# DEVELOPMENT OF HETEROSTRUCTURED TIN OXIDE NANOCATALYSTS FOR THE SYNTHESIS OF BIO-BASED MALEIC ACID

By

PETRUS MOLAOA MALIBO
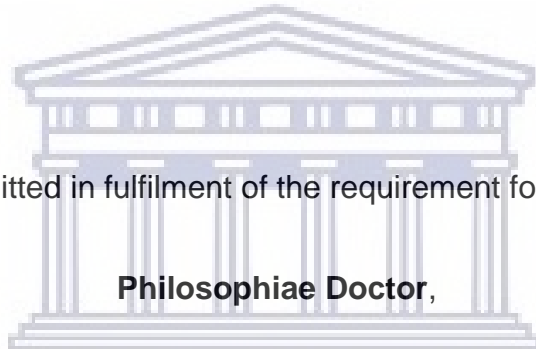
A thesis submitted in fulfilment of the requirement for the degree of,

Philosophiae Doctor,

in the Department of Chemistry, Faculty of Natural Science,

University of the Western Cape, South Africa

Supervisor: **Assoc. Prof. Peter R. Makgwane**

Co-supervisor: **Prof. Priscilla G.L. Baker**

September 2021

Keywords

Biomass

Furfural

5-Hydroxymethylfurfural

Oxidation

Maleic acid

Heterostructure metal oxides

Process intensification

Abstract

Maleic acid (MA) is a key intermediate for the synthesis of polyester resins, surface coatings, lubricant additives, plasticizers, copolymers, pharmaceuticals and agricultural chemicals. The current industrial production of MA is an energy-intensive gas-phase oxidation process of n-butane. The dwindling fossil resources and environmental issues have brought about a worldwide paradigm shift from fossil feedstocks to biomass resources for the sustainable production of fuel and chemicals. Furfural (FFR) and 5-hydroxymethylfurfural (HMF) are excellent biomass-derived platform chemicals, which present an alternative route for the production of renewable bio-based MA. There has been considerable success achieved in the oxidation of furfural and HMF to maleic acid and maleic anhydride with different catalysts in recent years. However, the main challenges which still exist are low selectivity, low feed volumes and high reaction temperatures for gas-phase oxidations, low catalyst stability (leaching of active sites) and recyclability. In this thesis, active heterostructured tin oxide-based nanocatalysts were developed for the oxidation process of FFR and HMF in the liquid-phase for the synthesis of MA. The bifunctional tin oxide interfaced with cheap and abundant metal oxides (vanadium, titanium, and base metal oxides (BMOs) of copper, iron, manganese and nickel) catalysts for the selective conversion of FFR and HMF to MA were synthesized following the concepts of nanoscale material architecture design with novel surface-enhanced intrinsic active sites employing a sol-gel polyol synthetic technique under microwave and conventional heating methods.

Among the VO_x-SnO_2 catalysts with varying vanadia content loading, it was discovered that the catalyst with 9.3 wt% V-metal presented a highly active catalyst for the oxidation of both FFR and HMF with H_2O_2 to maleic acid. The catalyst afforded maleic acid with

yields of 52 – 60% from FFR and HMF. The high activity of the catalyst was as a result of the presence of VO_x mono- and polymeric active sites populated with the balanced V^{5+}/V^{4+} redox pairs. Further, the CuO_x-SnO_2 nanocatalyst showed to be the most active among the heterostructured BMO-SnO_2 catalyst for the synthesis of MA from FFR affording yields up to 60% and 70% selectivity owing to the even distribution of the Cu^{2+}/Cu^+ redox pairs. The easily V^{4+}/V^{5+} and Cu^{2+}/Cu^+ redox pairs were important for accelerating the electron transfer processed and facilitating the C-C bond cleavage of the substrate for efficient maleic acid production. Moreover, the TiO_2-SnO_2 nanocatalyst with a Ti:Sn ratio of 1:4 and a high surface area (100.89 m^2/g) presented a highly active catalyst for oxidation of FFR and HMF with H_2O_2 to MA among TiO_2-SnO_2 catalysts with varying TiO_2 content loading. The common features of the three catalysts were maximized surface exposed metal active sites, low concentration of surface defects which negatively affected catalytic activity and high concentration of lattice oxygen necessary for facilitating electron transfer. In addition, the use of acetonitrile and acetic acid as co-solvents with water enhanced MA yield and selectivity due to the formation of peroxycarboximidic acid and peracetic acid complexes with increased oxidizing strength. A maximum MA yield of 74% was obtained with the TiO_2-SnO_2 catalyst. However, leaching and recyclability investigations revealed all the catalysts suffer leaching of the active sites. The oxidation reaction was successfully transferred from a flask small-scale to a benchtop laboratory reactor, thus demonstrating the feasibility to produce MA at a larger scale and thus the potential for industrial application. Furthermore, the MA synthesis process was successfully intensified using microwave heating as an alternative energy source, thus improving the FFR oxidation reaction rate and the space-time yield to afford a 42% MA yield in 20 minutes compared to a less than 1% yield in 20 minutes under the convention heating method.

Research outputs

Publications

1) <u>Petrus M. Malibo</u>, Peter R. Makgwane, and Priscilla G. Baker, Heterostructured redox-active V_2O_5/SnO_2 oxide nanocatalyst for aqueous-phase oxidation of furfural to renewable maleic acid, *ChemistrySelect*, **2020**, *5*, 6255–6267.

2) <u>Petrus M. Malibo</u>, Peter R. Makgwane, Mabel M. Mphahlele and Priscilla G. Baker, Synthesis of renewable maleic acid from oxidation of furfural over active SnO_2-M (M = Co, Cu, Mn, Ni) interfaced nano-oxide catalysts, (*Under review*).

3) <u>Petrus M. Malibo</u>, Peter R. Makgwane, and Priscilla G. Baker, Hetero-mixed TiO_2-SnO_2 interfaced nano-oxide catalyst with enhanced activity for selective oxidation of furfural to maleic acid, *Inorganic Chemistry Communications*, **2021**, *129*, 108637.

4) <u>Petrus M. Malibo</u>, Peter R. Makgwane, and Priscilla G. Baker. Bifunctional SnO_2-TiO_2 redox-acidic catalysts for biobased maleic acid synthesis, (*Under review*).

5) <u>Petrus M. Malibo</u> and Peter R. Makgwane, Synthesis of maleic acid by microwave-assisted oxidation of furfural over a heterostructured TiO_2-SnO_2 catalyst, (*Under review*).

Presentations

1) <u>Petrus M. Malibo</u> (**Poster presentation**): Design of Active and Recyclable Hetero-mixed V_2O_5-SnO_2 Nano-oxide Catalysts for the Aqueous-Phase Oxidation of Biomass Furfural to Maleic Acid. DST/MINTEK NIC 10th Year Anniversary Workshop, 14 - 16 October **2018**, CSIR ICC, Pretoria, South Africa.

Declaration

I hereby declare that **Development of Heterostructure Tin Oxide Nanocatalysts for the Synthesis of Bio-based Maleic Acid** is my own original work and that all sources have been accurately reported and acknowledged, and that this document has not previously in its entirety or in part been submitted at any university in order to obtain an academic qualification.

Petrus Molaoa Malibo   **January 2021**

Signed ……………………………

Acknowledgements

To my family, I would like to express my deepest gratitude for the support, love and patience you afforded me throughout my studies. To my mother, I will forever be grateful for all the sacrifices you have made for me.

Special thanks to Prof Peter Makgwane for the opportunity to work with him and for all the help and guidance throughout my doctorate studies. Your efforts are noticed and greatly appreciated. I also wish to extend my gratitude to Prof Priscilla Baker for all her help and inputs.

Many thanks to the CSIR characterization facility staff for all their help with the various instrumentation. Ms Rhandzu Rhikhotso is especially thanked for all the help with HRTEM operation and analysis.

To my friend Teboho Mokoena, thank you all for the help and guidance. Your help with XPS analysis and all the scientific discussions we had are greatly appreciated.

Thank you to all my friends for their encouragement and support over the years. Ta!

I would like to thank the UWC Department of Chemistry for the opportunity they afforded me.

Lastly, I am very grateful to the CSIR for the financial support that made this work posiible.
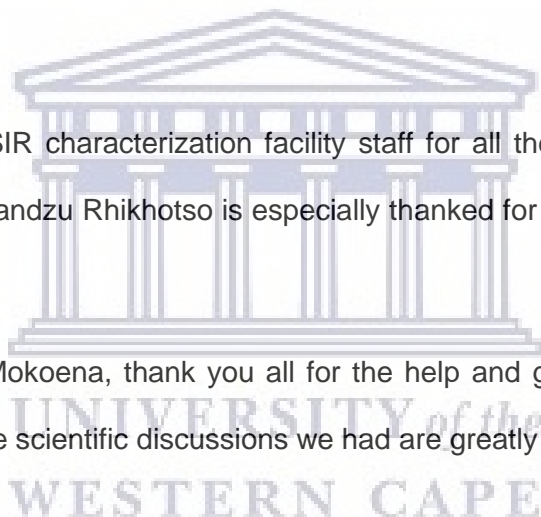
List of Abbreviations

AcOH – acetic acid

BET – Brunauer–Emmett–Teller

Dp – pore diameter

DFF – 2,5-diformylfuran

DMF – 2,5-dimethylfuran

EDX – energy dispersive x-ray spectroscopy

EPR – electron paramagnetic resonance

FA – 2-furoic acid

FDCA – 2,5-furandicarboxylic acid

FDM – 2,5-furandimethanol

FFA – furfuryl alcohol

FFCA – 2,5-formylfurancarboxylic acid

FMA – fumaric acid

FOA – formic acid

FTIR – fourier transform infrared spectroscopy

GVL – γ-valerolactone

HAADF-STEM – high-angle annular dark-field scanning transmission electron microscopy

HMF – 5-hydroxymethylfurfural

HMFCA – 5-hydroxymethyl-2-furancarboxylic acid

HPLC – high pressure liquid chromatography

HRTEM – high resolution transmission electron microscopy

LA – levulinic acid

MA – maleic acid

MAN – maleic anhydride

MeCN – acetonitrile

NH_3-TPD – ammonia temperature-programmed desorption

NPs – nanoparticles

OA – oxalic acid

PL – photoluminescence

S_{BET} – BET surface area
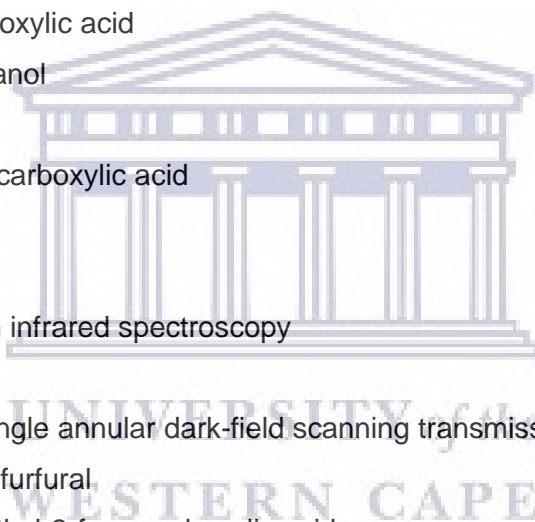
SA – succinic acid

SAED – selected area electron diffraction

SEM – scanning electron microscopy

TBHP – tert-butylhydroperoxide

TEM – transmission electron microscopy

THF – tetrahydrofuran

THFA – tetrahydrofurfuryl alcohol

THFDM – tetrahydrofurandimethanol

TPR – temperature-programmed reduction

Vp – pore volume

XRD – X-ray diffraction

XPS – X-ray photoelectron spectroscopy

CONTENTS

List of Figures

List of Schemes

List of Tables

UNIVERSITY *of the*

WESTERN CAPE

CHAPTER 1

Introduction

1.1 Research background

The push towards green, renewable and sustainable production of chemicals coupled with the diminishing availability of fossil resources and the increasing consumption of energy has directed more interest towards the development of new technologies for the production of renewable energy resources. Biomass, the largest annually renewable and environmentally friendly carbon source, is regarded as an ideal alternative to traditional fossil resources.[1,2] Biomass is readily available in different forms, such as waste materials (forest, agricultural and municipal), forest products, energy crops or aquatic biomass.[3,4] There are three main categories of biomass-derived feedstocks for the production of renewable fuels and chemicals: (**i**) lignocellulosic biomass, (**ii**) starch- and sugar-derived biomass and (**iii**) triglyceride-based biomass.[5] Vegetable biomass is produced by plants through photosynthesis consuming CO_2 and H_2O using sunlight as an energy source. This process produces O_2 as a sub-product and forms primary C_5 and C_6 sugar products; which then undergo polymerization to produce three components of lignocellulosic biomass: (**i**) cellulose, (**ii**) hemicelluloses and (**iii**) lignin.[2] The general composition of lignocellulosic biomass is 40-50 % cellulose, 25-35 % hemicellulose and 15-20 % lignin as shown in **Fig. 1-1**.[5] Further, other extractive organic molecules (e.g. lipids and terpenes) also make up a small percentage (less than 5%) of lignocellulosic biomass.[6] Among the different biomass conversion processes, there are three main approaches employed for the conversion of lignocellulosic biomass: gasification, pyrolysis, hydrolysis and fermentation.[7] These processes are carried out for the transformation of

lignocellulosic biomass into biofuels and a large variety of platform and value-added chemicals.
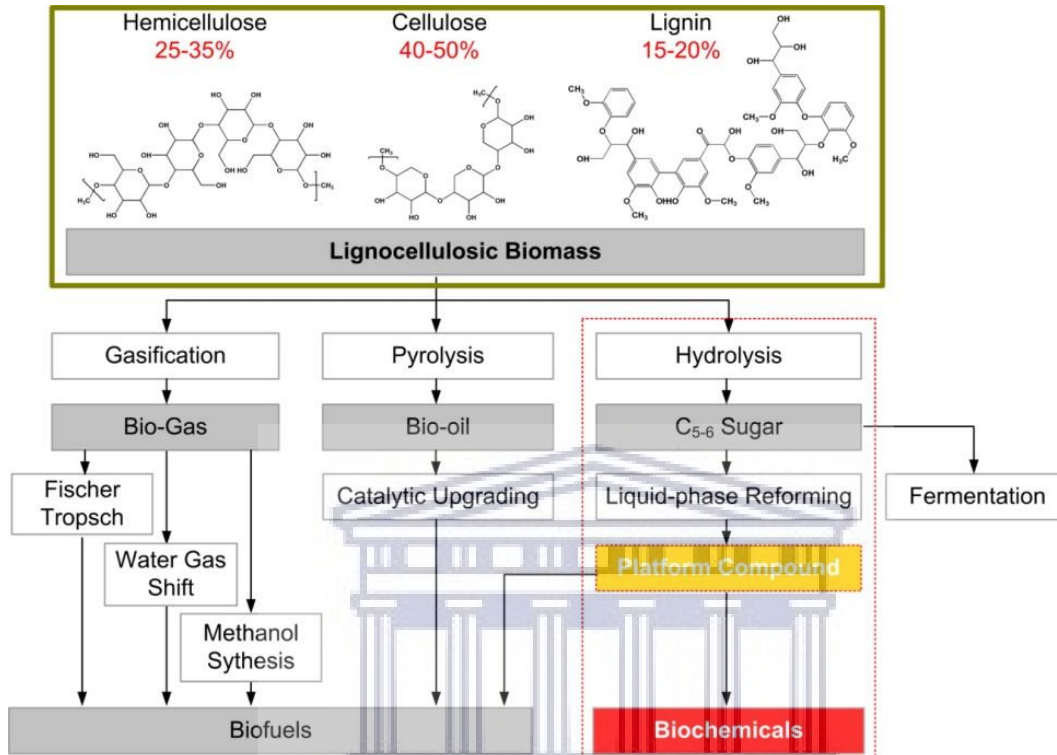
Fig. 1-1: A representation of lignocellulosic biomass composition and an overview of its conversion to biofuels and biochemical (Adapted from [7]).

1.2 Problem statement

The production of commodity and specialty chemicals from fossil-based carbon resources is a well established industry, however the processes employed possess their own limitations. These setbacks include: **(i)** diminishing fossil reserves needed as the starting material, **(ii)** the use of high temperatures and energy with multi-step processes, hence rendering the processes costly, and **(iii***)* the production of harmful gases as by-products, which makes the processes environmentally unfriendly. An alternative solution to these issues is to produce high-value chemicals through biomass valorisation. The valorisation of biomass is advantageous in that: **(i)** lignocellulose is the most abundant, globally

available biomass source inedible to humans, **(ii)** biomass is a renewable and versatile carbon source, **(iii)** biomass usage contributes to decreasing greenhouse gas emissions. The challenge for the utilization of biomass as a renewable carbon source for the production of value-added chemicals lies within the development of efficient and cost-effective processing methods for the transformation of highly functionalized carbohydrates. Part of improving on costs and biomass valorisation efficiency depends on the design and fabrication of heterogeneous catalysts based on cheap and abundant metals. As a result, this study was aimed at developing efficient heterogeneous catalysts based on SnO_2 support for use in the catalytic transformation of biomass furfural and 5-hydroxymethylfurfural to bio-based maleic acid, an industrially important functional performance intermediate fine chemical. The liquid phase oxidation of furfural and 5-hydroxymethylfurfural with hydrogen peroxide oxidant presents an alternative renewable route to maleic acid synthesis. Maleic acid is an important industrial intermediate or monomer for the manufacturing of unsaturated polyester resins, surface coatings, vinyl copolymers, lubricant additives, and plasticizers.[8]

1.3 Research objectives

The scope of this study was based on the design and fabrication of mixed heterostructure (SnO_2) nanocatalysts for selective oxidation of furfural and 5-hydroxymethylfurfural to maleic acid. The catalysts were synthesised at nanoscale size via a polyol synthetic route under conventional and microwave-assisted heating methods. The research work was carried out in four phases and the specific objectives of this study were as follows:

- To synthesize active vanadium-tin oxide (VO_x-SnO_2) nanocatalysts with varying vanadium metal loadings, characterization of catalysts structure properties and evaluation of their catalytic activity performance in furfural oxidation to maleic acid.

- To synthesize nanostructured composite catalysts based on heterostructure SnO_2 consisting of Cu, Co, Mn and Ni metal oxides. Characterization of the nanocatalysts and their catalytic activity performance evaluation in developing the process for synthesis of maleic acid from the liquid-phase oxidation reaction of furfural.

- To synthesize bifunctional TiO_2-SnO_2 nanostructured composite catalysts with varying titanium metal loadings, characterization of catalysts structure properties and evaluation of their catalytic activity performance in the oxidation of furfural and 5-hydroxymethylfurfural for maleic acid synthesis.

- To investigate the batch process scale up performance and process intensification in microwave-assisted oxidation reaction process of furfural conversion to maleic acid.

1.4 Brief chapter overview

This thesis describes the development of efficient SnO_2-based nanocatalysts for use in the oxidation of bio-sourced furfural and 5-hydroxymethylfurfural to renewable maleic acid. The thesis has been divided into eight chapters.

Chapter 1 gives a brief introduction to biomass valorisation and the production of furfural and 5-hydroxymethylfurfural from lignocellulosic biomass as an alternative, readily available and sustainable carbon source alternative. The subsequent transformation of furfural and 5-hydroxymethylfurfural to the targeted maleic acid is also briefly discussed.

Chapter 2 gives a literature review of biomass valorisation and furfural, 5-hydroxymethylfurfural, maleic acid and maleic anhydride production and their applications. The gas- and liquid-phase oxidation of furfural and 5-hydroxymethylfurfural is also discussed along with reaction mechanisms. A brief introduction to SnO_2, base metals oxides (Cu, Co, Mn and Ni), V_2O_5 and TiO_2 based catalysts and their applications in biomass catalytic conversions is also included.

In **Chapter 3**, the preparation and characterisation methods of the heterostructure SnO_2 mixed metal oxide nanocatalysts are described. Further, the chapter describes the characterization instrumentation specifications used to study the structure properties of the synthesised nanomaterials. The procedures to carry out the batch oxidation reaction in flask, bench top glass and microwave reactors as well as the liquid chromatographic analysis of organic products are also described.

Chapter 4 describes the catalytic activity results of the oxidation of furfural and 5-hydroxymethylfurfural using hydrogen peroxide over the heterostructure V_2O_5-SnO_2 composite nanocatalysts. The effect of different parameters such as solvent, temperature, H_2O_2 concentration, and catalyst dosage on furfural oxidation rates, products selectivity and yields were investigated.

Chapter 5 details the incorporation of different basic metal oxide (CuO_x, CoO_x, MnO_x, and NiO_x) onto SnO_2 support. The heterostructure nanocatalysts characterization and catalytic activity results in furfural oxidation to maleic acid are also presented.

Chapter 6 describes the preparation and characterisation of the heterostructure TiO_2-SnO_2 nanocatalysts, along the with their catalytic performance in the liquid-phase oxidations of furans (i.e. furfural, and 5-hydroxymethylfurfural) for maleic acid production using hydrogen peroxide (H_2O_2) oxidant

Chapter 7 describes the batch process scale up for furfural oxidation using the heterostructure SnO_2-based nanocatalysts.

Chapter 8 involves the process intensification in microwave-assisted furfural oxidation reaction using the heterostructure TiO_2-SnO_2 catalyst.

Chapter 9 gives a summary of the conclusions reached in this thesis and recommendations on future research are also presented.

1.5 References

[1] P. Gallezot, Conversion of biomass to selected chemical products. Chemical Society Reviews, **2012**, pp. 1538-1558.

[2] A. Corma, S. Iborra, A. Velty, Chemical routes for the transformation of biomass into chemicals. Chemical Reviews, **2007**, 107, pp. 2411-2502.

[3] S.K. Sansaniwal, M.A. Rosen, S.K. Tyagi, Global challenges in the sustainable development of biomass gasification: An overview. Renewable and Sustainable Energy Reviews, **2017**, 80, pp. 23-43.

[4] G.W. Huber, A. Corma, Synergies between bio- and oil refineries for the production of fuels from biomass. Angewandte Chemie International Edition, **2007**, 46, pp. 7184-7201.

[5] R. Mariscal, P. Maireles-Torres, M. Ojeda, I. Sádaba, M. López Granados, Furfural: a renewable and versatile platform molecule for the synthesis of chemicals and fuels. Energy & Environmental Science, **2016**, 9, pp. 1144-1189.

[6] I. Simakova L., A. Simakov V., D. Yu. Murzin, Valorization of biomass derived terpene compounds by catalytic amination. Catalysts, **2018**, 8, pp. 365.

[7] X. Li, P. Jia, T. Wang, Furfural: A Promising platform compound for sustainable production of C4 and C5 Chemicals. ACS Catalysis, **2016**, 6, pp. 7621-7640.

[8] G. Machado, S. Leon, F. Santos, Literature review on furfural production from lignocellulosic biomass. Natural Resources, **2016**, 7, pp. 115-129.

CHAPTER 2

Literature Review and Background

2.1 Introduction to biomass valorisation

A major drive to move from a fossil-based chemical industry towards a sustainable economy based on renewable biomass resources is currently underway globally. This transition is triggered by several factors such as the heavy dependency on fossil-fuel imports (for fuel and chemicals), the depletion of fossil-fuel reserves, increasing global energy demands, and the worldwide concern over excessive emissions of greenhouse gasses.[1] Biomass is regarded as a suitable alternative to traditional fossil-carbon resources for the production of energy, biofuel and chemicals. The reasons being that biomass is readily available, environmentally friendly, and renewable. As a result, biomass feedstocks are to the biorefinery industry what fossil-carbon (i.e. oil, natural gas and coal) is to the petrochemical industry. Biomass feedstocks generally refer to plants and their waste materials (forest, agricultural, aquatic and municipal), and aquatic biomass. These biomass feedstocks can be classified into three main categories; (**i**) lignocellulosic constituting the structural integrity of plants, (**ii**) sugar and starch comprised of glucose polysaccharides, and (**iii**) triglyceride-based comprised of fatty acids and glycerol from both plant and animal sources.[2]

Lignocellulosic biomass is the most attractive and studied feedstock because it is inexpensive and most abundant. Lignocellulose generally comprises a robust composite of three different oxygen-containing high-molecular weight polymers; (**i**) hemicellulose, (**ii**) cellulose and (**iii**) lignin. Hemicellulose is an amorphous polymer composed of C_5 (D-xylose and L-arabinose) and C_6 (D-glucose, D-mannose and D-galactose) sugar monomers

with xylose the most abundant monomer present. Cellulose is a crystalline polymer of C_6 glucose monomer units linked by β-1,4 glycosidic bonds and forms the major structural component of lignocellulose. Lignin is an amorphous polymer composed of methoxylated phenylpropane structures such as coniferyl, sinapyl and P-coumaryl alcohols.[3] The sugar-derived biomass comprise of a complex carbohydrate network of mono- (D-glucose and D-xylose) and disaccharides (sucrose, lactose and maltose) joined by glycosidic linkages. The starch biomass comprises a polysaccharide, which mainly consists of amylose and amylopectin, which are polymers of α-glucose. [4] Triglyceride-based biomass is based on tri-esters which consist of a glycerol bound to three fatty acid molecules.[5]

The three main approaches used in the conversion of lignocellulosic biomass are gasification, pyrolysis and hydrolysis.[6,7] The gasification process is the partial combustion of biomass at high temperatures (600-900 °C), and is used for the production of synthesis gas (syngas), a mixture of carbon monoxide and hydrogen. The syngas can then be converted into electrical power, hydrogen, steam and numerous fuels or chemicals through three conversion processes: (1) methanol synthesis, (2) Fischer-Tropsch (FT) synthesis and (3) the water gas shift (WGS) reaction.[8] Pyrolysis is the selective thermal decomposition of biomass at 'mild' temperatures (300-500 °C) to produce liquid products referred to as bio-oils. The process is often conducted at fast heating rates (100 °C/s) and is referred to as fast pyrolysis. The initial products of pyrolysis are vapour-phase products, which then react and subsequently condense (upon cooling) to produce a mixture of liquid products: acids, aldehydes, alcohols, sugars, esters, ketones and aromatics.[9] Fast pyrolysis can achieve high yields of bio-oil (70-80 %) and this is regarded as the most economic and promising technology for the production of biomass chemicals and fuels. Hydrolysis of biomass is carried out for the conversion of the hemicellulosic and cellulosic

fractions of biomass and is a more complicated process than pyrolysis and gasification. It is carried out at lower temperatures (100-200 °C) and is particularly appropriate if higher selectivity is required for efficient biomass utilization. Acid-catalysed hydrolysis is employed for the deconstruction of hemicellulose and cellulose into C_5 and C_6 sugars, which can be subsequently transformed into a series of platform chemicals.[10]

2.2 Conversion of biomass to platform chemicals

2.2.1 Hemicellulose to furfural

Furfural is a clear, colourless liquid produced from the dehydration of xylose/xylan obtained by the acid-catalysed hydrolysis of hemicellulose. It has an almond odour and the molecular formula of $C_5H_4O_2$ and with the following synonyms: 2-furancarboxyaldehyde, 2-furanaldehyde, 2-furfuralaldehyde, furalaldehyde, fural and furfurol.[11,12] The chemical structure of furfural is shown in **Fig. 2-1** below.
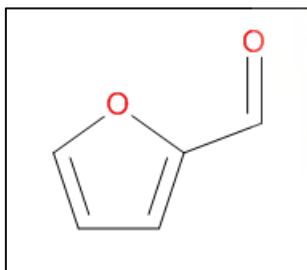
Fig. 2-1: Molecular chemical structure of furfural.

Upon exposure to oxygen in the presence of sunlight, furfural undergoes auto-oxidation and turns to a dark red/brown colour. The production of furfural requires raw materials rich in pentosans, which are aldose sugars, composed of small rings formed from short five-membered chains. Some of these raw materials are woody plants such as corncobs, sugar cane bagasse, rice, cotton and oat hulls, almond and sunflower husks, etc., with

sugar cane bagasse and corncobs responsible for more than 98% of the production of furfural.[13] Furfural is ranked among the top 30 biomass-derived platform chemicals by the US Department of Energy and among the top 10 value added chemicals by Bozell.[14,15] Approximately, over 300 000 tons of furfural is produced per year with China, the Republic of South Africa and the Dominican Republic being responsible for 90% of its global production.[2] It is used in several applications such as the production of antacids, fertilizers, plastics, inks, fungicides, nematicides, adhesives and flavouring compounds.[13] Moreover, furfural is also as an intermediate for the production of a variety of fine chemicals (as discussed in **Section 2-3**) due to its structure possessing both C=C bonds and an aldehyde functional group making it very reactive.

The synthesis of furfural is an acid catalysed two-step process where the pentosan (xylan) from the biomass hemicellulose is hydrolysed to pentose (xylose), and the pentose is then dehydrated to furfural as illustrated in **Scheme 2-1** and by **equations (1)** and **(2)** below. The process can be carried out in two ways: (**i**) a one-stage process where the hydrolysis of the pentosan and the dehydration of the pentose occur simultaneously in the same reactor and, (**ii**) a two-stage process where the hydrolysis of the pentosan occurs under mild conditions in one reactor followed by the dehydration of the pentose in another reactor. The two-stage process is advantageous over the one-stage process in that it produces higher yields and the solid residue obtained thereafter can be used in the synthesis of cellulose, glucose and ethanol by fermentation.[16]

$$(C_5H_8O_4)_n + nH_2O \rightarrow nC_5H_{10}O_5 \tag{1}$$

$$C_5H_{10}O_5 - 3H_2O \rightarrow C_5H_4O_2 \tag{2}$$
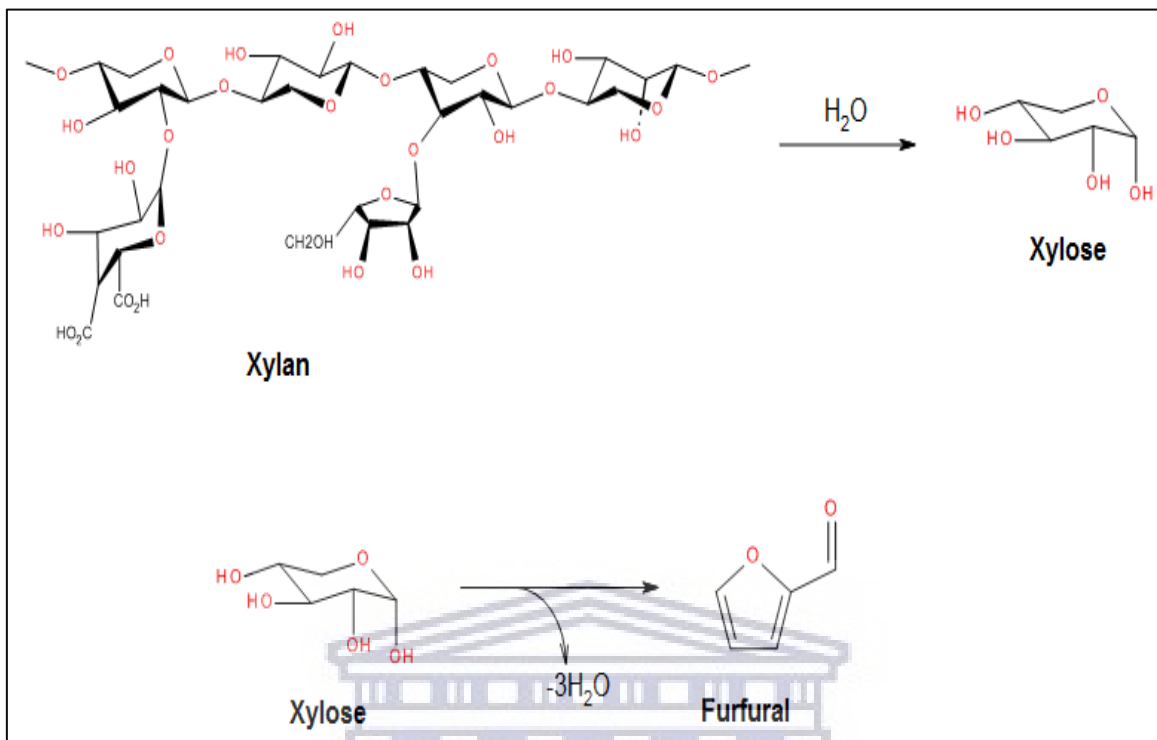
Scheme 2-1: Schematic illustration for the conversion of xylan to xylose, and subsequently xylose to furfural.

The first and oldest industrial process for producing furfural was developed in 1921 by the Quaker Oats company utilizing cookers originally meant for the production of an unprofitable cereal product. In the process, the raw material was mixed with sulphuric acid and introduced to a rotating cooker with passing steam at 153 °C. Since then several batch and continuous processes have been developed for the production of furfural.[11,13] However, these technologies are deemed inefficient due to low furfural yields (around 50% or less), use of corrosive homogenous acid catalysts, high energy consumption and environmental pollution. As a result, many efforts have been devoted to the use of heterogeneous solid acid catalysts to improve production and address these process issues. The approaches employed include the use of biphasic solvent systems and ionic liquids.[17] The production via heterogeneous acid catalysts proceeds through the

cyclodehydration mechanism (**Scheme 2-2**) over Brønsted and Lewis acidic sites of the catalysts.
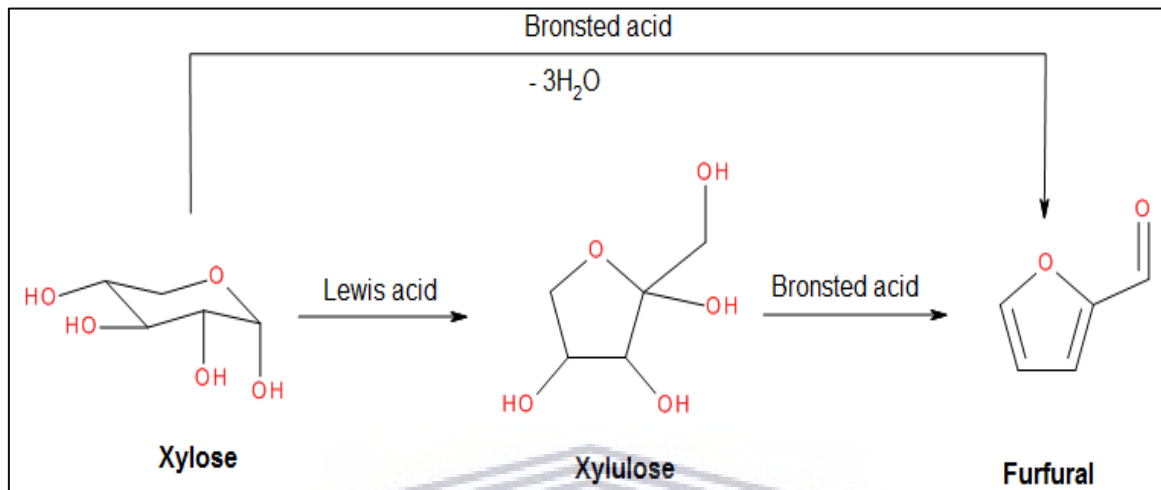
Scheme 2-2: The cyclodehydration mechanism for the conversion of xylose to furfural.

2.2.2 Cellulose to 5-hydroxymethylfurfural

5-hydroxymethylfurfural is a yellow, low melting crystalline solid synthesized by the dehydration of hexoses (preferably fructose and glucose) derived by the acid-catalysed hydrolysis of cellulose. It is characterized by a chamomile odour and has the molecular formula of $C_5H_4O_2$ and with the synonyms 5-(Hydroxymethyl)furan-2-carbaldehyde, and 5-(Hydroxymethyl)-2-furaldehyde.[18] The chemical structure of furfural is shown in **Fig. 2-2** below.
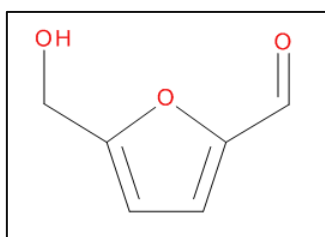
Fig. 2-2: Molecular chemical structure of 5-hydroxymethylfurfural.

The synthesis of 5-hydroxymethylfurfural is a multi-step acid-catalysed process beginning with the hydrolysis of cellulosic biomass to hexoses (mainly glucose and fructose) followed by the subsequent dehydration of the hexoses to 5-hydroxymethylfurfural as depicted in **Scheme 2-3**. Although 5-hydroxymethylfurfural can be synthesized from all hexoses (also directly from cellulose), the synthesis from glucose is more challenging and leads to lower yields. This is because of the very stable ring structure of glucose and the slow additional isomerization step that precedes fructose dehydration.[19,20] There are three possible mechanisms that have been proposed for the synthesis of 5-hydroxymethylfurfural from glucose and fructose. The first proposed mechanism involves the consecutive removal of three water molecules from the relevant hexose to 5-hydroxymethylfurfural (**Scheme 2-3**). The second proposed mechanism proceeds in the presence of amines and amino acids via the Maillard reaction of the hexose. The third and most studied mechanism is proposed to proceed through the direct dehydration of hexose via acyclic or cyclic intermediates. The acyclic pathway forms a 1,2-enediol as a key intermediate while the cyclic pathway forms fructofuranose as an intermediate.[21-23]
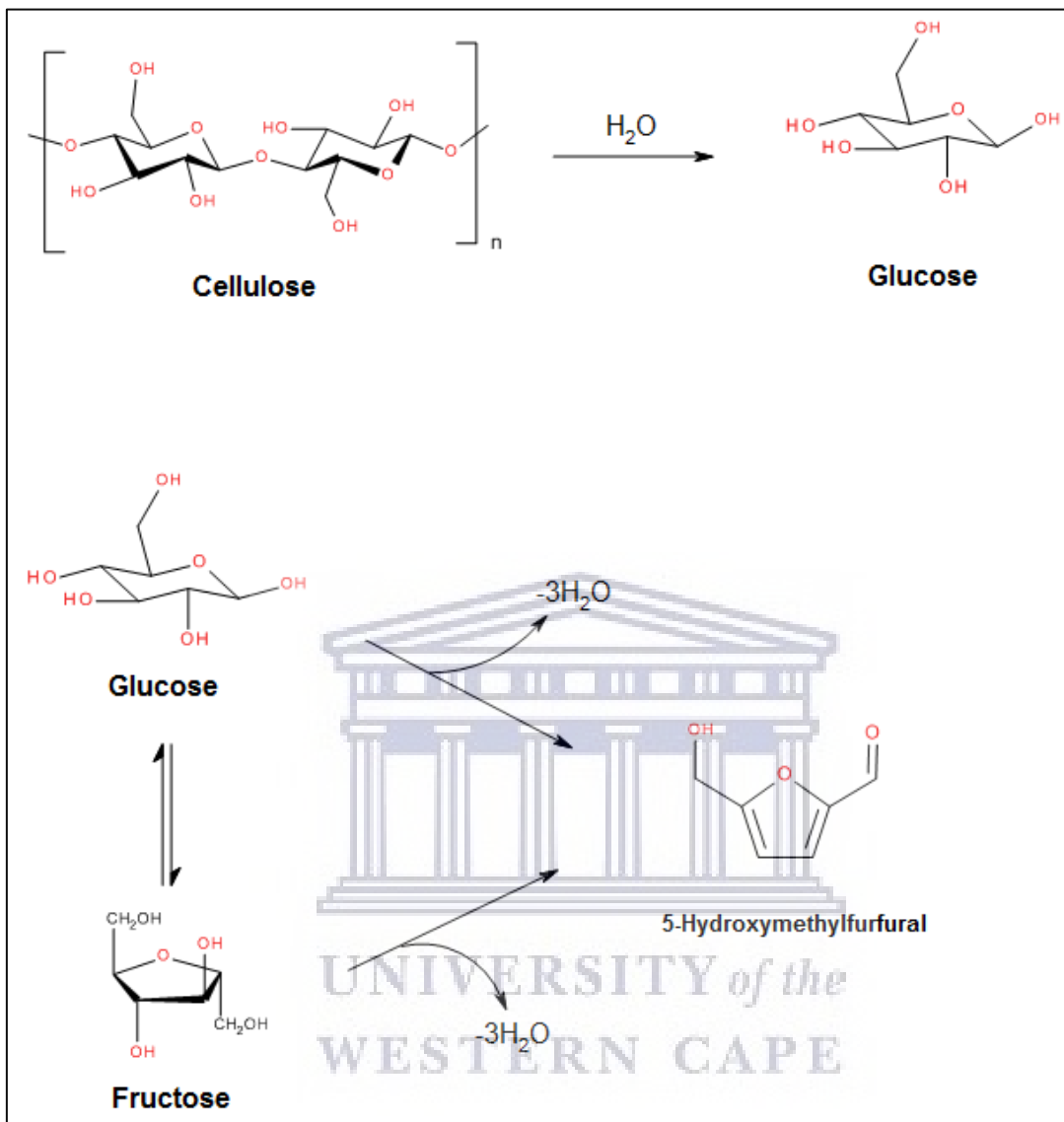
Scheme 2-3: Schematic illustration for the conversion of cellulose to glucose, and the subsequent conversion of cellulose to 5-hydroxymethylfurfural.

The synthesis of 5-hydroxymethylfurfural was first reported at the end of the 19th century. However, unlike furfural, its industrial commercialization has not been achieved yet due to the economic concerns arising from the use of increasingly complex reaction systems (anhydrous organic solvents, supercritical media, biphasic media, ionic liquids, water-immiscible extractive solvents, etc.). The use of such complex systems is driven by the unrestrained re-hydration of the produced 5-hydroxymethylfurfural to levulinic acid and

formic acid as well as the polymerization of 5-hydroxymethylfurfural or reaction intermediates to humins.[24,25] Due to the 5-hydroxymethylfurfural structure containing both the hydroxyl and aldehyde functional groups in addition to the C=C bonds, it is generally more reactive than furfural and can thus be transformed to many value-added chemicals (**Section 2-3**).

2.3 Conversion of furans to high value-added chemicals

The conversion of biomass derived furans platform chemicals such as furfural and 5-hydroxymethylfurfural have the potential application for the development of new, sustainable and environmentally cleaner technological processes for the synthesis of a plethora of high-value added downstream chemicals. The potential is made possible by the high functionality of these bio-based chemicals which allows them to undergo a variety of chemical transformations via processes that include dehydration, hydrogenation, oxidation, hydrogenolysis, decarboxylation, isomerization, metathesis, reforming and fermentation.[26]

2.3.1 Furfural to value-added chemicals

Furfural can be converted to C_4 and C_5 valuable chemicals and biofuels by several processes such as hydrogenation, oxidation, hydrogenolysis and decarboxylation (**Fig. 2-3**).[27] The main top value non-petroleum furfural derivatives include furfuryl alcohol, tetrahydrofurfuryl alcohol, levulinic acid, furan, succinic acid, furoic acid, tetrahydrofuran, and 2-methylfuran.[28-34] The most important derivative of furfural is furfuryl alcohol, with 60-70% of all produced furfural being consumed for furfuryl alcohol production. Furfuryl alcohol is produced by the gas or liquid-phase selective hydrogenation of the carbonyl group of furfural. Further, furfuryl alcohol is extensively used in the production of foundry

resins and also used in corrosion-resistant fibre-reinforced plastics, cements and mortars; as a reactive solvent in the refractory industry; as a chemical building block in the pharmaceuticals industry and as feedstock in the production of tetrahydrofurfuryl alcohol and levulinic acid.[28-30]
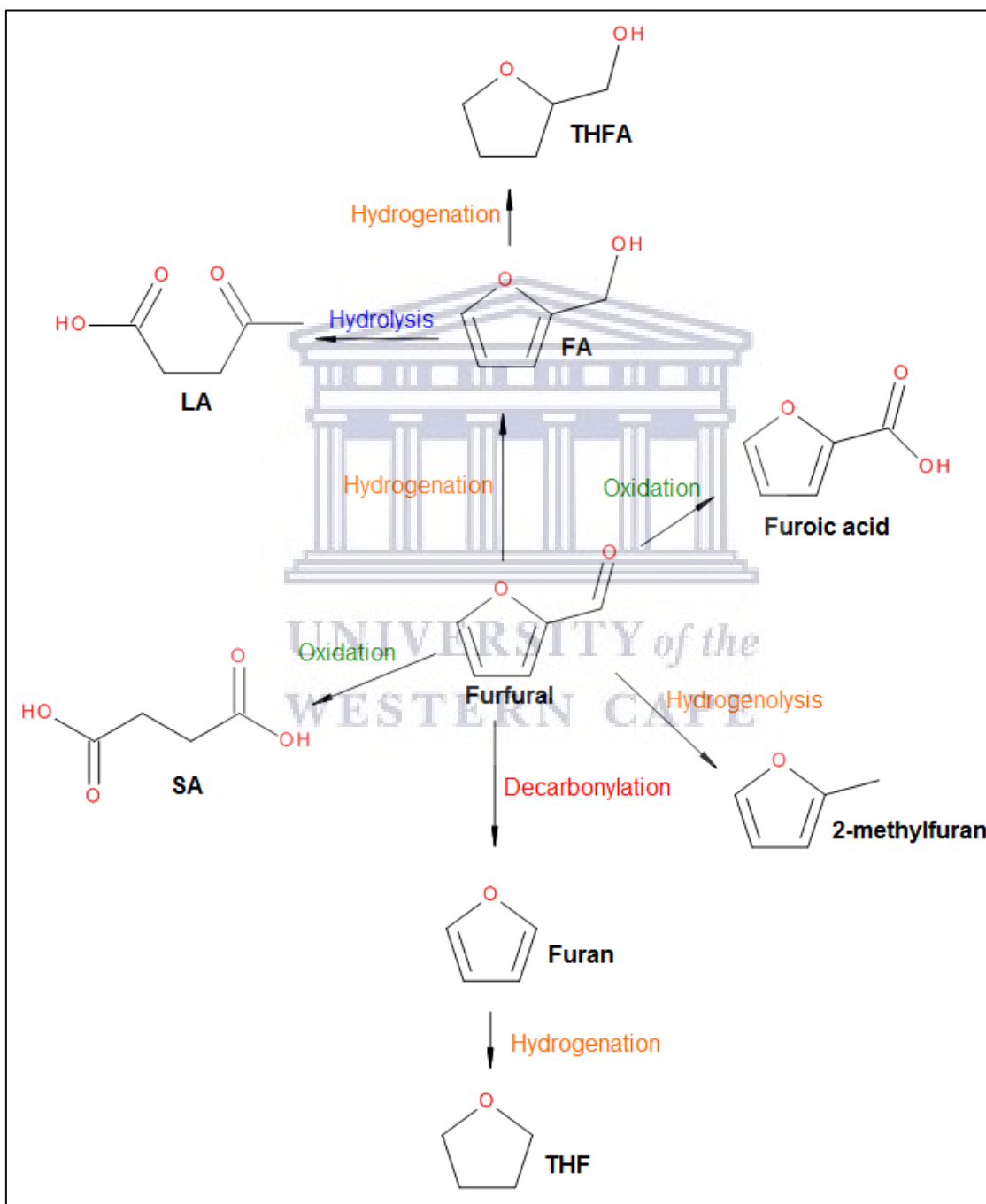
Fig. 2-3: Conversion routes of furfural to different chemical derivatives.

Furfural along with its derivatives can be processed further into several downstream commodity chemicals such as 1,5-pentanediol, 2-methylfuran, 5-hydroxymethylfurfural, etc.[2,15] Among these downstream chemicals, maleic acid, maleic anhydride and fumaric acid, synthesised via furfural and 5-hydroxymetylfurfural oxidation, are of interest to this project. As a result, they are discussed further in details in **section 2.4.1**.

2.3.2 5-Hydroxymethylfurfural to value-added chemicals

5-hydroxymethylfurfural can also undergo transformation into various value-added chemicals and biofuels derivatives by processes such as selective hydrogenation, oxidation, hydrogenolysis and decarboxylation. Among this variety of fine chemicals, the most industrially important are the 5-hydroxymethylfurfural oxidation products used in the production of renewable polymer monomers: 2,5-furandicarboxylic acid, 2,5-formylfurancarboxylic acid, 5-hydroxymethyl-2-furancarboxylic acid and 2,5-diformylfuran.[34] An extensive amount of research effort in the past decade has been devoted to the production of 2,5-furandicarboxylic acid via 5-hydroxymethylfurfural oxidation reaction, which is a highly important biopolymer monomer with applications in the plastics industry for products such as bottles, and food packages.[35,36] The oxidation of 5-hydroxymethylfurfural to 2,5-furandicarboxylic acid involves several intermediates as shown in **Fig. 2-4**, which are also important monomer chemical for biopolymers. Other applications of 2,5-furandicarboxylic acid include the production of polyamides, polyurethanes, thermosets, and plasticizers.[37] 2,5-formylfurancarboxylic acid is another important intermediated derived from the oxidation of 5-hydroxymethylfurfural with potential applications in medicine and furan-based polyesters.[38] 2,5-diformylfuran, another 5-hydroxymethylfurfural oxidation product, has versatile applications in the

synthesis of polymers, fluorescent materials, pharmaceuticals and ligands.[39] 5-hydroxymethyl-2-furancarboxylic acid finds applications as a monomer in the synthesis of polyesters and as a starting material for the manufacture of pharmaceuticals.[40]
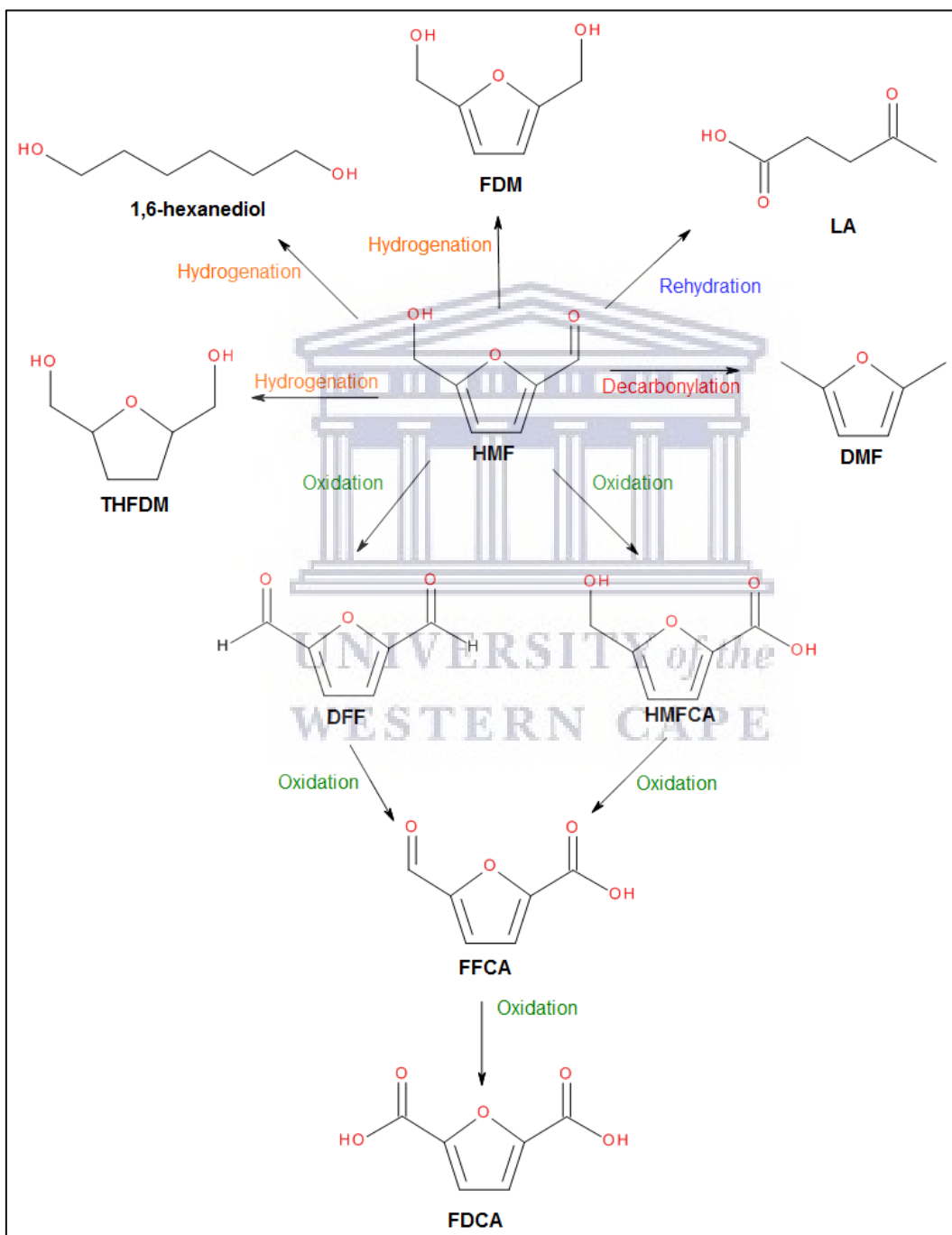
Fig. 2-4: Catalytic transformation routes to 5-hydroxymethylfurfural derivatives.

Another class of important 5-hydroxymethylfurfural derived chemicals are the so-called diols and triols, which are produced by the hydrogenation of 5-hydroxymethylfurfural and have significant applications as monomers in the synthesis of renewable polyesters.[41] These diols and triols include 1,5- and 1,6-hexanediool, 1,2,6-hexanetriol, 2,5-tetrahydrofurandimethanol and 2,5-furandimethanol. Another important 5-hydroxymethylfurfural hydrogenation (reductive decarbonylation) product is 2,5-dimethylfuran, which is used as a green carbon mitigation biofuel additive.[42,43] Levulinic acid is a versatile building block chemical with applications in fuel additives, polymers and resins.[44] Levulinic acid is produced by the rehydration of 5-hydroxymethylfurfural, usually during the synthesis of 5-hydroxymethylfurfural from cellulose or C_6 sugars.

2.4 Catalytic oxidation of furans to maleic acid and maleic anhydride

2.4.1 Oxidation of furfural to maleic acid and maleic anhydride

Industrially, maleic acid is synthesized from the hydrolysis of maleic anhydride, which is produced by the gas-phase oxidation of n-butane and benzene using vanadium oxide catalysts.[45] However, the industrial process for production of maleic anhydride is a fossil-carbon based process associated with several energy intensive steps producing greenhouse gasses.[46] These factors render the process economically costly and environmentally unfriendly. As a result, there is a need to develop new catalytic processes for the efficient and less costly production of maleic acid and maleic anhydride. The liquid- or vapour-phase oxidation of furfural provides an alternative route for the synthesis of renewable maleic acid and maleic anhydride. Further, both maleic acid and maleic anhydride are inter-convertible chemicals via the dehydration and hydration reaction processes, thus the production of one infers the availability of the other (**Scheme 2-4**).[47-

[50] For this reason, the work presented in this section not only focuses on the synthesis of maleic acid from furfural but also highlights some key results achieved in the oxidation of furfural to maleic anhydride as well.
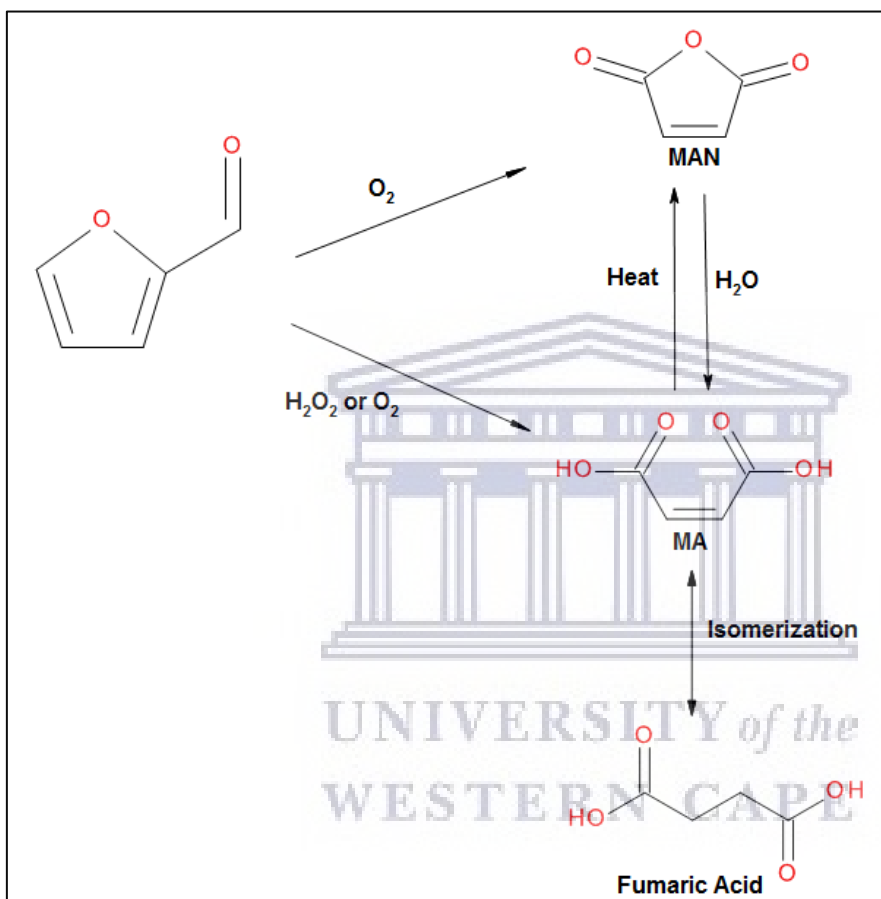
Scheme 2-4: Representation of chemical conversion routes for the production of maleic acid and maleic anhydride from furfural.

Since the first demonstration by Sessions in as early as 1928, there has been a considerable amount of effort directed towards improving the yield and selectivity towards maleic acid and maleic anhydride from furfural oxidation.[51] It was not until 1948 that an improvement on vapour-phase oxidation of furfural was reported by Nielsen.[52] Using an iron molybdate catalyst, over 70% selectivity of maleic anhydride was achieved based on

the converted furfural. However, since then progress on studies of furfural oxidation to maleic anhydride was very stagnant, possibly due to poor competition to the on-going petroleum process based on butane oxidation. In fact, it was not until after 2010 that real progress was made in terms of catalyst design, yield and selectivity towards maleic acid and maleic anhydride in the furfural oxidation reaction.

2.4.1.1 Oxidation using molecular oxygen

A variety of catalyst have been developed for the vapour- and liquid-phase oxidation of furfural to synthesise maleic acid and maleic anhydride based on metal oxides, molecular sieves and carbonaceous materials. Whilst maleic anhydride is preferably produced through the vapour-phase oxidation of furfural using molecular oxygen, maleic acid can be produced in both the vapour- and liquid-phases using molecular oxygen or hydrogen peroxide as oxidants (**Table 2-1**). With regards to furfural oxidation to maleic acid and maleic anhydride, the most promising results was the vapour-phase oxidation process using VO_x/Al_2O_3 to achieve 73% yield of maleic anhydride.[53] Recently, $V_2O_5/\gamma-Al_2O_3$ showed improved maleic anhydride yield of 75% in the vapour-phase oxidation of furfural.[54] In another study, the use of binary Mo-V oxides achieved a 65% combined yield of maleic acid and maleic anhydride in acetic acid solvent.[55] The highest yield of maleic anhydride of 90% from furfural to date has been achieved using vanadium phosphorous oxide catalyst under gas-phase oxidation at 360 °C.[56]

The use of molecular sieves catalysts in furfural oxidation has up to so far been very limited with few examples reported. A recent study reported on the use three different molecular sieves (MCM-41, SBA-15 and ZSM-5) as supports for an iron porphyrin catalyst for liquid-phase furfural oxidation with molecular oxygen.[57] Under optimized reaction

conditions, a 56 % yield of maleic acid at 74% selectivity was obtained with the catalyst supported on SBA-15. The use of carbonaceous materials in furfural oxidation has been demonstrated recently with molecular oxygen and H_2O_2 as oxidants. The oxidation of furfural to maleic anhydride with molecular oxygen oxidant has been recently demonstrated using vanadium-oxo nanosheets fabricated on graphene oxide as a catalyst. Under optimized conditions, a total yield of maleic anhydride of 59.9% was achieved after 4 h reaction time.[58]

2.4.1.2 Oxidation using hydrogen peroxide

Reports on the catalytic oxidation of furfural to maleic acid with H_2O_2 are scarce partly due to the cheaper price and slightly better atom efficiency of O_2 oxidant compared to H_2O_2.[59] However, the use of H_2O_2 oxidant presents the potential opportunity to conduct reactions at lower temperatures and while eliminating safety issues associated with using high O_2 pressures. Araji et al.[60] demonstrated the oxidation of furfural with H_2O_2 in aqueous solvent using betaine hydrochloride (BHC, a quaternary ammonium salt) homogeneous catalyst to obtain 61% yield of maleic acid. However, the reuse of BHC required an extra step to recover the catalyst by dehydration, which will incur additional costs to the process economics. The zeolite ZSM-5 catalyst was used for the liquid-phase oxidation of furfural to succinic acid as the main product with a yield of 30% while maleic acid was only obtained in trace amounts.[61] A yield of 62.8% was achieved over a vanadium-oxo catalyst immobilised on a Schiff base modified graphene oxide support after 8 h using H_2O_2 oxidant.[62] The use of Amberlyst-70 sulphonic-resin catalyst with strong acid-sites concentration utilizing H_2O_2 oxidant produced succinic acid with a yield of 50% while maleic acid yield was 15%.[61] Similarly, other sulphonic-resin designed catalysts such as

Amberlyst 15, Nafion NR50 and p-TsOH, all achieved the formation of succinic acid as the main product and while maleic acid was only obtained with yields of up to 11%.[63]

Alonso-Fagúndez et al.[61] reported the catalytic activity of a poly-(styrene sulphonic acid) catalyst for furfural oxidation with H_2O_2 to obtain up to 34% yield of maleic acid. Utilizing a titanium-silicate (TS-1) molecular sieve catalyst, a yield of 78% for maleic acid was reported, the highest to date, from furfural oxidation at 50 °C with H_2O_2 oxidant although leaching of the Ti active sites was detected. In a later related study, leaching of the Ti active sites was mitigated with the use of γ-valerolactone.[64] The results of these studies demonstrate the need for a chemically stable, highly active and reusable catalyst exists to avert issues of low conversion or yield, long reaction times and catalyst leaching without the use of additives.

Progressive developments have been achieved in the oxidation of furfural to maleic acid and maleic anhydride with different catalysts. Some of these catalysts include mixed metal oxides, molecular sieves, carbonaceous materials and resins. However, the main drawback with these catalysts is low selectivity, and other related issues are low feed volumes and high reaction temperatures (for gas-phase oxidations), low catalyst stability (leaching of active sites) and recyclability. It is thus highly desirable to design an active catalyst that could improve the yield and selectivity of maleic acid and maleic anhydride in the oxidation of furfural under very mild conditions. Mostly, this catalyst should give high selectivity toward maleic acid formation under liquid phase oxidation which can be easily transformed to maleic anhydride.

Table 2-1: Comparison of state-of-the-art catalytic systems for furfural and 5-hydroxymethylfurfural oxidation to produce maleic acid and maleic anhydride.

Entry	Catalyst	Reaction conditions					Catalytic results			Ref
		Substrate (Oxidant)	Catalytic System	Solvent / Feed volume	Temp. /°C	Time /h	Product	X /%	Y /%	
1	VO_x/Al_2O_3	FFR (O_2)	Fixed-bed	10%	320	-	MAN	100	73	[53]
2	$V_2O_5/\gamma\text{-}Al_2O_3$	FFR (O_2)	Fixed-bed	20%	300	-	MAN	100	75	[54]
3	Mo_4VO_{14}	FFR (O_2)	Batch	AcOH	100	4	MA+MAN	93	65	[55]
4	Plate VPO	FFR (O_2)	Continuous flow	10%	360	-	MAN	100	90	[56]
5	FeT(p-Br)PPCl/SBA-15	FFR (O_2)	Batch	H_2O	100	6	MA	76	56	[57]
6	$VO\text{-}NH_2\text{-}GO$	FFR (O_2)	Batch	AcOH	90	8	MA+MAN	82	62	[62]
7	TS-1	FFR (H_2O_2)	Batch	H_2O	50	24	MA	100	78	[61]
8	$KBr/g\text{-}C_3N_4$	FFR (H_2O_2)	Batch	H_2O	100	3	MA	>99	70.4	[74]
9	N-doped carbon	FFR (H_2O_2)	Batch	H_2O	80	5	MA	100	61	[75]
10	TS-1	FFR (H_2O_2)	Batch	AcOH	80	4	MA	100	60	[76]
11	Cu-Pd@HPC	FFR (H_2O_2)	Batch	H_2O	50	4	MA	100	97.8	[77]
12	$H_5PV_2Mo_{10}O_{40}$	HMF (O_2)	Batch	AcOH	90	4	MA+MAN	100	64	[71]
13	V_2O_5	HMF (O_2)	Batch	AcOH	100	4	MA+MAN	99	78	[67]
14	$VO\text{-}NH_2\text{-}GO$	HMF (O_2)	Batch	AcOH	90	4	MA+MAN	99.8	95.3	[62]
15	Ru@AC	HMF (H_2O_2)	Batch	H_2O	75	6	FDCA	100	91.3	[73]

Symbol: FFR = furfural, HMF = 5-hydroxymethylfurfural, MA = maleic acid, MAN = maleic anhydride, NC = not communicated, X= conversion, Y = yield, S = selectivity towards maleic acid.

2.4.2 Oxidation of 5-hydroxymethylfurfural to maleic anhydride

The oxidation of 5-hydroxymethylfurfural can be carried out in the liquid-phase to produce maleic anhydride via C-C bond cleavage of the hydroxymethyl group in 5-hydroxymethylfurfural.[65-68] However, this route is deemed less attractive due to the fact that 5-hydroxymethylfurfural is currently only produced at lab-scale compared to furfural, which has an established industrial production line.[69,70] There have been very few reports on the oxidation of HMF with molecular O_2 producing maleic anhydride as the product, however maleic acid is almost always found in the reaction mixture due to the inevitable and easy hydrolysis of maleic anhydride to maleic acid under elevated temperatures by the in-situ generated water and/or moisture in the solvent. Further, the majority of literature reports on the aerobic oxidation 5-hydroxymethylfurfural to maleic anhydride using O_2 are focused on vanadium-based catalysts.

Li and Zhang et al.[67] reported on the conversion of 5-hydroxymethylfurfural to maleic anhydride using vanadium-based heterogeneous catalysts. By employing an O_2 pressure of 10 bar and a temperature of 100 °C, after 4 h reaction time a combined yield of maleic anhydride and maleic acid of 78% was achieved over bulk V_2O_5 catalyst in acetic acid solvent. The ratio of maleic anhydride to maleic acid from the products was determined to be 2:1. By dispersing the V_2O_5 over a traditional SiO_2 support a comparable yield just below 75% was obtained with the supported catalyst showing better recyclability. However, both the bulk V_2O_5 and V_2O_5/SiO_2 catalysts suffered from a very small degree of leaching of the vanadia active sites. The authors also demonstrated the conversion of 5-hydroxymethylfurfural to maleic anhydride and maleic acid over vanadium phosphorous oxide (VPO), ($VOHPO_4$ and $(VO)_2P_2O_7$) catalysts with comparable yields of 78-79%. Du et al.[68] carried out the oxidation of 5-hydroxymethylfurfural with molecular oxygen (1 MPa)

using different transition metal oxide catalysts. After 4 h reaction time in acetonitrile solvent the highest yield of maleic anhydride of 52% was achieved with a homogeneous $VO(acac)_2$ catalyst. While employing heteropolyacid catalysts, Lan et al.[71] demonstrated a combined total yield of maleic acid and maleic anhydride of 64% under optimized reaction conditions also using 1 MPa molecular oxygen oxidant. These catalysts suffered from a lack of selectivity as several other products such as 2,5-diformylfuran and 2,5-furandicarboxylic acid were detected in the reaction mixture. Lv et al.[62] reported on the use of a catalyst system based on vanadium-oxo immobilized on a Schiff base modified graphene oxide support ($VO-NH_2-GO$) for the oxidation of 5-hydroxymethylfurfural to maleic anhydride. A total combined yield of maleic anhydride and maleic acid reaching 95.3% was achieved in acetic acid solvent at 90 °C after 4 h under 20 bar O_2. The ratio of maleic acid to maleic anhydride under this catalyst system was 2.5:1 with 2,5-formylfuran the only side-product of the reaction.

In another more recent study by the same group, the use of vanadium oxide nanosheets fabricated onto exfoliated graphene oxide support for 5-hydroxymethylfurfural oxidation to maleic anhydride led to a total yield of 90.9% (maleic acid:maleic anhydride = 2.8:1) also in acetic acid solvent at 90 °C after 4 h and under 20 bar O_2.[58] The researchers also demonstrated the transformation of 5-hydroxymethylfurfural to maleic anhydride and maleic acid over V_2O_5 supported on SiO_2 and activated-carbon (AC) achieving yields of 74.5% and 62.3% for the V_2O_5/SiO_2 and V_2O_5/AC catalysts, respectively. Tirsoaga et al.[72] also recently reported on $Fe_3O_4@SiO_2$-based multifunctional catalyst for use in 5-hydroxymethylfurfural oxidation with molecular O_2. Utilizing water as a solvent, at 110 °C and under 10 bar O_2, a 72% selectivity towards maleic acid was achieved with a $Fe_3O_4@SiO_2-MnO_x$ catalysts after 8 h. However, 5-hydroxymethylfurfural conversion was

very low at 5% and was only slightly improved when an amino group functionalized (Fe_3O_4@SiO_2-NH_2) catalyst was employed instead with selectivity towards maleic acid reaching 85%. Following an extensive literature search only one study was found for the 5-hydroxymethylfurfural oxidation with H_2O_2 oxidant. Chen et al.[73] employed a ruthenium supported on activated-carbon catalyst for the H_2O_2-mediated oxidation of 5-hydroxymethylfurfural in water. However, 5-formyl-2-furoic acid and 2,5-furandicarboxylic acid were obtained (with excellent yields) as the products at short (1 h) and longer (6 h) reaction times, respectively. In summary, the catalysts employed for the oxidation of 5-hydroxymethylfurfural to maleic anhydride (and maleic acid) depend on the use of elevated reaction temperatures (≥ 90 °C) for good yields but otherwise are susceptible to low selectivity, low 5-hydroxymethylfurfural conversion or catalyst recyclability. Thus, from a sustainable chemistry viewpoint, there exists the need to explore the conversion of 5-hydroxymethylfurfural to maleic anhydride and maleic acid under mild reaction conditions.

2.5 Factors controlling activity and selectivity in maleic acid synthesis

Selective liquid-phase oxidation reactions with either O_2 or H_2O_2 involves the formation of reactive oxygen species (ROS) or free radicals such as $OH^•$, $HO_2^•$ and $O_2^{•-}$ which can lead to either partial or total over-oxidation of the target product, thus formation of unwanted side-products which compromises selectivity.[59] The adverse effect of free radicals can be mitigated with the use of scavenger additives or designing catalysts with the active sites capable of suppressing the non-selective ROS in order to improve products selectivity. In addition to these effects, other factors such as mass (and heat) transfer limitations, surface reaction of adsorbates, hydrolysis and structural deformation of the catalyst active sites, catalyst deactivation through leaching, fouling, coking and humin formation can impart on the overall catalytic activity.[78-81]

To understand the structure-activity relationship and thus the rational design for an effective catalyst for maleic acid synthesis, several researchers have focused on studying the furfural oxidation reaction mechanism.[82-85] For this purpose, the understanding of the activation/desorption processes at the molecular level i.e. at the C=O, C–O bonds and the furan ring and thus the role of the catalyst active sites is fundamental to elucidating a plausible reaction mechanism. Lan et al. [82] studied the mechanism for furfural oxidation to maleic anhydride with O_2 over a $H_5PV_2MoO_{40}$ heteropolyacid catalyst in the liquid-phase (acetonitrile/acetic acid solvent mixture). A 54% maleic anhydride yield was obtained with the use of a $Cu(CF_3SO_3)_2$ Lewis acid additive. The proposed most plausible mechanism (**Scheme 2-5**) first involves the abstraction of hydrogen by O_2 or the catalyst to form a furfural radical (**1**) which undergoes electron transfer by $H_5PV_2Mo_{10}O_{40}$ to generate a furfural cation (**2**). The cation then reacts with water to form 5-hydroxyfurfural (**3**) which undergoes a 1,4-rearrangement to intermediate **4**. The intermediate then undergoes decarbonylation and electron transfer to form a 2-(5H)-furanone cation (**5**) which undergoes 1,4-rearrangement and reacts with water to form 5-hydroxy-2-(5H)-furanone (**6**). 5-Hydroxy-2-(5H)-furanone is then oxidized to form maleic anhydride.

The $Cu(CF_3SO_3)_2$ Lewis acid additive was reported to improve the yield of maleic anhydride by accelerating the electron transfer rates via linkage to the redox metal ions, thus enhancing their redox potential. In addition, the promotional effect of the Lewis acid was also attributed to trapping the generated organic radical intermediates from the competing polymerization reaction which leads to the formation of resins and humins.
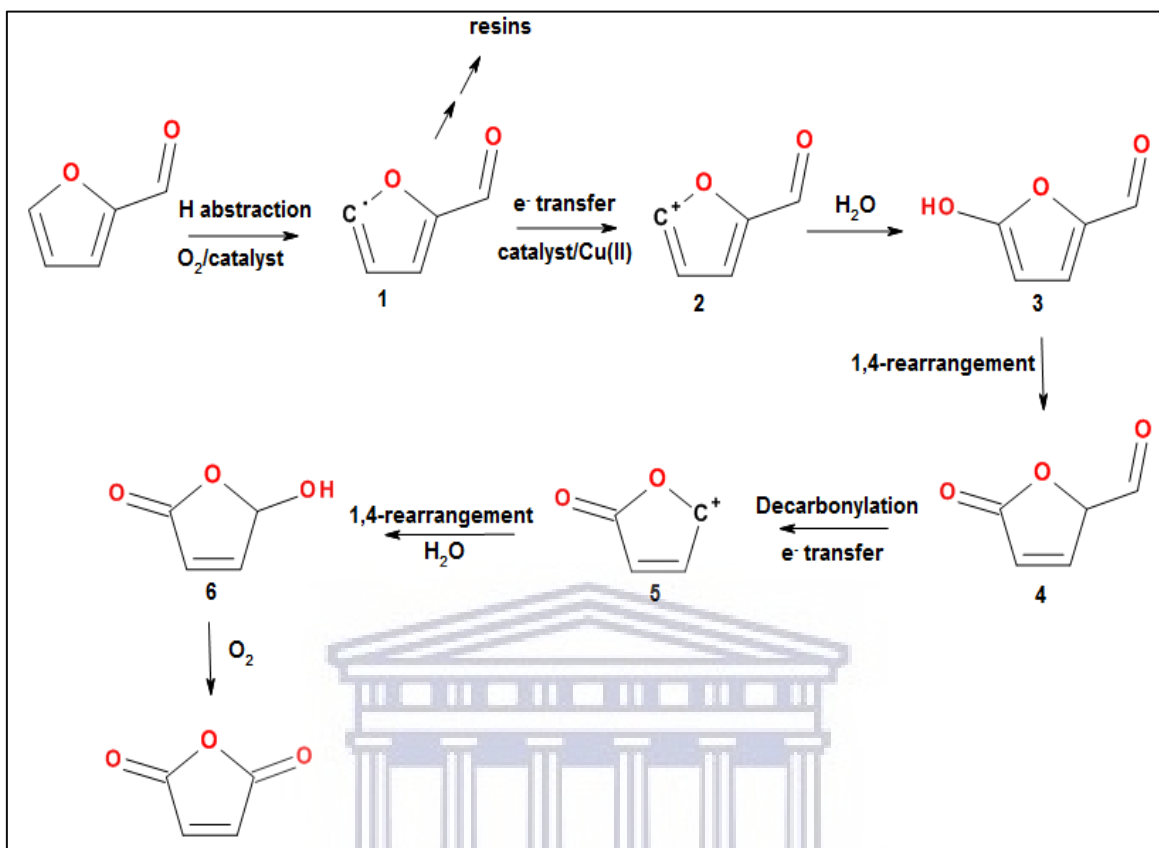
Scheme 2-5: Plausible reaction mechanism for furfural oxidation to maleic anhydride with O_2 over $H_5PV_2Mo_{10}O_{40}$ and $Cu(CF_3SO_3)_2$. Adopted from [82].

A second minor pathway which proceeds via the formation of 2-(5H)-furanone was also reported. The mechanism involves the hydrogen abstraction from the 1-position (aldehyde functional group) instead of the 5-position as shown in **Scheme 2-6**. The hydrogen abstraction is followed by decarbonylation and electron transfer to generate a furan cation (**2**) which then reacts with water to form 2-hydroxyfuran (**3**). 2-hydroxyfuran then undergoes a 1,4-rearrangement forming 2-(5H)-furanone (**4**). The generated 2-(5H)-furanone then undergoes hydrogen abstraction and electron transfer to generate a 2-(5H)-furanone cation (**5**). The reaction then proceeds as in **Scheme 2-5** to form maleic anhydride. Interestingly, maleic acid was always produced during the reactions performed without the Cu^{2+} additive and during the reactions with other additives. It was discovered

that the Cu^{2+} additive led to the decomposition of all the produced maleic acid and to some extent maleic anhydride as well.
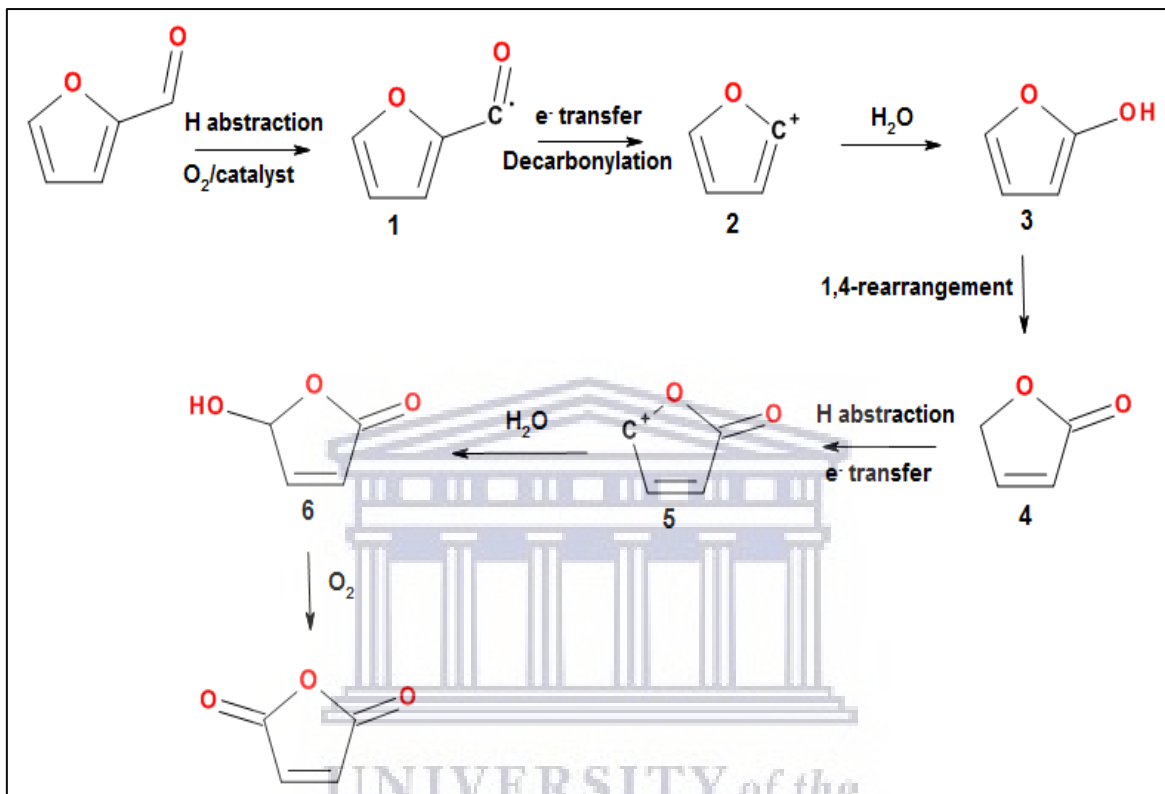
Scheme 2-6: A minor reaction pathway for furfural oxidation to maleic anhydride via 2(5H)-furanone over $H_5PV_2Mo_{10}O_{40}$ and $Cu(CF_3SO_3)_2$. Adopted from [83].

Guo and Yin [83] in 2011 reported a 34.5% yield of maleic acid with 68.6% selectivity from furfural oxidation in a biphasic solvent system (water/tetrachloroethane mixture) using phosphomolybdic acid catalyst. The proposed mechanism therein involves a two-step furan ring-opening and decarboxylation as shown in **Scheme 2-7**. The reaction starts with hydrogen abstraction from the 5-position by the catalyst or O_2 to generate a furfural radical (**1**) followed by electron transfer to the phosphomolybdic catalyst forming a furfural cation (**2**). The cation then reacts with water to form 5-hydroxyfurfural (**3**) which then undergoes a 1,4-rearrangement to intermediate **4**. The intermediate is thereafter hydrolysed

undergoing furan ring-opening to form intermediate **5** which is then oxidized to produce maleic acid.
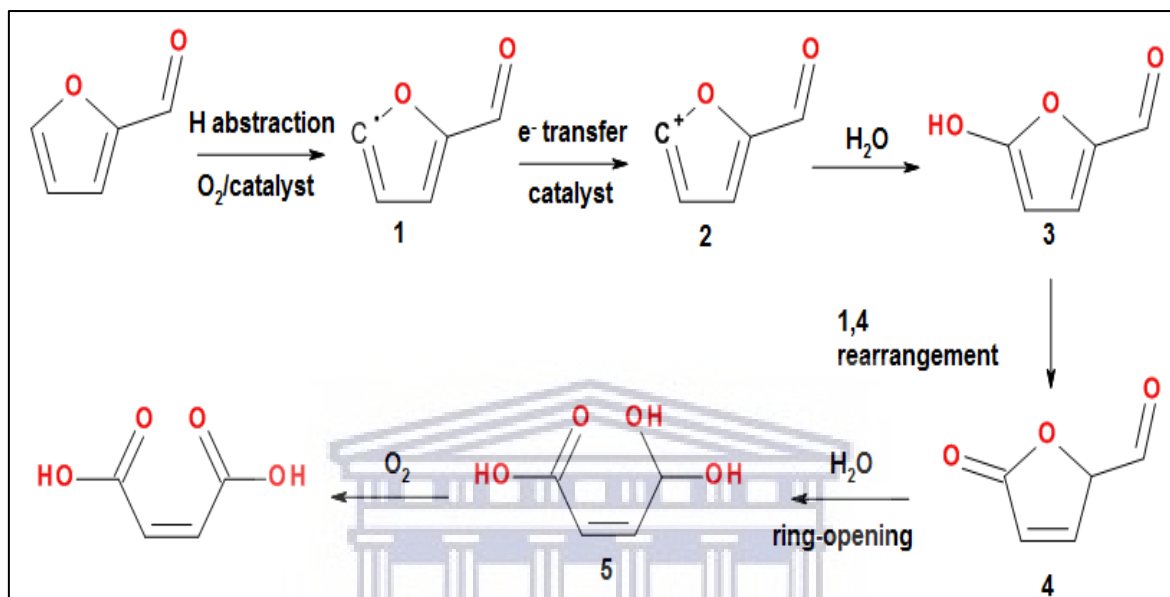
Scheme 2-7: Proposed reaction mechanism for furfural oxidation to maleic acid with O_2 over $H_5PMo_{10}O_{40}$. Adopted from [83].

The phosphomolybdic acid catalyst was reported to facilitate the electron transfer from the furfural radical due to its higher redox potential compared to other heteropolyacid catalysts explored. The water/tetrachloroethane solvent mixture was also reported to assist the oxidation process with oxidation occurring in the aqueous phase while the organic phase served as a furfural reservoir minimizing the polymerization of furfural. Thus, the gradual mass transfer of furfural from the organic phase was driven by its depletion in the aqueous phase. Choudhary et al.[84] also studied the oxidation of furfural with H_2O_2 oxidant over Amberlyst-15 acid catalyst in H_2O solvent. The catalyst produced succinic acid (74.2% yield) as the main product with 11.0% maleic acid being produced and the authors proposed a mechanism for the production of both acids (**Scheme 2-8**).
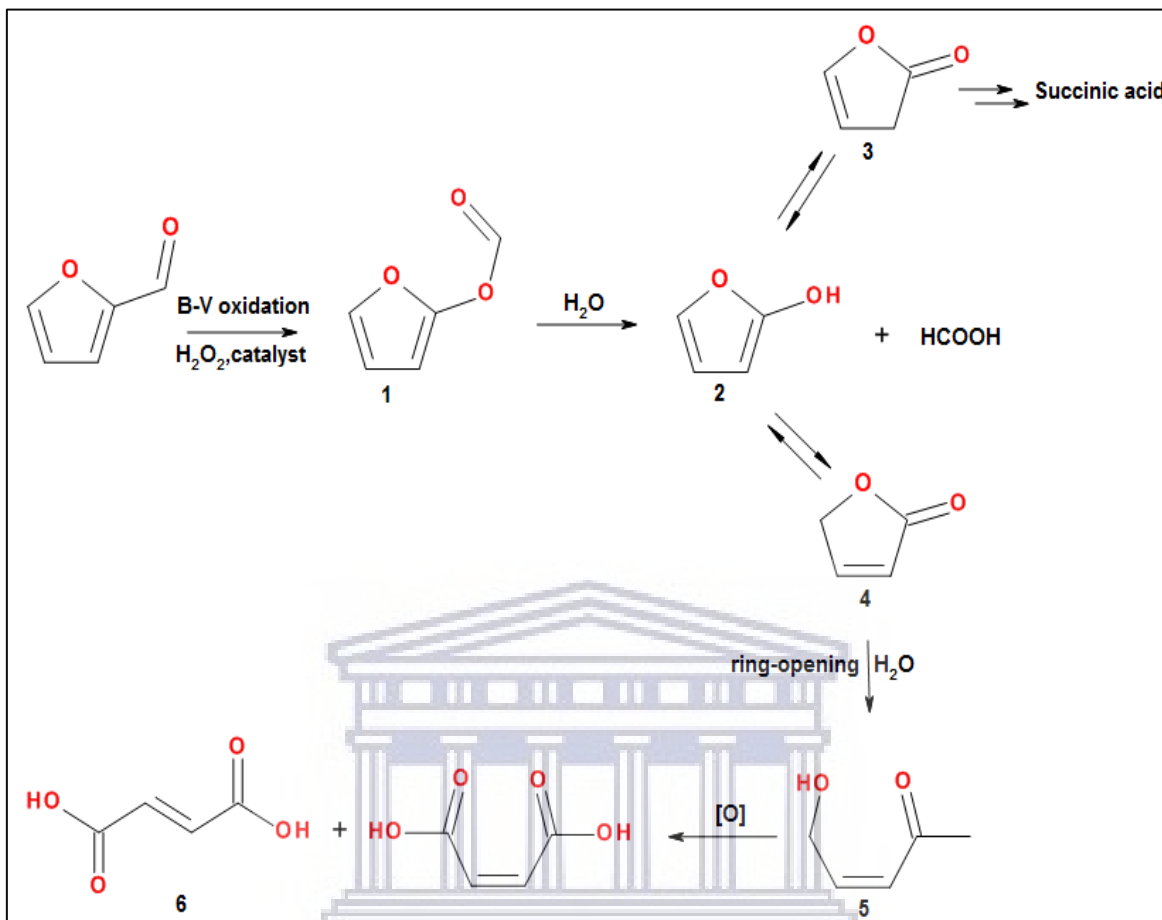
Scheme 2-8: Proposed reaction mechanism for maleic acid production from furfural via Baeyer-Villager oxidation with H_2O_2 over Amberlyst-15. Adopted from [84].

The reaction proceeds via the Baeyer-Villager (B-V) oxidation of furfural over the catalyst to generate 2-furanol formate (**1**) which undergoes rapid hydrolysis to produce 2-furanol and formic acid. The 2-furanol intermediate is in equilibrium with two tautomeric isomers, 2-(3H)-furanone (**3**) and 2-(5H)-furanone (**4**) with the former leading to the formation of succinic acid by further oxidation. 2-(5H)-furanone leads to maleic acid by undergoing hydrolysis and furan ring-opening to form intermediate **5** which is further oxidized to produce maleic acid and its isomer, fumaric acid (**6**). The high selectivity of the catalyst towards SA was attributed to the strongly acidic $–SO_3H$ functional group of the catalyst. In addition, the π-π interaction between the tolyl ring of the catalyst and the furan ring was

reported to favour a suitable catalyst-substrate confirmation via a five-membered ring intermediate involving the sulphur atom thus leading to the formation of the 2-(3H)-furanone (**3**) intermediate.[63] Thus, suggesting a less acidic functional group than –SO$_3$H and/or a different catalyst-substrate confirmation results in the observed low yield of maleic acid through the 2-(5H)-furanone (**4**) intermediate. Furthermore, the catalyst was shown to improve the efficiency of H$_2$O$_2$ by enhancing its decomposition to generate O$_2$.

Another plausible mechanism for furfural oxidation with H$_2$O$_2$ oxidant also involving the Baeyer-Villager oxidation was proposed by Alonso-Fagúndez et al.[61] A 78% yield of maleic acid was obtained after 24 hours over a titanium silicate (TS-1) zeolite catalyst. The proposed mechanism showed in **Scheme 2-9** begins with the epoxidation of the furan ring double-bond with less steric hindrance (i.e. at the 4-position) to a furfural-epoxide (**1**) which undergoes rapid rearrangement and ring-opening to generate intermediate **2**. The intermediate then undergoes Baeyer-Villager oxidation with H$_2$O$_2$ to generate intermediate **3** which in-turn is rapidly hydrolysed to β-formylacrylic acid (**4**) while generating formic acid in the process. The β-formylacrylic acid is in equilibrium with 5-hydroxy-2-(5H)-furanone (**5**) with the equilibrium strongly shifted towards hydroxyfuranone. Both β-formylacrylic acid and hydroxyfuranone are further oxidized to produce maleic acid. The TS-1 catalyst employed possessed the largest possible incorporation of Ti within the silicate, thus the catalyst possessed extraframework Ti species which is present as anatase TiO$_2$ in octahedral geometry located at the external zeolite surface and Ti oxide nanodomains occluded within the channels and cavities of the zeolite. This is in addition to the isolated tetrahedral Ti(IV) Lewis acid sites which are attributed to the high selectivity of the catalyst towards maleic acid.
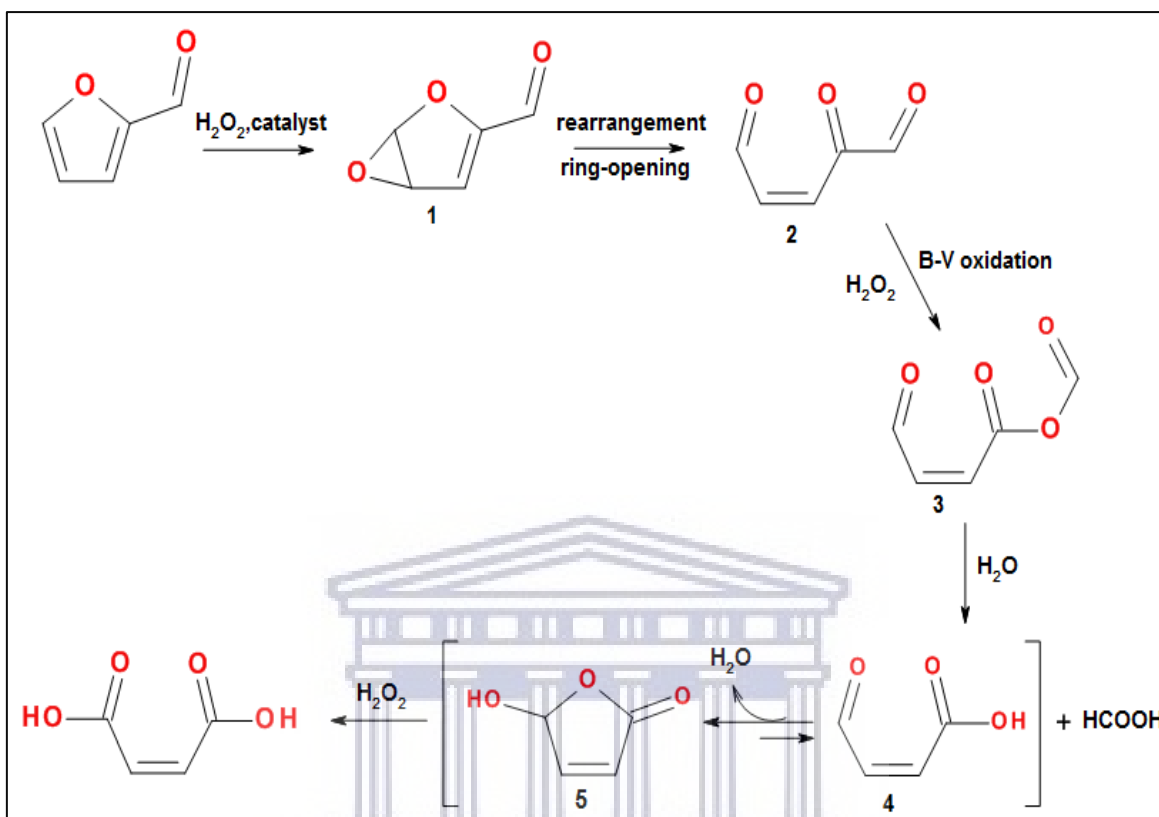
Scheme 2-9: Proposed reaction mechanism for maleic acid production from furfural via epoxidation and Baeyer-Villager oxidation with H_2O_2 over TS-1. Adopted from [61].

A second possible mechanism was proposed by Alonso-Fagúndez's group over the TS-1 catalyst which proceeds via the formation of 2-furoic acid (**Scheme 2-10**). First, furfural is oxidised to form 2-furoic acid (**2**) which undergoes decarbonylation to generate furan (**3**) and formic acid. Furan then undergoes epoxidation to form a furan-epoxide **4** which undergoes rapid rearrangement and ring-opening to generate intermediate **5**. Oxidation of intermediate **5** to produces β-formylacrylic acid (**6**) which is in equilibrium with 5-hydroxy-2-(5H)-furanone (**7**) with the equilibrium again strongly shifted towards hydroxyfuranone. Both β-formylacrylic acid and hydroxyfuranone are subsequently oxidized to produce maleic acid.
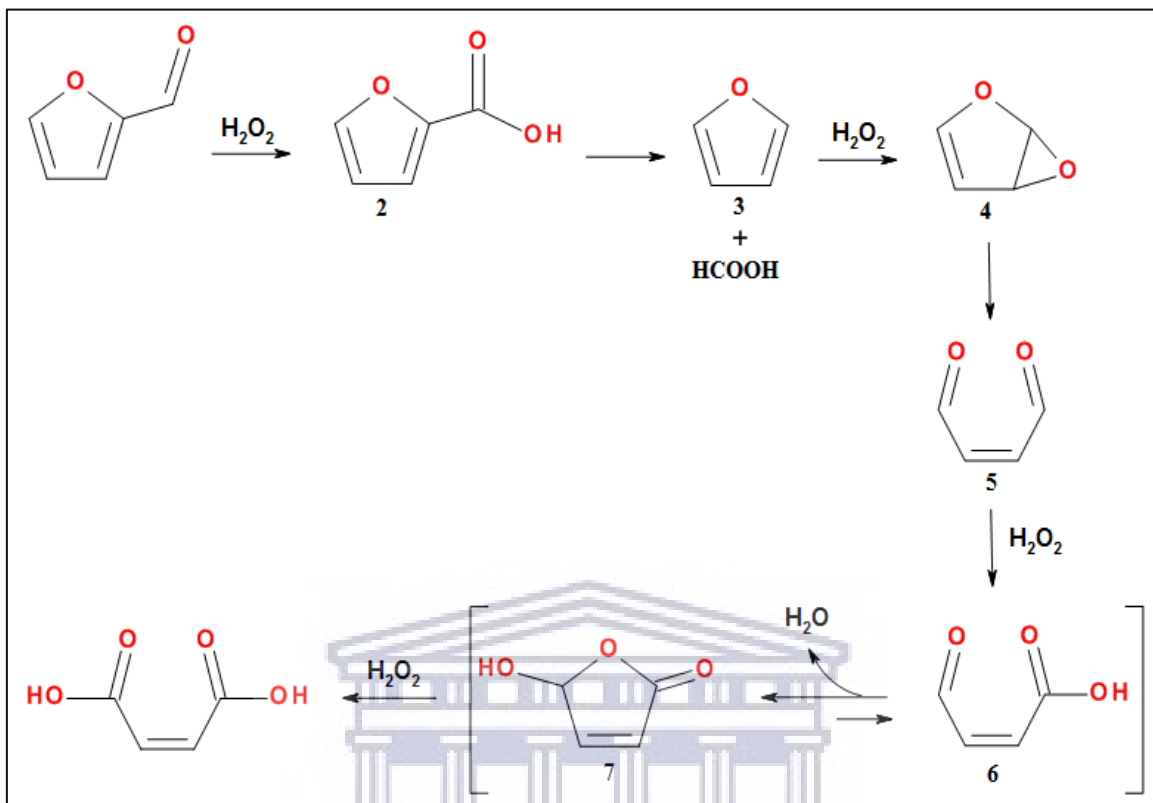
Scheme 2-10: Proposed reaction mechanism for maleic acid synthesis from furfural via the formation of 2-furoic acid with H_2O_2 over TS-1. Adopted from [61].

Alba-Rubio et al.[85] investigated the role of these extraframework Ti species in furfural oxidation with H_2O_2 and uncovered that the extraframework Ti species enhance decomposition of H_2O_2 and the Ti oxide nanodomains are more active for the oxidation of hydroxyfuranone to maleic acid than the tetrahedral Ti(IV) Lewis acid sites hence the high selectivity towards maleic acid was observed with the TS-1 catalyst. It should be noted that the TS-1 catalyst suffered serious leaching of the Ti active sites. However, this issue was mitigated by the use of a γ-valerolactone (GVL) and H_2O solvent mixture with the catalyst retaining its activity after 17 catalytic runs.[64] The use of GVL was reported to prevent the deposition of the by-products on the surface and within the channels and cavities of the zeolite catalyst while also improving the maleic acid yield and its separation from the reaction mixture.

Efforts have also been made to uncover the reaction mechanism and the role of catalyst active sites for the oxidation of 5-hydroxymethylfurfural to maleic acid and maleic anhydride. However, studies pertaining to this are extremely limited to vanadium-based catalysts proving to be the most common and effective for the formation of maleic anhydride and no consensus has yet been reached regarding the reaction mechanism for 5-hydroxymethylfurfural oxidation to maleic anhydride. The oxidation of 5-hydroxymethylfurfural to maleic anhydride involves a C–C bond cleavage and the removal of two carbon atoms (compared to one carbon atom for furfural). Du et al.[68] reported the oxidation 5-hydroxymethylfurfural to maleic anhydride with molecular O_2 achieving a 52% yield for both maleic anhydride and maleic acid in acetonitrile solvent using a $VO(acac)_2$ homogenous catalyst. Their proposed reaction mechanism (**Scheme 2-11**) was partially based on theoretical calculations and takes place at the hydroxymethyl functional group with the aldehyde group proving to be stable in an oxygen atmosphere.
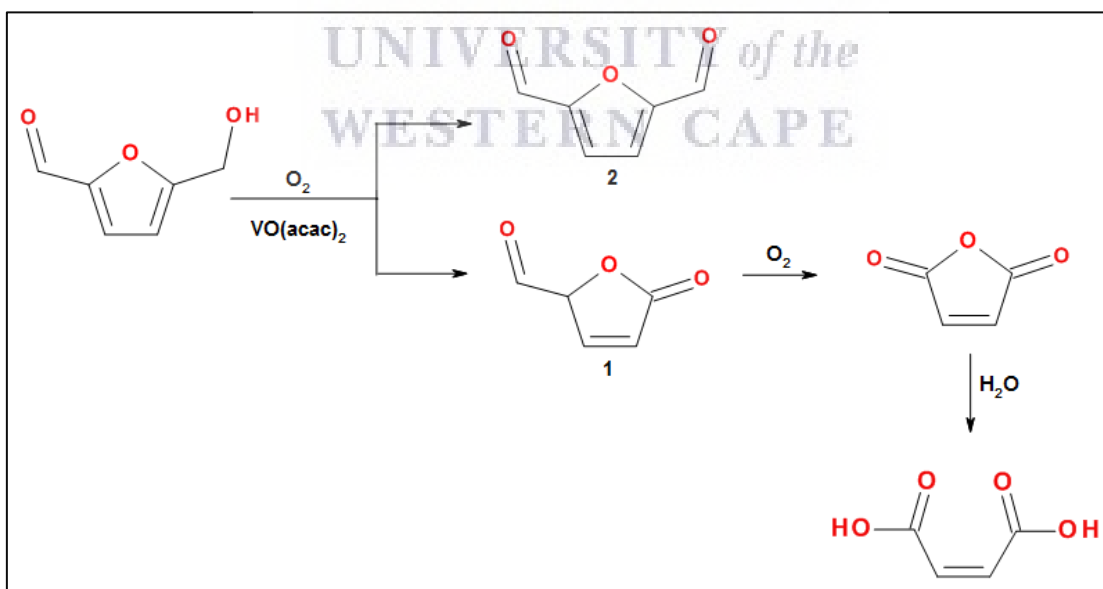
Scheme 2-11: Reaction pathway for maleic acid production from 5-hydroxymethylfurfural with O_2 using $VO(acac)_2$. Adopted from [68].

The reaction proceeds via C–C bond cleavage of the hydroxymethyl and oxidation generating intermediate **1** and formic acid. Intermediate **1** is then further oxidized with O_2 to form maleic anhydride and CO_2. The rapid and easy hydrolysis of maleic anhydride then generates maleic acid. Oxidation of the alcohol functional group also takes place to generate 2,5-diformylfuran (**2**). Unfortunately, the exact role of the V^{5+}/V^{4+} redox centres in the reaction mechanism was not investigated. Lan et al.[71] studied the production of maleic anhydride from 5-hydroxymethylfurfural with O_2 over heteropolyacid catalysts and achieved a yield of maleic anhydride and maleic acid of 64% with a vanadium-substituted heteropolyacid catalyst ($H_5PV_2Mo_{10}O_{40}$). A more elaborate mechanism based on the same C–C bond cleavage route by Du et al. was elucidated as shown in **Scheme 2-12**.
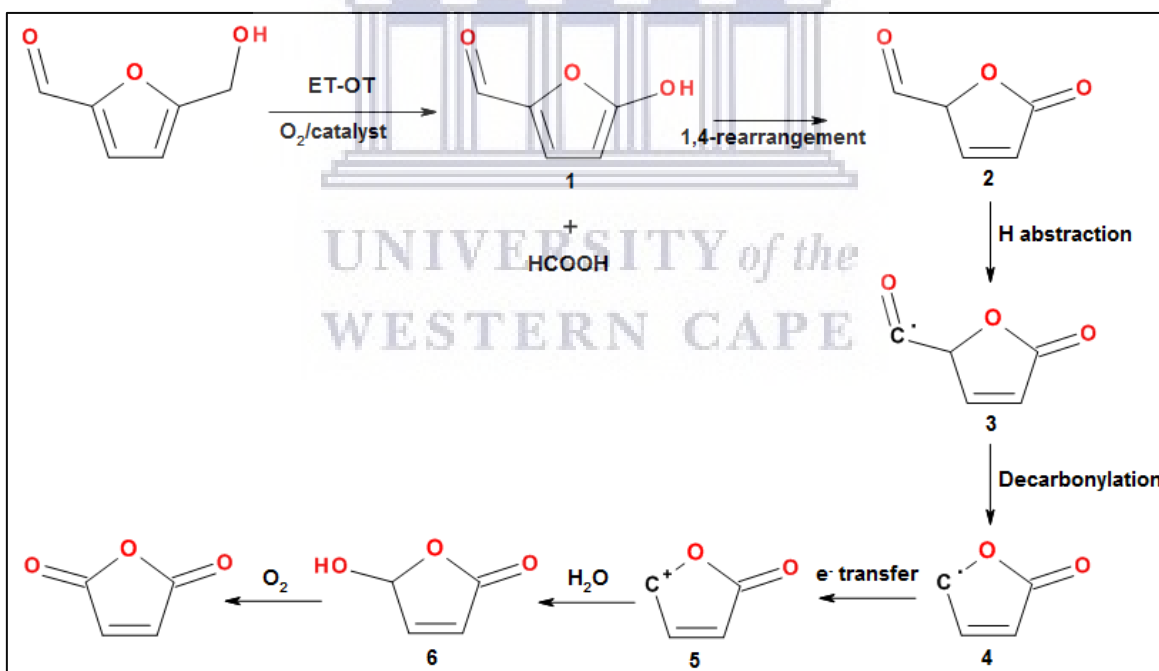
Scheme 2-12: Plausible reaction mechanism for 5-hydroxymethylfurfural oxidation to maleic anhydride with O_2 over $H_5PV_2Mo_{10}O_{40}$. Adopted from [71].

Firstly, C–C bond cleavage by $H_5PV_2Mo_{10}O_{40}$ takes place between the hydroxymethyl group and the furan ring via an electron transfer and oxygen transfer (ET-OT) reaction

mechanism producing intermediate **1** and formaldehyde which is readily oxidised to formic acid. Intermediate **1** then undergoes a 1,4-rearrangement to intermediate **2** which goes through hydrogen abstraction by O_2 or $H_5PV_2Mo_{10}O_{40}$ to form intermediate **3**. Intermediate **3** then undergoes decarbonylation to generate Intermediate **4** and electron transfer takes place to form a 2-(5H)-furanone cation (**5**). Hydrolysis of the 2-(5H)-furanone cation generates 5-hydroxy-2-(5H)-furanone (**6**) which then yields maleic anhydride by further oxidation. Maleic acid is then formed by hydrolysis of maleic anhydride. The higher activity of $H_5PV_2Mo_{10}O_{40}$ was attributed to its well-known ability to activate dioxygen as well as its better ability to facilitate the C–C bond cleavage (compared to other heteropolyacids studied) due to the easy exchange of the V^{5+}/V^{4+} redox centres.

In summary, the results of these investigations indicate that for improved selectivity towards maleic acid production from furfural and 5-hydroxymethylfurfural the following key points must be considered during catalyst design;

➢ Moderate to strong Lewis acid sites must be present as they are critical for accelerating the electron transfer process on their own or by linkage to the redox metal ions present on the catalyst.

➢ The Lewis acid sites must also be present for trapping the generated organic radicals, thus eliminating the formation of resins/humins.

➢ The presence of easily exchangeable metal redox centres is a crucial requirement for facilitating the C–C bond cleavage.

➢ The use of a biphasic solvent is also important as this prevents deposition of the by-products on the catalyst surface and also for easy product separation.

➢ The choice of solvent is also important in the case of 5-hydroxymethylfurfural oxidation where an environment that drives the C-C bond cleavage of the hydroxymethyl group and stabilizes the aldehyde group is important in order to prevent the synthesis of 2,5-furandicarboxylic acid (FDCA), 5-hydroxymethyl-2- furancarboxylic acid (HMFCA) and 5-formyl-2-furancarboxylic acid (FFCA).

2.6 Design of active bifunctional redox-acidic catalysts for furfural oxidation

Transition metal oxides (TMOs) have for long been applied as catalysts because they provide featured active sites to adsorb molecules for chemical transformations to targeted products. Mixed metal oxides (MMOs), tailored by doping or dispersing a metal oxide into/onto a metal oxide matrix or heterostructuring two or more metal oxides have attracted immense catalytic interest because they generate new intrinsic surface states or electronic structures, influence chemical nature (redox and acid-base character) and the electron density of active sites. All these factors affect the products distribution and yield in catalytic oxidation reactions.

The concept of rational design has made is possible develop catalytically active MMOs with desirable physicochemical properties for a specific reaction. For instance, by dispersing a redox-active metal oxide possessing multiple oxidation states onto a reducible metal oxide support a catalyst highly active for CO oxidation can be obtained (e.g. CuO_x/CeO_2).[86] Wang et al.[87] demonstrated the rational design of a highly efficient mixed Fe-Mn oxide catalyst by exploiting the acidity of Fe_2O_3 and the redox properties of MnO_2. By varying the amount of each oxide in the MMO, the reducibility and surface acidity of the catalyst were optimized to afford a highly active catalyst for the oxidation of chlorobenzene. Thus through rational design, highly active MMOs can be harnessed with various physicochemical properties such as morphology, size, crystal structure,

surface/structural defects, distinct active facets, electronic states, acid-base character and adsorption-desorption ability towards reactants.[88-91] All these properties can exert a profound influence on the catalytic activity of MMOs and by fundamentally understanding the influence of each and the interplay between them , which is often challenging, can lead to the development of catalytic materials with desirable cost, activity, selectivity and stability.[88]

In addition, the metal-support interactions (MSI) need to be considered when designing MMOs as they can also affect catalytic performance by altering the stability, morphology, reducibility of the metal oxide support, inducing lattice strains, enabling spill over effects and by modifying the electronic structure via charge transfer processes.[92,93] Moreover, other synergistic effects such as interfacial reactivity of the metal oxides, presence of defects , reducibility of the MMOs compared to the individual ones and the interplay between interfacial redox-pairs of the two metal oxides also need to be considered and understood. Thus, by fine-tuning one or a combination of these factors it is possible to control the MSI and rationally design a catalyst with superior performance by optimising the material properties that determine activity, selectivity and stability.[94] In this context, the work herein seeks to develop SnO_2-based MMOs through heterostructuring with active, cheap and abundant metal oxides which are discussed below.

2.6.1 Tin based catalysts

SnO_2 on its own has shown poor oxidation activity in the liquid-phase reaction due to its low or slow redox reactivity. However, the mixing of SnO_2 with other transition metal oxide or using it as a catalyst support has been shown to be very effective for certain oxidation reactions such as the oxidation of methane[95,96], carbon monoxide[97,98], both CO and CH_4[99,100], organic molecules such as methanol, ethanol, formaldehyde and toluene.[100-103]

Although SnO_2-based catalysts are widely used for the oxidation of fossil-fuel derived compounds, a number of SnO_2-based catalysts have been used in the conversion of lignocellulose and model compounds to produce furfural and HMF.[104-107] The hydrolysis of lignocellulose and model compounds with SnO_2-based catalysts in these reactions is made possible by the effective Lewis acidic active sites of SnO_2. For instance, Choudary et al.[107] reported the single-pot dehydration of xylose to furfural with a modified Sn-beta zeolite Lewis acid catalyst preceded by isomerization to xylulose. In the presence of an HCl Bronsted acid catalyst, a 14.3% yield of furfural was obtained at 110 °C in an aqueous solvent with 83.9% conversion. Moliner et al.[108,109] also demonstrated the synthesis of 5-hydroxymethylfurfural from glucose via fructose with the Sn-beta zeolite catalyst achieving up to 70% selectivity toward 5-hydroxymethylfurfural at 110 °C with 79% conversion. The critical role of the Lewis acidity of SnO_2 was invesitigated by Lin et al.[101] with a SnO_2-Co_3O_4/C biochar catalyst for synthesis of furfural by corncob hydrolysis. The catalyst with the highest acidity (low Sn content) afforded the best catalytic performance with a corncob conversion of 60.4% and 24.4% furfural yield. Behera and Parida[110] reported a tin promoted vanadium phosphate (Sn-VPO) catalyst for the one-pot synthesis of 5-hydroxymethylfurfural from glucose achieving a 74% yield. The presence of both Lewis and Bronsted acids sites was determined to be crucial for the improved selectivity toward 5-hydroxymethylfurfural with Lewis acid sites facilitating the isomerization of glucose to fructose and the Bronsted acids sites the conversion of fructose to 5-hydroxymethylfurfural. SnO_2-based catalysts have also been used for the acetalization of bio-glycerol into industrially useful chemicals such glycerol acetals and ketals, which are extensively used as effective fuel additives, bases, protecting agents, scents, fragrance and flavours in several industries. In particular, WO_3/SnO_2, MoO_3/SnO_2, SO_4^{2-}/SnO_2 catalysts applied for this reaction were found to possess both Lewis and

Bronsted acids sites with SO_4^{2-}/SnO_2 displaying super acid strength.[111,112] MoO_3/SnO_2 and SO_4^{2-}/SnO_2 were reported to be effective for the acetalization of glycerol with acetone and furfural to achieve 98-99% conversions.

2.6.2 Vanadium based catalysts

Among the many transition metals utilized as catalysts in heterogeneous catalysis, vanadium is one of the most important as it forms a crucial component of many catalyst systems due to its high activity. This high activity is attributed to the strong redox character of vanadium constituting easily exchangeable multiple oxidation states, $V^{5+}/V^{4+}/V^{3+}$, which affords different active phases such as monovanadate, metavanadate, pyrovanadate and orthovanadate.[113,114] Consequent to its high activity, vanadium-based compounds have found extensive applications in many industrially important applications including, but not limited to; the reduction of NO, oxidation of SO_2 to SO_3, the oxidation of C_2-C_6 hydrocarbons, oxidation of alcohols, ketones and aldehydes, hydrogenation of CO, CO_2 and substituted hydrocarbons.[115-118] The structure and redox properties of the surface VO_x species on these catalysts is strongly dependent on the metal oxide used as a support and the vanadium loading. The acid-base makeup of the metal oxide support not only influences the dispersion and nature of VO_x species through modifications of the environment and coordination of vanadium species, but also affects the overall redox and acid-base properties and consequently the catalytic activity of the supported catalyst.[119-122] The various vanadium-based catalysts used in the oxidation reactions of furfural and 5-hydroxymethylfurfural to maleic acid and maleic anhydride have already been mentioned in **sections 2.4.1** and **2.4.2**.

Chai et al.[123] recently explored the oxidation of 5-hydroxymethylfurfural to maleic acid with O_2 oxidant over a vanadium catalyst supported on graphene oxide. A combined yield of maleic acid and maleic anhydride of 53.7% was achieved in γ-valerolactone solvent. Chatzidimitriou and Bond[124] also reported the synthesis of maleic acid over VO_x supported on SiO_2 using O_2 and achieved a total yield of 71%. There are several other vanadium-based catalysts which have been developed for the selective aerobic oxidation of 5-hydroxymethylfurfural to 2,5-diformylfuran such as V_2O_5 on activated carbon, VO_x/TiO_2, $Cu(NO_3)_2/VOSO_4$, VO_2 on carbon microspheres and V_2O_5/H-beta zeolite with selectivities ranging from 69% to over 99%.[125-129] The excellent activity of these catalysts was attributed to the redox reactivity of the V^{4+}/V^{5+} redox pairs. The synthesis of 2,5-furandicarboxylic acid by aerobic oxidation of 5-hydroxymethylfurfural has also been reported over a V_2O_5/TiO_2 catalyst achieving 97% selectivity.[130]

There are other biomass conversion reactions catalysed by vanadium which have been studied such as α-pinene oxidation with H_2O_2[131], C-C and C-O bond cleavage of lignin and model compounds[132-134], and pyrolysis of biomass to produce bio-oils and furans.[135,136]

In summary, the above results demonstrate the effectiveness of vanadium active sites for the conversion of biomass derivatives to valuable chemicals due to the strong redox character of vanadium as a result of its exchangeable multiple oxidation states, $V^{5+}/V^{4+}/V^{3+}$. It thus anticipated the heterostructuring of vanadium with SnO_2 will present a highly active catalyst for synthesis of maleic acid from the oxidation of furfural and 5-hydroxymethylfurfural. This can be achieved by taking advantage of the redox nature of SnO_2 (Sn^{4+}/Sn^{2+}) and that of V_2O_5 as well as the Lewis acid character of both oxides.

2.6.3 Base metal oxide catalysts based on Co, Cu, Mn and Ni

The utilization of transition metal based heterogeneous catalyst with adequate acid, basic or redox properties have long been exploited in catalysis. Be it in the form of metal oxides, supported metal or metal oxides as well as mixed metal oxides these catalysts have found application in a wide variety of oxidation reactions which include the oxidation of NH_3 to NO, SO_2 to SO_3, the oxidation of C_2-C_6 hydrocarbons and alcohols.[137-150] In particular, the use of basic (and redox) Co, Cu, Mn and Ni based catalysts for the conversion of biomass-derived furans has been recently reported and some of these results are presented in **Table 2-2**. As shown, oxides of Co, Cu and Mn have been successfully applied in the oxidation of 5-hydroxymethylfurfural using molecular oxygen, *tert*-butylhydroperoxide (TBHP) and air as oxidants.

Ning et al.[151] studied the oxidation of 5-hydroxymethylfurfural for the production of 2,5-diformylfuran with a Co_XO_Y-N@TiO$_2$ catalyst using *tert*-butylhydroperoxide oxidant. At 91% 5-hydroxymethylfurfural conversion, 40% selectivity toward 2,5-diformylfuran was achieved in acetonitrile solvent. XPS analysis of the catalyst showed the existence of Co^{3+}/Co^{2+} redox pairs which can be used to explain the activity of the catalyst. A spinel $CoMn_2O_4$ catalyst and $RuCo(OH)_2CeO_2$ trimetallic mixed oxide catalyst have also been shown to be effective for 2,5-diformylfuran synthesis from 5-hydroxymethylfurfural with 100% selectivity for $CoMn_2O_4$ and a yield of 82.6% for the mixed oxide being obtained.[152,153] Cobalt was reported to facilitate selectivity towards 2,5-diformylfuran for $RuCo(OH)_2CeO_2$ while for the spinel $CoMn_2O_4$ catalyst a synergistic effect between cobalt and manganese was reported to improve oxygen mobility and the reducibility of the catalyst and thus selectivity. Copper based catalysts have been shown to be efficient for the catalytic upgrading of 5-hydroxymethylfurfural. For instance, Zhang et al.[154]

synthesised a V_2O_5@Cu-modernite zeolite catalyst and employed it in the synthesis of 2,5-diformylfuran by aerobic oxidation of 5-hydroxymethylfurfural under ambient pressure. The framework Cu^{2+} species was reported to strongly interact with the V^{5+} species by altering their surface state, and thus resulted in a highly efficient catalyst producing 91.5% 2,5-diformylfuran yield with O_2 oxidant and 72.1% yield using air as oxidant. 5-fomyl-2-furancarboxylic acid, a platform chemical for other high value chemicals, has also been synthesised from 5-hydroxymethylfurfural oxidation over a $CuO-CeO_2$ mixed oxide catalyst.[155] With full conversion of 5-hydroxymethylfurfural, 90% selectivity toward the product was obtained and this was consequence to the increased basicity and good acidity of the catalyst as a result of mixing the two oxides. Yang et al.[156] prepared a nitrogen-doped graphene catalyst encapsulated with copper NPs for production of 2,5-furandicarboxylic acid from 5-hydroxymethylfurfural using *tert*-butylhydroperoxide oxidant obtaining a product yield of 95.2%.

MnO_2 has been recently demonstrated to be efficient for the oxidation of 5-hydroxymethylfurfural to 2,5-furandicarboxylic acid with O_2.[157] The different crystal structures of MnO_2 studied by computational and experimental techniques revealed that $β$-MnO_2 with the lowest oxygen vacancy formation energy to be most active among the different crystal structures. These oxygen vacancies are crucial for facilitating oxygen mobility which is vital for oxidation reactions. The catalyst gave 2,5-furandicarboxylic acid with a good yield of 86% as a result. Several other manganese catalysts have been developed for 2,5-furandicarboxylic acid synthesis from 5-hydroxymethylfurfural oxidation.[158-161] Gui et al.[162] carried out the oxidation of 5-hydroxymethylfurfural to 2,5-diformylfuran with O_2 and obtained 98% selectivity over a Mn-Co binary oxide catalyst. The excellent selectivity toward 2,5-diformylfuran was as a result of the increased

Mn^{4+}/Mn^{3+} redox pair atomic ratio and the exposed lattice oxygen which were reported to enhance oxygen mobility.

Table 2-2: Summary results for the furans oxidation using Co, Cu, Mn and Ni based catalysts.						
Entry	Catalyst	Substrate (Oxidant)	Product	X/%	Y/% (S/%)	Ref
1	Co_XO_Y-N@TiO_2	HMF (TBHP)	DFF	91	NC (40)	[151]
2	$CoMn_2O_4$	HMF (O_2)	DFF	41.6	NC (100)	[152]
3	$RuCo(OH)_2CeO_2$	HMF (O_2)	DFF	96.5	82.6 (85.6)	[153]
4	V_2O_5@Cu-modernite	HMF (O_2)	DFF	100	91.5 (NC)	[154]
5	V_2O_5@Cu-modernite	HMF (Air)	DFF	100	72.1 (NC)	[154]
6	CuO-CeO_2	HMF (O_2)	FFCA	99	90 (90)	[155]
7	Cu@N-graphene	HMF (TBHP)	FDCA	100	95.2 (NC)	[156]
8	MnO_2	HMF (O_2)	FDCA	>99	86 (NC)	[157]
9	Mn-Co binary oxide	HMF (O_2)	DFF	42.6	NC (98)	[162]
10	nickel-palladium alloy	FFR (Air)	FA	99	NC (99)	[163]
11	nickel-palladium alloy	HMF (Air)	FDCA	99	NC (86)	[163]
12	Ni/NiOOH electrodes	HMF (-)	FDCA	100	90 (NC)	[164]

Symbol: FFR = furfural, HMF = 5-hydroxymethylfurfural, FA = 2-furoic acid, FDCA = 2.5-furandicarboxylic acid, DFF = 2.5-diformylfuran. NC = not communicated, TBHP = *tert*-butylhydroperoxide, X= conversion, Y = yield, S = selectivity.

Nickel based catalysts are known not to be catalytically active for oxidation reactions and as such are hardly employed. However, very few studies exist were nickel-based catalyst are applied in the oxidation of biomass-derived chemicals. Gupta et al.[163] investigated a bimetallic nickel-palladium alloy catalyst for the oxidation of a variety of bio-based furans such as furfural, furfuryl alcohol, 5-hydroxymethylfurfural, 5-methyl-2-furfural and 5-methyl-2-furfuryl alcohol to their corresponding carboxylic acids with air. The catalyst showed remarkable activity to produce 2-furoic acid from furfural and furfuryl alcohol with

over 99% selectivity and over 99% conversion of the substrate. Similar turnover numbers were obtained to produce the corresponding carboxylic acids of 5-methyl-2-furfural and 5-methyl-2-furfuryl alcohol, while the oxidation of 5-hydroxymethylfurfural produced 2,5-furandicarboxylic acid with 86% selectivity in the presence of a base. The catalyst was further shown to be effective for the one-pot transformation of fructose to produce 2,5-hydroxyfurancarboxylic acid and 2,5-furandicarboxylic acid with 74% and 22% selectivity, respectively. The presence of nickel on the catalyst was reported to enhance the activity and stability of the catalyst. Latsuzbaia et al.[164] studied the electrochemical oxidation of 5-hydroxymethylfurfural to produce 2,5-furandicarboxylic acid with a yield of almost 90% using Ni/NiOOH electrodes.

In light of the results presented herein, it is envisaged the combination of the metal oxides of Co, Cu, Mn and Ni with of SnO_2 will present a stable and active catalyst for the oxidation of furfural. This hypothesis is based on the easily exchangeable oxidation states of the above-mentioned metals which give rise to redox couples which could induce various structural modifications thus leading to different phase compositions, shapes and much different catalytic activities. Furthermore, the varying degree of Lewis acidity of these metal oxides coupled with the moderate Lewis acid character of SnO_2 could bring about enhanced acid-base properties required for an efficient oxidation of furfural.

2.6.4 Titanium based catalysts

The Lewis acidity of TiO_2 has also been exploited for the conversion of lignocellulose to bio-based model compounds. Noma et al.[165] employed bare TiO_2 and phosphated TiO_2 for the dehydration of glucose to 5-hydroxymethylfurfural. Interestingly, the reaction proceeded via 3-deoxyglucosone instead of isomerisation to fructose affording a 10%

yield with both catalysts. The conversion was much higher for TiO_2 (85%) compared to PO_4^{2-}/TiO_2 (18%) however PO_4^{2-}/TiO_2 resulted in better selectivity than bare TiO_2 (56% compared to 12%). Atanda et al.[166] also reported the use of phosphated TiO_2 with enhanced acidity and stability for the synthesis of 5-hydroxymethylfurfural from glucose with 81% yield and 97% conversion. De et al.[167] employed TiO_2 nanospheres with high Lewis acidity synthesised with aspartic acid template for the production of 5-hydroxymethylfurfural from glucose and fructose by microwave irradiation. In a dimethylacetamide/lithium chloride solvent, respective maximum yields of 82.3% and 30.2% from fructose and glucose were obtained at 130 °C. Mixed oxide TiO_2-ZrO_2 catalysts synthesised by different methods were also investigated for the production of furfural and 5-hydroxymethylfurfural under hot compressed water from sugarcane bagasse, rice husk and corncob.[168] The TiO_2-ZrO_2 catalyst synthesised by sol-gel method was reported to possess the higher Lewis acidity and consequently led to higher activity producing 10.3% furfural and 8.6% 5-hydroxymethylfurfural from corncob. Li et al.[169] also studied the production of furfural from xylose dehydration over a SO_4^{2-}/TiO_2-ZrO_2/La^{3+} solid acid catalyst in biphasic solvent systems achieve a yield of 3563.3 μmol/g of xylose with 98% xylose conversion. The same research group also investigated the photocatalytic dehydration of xylose to furfural with the same catalyst and achieved 216.6 μmol/g of xylose with 32% xylose conversion.[170]

There are currently no literature reports of Ti-based catalysts being employed for furfural oxidation, with the exception of titanium silicate (TS-1) catalyst. Thus, it is envisaged the heterostructuring of TiO_2 and SnO_2 can lead to a strong Lewis acidic catalyst capitalizing on the Lewis acid properties SnO_2 and TiO_2. In addition, by taking advantage of the redox nature of SnO_2 (Sn^{4+}/Sn^{2+}) and that of TiO_2 (Ti^{4+}/Ti^{3+}) a highly active redox catalyst can be

designed that can contribute to the catalytic activity influence of the heterostructure TiO_2-SnO_2 composite by the synergistic effect.

2.6.5 SnO_2 coupled with V_2O_5, TiO_2 and oxides of Co, Cu, Mn and Ni

The catalytic results presented above indicate the effectiveness of SnO_2 as a catalyst support and the effectiveness of Ti, V, Co, Cu, Mn and Ni as catalyst active sites. Thus, the catalyst design strategy herein intends to exploit the redox nature, low cost and abundance of these metals for the development of efficient catalysts for the conversion of furfural and 5-hydroxymethylfurfural to maleic acid. It is envisaged that the combination of the above-mentioned metal oxides with SnO_2 will present stable and active catalysts. Although SnO_2 on its own represents a poor oxidation catalyst, coupling with other metal oxides provides a dynamic approach to heterogeneous catalysis capitalizing on the consequential electronic and structural properties of the metal oxides. Furthermore, the varying degree of Lewis acidity and redox character of these metal oxides coupled with the moderate Lewis acid character of SnO_2 could bring about enhanced acid-base properties required for efficient catalytic oxidations of the bio-based chemicals.

It is therefore hypothesised that the enhanced activity of these SnO_2 designed heterostructure catalysts would result from;

> ➢ An accelerated electron transfer process due to linkage of SnO_2 Lewis sites to the redox metal ions of V, Cu, Co, Mn and Ni.
>
> ➢ An accelerated electron transfer process due to SnO_2 and TiO_2 Lewis sites.
>
> ➢ The presence of easily exchangeable metal redox centres of V, Cu, Co, Mn and Ni for facilitating the C–C bond cleavage.

➢ The presence of SnO_2 and TiO_2 Lewis sites for trapping generated organic radicals to prevent side reactions which lead to formation of resins/humins.

2.7 References

[1] D.M. Alonso, J.Q. Bond, J.A. Dumesic, Catalytic conversion of biomass to biofuels. Green Chemistry, **2010**, 12, pp. 1493-1513.

[2] L.T. Mika, E. Cséfalvay, Á. Németh, Catalytic conversion of carbohydrates to initial platform chemicals: Chemistry and sustainability. Chemical Reviews, **2018**, 118, pp. 505-613.

[3] C. Chatterjee, F. Pong, A. Sen, Chemical conversion pathways for carbohydrates. Green Chemistry, **2015**, 17, pp. 40-71.

[4] P. Bhaumik, P.L. Dhepe, Solid acid catalyzed synthesis of furans from carbohydrates. Catalysis Reviews, **2016**, 58, pp. 36-112.

[5] S.N. Khot, J.J. Lascala, E. Can, S.S. Morye, G.I. Williams, G.R. Palmese, S.H. Kusefoglu, R.P. Wool, Development and application of triglyceride-based polymers and composites. Journal of Applied Polymer Science, **2001**, 82, pp. 703-723.

[6] P. Gallezot, Conversion of biomass to selected chemical products. Chemical Society Reviews, **2012**, pp. 1538-1558.

[7] Y. Jiang, X. Wang, Q. Cao, L. Dong, J. Guan, X. Mu, Chemical conversion of biomass to green chemicals, In: M. Xian (Ed.), Sustainable production of bulk chemicals. Springer, Netherlands, Dordrecht, **2015**, pp 19-49.

[8] G.W. Huber, S. Iborra, A. Corma, Synthesis of transportation fuels from biomass: Chemistry, catalysts, and engineering. Chemical Reviews, **2006**, 37, pp. 4044-4098.

[9] Y. Lin, G.W. Huber, The critical role of heterogeneous catalysis in lignocellulosic biomass conversion. Energy & Environmental Science, **2008**, 2, pp. 68-80.

[10] S.E. Jacobsen, C.E. Wyman, Cellulose and hemicellulose hydrolysis models for application to current and novel pretreatment processes. Applied Biochemistry and Biotechnology, **2000**, 84, pp. 81-96.

[11] D.T. Win, Furfural-gold from garbage. AU Journal of Technology, 8, pp. 185-190.

[12] K. Yan, G. Wu, T. Lafleur, C. Jarvis, Production, properties and catalytic hydrogenation of furfural to fuel additives and value-added chemicals. Renewable and Sustainable Energy Reviews, **2014**, 38, pp. 663-676.

[13] G. Machado, S. Leon, F. Santos, Literature review on furfural production from lignocellulosic biomass. Natural Resources, **2016**, 7, pp. 115-129.

[14] J.J. Bozell, G.R. Petersen, Technology development for the production of biobased products from biorefinery carbohydrates-the US Department of Energy's "Top 10" revisited. Green Chemistry, **2010**, 12, pp. 539-554.

[15] X. Li, P. Jia, T. Wang, Furfural: A promising platform compound for sustainable production of C4 and C5 chemicals. ACS Catalysis, **2016**, 6, pp. 7621-7640.

[16] L. Mesa, M. Morales, E. González, C. Cara, I. Romero, E. Castro, S.I. Mussatto, Restructuring the processes for furfural and xylose production from sugarcane bagasse in a biorefinery concept for ethanol production. Chemical Engineering & Processing: Process Intensification, **2014**, 85, pp. 196-202.

[17] K. Gupta, R.K. Rai, S.K. Singh, Metal catalysts for the efficient transformation of biomass-derived HMF and furfural to value added chemicals. ChemCatChem, **2018**, 10, pp. 2326-2349.

[18] R. van Putten, J.C. van der Waal, E. de Jong, C.B. Rasrendra, H.J. Heeres, J.G. de Vries, Hydroxymethylfurfural, a versatile platform chemical made from renewable resources. Chemical Reviews, **2013**, 113, pp. 1499-1597.

[19] B.F.M. Kuster, 5-Hydroxymethylfurfural (HMF). A review focussing on its manufacture. Starch/Stärke **1990**, 42, pp. 314-321.

[20] X. Zhang, K. Wilson, A.F. Lee, Heterogeneously catalyzed hydrothermal processing of C_5–C_6 Sugars. Chemical Reviews, **2016**, 116, pp. 12328-12368.

[21] H. Li, Q. Zhang, P.S. Bhadury, S. Yang, Furan-type compounds from carbohydrates via heterogeneous catalysis. Current Organic Chemistry, **2014**, 18, pp. 547-597.

[22] A.A. Rosatella, S.P. Simeonov, R.F.M. Frade, C.A.M. Afonso, Hydroxymethylfurfural (HMF) as a building block platform: Biological properties, synthesis and synthetic applications. Green Chemistry, **2011**, 13, pp. 754-793.

[23] J.G. de Vries, Chapter Eight - Green syntheses of heterocycles of industrial importance. 5-Hydroxymethylfurfural as a platform chemical. In: E.F.V. Scriven, C.A. Ramsden (Ed.), Advances in Heterocyclic Chemistry. Academic Press, **2017**, Vol, 121, pp. 247-293.

[24] J.N. Chheda, Y. Román-Leshkov, J.A. Dumesic, Production of 5-hydroxymethylfurfural and furfural by dehydration of biomass-derived mono- and poly-saccharides. Green Chemistry, **2007**, 9, pp. 342-350.

[25] B. Agarwal, K. Kailasam, R.S. Sangwan, S. Elumalai, Traversing the history of solid catalysts for heterogeneous synthesis of 5-hydroxymethylfurfural from carbohydrate sugars: A review. Renewable and Sustainable Energy Reviews, **2018**, 82, pp. 2408-2425.

[26] S. Chen, R. Wojcieszak, F. Dumeignil, E. Marceau, S. Royer, How catalysts and experimental conditions determine the selective hydroconversion of furfural and 5-hydroxymethylfurfural. Chemical Reviews, **2018**, 118, pp. 11023-11117

[27] R. Mariscal, P. Maireles-Torres, M. Ojeda, I. Sádaba, M.L. Granados, Furfural: a renewable and versatile platform molecule for the synthesis of chemicals and fuels. Energy & Environmental Science, **2016**, 9, pp. 1144-1189.

[28] K.J. Zeitsch, The chemistry and technology of furfural and its many by-products; Elsevier: **2000**; Vol. 13.

[29] J. Kijeński, P. Winiarek, T. Paryjczak, A. Lewicki, A. Mikołajska, Platinum deposited on monolayer supports in selective hydrogenation of furfural to furfuryl alcohol. Applied Catalysis A: General, **2002**, 233, pp. 171-182.

[30] D. Vargas-Hernández, J.M. Rubio-Caballero, J. Santamaría-González, R. Moreno-Tost, J.M. Mérida-Robles, M.A. Pérez-Cruz, A. Jiménez-López, R. Hernández-Huesca, P. Maireles-Torres, Furfuryl alcohol from furfural hydrogenation over copper supported on SBA-15 silica catalysts. Journal of Molecular Catalysis A: Chemical, **2014**, 383-384, pp. 106-113.

[31] Y. Yang, J. Ma, X. Jia, Z. Du, Y. Duan, J. Xu, Aqueous phase hydrogenation of furfural to tetrahydrofurfuryl alcohol on alkaline earth metal modified Ni/Al$_2$O$_3$. RSC Advances, **2016**, 6, pp. 51221-51228.

[32] G.M.G. Maldonado, R.S. Assary, J. Dumesic, L.A. Curtiss, Experimental and theoretical studies of the acid-catalyzed conversion of furfuryl alcohol to levulinic acid in aqueous solution. Energy & Environmental Science, **2012**, 5, pp. 6981-6989.

[33] H. Zheng, Y. Zhu, B. Teng, Z. Bai, C. Zhang, H. Xiang, Y. Li, Towards understanding the reaction pathway in vapour phase hydrogenation of furfural to 2-methylfuran. Journal of Molecular Catalysis A: Chemical, **2006**, 246, pp. 18-23.

[34] M.A. Lilga, R.T. Hallen, M. Gray, Production of oxidized derivatives of 5-hydroxymethylfurfural (HMF). Topics in Catalysis, **2010**, 53, pp. 1264-1269.

[35] E. Hayashi, T. Komanoya, K. Kamata, M. Hara, Heterogeneously-catalyzed aerobic oxidation of 5-hydroxymethylfurfural to 2,5-furandicarboxylic acid with MnO$_2$. ChemSusChem, **2017**, 10, pp. 654.

[36] M. Sajid, X. Zhao, D. Liu, Production of 2,5-furandicarboxylic acid (FDCA) from 5-hydroxymethylfurfural (HMF): recent progress focusing on the chemical-catalytic routes. Green Chemistry, **2018**, 20, pp. 5427-5453.

[37] H. Ait Rass, N. Essayem, M. Besson, Selective aerobic oxidation of 5-HMF into 2,5-furandicarboxylic acid with Pt catalysts supported on TiO$_2$- and ZrO$_2$-based supports. ChemSusChem, **2015**, 8, pp. 1206-1217.

[38] Y. Zhu, Y. Zhang, L. Cheng, M. Ismael, Z. Feng, Y. Wu, Novel application of g-C$_3$N$_4$/NaNbO$_3$ composite for photocatalytic selective oxidation of biomass-derived HMF to FFCA under visible light irradiation. Advanced Powder Technology, **2020**.

[39] F. Neaţu, N. Petrea, R. Petre, V. Somoghi, M. Florea, V.I. Parvulescu, Oxidation of 5-hydroxymethyl furfural to 2,5-diformylfuran in aqueous media over heterogeneous manganese based catalysts. Catalysis Today, **2016**, 278, pp. 66-73.

[40] Z. Zhang, B. Liu, K. Lv, J. Sun, K. Deng, Aerobic oxidation of biomass derived 5-hydroxymethylfurfural into 5-hydroxymethyl-2-furancarboxylic acid catalyzed by a montmorillonite K-10 clay immobilized molybdenum acetylacetonate complex. Green Chemistry, **2014**, 16, pp. 2762-2770.

[41] L. Hu, L. Lin, S. Liu, Chemoselective hydrogenation of biomass-derived 5-hydroxymethylfurfural into the liquid biofuel 2,5-dimethylfuran. Industrial & Engineering Chemistry Research, **2014**, 53, pp. 9969-9978.

[42] A.J. Kumalaputri, G. Bottari, P.M. Erne, H.J. Heeres, K. Barta, Tunable and selective conversion of 5-HMF to 2,5-furandimethanol and 2,5-dimethylfuran over copper-doped porous metal oxides. ChemSusChem, **2014**, 7, pp. 2266-2275.

[43] R. Goyal, B. Sarkar, A. Bag, N. Siddiqui, D. Dumbre, N. Lucas, S.K. Bhargava, A. Bordoloi, Studies of synergy between metal–support interfaces and selective hydrogenation of HMF to DMF in water. Journal of Catalysis, **2016**, 340, pp. 248-260.

[44] B. Girisuta, L. Janssen, H.J. Heeres, A kinetic study on the decomposition of 5-hydroxymethylfurfural into levulinic acid. Green Chemistry, **2006**, 8, pp. 701-709.

[45] G. Mazzoni, F. Cavani, G. Stefani, to Lonza (**1997**) EP 0804963A1

[46] F. Trifirò, R. Grasselli, How the yield of maleic anhydride in n-nutane oxidation, using VPO catalysts, was improved over the years. Topics in Catalysis, **2014**, 57, pp. 1188-1195.

[47] L. Zhang, G. Xi, K. Yu, H. Yu, X. Wang, Furfural production from biomass–derived carbohydrates and lignocellulosic residues via heterogeneous acid catalysts. Industrial Crops & Products, **2017**, 98, pp. 68-75.

[48] O.M. Musa, Handbook of maleic anhydride based materials: Syntheses, properties and Aplications; Springer International Publishing: Cham, **2016**.

[49] T.R. Felthouse, J.C. Burnett, B. Horrell, M.J. Mummey, Y. Kuo, Maleic Anhydride, Maleic acid, and fumaric acid. Kirk-Othmer Encyclopedia of Chemical Technology **2001**.

[50] B.C. Trivedi, B.M. Culbertson, Maleic anhydride; Springer US: **1982**.

[51] W.V Sessions, Catalytic oxidation of furfural in the vapor phase. Journal of the American Chemical Society, **1928**, 50, pp. 1696-1698.

[52] E.R. Nielsen, Vapor phase oxidation of furfural. Industrial & Engineering Chemistry Research, **1949**, 41, pp. 365-368.

[53] N. Alonso-Fagúndez, M.L. Granados, R. Mariscal, M. Ojeda, Selective conversion of furfural to maleic anhydride and furan with VO_x/Al_2O_3 Catalysts. ChemSusChem, **2012**, 5, pp. 1984-1990.

[54] N. Alonso-Fagúndez, M. Ojeda, R. Mariscal, J.L.G. Fierro, M.L. Granados, Gas phase oxidation of furfural to maleic anhydride on $V_2O_5/\gamma\text{-}Al_2O_3$ catalysts: Reaction conditions to slow down the deactivation. Journal of Catalysis, **2017**, 348, pp. 265-275.

[55] X. Li, B. Ho, Y. Zhang, Selective aerobic oxidation of furfural to maleic anhydride with heterogeneous Mo–V–O catalysts. Green Chemistry, **2016**, 18, pp. 2976-2980.

[56] X. Li, J. Ko, Y. Zhang, Highly efficient gas-phase oxidation of renewable furfural to maleic anhydride over plate vanadium phosphorus oxide catalyst. ChemSusChem, **2018**, 11, pp. 612-618.

[57] Y. Xie, Y. Huang, C. Wu, W. Yuan, Y. Xia, X. Liu, H. Wang, Iron-based metalloporphyrins as efficient catalysts for aerobic oxidation of biomass derived furfural into maleic acid. Molecular Catalysis, **2018**, 452, pp. 20-27.

[58] G. Lv, S. Chen, H. Zhu, M. Li, Y. Yang, Determination of the crucial functional groups in graphene oxide for vanadium oxide nanosheet fabrication and its catalytic application in 5-hydroxymethylfurfural and furfural oxidation. Journal of Cleaner Production, **2018**, 196, pp. 32-41.

[59] G. Strukul, A. Scarso, Environmentally benign oxidants. Liquid phase oxidation via heterogeneous catalysis, **2013**, pp. 1-20.

[60] N. Araji, D.D. Madjinza, G. Chatel, A. Moores, F. Jérôme, K.D.O. Vigier, Synthesis of maleic and fumaric acids from furfural in the presence of betaine hydrochloride and hydrogen peroxide. Green chemistry, **2017**, 19, pp. 98-101.

[61] N. Alonso-Fagúndez, I. Agirrezabal-Telleria, P.L. Arias, J.L.G. Fierro, R. Mariscal, M.L. Granados, Aqueous-phase catalytic oxidation of furfural with H_2O_2: high yield of maleic acid by using titanium silicalite-1. RSC Advances, **2014**, 4, pp. 54960-54972.

[62] G. Lv, C. Chen, B. Lu, J. Li, Y. Yang, C. Chen, T. Deng, Y. Zhu, X. Hou, Vanadium-oxo immobilized onto Schiff base modified graphene oxide for efficient catalytic oxidation of 5-hydroxymethylfurfural and furfural into maleic anhydride. RSC Advances, **2016**, 6, pp. 101277-101282.

[63] H. Choudhary, S. Nishimura, K. Ebitani, Metal-free oxidative synthesis of succinic acid from biomass-derived furan compounds using a solid acid catalyst with hydrogen peroxide. Applied Catalysis A, General, **2013**, 458, pp. 55-62.

[64] Y. Rodenas, R. Mariscal, J.L.G. Fierro, D.M. Alonso, J.A. Dumesic, M.L. Granados, Improving the production of maleic acid from biomass: TS-1 catalysed aqueous phase oxidation of furfural in the presence of γ-valerolactone. Green Chemistry, **2018**, 20, pp. 2845-2856.

[65] M.E. Zakrzewska, E. Bogel-Łukasik, R. Bogel-Łukasik, Ionic liquid-mediated formation of 5-hydroxymethylfurfural-A promising biomass-derived building block. The American Journal of Cardiology, **2019**, 111, pp. 397-417.

[66] X. Kong, Y. Zhu, Z. Fang, J.A. Kozinski, I.S. Butler, L. Xu, H. Song, X. Wei, Catalytic conversion of 5-hydroxymethylfurfural to some value-added derivatives. Green Chemistry, **2018**, 20, pp. 3657-3682.

[67] X. Li, Y. Zhang, The conversion of 5-hydroxymethyl furfural (HMF) to maleic anhydride with vanadium-based heterogeneous catalysts. Green Chemistry, **2016**, 18, pp. 643-647.

[68] Z. Du, J. Ma, F. Wang, J. Liu, J. Xu, Oxidation of 5-hydroxymethylfurfural to maleic anhydride with molecular oxygen. Green Chemistry, **2011**, 13, pp. 554.

[69] A. Takagaki, S. Nishimura, K. Ebitani, Catalytic transformations of biomass-derived materials into value-added chemicals. Catalysis Surveys from Asia, **2012**, 16, pp. 164-182.

[70] J.C. Serrano-Ruiz, R. Luque, A. Sepúlveda-Escribano, Transformations of biomass-derived platform molecules: from high added-value chemicals to fuels via aqueous-phase processing. Chemical Society Reviews, **2011**, 40, pp. 5266-5281.

[71] J. Lan, J. Lin, Z. Chen, G. Yin, Transformation of 5-hydroxymethylfurfural (HMF) to maleic anhydride by aerobic oxidation with heteropolyacid catalysts. ACS Catalysis, **2015**, 5, pp. 2035-2041.

[72] A. Tirsoaga, M. El Fergani, V.I. Parvulescu, S.M. Coman, Upgrade of 5-hydroxymethylfurfural to dicarboxylic acids onto multifunctional-based $Fe_3O_4@SiO_2$ Magnetic Catalysts. ACS Sustainable Chemistry & Engineering, **2018**, 6, pp. 14292-14301.

[73] C. Chen, C.V. Nguyen, Z. Wang, Y. Bando, Y. Yamauchi, M.T.S. Bazziz, A. Fatehmulla, W.A. Farooq, T. Yoshikawa, T. Masuda, K.C.- Wu, Hydrogen peroxide assisted selective oxidation of 5-hydroxymethylfurfural in water under mild conditions. ChemCatChem, **2018**, 10, pp. 361-365.

[74] T. Yang, W. Li, Q. Liu, M. Su, T. Zhang, J. Ma, Synthesis of maleic acid from biomass-derived furfural in the presence of KBr/graphitic carbon nitride (g-C_3N_4) catalyst and hydrogen peroxide. Bioresources, **2019**, 14, pp. 5025-5044.

[75] C. Van Nguyen, J.R. Boo, C.H. Liu, T. Ahamad, S.M. Alshehri, B.M. Matsagar, K.C.W. Wu, Oxidation of biomass-derived furans to maleic acid over nitrogen-doped carbon catalysts under acid-free condition. Catalysis Science & Technology, **2020**, 10, pp. 1498-1506.

[76] Y. Lou, S. Marinkovic, B. Estrine, W. Qiang, G. Enderlin, Oxidation of furfural and furan derivatives to maleic acid in the presence of a simple catalyst system based on acetic acid and TS-1 and hydrogen peroxide. ACS Omega, **2020**, 5, pp. 2561-2568.

[77] X. Zhao, X. Kong, F. Wang, R. Fang, Y. Li, Metal sub-nanoclusters confined within hierarchical porous carbons with high oxidation activity. Angewandte Chemie International Edition, **2021**, 60, pp.10842-10849.

[78] C.H. Bartholomew, Mechanisms of catalyst deactivation. Applied Catalysis A: General, **2001**, 212, pp. 17-60.

[79] D.M. Argyle, H.C. Bartholomew, Heterogeneous catalyst deactivation and regeneration: A review. Catalysts, **2015**, 5.

[80] J.A. Moulijn, A.E. van Diepen, F. Kapteijn, Catalyst deactivation: is it predictable?: What to do? Applied Catalysis A: General, **2001**, 212, pp. 3-16.

[81] U.K. Singh, M.A. Vannice, Kinetics of liquid-phase hydrogenation reactions over supported metal catalysts — a review. Applied Catalysis A: General, **2001**, 213, pp. 1-24.

[82] J. Lan, Z. Chen, J. Lin, G. Yin, Catalytic aerobic oxidation of renewable furfural to maleic anhydride and furanone derivatives with their mechanistic studies. Green Chemistry, **2014**, 16, pp. 4351-4358.

[83] H. Guo, G. Yin, Catalytic aerobic oxidation of renewable furfural with phosphomolybdic acid catalyst: an alternative route to maleic acid. The Journal of Physical Chemistry C, **2011**, 115, pp. 17516-17522.

[84] H. Choudhary, S. Nishimura, K. Etibani, Highly efficient aqueous oxidation of furfural to succinic acid using reusable heterogeneous acid catalyst with hydrogen peroxide. Chemistry Letters, **2012**, 41, pp. 409-411.

[85] A.C. Alba-Rubio, J.L.G. Fierro, L. León-Reina, R. Mariscal, J.A. Dumesic, M.L. Granados, Oxidation of furfural in aqueous H_2O_2 catalysed by titanium silicalite: Deactivation processes and role of extraframework Ti oxides. Applied Catalysis B, **2017**, 202, pp. 269-280.

[86] M. Konsolakis, M. Lykaki, Facet-dependent reactivity of ceria nanoparticles exemplified by CeO_2-based transition metal catalysts: A critical review. Catalysts, **2021**, 11, pp. 452.

[87] Y. Wang, G. Wang, W. Deng, J. Han, L. Qin, B. Zhao, L. Guo, F. Xing, Study on the structure-activity relationship of Fe-Mn oxide catalysts for chlorobenzene catalytic combustion. Chemical Engineering Journal, **2020**, 395, pp.125172.

[88] M. Konsolakis, M. Lykaki, Recent advances on the rational design of non-precious metal oxide catalysts exemplified by CuO_x/CeO_2 binary system: Implications of size, shape and electronic effects on intrinsic reactivity and metal-support interactions. Catalysts, **2020**, 10, pp. 160.

[89] S. Cao, F. Tao, Y. Tang, Y. Li, J. Yu, Size- and shape-dependent catalytic performances of oxidation and reduction reactions on nanocatalysts. Chemical Society Reviews, **2016**, 45, pp. 4747.

[90] P. Bhaumik, P.L. Dhepe, Mixed transition-metal oxides: Design, synthesis, and energy-related applications. Angewandte Chemie International Edition, **2014**, 53, pp. 1488-1504.

[91] P.N. Kapoor, A.K. Bhagi, R.S. Mulukutla, K.J. Klabunde, Mixed metal oxide nanoparticles. Dekker Encyclopedia of Nanoscience and Nanotechnology, **2004**, pp. 2007-2015.

[92] M. Ahmadi, H. Mistry, B. Roldan Cuenya, Tailoring the catalytic properties of metal nanoparticles via support interactions. The Journal of Physical Chemistry Letters, **2016**, 7, pp. 3519-3533.

[93] I. Ro, J. Resasco, P. Christopher, Approaches for understanding and controlling interfacial effects in oxide-supported metal catalysts. ACS Catalysis, **2018**, 8, pp. 7368-7387.

[94] T.W. van Deelen, C.H. Mejía, K.P. de Jong, Control of metal-support interactions in heterogeneous catalysts to enhance activity and selectivity. Nature Catalysis. **2019**, 2, pp. 955–970.

[95] K. Sekizawa, H. Widjaja, S. Maeda, Y. Ozawa, K. Eguchi, Low temperature oxidation of methane over Pd/SnO$_2$ catalyst. Applied Catalysis A: General, **2000**, 200, pp. 211-217.

[96] X. Wang, Y. Xie, Preparation and characterization of SnO$_2$-based composite metal oxides: Active and thermally stable catalysts for CH$_4$ Oxidation. Catalysis Letters, **2001**, 75, pp. 73-80.

[97] K. Yu, Z. Wu, Q. Zhao, B. Li, Y. Xie, High-temperature-stable Au@SnO$_2$ core/shell supported catalyst for CO oxidation. The Journal of Physical Chemistry C, **2008**, 112, pp. 2244-2247.

[98] S. Wang, J. Huang, Y. Zhao, S. Wang, X. Wang, T. Zhang, S. Wu, S. Zhang, W. Huang, Preparation, characterization and catalytic behavior of SnO2 supported Au catalysts for low-temperature CO oxidation. Journal of Molecular Catalysis A: Chemical, **2006**, 259, pp. 245-252.

[99] X. Xu, R. Zhang, X. Zeng, X. Han, Y. Li, Y. Liu, X. Wang, Effects of La, Ce, and Y oxides on SnO$_2$ catalysts for CO and CH$_4$ oxidation. ChemCatChem, **2013**, 5, pp. 2025-2036.

[100] J. Yu, D. Zhao, X. Xu, X. Wang, N. Zhang, Study on RuO$_2$/SnO$_2$: Novel and active catalysts for CO and CH$_4$ oxidation. ChemCatChem, **2012**, 4, pp. 1122-1132.

[101] M. Niwa, J. Igarashi, Role of the solid acidity on the MoO$_3$ loaded on SnO$_2$ in the methanol oxidation into formaldehyde. Catalysis Today, **1999**, 52, pp. 71-81.

[102] F. Gonçalves, P.R.S. Medeiros, J.G. Eon, L.G. Appel, Active sites for ethanol oxidation over SnO$_2$-supported molybdenum oxides. Applied Catalysis A: General, **2000**, 193, pp. 195-202.

[103] T. Lv, C. Peng, H. Zhu, W. Xiao, Heterostructured Fe_2O_3@SnO_2 core–shell nanospindles for enhanced Room-temperature HCHO oxidation. Applied Surface Science, **2018**, 457, pp. 83-92.

[104] N. Kamiuchi, T. Mitsui, N. Yamaguchi, H. Muroyama, T. Matsui, R. Kikuchi, K. Eguchi, Activation of Pt/SnO_2 catalyst for catalytic oxidation of volatile organic compounds. Catalysis Today, **2010**, 157, pp. 415-419.

[105] Q. Liu, F. Yang, Z. Liu, G. Li, Preparation of SnO_2–Co_3O_4/C biochar catalyst as a Lewis acid for corncob hydrolysis into furfural in water medium. Journal of Industrial and Engineering Chemistry, **2015**, 26, pp. 46-54.

[106] T. Suzuki, T. Yokoi, R. Otomo, J.N. Kondo, T. Tatsumi, Dehydration of xylose over sulfated tin oxide catalyst: Influences of the preparation conditions on the structural properties and catalytic performance. Applied Catalysis A: General, **2011**, 408, pp. 117-124.

[107] V. Choudhary, A.B. Pinar, S.I. Sandler, D.G. Vlachos, R.F. Lobo, Xylose isomerization to xylulose and its dehydration to furfural in aqueous media. ACS Catalysis, **2011**, 1, pp. 1724-1728.

[108] M. Moliner, Y. Roman-Leshkov, M.E. Davis, Tin-containing zeolites are highly active catalysts for the isomerization of glucose in water. Proceedings of the National Academy of Sciences. **2010**, 107, pp. 6164-6168.

[109] E.N.E. Nikolla, Y. Roman-Leshkov, M. Moliner, M.E. Davis, "One-pot" synthesis of 5-(hydroxymethyl) furfural from carbohydrates using tin-beta zeolite. ACS Catalysis. **2011**, 1, pp. 408-410.

[110] G.C. Behera, K.M. Parida, One-pot synthesis of 5-hydroxymethylfurfural: a significant biomass conversion over tin-promoted vanadium phosphate (Sn–VPO) catalyst. Catalysis Science & Technology, **2013**, 3, pp. 3278.

[111] B. Mallesham, P. Sudarsanam, H. Raju, B.M. Reddy, Design of highly efficient Mo and W-promoted SnO_2 solid acids for heterogeneous catalysis: acetalization of bio-glycerol. Green Chemistry, **2013**, 15, pp. 478-489.

[112] B. Mallesham, P. Sudarsanam, B.M. Reddy, Eco-friendly synthesis of bio-additive fuels from renewable glycerol using nanocrystalline SnO_2 -based solid acids. Catalysis Science & Technology, **2014**, 8, pp. 803-813.

[113] P. Mars, D.W. van Krevelen, Oxidations carried out by means of vanadium oxide catalysts. Chemical Engineering Science, **1954**, 3, pp. 41-59.

[114] G.L. Simard, J.F. Steger, R.J. Arnott, L.A. Siegel, Vanadium oxides as oxidation catalysts. Industrial & Engineering Chemistry, **1955**, 47, pp. 1424-1430.

[115] R.R. Langeslay, D.M. Kaphan, C.L. Marshall, P.C. Stair, A.P. Sattelberger, M. Delferro, Catalytic applications of vanadium: A mechanistic perspective. Chemical Reviews, **2019**, 119, pp. 2128-2191.

[116] V. Conte, A. Coletti, B. Floris, G. Licini, C. Zonta, Mechanistic aspects of vanadium catalysed oxidations with peroxides. Coordination Chemistry Reviews, **2011**, 255, pp. 2165-2177.

[117] G. Licini, V. Conte, A. Coletti, M. Mba, C. Zonta, Recent advances in vanadium catalyzed oxygen transfer reactions. Coordination Chemistry Reviews, **2011**, 255, pp. 2345-2357.

[118] E.A. Mamedov, V. Cortés Corberán, Oxidative dehydrogenation of lower alkanes on vanadium oxide-based catalysts. The present state of the art and outlooks. Applied Catalysis A: General, **1995**, 127, pp. 1-40.

[119] I.E. Wachs, Catalysis science of supported vanadium oxide catalysts. Dalton Transactions, **2013**, 42, pp. 11762-11769.

[120] Y. Habuta, N. Narishige, K. Okumura, N. Katada, M. Niwa, Catalytic activity and solid acidity of vanadium oxide thin layer loaded on TiO_2, ZrO_2, and SnO_2. Catalysis Today, **2003**, 78, pp. 131-138.

[121] L. Artiglia, S. Agnoli, G. Granozzi, Vanadium oxide nanostructures on another oxide: The viewpoint from model catalysts studies. Coordination Chemistry Reviews, **2015**, 301-302, pp. 106-122.

[122] G.C. Bond, S.F. Tahir, Vanadium oxide monolayer catalysts Preparation, characterization and catalytic activity. Applied Catalysis, **1991**, 71, pp. 1-31.

[123] L. Chai, X. Hou, X. Cui, H. Li, N. Zhang, H. Zhang, C. Chen, Y. Wang, T. Deng, 5-Hydroxymethylfurfural oxidation to maleic acid by O_2 over graphene oxide supported vanadium: Solvent effects and reaction mechanism. Chemical Engineering Journal, **2020**, 388, pp. 124187.

[124] A. Chatzidimitriou, J.Q. Bond, Oxidation of levulinic acid for the production of maleic anhydride: breathing new life into biochemicals. Green Chemistry, **2015**, 17, pp. 4367-4376.

[125] C.A. Antonyraj, B. Kim, Y. Kim, S. Shin, K.Y. Lee, I. Kim, J.K. Cho, Heterogeneous selective oxidation of 5-hydroxymethyl-2-furfural (HMF) into 2,5-diformylfuran catalyzed by vanadium supported activated carbon in MIBK, extracting solvent for HMF. Catalysis Communications, **2014**, 57, pp. 64-68.

[126] J. Nie, H. Liu, Aerobic oxidation of 5-hydroxymethylfurfural to 2, 5-diformylfuran on supported vanadium oxide catalysts: Structural effect and reaction mechanism. Pure and Applied Chemistry, **2011**, 84, pp. 765-777.

[127] J. Ma, Z. Du, J. Xu, Q. Chu, Y. Pang, Efficient aerobic oxidation of 5-hydroxymethylfurfural to 2, 5-diformylfuran, and synthesis of a fluorescent material. ChemSusChem, **2011**, 4, pp. 51-54.

[128] J. Zhao, X. Chen, Y. Du, Y. Yang, J.M. Lee, Vanadium-embedded mesoporous carbon microspheres as effective catalysts for selective aerobic oxidation of 5-hydroxymethyl-2-furfural into 2, 5-diformylfuran. Applied Catalysis A: General, **2018**, 568, pp. 16-22.

[129] I. Sádaba, Y.Y. Gorbanev, S. Kegnæ, S.S. Putluru, R.W. Berg, A. Riisager, Catalytic performance of zeolite-supported vanadia in the aerobic oxidation of 5-hydroxymethylfurfural to 2, 5-diformylfuran. ChemCatChem, **2013,** 5, pp. 284-293.

[130] C. Moreau, R. Durand, C. Pourcheron, D. Tichit, Selective oxidation of 5-hydroxymethylfurfural to 2, 5-furan-dicarboxaldehyde in the presence of titania

supported vanadia catalysts. Studies in Surface Science and Catalysis, **1997**, 108, pp. 399-406.

[131] A.L. Cánepa, C.M. Chanquía, V.M. Vaschetti, G.A. Eimer, S.G. Casuscelli, Biomass toward fine chemical products: Oxidation of α-pinene over sieves nanostructured modified with vanadium. Journal of Molecular Catalysis A: Chemical, **2015**, 404, pp. 65-73.

[132] Y. Ma, Z. Du, J. Liu, F. Xia, J. Xu, Selective oxidative C–C bond cleavage of a lignin model compound in the presence of acetic acid with a vanadium catalyst. Green Chemistry, **2015**, 17, pp. 4968-4973.

[133] J. Filley, C. Roth, Vanadium catalyzed guaiacol deoxygenation. Journal of Molecular Catalysis A: Chemical, **1999**, 139, pp. 245-252.

[134] S. Son, F.D. Toste, Non-oxidative vanadium-catalyzed C-O bond cleavage: Application to degradation of lignin model compounds. Angewandte Chemie International Edition, **2010**, 49, pp. 3791-3794.

[135] E. Kantarelis, W. Yang, W. Blasiak, Effects of silica-supported nickel and vanadium on liquid products of catalytic steam pyrolysis of biomass. Energy & Fuels, **2014**, 28, pp. 591-599.

[136] B.S. Kim, C.S. Jeong, J.M. Kim, S.B. Park, S.H. Park, J.K. Jeon, S.C. Jung, S.C. Kim, Y.K. Park, Ex situ catalytic upgrading of lignocellulosic biomass components over vanadium contained H-MCM-41 catalysts. Catalysis Today, **2016**, 265, pp. 184-191.

[137] Y. Li, J.N. Armor, Selective NH_3 oxidation to N_2 in a wet stream. Applied Catalysis B: Environmental, **1997**, 13, pp. 131-139.

[138] T. Pignet, L.D. Schmidt, Kinetics of NH_3 oxidation on Pt, Rh, and Pd. Journal of Catalysis, **1975**, 40, pp. 212-225.

[139] L. Gang, J. van Grondelle, B.G. Anderson, R.A. van Santen, Selective low temperature NH_3 oxidation to N_2 on copper-based catalysts. Journal of Catalysis, **1999**, 186, pp. 100-109.

[140] L. Gang, B.G. Anderson, J. van Grondelle, R.A. van Santen, NH_3 oxidation to nitrogen and water at low temperatures using supported transition metal catalysts. Catalysis Today, **2000**, 61, pp. 179-185.

[141] C.G. Vayenas, H.M. Saltsburg, Chemistry at catalytic surfaces: The SO_2 oxidation on noble metals. Journal of Catalysis, **1979**, 57, pp. 296-314.

[142] H. Tseng, M. Wey, C. Fu, Carbon materials as catalyst supports for SO_2 oxidation: catalytic activity of CuO–AC. Carbon, **2003**, 41, pp. 139-149.

[143] H. Kamata, H. Ohara, K. Takahashi, A. Yukimura, Y. Seo, SO_2 oxidation over the V_2O_5/TiO_2 SCR catalyst. Catalysis Letters, **2001**, 73, pp. 79-83.

[144] I. Amon-Mézière, F. Castagna, M. Prigent, A. Pentenero, Speciated hydrocarbon conversion on a fresh Pd/Rh three-way catalyst. SAE Technical Paper 950932, **1995**.

[145] J.J. Spivey, Complete catalytic oxidation of volatile organics. Industrial & Engineering Chemistry Research, **1987**, 26, pp. 2165-2180.

[146] A.S. Bodke, D.A. Olschki, L.D. Schmidt, E. Ranzi, High selectivities to ethylene by partial oxidation of ethane. Science, **1999**, 285, pp. 712.

[147] M.A. Pepera, J.L. Callahan, M.J. Desmond, E.C. Milberger, P.R. Blum, N.J. Bremer, Fundamental study of the oxidation of butane over vanadyl pyrophosphate. Journal of the American Chemical Society, **1985**, 107, pp. 4883-4892.

[148] M.M. Bettahar, G. Costentin, L. Savary, J.C. Lavalley, On the partial oxidation of propane and propylene on mixed metal oxide catalysts. Applied Catalysis A: General, **1996**, 145, pp. 1-48.

[149] S.Y. Shen, T.S. Zhao, J.B. Xu, Y.S. Li, Synthesis of PdNi catalysts for the oxidation of ethanol in alkaline direct ethanol fuel cells. Journal of Power Sources, **2010**, 195, pp. 1001-1006.

[150] J. Peral, D.F. Ollis, Heterogeneous photocatalytic oxidation of gas-phase organics for air purification: acetone, 1-butanol, butyraldehyde, formaldehyde, and m-xylene oxidation. Journal of Catalysis, **1992**, 136, pp. 554-565.

[151] L. Ning, S. Liao, Y. Sun, L. Yu, X. Tong, The efficient oxidation of biomass-derived 5-hydroxymethyl furfural to produce 2, 5-diformylfuran over supported cobalt catalysts. Waste and Biomass Valorization, **2018**, 9, pp. 95-101.

[152] L. Ding, W. Yang, L. Chen, H. Cheng, Z. Qi, Fabrication of spinel $CoMn_2O_4$ hollow spheres for highly selective aerobic oxidation of 5-hydroxymethylfurfural to 2,5-diformylfuran. Catalysis Today, **2020**, 347, pp. 39-47

[153] Y. Wang, B. Liu, K. Huang, Z. Zhang, Aerobic oxidation of biomass-derived 5-(hydroxymethyl)furfural into 2,5-diformylfuran catalyzed by the trimetallic mixed oxide (Co–Ce–Ru). Industrial & Engineering Chemistry Research, **2014**, 53, pp. 1313-1319.

[154] W. Zhang, J. Xie, W. Hou, Y. Liu, Y. Zhou, J. Wang, One-pot template-tree synthesis of Cu–MOR zeolite toward efficient catalyst support for aerobic oxidation of 5-hydroxymethylfurfural under ambient pressure. ACS Applied Materials & Interfaces, **2016**, 8, pp. 23122-23132.

[155] M. Ventura, M. Aresta, A. Dibenedetto, Selective aerobic oxidation of 5-(hydroxymethyl)furfural to 5-formyl-2-furancarboxylic acid in water. ChemSusChem, **2016**, 9, pp. 1096-1100.

[156] C. Yang, X. Li, Z. Zhang, B. Lv, J. Li, Z. Liu, W. Zhu, F. Tao, G. Lv, Y. Yang, High efficient catalytic oxidation of 5-hydroxymethylfurfural into 2,5-furandicarboxylic acid under benign conditions with nitrogen-doped graphene encapsulated Cu nanoparticles. Journal of Energy Chemistry, **2020**, 50, pp. 96-105.

[157] E. Hayashi, Y. Yamaguchi, K. Kamata, N. Tsunoda, Y. Kumagai, F. Oba, M. Hara, Effect of MnO_2 crystal structure on aerobic oxidation of 5-hydroxymethylfurfural to 2,5-furandicarboxylic Acid. Journal of the American Chemical Society, **2019**, 141, pp. 890-900.

[158] H. Zhou, H. Xu, Y. Liu, Aerobic oxidation of 5‑hydroxymethylfurfural to 2,5-furandicarboxylic acid over Co/Mn-lignin coordination complexes-derived catalysts. Applied Catalysis B: Environmental, **2019**, 244, pp. 965-973.

[159] X. Han, C. Li, X. Liu, Q. Xia, Y. Wang, Selective oxidation of 5-hydroxymethylfurfural to 2,5-furandicarboxylic acid over MnO_x–CeO_2 composite catalysts. Green Chemistry, **2017**, 19, pp. 996-1004.

[160] A.S. Amarasekara, D. Green, E. McMillan, Efficient oxidation of 5-hydroxymethylfurfural to 2,5-diformylfuran using Mn(III)–salen catalysts. Catalysis Communications, **2008**, 9, pp. 286-288.

[161] K.T. Rao, J.L. Rogers, S. Souzanchi, L. Dessbesell, M.B. Ray, C. Xu, Inexpensive but highly efficient Co–Mn mixed-oxide catalysts for selective oxidation of 5-hydroxymethylfurfural to 2,5-furandicarboxylic acid. ChemSusChem, **2018**, 11, pp. 3323-3334.

[162] Z. Gui, S. Saravanamurugan, W. Cao, L. Schill, L. Chen, Z. Qi, A. Riisager, Highly selective aerobic oxidation of 5-hydroxymethylfurfural into 2,5-diformylfuran over Mn–Co binary oxides. Chemistry Select, **2017**, 2, pp. 6632-6639.

[163] K. Gupta, R.K. Rai, A.D. Dwivedi, S.K. Singh, Catalytic aerial oxidation of biomass-derived furans to furan carboxylic acids in water over bimetallic nickel–palladium alloy nanoparticles. ChemCatChem, **2017**, 9, pp. 2760-2767.

[164] R. Latsuzbaia, R. Bisselink, A. Anastasopol, H. van der Meer, R. van Heck, M.S. Yagüe, M. Zijlstra, M. Roelands, M. Crockatt, E. Goetheer, E. Giling, Continuous electrochemical oxidation of biomass derived 5-(hydroxymethyl)furfural into 2,5-furandicarboxylic acid. Journal of Applied Electrochemistry, **2018**, 48, pp. 611–626.

[165] R. Noma, K. Nakajima, K. Kamata, M. Kitano, S. Hayashi, M. Hara, Formation of 5-(hydroxymethyl)furfural by stepwise dehydration over TiO_2 with water-tolerant Lewis acid sites. The Journal of Physical Chemistry C, **2015**, 119, pp. 17117-17125.

[166] L. Atanda, S. Mukundan, A. Shrotri, Q. Ma, J. Beltramini, Catalytic conversion of glucose to 5-hydroxymethyl-furfural with a phosphated TiO_2 catalyst. ChemCatChem, **2015**, 7, pp. 781-790.

[167] S. De, S. Dutta, A.K. Patra, A. Bhaumik, B. Saha, Self-assembly of mesoporous TiO_2 nanospheres via aspartic acid templating pathway and its catalytic application for 5-hydroxymethyl-furfural synthesis. Journal of Materials Chemistry, **2011**, 21, pp. 841-849.

[168] A. Chareonlimkun, V. Champreda, A. Shotipruk, N. Laosiripojana, Catalytic conversion of sugarcane bagasse, rice husk and corncob in the presence of TiO_2, ZrO_2 and mixed-oxide TiO_2–ZrO_2 under hot compressed water (HCW) condition. Bioresource Technology, **2010**, 101, pp. 4179-4186.

[169] H. Li, A. Deng, J. Ren, C. Liu, W. Wang, F. Peng, R. Sun, A modified biphasic system for the dehydration of d –xylose into furfural using SO_4^{2-}/TiO_2-ZrO_2/La^{3+} as a solid catalyst. Catalysis Today, **2014**, 234, pp. 251-256.

[170] H. Li, W. Wang, J. Ren, F. Peng, R. Sun, Preparation and characterization of SO_4^{2-}/TiO_2-ZrO_2/La^{3+} and their photocatalytic performance for the dehydration of xylose to furfural. Journal of Biobased Materials and Bioenergy, **2014**, 8, pp. 50-58.

CHAPTER 3

Experimental Design and Methods

3.1 Materials and reagents

All reagents and materials were used as received without purification. The inorganic metal precursors, tin oxalate (SnC_2O_4; 98%), vanadyl (II) acetylacetonate ($VO(acac)_2$; copper (II) nitrate trihydrate ($Cu(NO_3)_2 \cdot 3H_2O$; 99%), cobalt (II) nitrate hexahydrate ($Co(NO_3)_2 \cdot 6H_2O$; 99.999%), manganese (II) nitrate tetrahydrate ($Mn(NO_3)_2 \cdot 4H_2O$; 98%), nickel (II) nitrate hexahydrate ($Ni(NO_3)_2 \cdot 6H_2O$; 99.999%), and titanium isopropoxide ($Ti[OCH(CH_3)_2]_4$, 97%) were all purchased from Sigma-Aldrich (South Africa). Ammonium hydroxide ($NH_3 \cdot H_2O$, 28% in water) and hydrogen peroxide (H_2O_2, 30% and 50% in water) were also purchased from Sigma-Aldrich (South Africa).

The following organic compounds; oxalic acid dehydrate (≥ 99%), maleic acid (≥ 99%), maleic anhydride (99%), fumaric acid (≥ 99%), succinic acid (≥ 99%), 2-furoic acid (98%), 2-(5H)-furanone (98%), 5-hydroxymethylfurfural (99%) and furfural (99%) purchased from Sigma-Aldrich (South Africa) were used to prepare standard solutions for HPLC product identification and quantification.

The organic chemicals, toluene (anhydrous, 99.8%), dimethylformamide (DMF; 99%), 1,4-dioxane (≥ 99.5%), benzyl alcohol (BA; ≥ 99%), polyvinylpyrrolidone (10 000 mol wt), γ-valerolactone (99.9%), isobutanol (≥ 99%), 1,4-dioxane (≥ 99.5%), dimethylformamide (DMF; 99%), tetrahydrofuran (THF; anhydrous, ≥99.9%), toluene (anhydrous, 99.8%), dimethyl sulfoxide (DMSO, ≥ 99.9%) and ethyl acetate (anhydrous, 99.8%) were also purchased from Sigma-Aldrich (South Africa). The deionized water produced from a Meck

Milli-Q water purification system (Millipore) was used for catalyst preparation, washing and also as reaction solvent. Acetonitrile (≥ 99.9%), acetic acid (glacial, 100%), and formic acid (98-100%) all analytical grade were purchased from Merck (South Africa). The following solvents: acetone (≥ 99.5%), methanol and ethanol (both 99.9%), ethylene glycol (AR grade), and dichloroethane (AR grade); were all purchased from Minema Chemicals (South Africa).

3.2 Synthesis of heterostructured SnO_2 nanocatalysts

3.2.1 Synthesis of hetero-mixed VO_x-SnO_2 nanocatalysts

The heterostructure VO_x-SnO_2 catalysts were prepared via a surfactant-free sol-gel method as shown in **Fig. 3-1**. A series of VO_x-SnO_2 catalysts were prepared with vanadium loading ranging from 5 to 30 wt% by dissolving (separately) the appropriate amounts of tin oxalate and vanadyl acetylacetonate each in 40 mL of benzyl alcohol in 100 mL round-bottom flasks and sonicated for 30 min to dissolve. The two solutions were then mixed in 250 mL round-bottom flask fitted with a magnetic stirrer bar and this mixture was further stirred for 30 min on a magnetic stirrer to homogenize and 10 mL of ammonium hydroxide was then added. The resultant precipitate was aged at room temperature for 8 h then transferred to another 250 mL round-bottom flask and heated under reflux for 20 h at 180 °C. The resultant reaction mixture was allowed to cool to room temperature then collected and washed two times with acetone and twice more with deionised water by centrifuge.
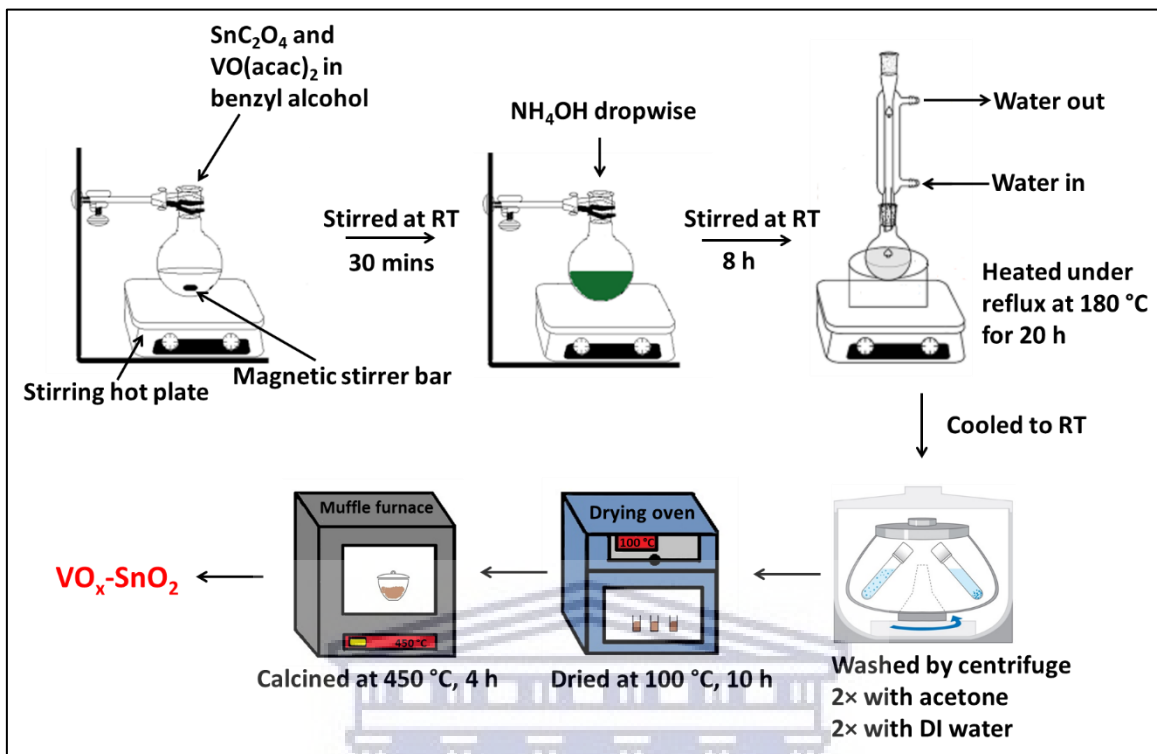
Fig. 3-1: Schematic representation of the surfactant-free sol-gel procedure for preparing VO$_x$-SnO$_2$ nanocatalysts.

The supernatant was then dried in an oven at 100 °C for 10 h and the powder sample calcined in air in a muffle furnace at a rate of 3 °C/min from room temperature to 450 °C and held at 450 °C for 4 h. Pure SnO$_2$ and V$_2$O$_5$ were prepared following the same procedure. The synthesised heterostructure VO$_x$-SnO$_2$ catalyst materials were denoted as VSn-1, VSn-2, VSn-3, VSn-4, VSn-5 and VSn-6, respectively corresponding to nominal loadings of 5, 10, 15, 20, 25 and 30 wt% vanadium dispersed onto the SnO$_2$ support.

3.2.2 Synthesis of SnO$_2$-M (M= Co, Cu, Ni Mn) nanocatalysts

For preparation of the heterostructure metal oxide (MO$_x$)-SnO$_2$ catalysts, 3 mmol (6.2019 g) of SnC$_2$O$_4$ was added to 80 mL of BA into a 250 mL round-bottom flask and stirred for 30 min to dissolve completely. Then, the respective metal salts of Cu, Co, Mn and Ni were

added to give 20 wt% loading of the metals onto SnO_2 composite mixture. After addition of respective base metals salts with continuous stirring for 30 min, the solution mixture was precipitated with $NH_3 \cdot H_2O$ to adjust the pH to 9. The resultant precipitate solid slurries were stirred at room temperature for 2 h, thereafter the reaction temperature was raised to 160 °C for 20 h under reflux with continuous stirring. After 20 h, the reaction mixture was stopped and allowed to cool to room temperature, then collected and washed three times with the mixture of acetone/deionized water (50%/50%; v/v) by centrifuge. The final washed solids were then dried in an oven at 100 °C for 12 h, followed by calcination in a muffle furnace under air condition at a heating rate of 3 °C/min from 30 to 400 °C and held at 400 °C for 4 h. The synthesized heterostructure MO_x-SnO_2 catalysts were denoted as CoO_x-SnO_2, CuO_x-SnO_2, MnO_x-SnO_2, and NiO_x-SnO_2, respectively. Further, the pure SnO_2 was also synthesized following the same procedure.
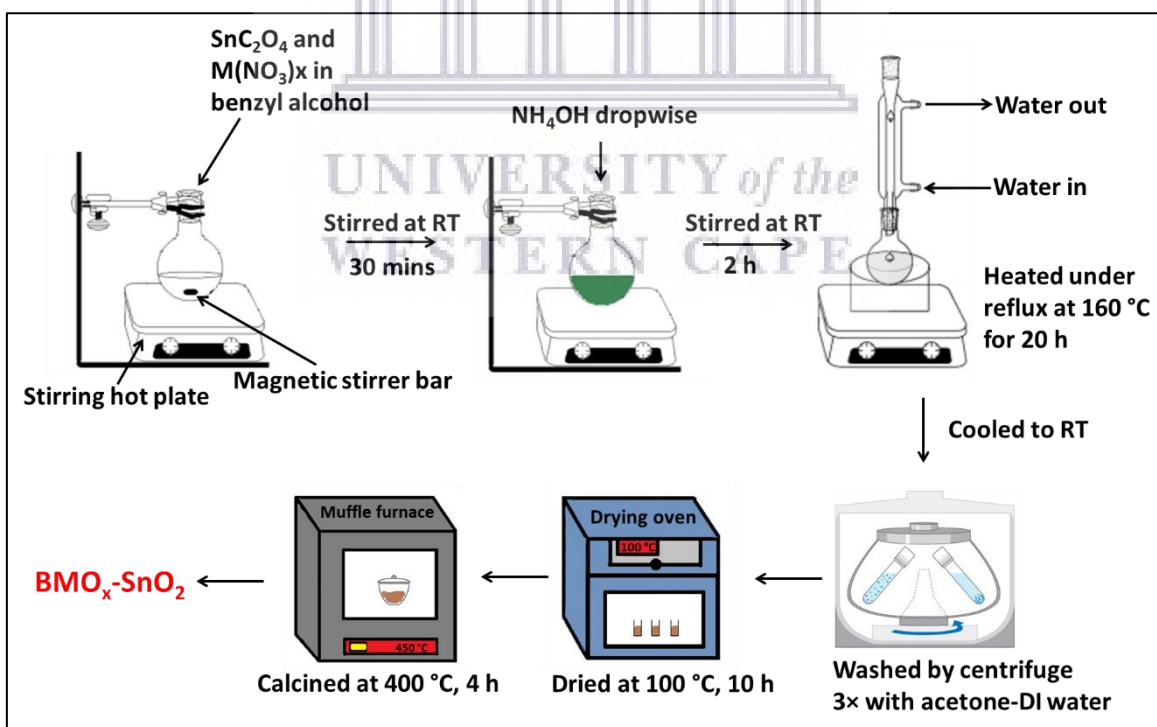
Fig. 3-2: Schematic representation of the procedure for preparing the base metal doped SnO_2 heterostructure catalysts.

3.2.3 Synthesis of TiO$_2$-SnO$_2$ nanocatalysts

The synthesis of the heterostructured TiO$_2$-SnO$_2$ nanocatalysts was carried by a microwave-assisted method through the following procedure outlined in **Fig. 3-3**. 8.42 mmol (1.0 g) of SnC$_2$O$_4$ was dissolved in an 80 mL solvent mixture of ethanol and ethylene glycol (3:2, v/v) in a 250 mL round-bottom flask by stirring for 30 min. Then, 20.89 mmol (1.0 g) of titanium isopropoxide was added to this solution and the mixture was stirred for a further 30 min to homogenize. The solution mixture was precipitated with NH$_3$·H$_2$O to adjust the pH to 9. The resultant precipitate solid slurries were stirred at room temperature for 4 h and thereafter transferred to 80 mL Teflon vessels, which were then transferred to a microwave oven and irradiated at 1200 W from room temperature to 180 °C in 15 min and held at 180 °C for 15 min. The reaction mixture was allowed to cool to room temperature, then collected and washed three times with the mixture of ethanol/deionized water (50%/50%; v/v) by centrifuge. The mixture contain Ti and Sn in composition ratio of 1:1. Other compositions of Ti:Sn such as 0:1, 1:0, 4:1 and 1:4 were respectively prepared.

The resultant final washed solids were then dried in an oven at 100 °C for 12 h, followed by calcination in a muffle furnace under air condition at a heating rate of 3 °C/min from 30 to 500 °C and held at 500 °C for 4 h. The synthesized heterostructure TiO$_2$-SnO$_2$ nanocatalysts were denoted as Ti1Sn4, Ti1Sn1, and Ti4Sn1 corresponding to TiO$_2$ loadings of 25%, 50% and 75% (wt%), respectively. Further, pristine SnO$_2$ and TiO$_2$ oxides were also synthesized following the same procedure.
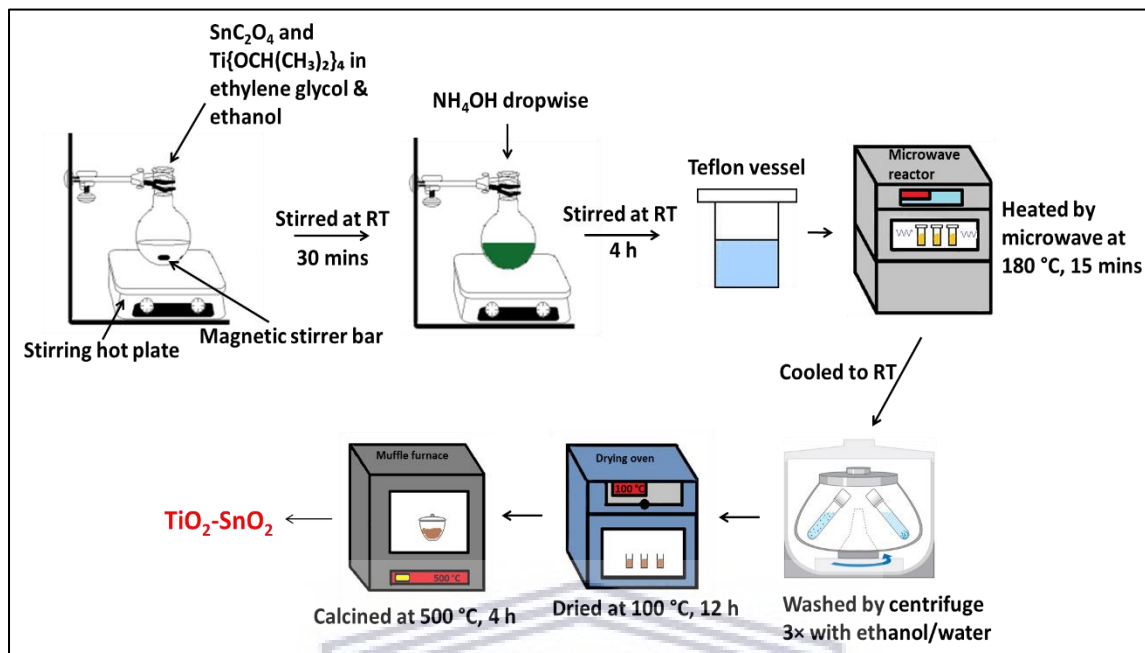
Fig. 3-3: Schematic outline of the procedure for microwave-assisted synthesis of TiO$_2$-SnO$_2$ heterostructure catalysts.

3.3 Characterization of catalysts

3.3.1 Nitrogen sorption analysis

To determine the textural properties of the catalyst materials, BET surface area, pore diameter and volume measurements were conducted on a Micromeritics TRISTAR 3000 surface area analyzer employing N$_2$ physisorption at -196 °C without degassing.

3.3.2 X-Ray diffraction analysis

Powder X-Ray diffraction (XRD) patterns of the catalysts were measured in order to determine the crystal structure and phases compositions of the heterostructure SnO$_2$ catalyst materials. XRD measurements were run on a PANalytical X'Pert PRO diffractometer with a Ni-filtered Cu K$_\alpha$ radiation of 0.1542 nm wavelength. The diffractometer was operated at a voltage of 45 kV and a current of 40 mA. The samples

were scanned at a 5 - 90 ° range with a scan speed of 0.02 °/s. The average crystallite size of the nanoparticles was determined using the Debye-Scherrer equation:

$$D = \frac{k\lambda}{\beta cos\theta}$$

where λ is the radiation of wavelength, β is the full width at half maximum (FWHM) of the most intense diffraction peak, θ is the Bragg angle and *k* is the shape factor (0.89 for spherical particles).

3.3.3 Photoluminescence spectroscopy analysis

The optical properties of the nanocatalysts were determined using a Jobin-Yvon Nanolog® Pulsed laser photoluminescence (PL) spectrometer operated at an excitation wavelength of 325 nm. The emission peaks were collected in wavelength region 350-1000 nm. Sample preparation was carried out by dispersing the samples (10mg) in ethanol (~10 mL) then sonicating for 30 min.

3.3.4 Transmission electron microscopy analysis

Transmission electron microscopy (TEM) and high resolution transmission electron microscopy (HRTEM) analysis was performed to determine the morphology and nanostructure of the catalysts. TEM and HRTEM images as well as selected area electron diffraction (SAED) patterns of the samples were captured with a JEOL JEM-2100 microscope operating at a voltage of 200 kV and beam current of 110 µA. The high-angle annular dark-field scanning transmission electron microscopy (HAADF-STEM) images and elemental mappings were performed employing the attached respective HAADF-STEM and energy dispersive X-ray spectroscopy (EDX) detectors. Sample preparation

was carried out by dispersing the samples (~ 5 mg) in ethanol (~2 mL) then sonicating for 30 min before mounting on carbon-coated copper grids.

3.3.5 Scanning electron microscopy analysis

Scanning electron microscopy (SEM) analysis was performed to analyse the morphology, microstructure and elemental composition of the synthesised catalysts. SEM and (EDX) analysis of the samples were carried out on a ZEISS Auriga Cobra FIB Field emission SEM microscope equipped with an X-Man Silicon Drift EDS detector operated at 3 kV for imaging and 15 kV for EDX analysis. Samples were prepared by loading a small amount (~ 5 mg) onto specimen stubs using carbon tape and coated with carbon to prevent charging during analysis.

3.3.6 Fourier transform infrared spectroscopy analysis

Fourier transform infrared spectroscopy analysis (FTIR) spectroscopy analysis of the samples was performed on a Perkin Elmer Spectrum100 spectrometer using the Attenuated Total Reflectance (ATR) technique applying a germanium crystal. The analysis was performed to reveal the chemical fingerprint and functional groups present on the nanocomposite catalysts. The selected range of the infrared radiation was 4000 - 500 cm^{-1} at a spatial resolution of 8 cm^{-1} using 32 scans.

3.3.7 X-ray photoelectron spectroscopy (XPS) analysis

X-ray photoelectron spectroscopy (XPS) analysis was carried to study the nature of interactions, elemental chemical state and electronic structure in the heterostructure composite nanocatalysts. X-ray photoelectron spectroscopy (XPS) analysis was performed using a PHI 5000 scanning ESCA Microprobe spectrometer. The instrument

was operated at a source power of 10 kV and 5 mA with an analysis chamber pressure lower than 10^{-8} Pa. The survey scans were performed at a 1 eV step size from -10 eV to 1350 eV and the high resolution scans at a step size of 0.2 eV. The binding energy (BE) positions of were corrected using the C1s contamination carbon peak (284.60 eV). The XPS high resolution data was deconvoluted using the Gaussian method by first removing the Shirley background.

3.3.8 Electron paramagnetic resonance spectroscopy analysis

A JEOL X-band JES FA 200 electron paramagnetic resonance (EPR) spectrometer operating at 9.4 GHz at room temperature was used to analyse the paramagnetic defects of the catalysts. The magnetization analyses were extracted at room temperature employing a Lakeshore 735 vibrating sample magnetometer (VSM).

3.3.9 Hydrogen temperature-programmed reduction (H$_2$-TPR) analysis

H$_2$-TPR studies were performed on a Micromeritics Autochem AC2920 apparatus (USA; Atlanta, Norcross) gaseous mixture of 10% H$_2$/Ar at a heating rate of 10 °C/min from 50 to 1000 °C and total gas flow rate of 50 mL/min. A calibrated thermal conductivity detector (TCD) monitored the H$_2$ consumption. Prior to TPR analysis, the samples were prepared to remove moisture under an argon gas flow at 70 °C for 1 h.

3.4 Procedure for oxidation of furfural and HMF and products analysis

This section describes the general procedures followed for the oxidation of both furfural HMF. The actual amount of substrate, oxidant, solvent and catalyst utilized are provided in the relevant results figure captions and table footnotes.

3.4.1 Procedure for small-scale batch oxidation of furfural and HMF

The oxidation reaction of furfural and 5-hydroxymethylfurfural was carried out in a 25/50 mL round-bottom flask fitted with a magnetic stirrer bar and a reflux condenser (**Fig. 3-4**). Furfural/5-hydroxymethylfurfural, catalyst and solvent were placed in the flask and aqueous H_2O_2 was added to the mixture. The flask was then quickly sealed and placed in a sand-bath preheated to the reaction temperature with a heating mantle. This mixture was then vigorously stirred at 700 rpm and kept at constant temperature for the duration of the reaction. The reaction was then stopped and allowed to cool before a small aliquot of the products was sampled for analysis using high-pressure liquid chromatography (HPLC).
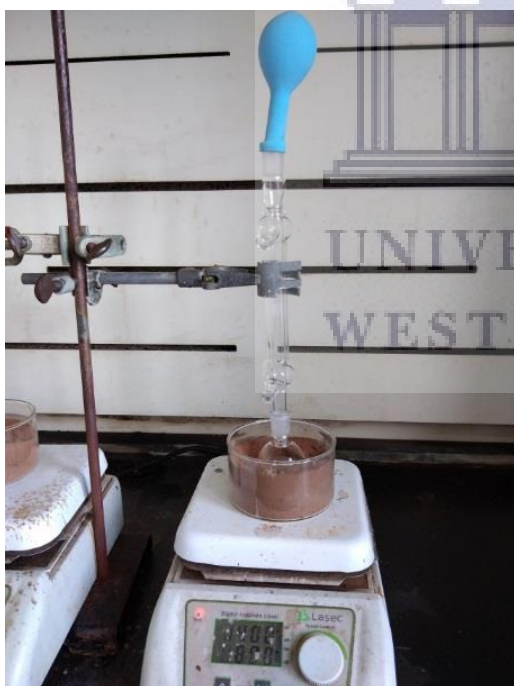
Fig. 3-4: Experimental setup for small-scale batch oxidation of furfural and 5-hydroxymethylfurfural.

3.4.2 Procedure for batch oxidation of furfural

The batch oxidation of furfural was carried out in Radleys Reactor-Ready 100 mL glass lab batch bench top reactor equipped with a reflux condenser, a Heidolph RZR 2020 overhead stirrer, and a Julabo F32-HE refrigerated - heating circulator (**Fig. 3-5**). For the oxidation procedure, the heating circulator was set at 75 °C and allowed to stabilize before adding furfural, catalyst and solvent into the reactor. This mixture heated to the reaction temperature for 10 minutes while stirring, thereafter aqueous H_2O_2 was added to the mixture to start the reaction. The reaction mixture was then vigorously stirred with the overhead stirrer set at level 6 and kept at constant temperature for the duration of the reaction. The reaction was then stopped and allowed to cool before a small aliquot of the products was sampled for analysis using HPLC.

Fig. 3-5: Experimental setup for batch oxidation of furfural using a glass batch reactor.

3.4.3 Procedure for batch microwave-assisted oxidation of furfural

The batch microwave-assisted oxidation of furfural was performed using the microwave reactor employed for the synthesis of the TiO_2-SnO_2 nanocatalysts (**section 3.2.3**). Furfural, catalyst and solvent were placed into a 80 mL Teflon vessel. Immediately after the addition of aqueous H_2O_2, the vessel was quickly sealed and transferred to a microwave reactor and irradiated at 1200 W from room temperature to 100 °C in 10 min and held at 100 °C for 20 min. The reaction was then stopped and allowed to cool before a small aliquot of the products was sampled for analysis using high-pressure liquid chromatography (HPLC).

3.4.4 Procedure for analysis of oxidation products

The oxidation products were analysed using a high pressure liquid chromatography (HPLC-Thermo Scientific, UltiMate 3000) system with photodiode array detector (PDA) (254 nm and 280 nm) and refractive index (RI) detectors and equipped with a BioRAD Aminex HPX-87H column (300 × 7.8 mm) operated at 45 °C. The eluent was a solution of H_2SO_4 (0.0005 M) at a flow rate of 0.7 mL.min^{-1}. The wavelength of 284 nm was chosen for the PDA because furfural is more responsive at 284 nm than at 254 nm. The substrate conversion rate, product yield and selectivity were calculated according to the following equations:

$$Conversion\ (mol\ \%) = \frac{n^o_{substrate} - n_{substrate}}{n^o_{substrate}} \times 100$$

$$Yield\ (mol\ \%) = \frac{n_{product}}{n^o_{substrate}} \times 100$$

$$Selectivity\ (\%) = \frac{yield}{conversion} \times 100$$

where $n^o_{substrate}$ refers to the mole quantity of the substrate initially loaded reaction flask, $n_{substrate}$ and $n_{product}$ correspond to the respective mole quantity of the substrate and products at any given time. The HPLC retention times determined with standard solutions of authentic samples were 4.8 min for oxalic acid, 6.9 min for maleic acid, 12.8 min for fumaric acid, 13.8 min for succinic acid, 8.3 min for formic acid, 20.2 min for 2-furoic acid, 22.1 min for 2-(5H)-furanone and 35.6 for furfural.

CHAPTER 4

Nanostructured VO$_x$-SnO$_2$ Catalyst for Maleic Acid Synthesis

4.1 Introduction

The growing use of biomass in recent times has been tipped as an ideal alternative to fossil-fuel based resources due to its readily availability as renewable and environmentally-friendly carbon source for the production of organic chemical derivatives and chemical fuel energy.[1-3] Furfural, a derivative of C$_5$ sugar (xylose) obtained from lignocellulosic biomass, is one of the critical building-block platform chemical that can undergo a variety of organic chemical transformations into several value-added chemicals.[4,5] The liquid- or vapour-phase oxidation of furfural provides an alternative route for the synthesis of bio-based renewable maleic acid and maleic anhydride which are important intermediates or monomers for the manufacturing of unsaturated polyester resins, surface coatings, vinyl copolymers, lubricant additives, and plasticizers.[6,7] Currently, maleic anhydride is produced on the industrial scale by the vapour-phase oxidation of n-butane and benzene using vanadium-based catalysts.[8] The synthesis of both maleic acid and maleic anhydride are inter-convertible reactions via the dehydration and hydration reactions processes, thus the production of one infers the availability of the other.[9-11]

Whilst maleic anhydride is preferably produced through the vapour-phase oxidation of furfural using molecular oxygen, maleic acid can be produced in both the vapour- and liquid-phases using O$_2$ or H$_2$O$_2$ as oxidants. The gas-phase oxidation of furfural to maleic anhydride was recently demonstrated by Lan et.al[12] along with their mechanistic studies using molecular O$_2$ as an oxidant. The liquid-phase oxidation to maleic acid with O$_2$ has

been most recently investigated by Soták et al.[13] using a copper phosphate catalyst, following the earlier work of Guo and Yin.[14,15] The liquid-phase oxidation to maleic acid with H_2O_2 was demonstrated by Alonso-Fagúndes et al.[16] using TS-1 as a catalyst. Wojcieszak et al.[17] reviewed the recent developments in the synthesis of renewable maleic acid from biomass chemicals using both homogenous and heterogeneous catalysts, respectively. Generally, the main drawback with these catalysts is low selectivity, and other related issues such as low feed volumes (for gas-phase oxidations), poor catalyst stability and recyclability with respect to the homogeneous based catalysts. There have been few reports on furfural oxidation using vanadium-based catalysts.[18-20] Unfortunately, these catalytic systems required the gas-phase furfural oxidation conditions to give mainly maleic anhydride product.

Based on the studies of the developed catalysts to date in the oxidation of furfural, the quest to design recyclable and active solid catalysts that could improve on both selectivity and yields of maleic acid under mild reaction conditions is still on-going. The combination of relatively cheap and abundant V_2O_5 and SnO_2 designed as nanostructured mixed oxide is proposed as ideal to afford an active and selective catalyst for furfural oxidation to the desirable maleic acid. This envisaged catalytic activity effect is prompted by the previous good catalytic activity displayed by the supported V_2O_5 in various oxidation reactions, which was ascribed to the reactive redox character of V_2O_5 based on multiple oxidation states of $V^{5+}/V^{4+}/V^{3+}$.[21-23] On the other hand, SnO_2 on its own has shown poor oxidation activity in the liquid-phase reaction due to its low or slow redox reactivity. However, mixing SnO_2 with other transition metal oxide or using it as a catalyst support has been shown to be very effective for certain oxidation reactions.[24-27] Therefore, a highly active redox

catalyst can be produced by taking advantage of the Lewis acid sites and redox nature of SnO$_2$ (Sn^{4+}/Sn^{2+}) coupled to that of V$_2$O$_5$.

In this chapter, the surfactant-free polyol synthesis of heterostructured VO$_x$-SnO$_2$ nanocatalysts and their catalytic investigation in furfural and 5-hydroxymethylfurfural oxidation to maleic acid using hydrogen peroxide (H$_2$O$_2$) oxidant is reported. Several oxidation reaction parameters such as the effects of solvent, oxidant concentration and dosage, catalyst dosage and temperature were studied with the aim of optimizing the maleic acid yield and selectivity. The leaching of the catalyst active sites was also investigated to ascertain the stability of the catalyst.

4.2 Characterisation of the catalyst structure

4.2.1 Nitrogen sorption analysis

The average surface areas (S_{BET}), pore diameter (D_p) and volume (V_p) analysis results obtained from nitrogen sorption of the heterostructured VO$_x$-SnO$_2$ catalysts are summarized in **Table 4-1** and the corresponding adsorption-desorption isotherms are in **Fig. 4-1**.

Table 4-1: Textural and physical characterization data of the heterostructured VO$_x$-SnO$_2$ catalysts.								
Catalysts	SnO$_2$	V$_2$O$_5$	VSn-1	VSn-2	VSn-3	VSn-4	VSn-5	VSn-6
S_{BET} (m^2/g)	111.3	15.42	93.8	88.5	85.8	74.0	30.6	18.4
D_p (nm)	5.2	16.0	6.07	5.8	7.3	9.1	11.0	14.3
V_p (cm³/g)	0.20	0.06	0.12	0.11	0.17	0.11	0.11	0.05
[a] Crystallite size (nm)	22.2	257.3	11.1	20.8	23.8	27.8	16.7	19.1
[b] V metal loading (wt%)	N/A	-	3.8	9.3	14.4	18.8	23.9	28.1
[c] Surface V atomic %	-	27.8	2.2	6.3	7.2	5.3	9.6	6.8
[c] Surface Sn atomic %	21.5	-	26.0	23.4	21.3	20.2	16.4	14.2
[c] Surface O atomic %	78.5	72.2	70.8	70.3	71.5	74.5	74.0	79.0
Surface V/actual V	-	-	0.58	0.68	0.50	0.28	0.40	0.24

[a] For SnO$_2$ phase estimated from XRD using Scherrer equation. [b] ICP analysis. [c] XPS analysis.

The synthesized SnO_2 possessed a S_{BET} of 111.3 m^2/g and V_2O_5 of 15.42 m^2/g. The V_p of the SnO_2 (0.20 cm³/g) was also larger than that of V_2O_5 (0.06 cm³/g). However, the V_2O_5 appeared to be more porous with a D_p of 16.07 nm, larger than that of SnO_2 of 9.23 nm. For heterostructured catalysts the S_{BET} decreased relatively with the increasing amount of vanadium metal loadings onto SnO_2 oxide from 5 wt% (93.8 m^2/g) for VSn-1 to 30 wt% (18.4 m^2/g) for VSn-6 (**Table 4-1**). The V_p of the heterostructured VO_x-SnO_2 catalysts showed to be within the range of 0.05 – 0.17 cm^3/g, with the VSn-3 catalyst displaying the highest V_p and the VSn-6 catalyst the smallest. The pore sizes distribution varied significantly over a broad range of 5 -100 nm with respect to increase in V-metal loadings. The decrease in S_{BET} with increasing vanadium content could be related to the crystallinity of the heterostructure catalysts (which also decreases with increasing vanadium loading). There is no systematic trend observed with regards to D_p and V_p. The largest D_p was observed on the VSn-5 catalyst and the smallest on the VSn-2 catalyst with all the catalysts being mesoporous. In terms of V_p, the largest and smallest volumes were observed on the VSn-3 and VSn-6 catalysts, respectively. The pore size distribution plots of the prepared catalysts are presented in **Fig. A-1** (**Appendix A**). The isotherms of all the catalysts present as type IV with classified H2 hysteresis loops characteristic of mesoporous materials according to the IUPAC physisorption isotherms classification guidelines.[28] This type of isotherm is indicative of agglomerates arranged in a fairly uniform way that have pores with narrow mouths and relatively uniform channel-like pores.
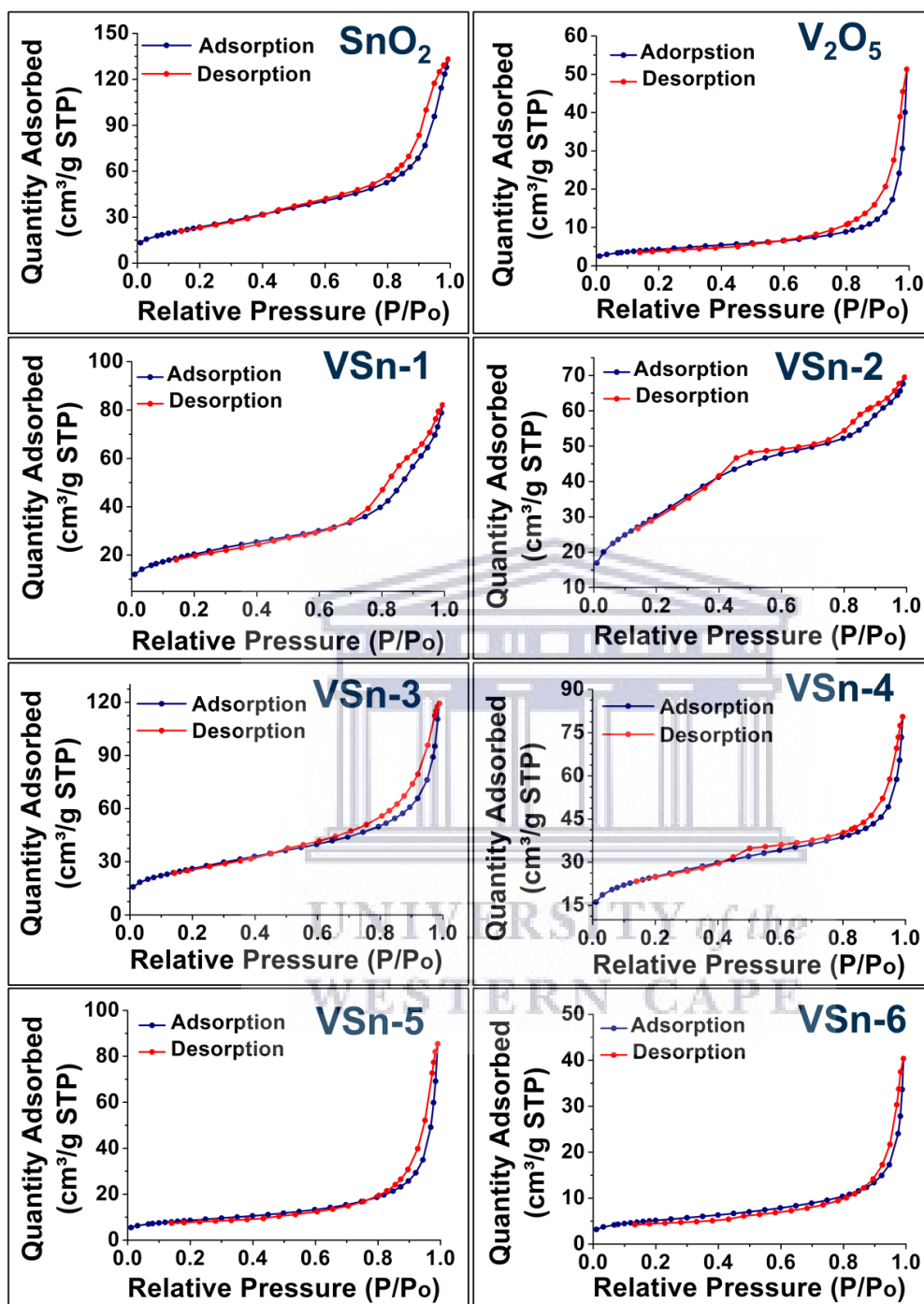
Fig. 4-1: The N_2 isotherms of the heterostructured VO_x-SnO_2 catalysts.

4.2.2   X-ray diffraction (XRD) analysis

The powder XRD patterns of the catalysts were measured in order to determine the crystal structure and phase compositions of the heterostructured VO_x-SnO_2 nanocatalysts.

Fig. 4-2 illustrates the XRD crystalline structure patterns of the calcined heterostructured VO_x-SnO_2 catalysts. The peaks at 2θ values of 26.6°, 34.2°, 38.0°, 51.8° and 54.7° could all be indexed to the respective (110), (101), (200), (211) and (220) crystallographic planes of SnO_2 oxide with a tetragonal rutile structure (JCPDS no. 41-1445).[29,30] There is also an additional peak at 2θ of 29.3° and this peak is associated with the SnO (101) phase.[31] Also, the XRD peak at 2θ of 36.3° belong to the SnO (002) plane. No clear XRD peaks could be correlated to the crystal planes structure of V_2O_5, thus all the peaks in the heterostructured VO_x-SnO_2 catalysts were all indexed to SnO_2 oxide phase. The XRD pattern of the synthesised pure V_2O_5 is presented in (**Fig. 4.3**) to confirm the absence of V_2O_5 peaks on the VO_x-SnO_2 patterns. The main vanadia characteristic peaks on the pattern are those at 2θ values of 15.6°, 20.5°, 26.4° and 31.2° which are indexed respectively to the (200), (001), (110), and (301) crystallographic planes of V_2O_5 (Shcherbinaite) with an orthorhombic crystal structure (JCPDS no. 41-1426). None of these main peaks were observed for the VO_x-SnO_2 catalysts.
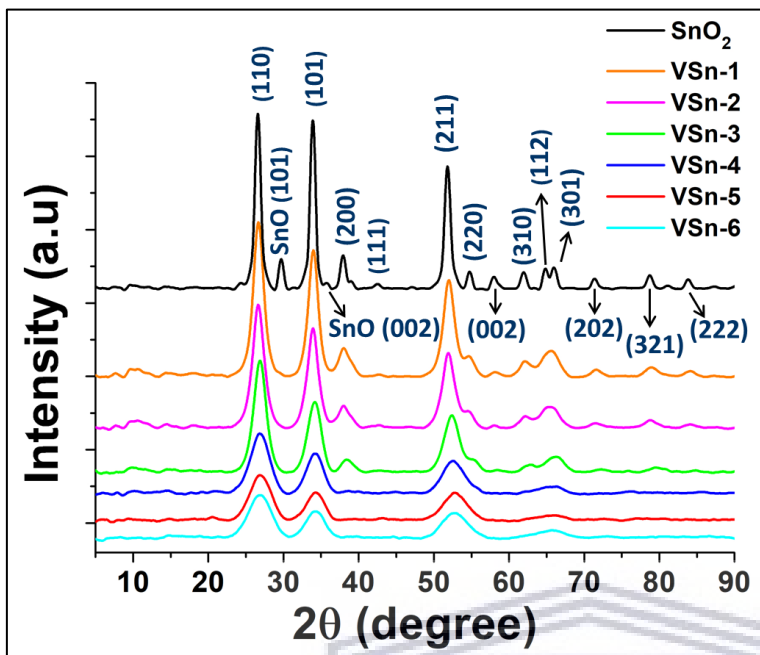
Fig. 4-2: Powder XRD patterns of the heterostructured VO_x-SnO_2 catalysts.

The crystallinity of the VO_x-SnO_2 catalysts decreased relatively with increasing V_2O_5 loading content as evidenced by the decrease in their respective peak intensity and sharpness (i.e. peaks became shorter and broader as the vanadium-metal loading increased). The decrease in crystallinity was also observed due to the disappearance of the respective (200), (111), (220), (002), (202) and (222) peaks of SnO_2 when the V_2O_5 content was increased beyond 20 wt%. In addition, the absence of the detectable peaks due to vanadium metal in the form of vanadium dioxide or pentoxide (i.e. VO_2 or V_2O_5) indicated high dispersion even at high vanadium-metal loadings. Normally, in the bulk designed vanadium metal catalysts with vanadium-metal loadings of above 20 wt%, the presence of peaks due to V_2O_5 had been previously evoked.[32-35] Consequently, the absence of V_2O_5 peaks in the heterostructure VO_x-SnO_2 catalysts indicated the inherent structural alterations of V_2O_5 dispersion behaviour when fabricated in the typical nanoscale compared to the bulk designed vanadia based catalysts. This structural dispersion could

profoundly bring about enhanced catalytic activity effect improvements. The average crystalline sizes of the heterostructured VO_x-SnO_2 catalysts were determined by using the Scherrer equation and (110) peak (**Fig. 4-2**). The results obtained are summarized in **Table 4-1** indicating the increase in the crystal size of the VO_x-SnO_2 catalysts relative to the increase in V-metal loadings. The crystallite sizes of the SnO_2 phase of heterostructured VO_x-SnO_2 catalysts increases from 3.8 nm (VSn-1) to 18.8 nm (VSn-4) with increasing vanadium loading up to 20 wt% (VSn-4). The increase of the vanadium loading beyond 20 wt% resulted in further increase of the crystallite size to 23.9 nm for the VSn-5 catalyst (25 wt%) and 28.1 nm for the VSn-6 catalyst (30 wt%).
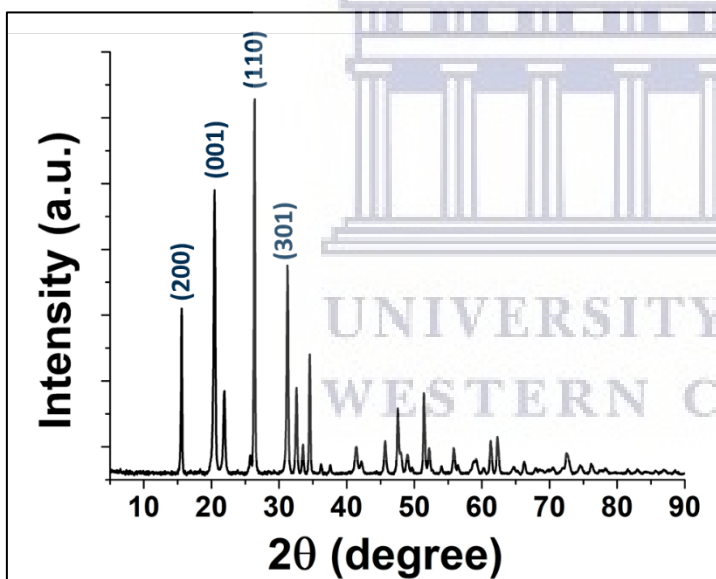
Fig. 4-3: XRD pattern of the synthesised V_2O_5 showing the main characteristic peaks.

4.2.3 Fourier transform infrared (FTIR) spectroscopy analysis

The FTIR spectra of the V_2O_5, SnO_2 and heterostructured VO_x-SnO_2 catalysts are illustrated in **Fig. 4-4**. The broad band observed at 3000 - 3500 cm^{-1} and the small band at 1630 cm^{-1} are due to the vibration of hydroxyl (–OH) group and water molecules adsorbed on the SnO_2 surface, respectively.[36,37] The band at 3346 cm^{-1} is only observed for the

VSn-3, VSn-4, VSn-5 and VSn-6 nano-oxide catalysts and its intensity is highest on the VSn-3 catalyst. At lower vanadium loading (5 and 10 wt%), this band is observed at a higher wavenumber of ~ 3600 cm^{-1} and its intensity is very small.
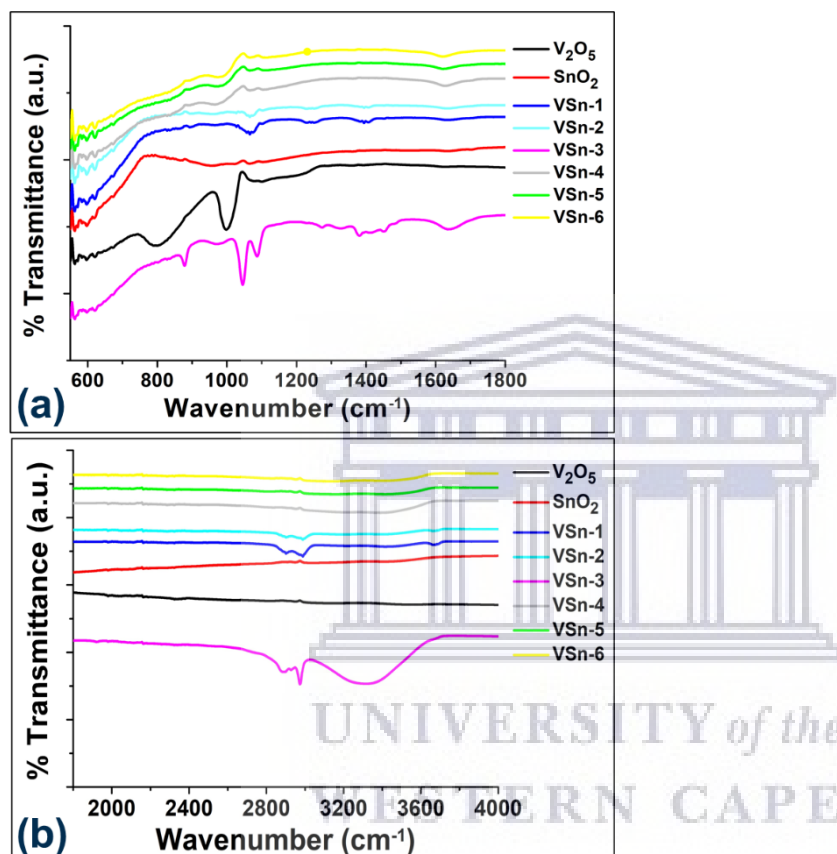
Fig. 4-4: FTIR spectra of the heterostructured VO$_x$-SnO$_2$ catalysts enlarged in the ranges of (a) 550 – 1800 cm^{-1} and (b) 1800 – 4000 cm^{-1}.

The band at 1630 cm^{-1} is observed on all the heterostructure nano-oxide catalysts except for the pure V$_2$O$_5$ and is also appearing as a shoulder for SnO$_2$ oxide. The intensity of the 1630 cm^{-1} band increased with increasing vanadium metal loading up to 20 wt% and thereafter it was unaffected. The small band observed on the SnO$_2$ spectrum at 944 cm^{-1} corresponds to the O–Sn–O stretching vibration mode.[38] The 944 cm^{-1} band is masked by the V=O stretching vibration band in the heterostructure VO$_x$-SnO$_2$ catalysts. The low

intensity typical SnO_2 bands observed appearing at 600–660 cm^{-1} vibration region correspond to the antisymmetric Sn–O–Sn bond mode.[39,40]

The sharp bands observed at 786 cm^{-1} and 996 cm^{-1} in the V_2O_5 catalyst are attributed to the vibrational stretching bands of V–O and V=O bond modes, respectively.[41,42] The band assigned to the V=O bond was also observed in all the heterostructured VO_x-SnO_2 catalysts although at a slightly higher wavenumber shift for the VSn-1, VSn-2 and VSn-3 catalysts (1045 cm^{-1}). This shift in the wavenumber vibration modes of the VSn-1 to VSn-3 is the indication of the vanadia phases structure transitions and their respective varying interactions with the SnO_2 oxide, thus resulting into modified structural interface of V_2O_5 and SnO_2 metal oxides in their heterostructured catalysts. With increasing vanadium loading content of the heterostructure VO_x-SnO_2 catalysts beyond 20 wt% there was a decrease in the intensity and shift to lower wavenumber for the 1045 cm^{-1} band. Overall, the variation in V-metal loadings in the heterostructure VO_x-SnO_2 catalysts exhibited a profound structural vibration mode changes, which indicated the development of different interactions of the V_2O_5 and SnO_2 metal oxides interfaces in the heterostructured catalysts.

4.2.4 Scanning electron microscopy (SEM) analysis

The SEM images of the heterostructured VO_x-SnO_2 catalysts, including SnO_2 and V_2O_5 are presented in **Fig. 4-5**. The SEM of SnO_2 showed the formation of agglomerated nanoparticles morphology with spherical shapes of various sizes. On the other hand, V_2O_5 appeared to compose of platelets-like morphology, of varying diameter sizes. The morphology of the VO_x-SnO_2 catalysts showed to vary relatively with the vanadium metal loading content (**Fig. 4-5**).
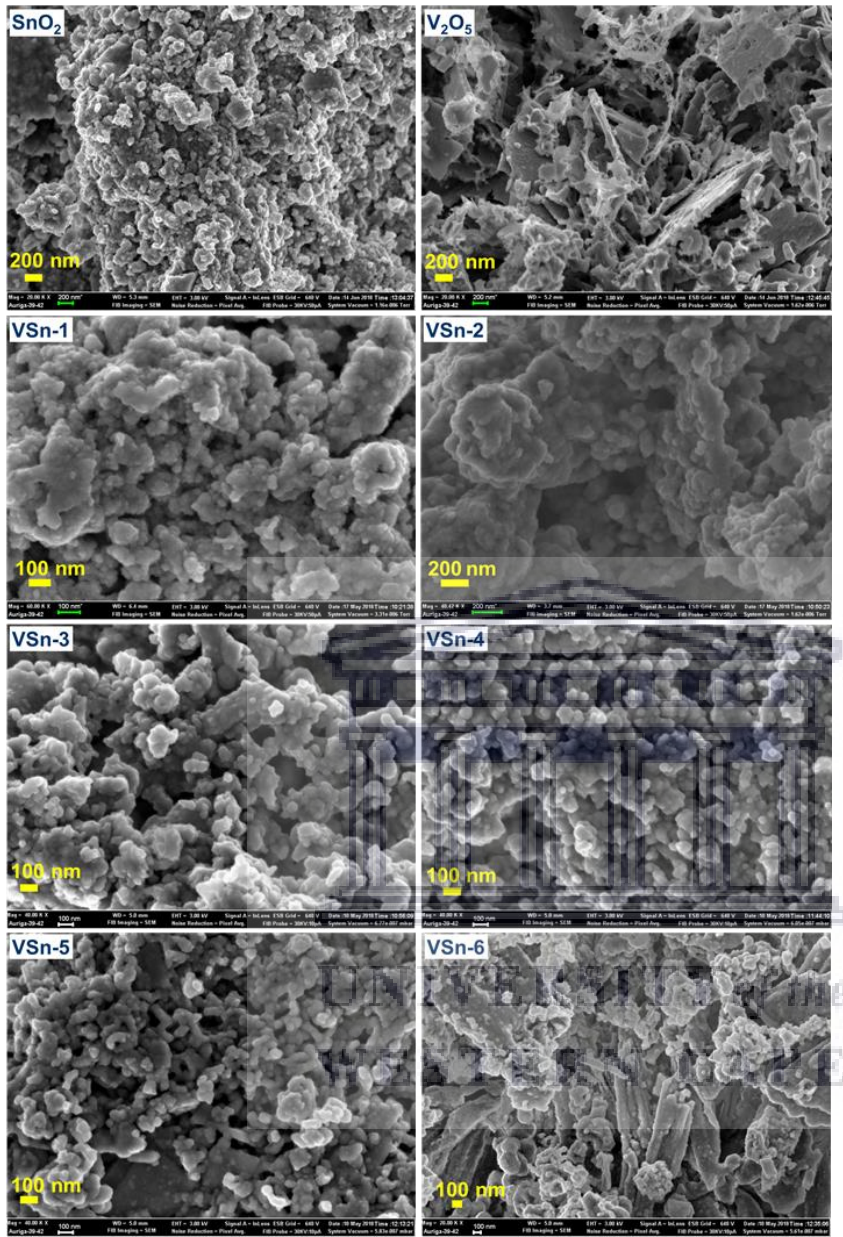
Fig. 4-5: SEM micrograph images of the heterostructured VO_x-SnO_2 catalysts.

The VSn-1 and VSn-2 catalysts showed an agglomeration of densely packed NPs with non-uniform shapes and sizes. The VSn-3 catalyst showed closely similar morphology to that of VSn-1 and VSn-2 catalysts but with the agglomeration showing to be more porous. The VSn-4 and VSn-5 catalysts showed porous agglomerate of NPs with non-uniform shapes and sizes. The VSn-6 catalyst showed the most distinctive morphology amongst

all the heterostructure VO_x-SnO_2 catalysts. For VSn-6 catalyst, the observed NPs for the VSn-1 to VSn-5 catalysts showed to self-assemble into a formation of nanorods-like morphology. This alteration in morphology was attributed to the effect of the high content of vanadium, which indicated to be initiating the preferential growth of NPs into self-assembled nanorods.

The elemental composition of the synthesized heterostructure VO_x-SnO_2 catalysts as determined by X-ray energy dispersive (EDX) spectroscopy, the resulting spectra and elemental mapping images obtained are shown in **Appendix A** (**Figs. A-2** and **A-3**). The EDX spectra show the heterostructure VO_x-SnO_2 catalysts to comprise of Sn and V with only trace amounts of Si impurities (dust from the instrument specimen chamber). The tentative amount of vanadium content in the heterostructure VO_x-SnO_2 catalysts as shown on the EDX spectra (**Fig. A-2**) were relatively closer to the nominal loadings (**Table 4-1**). The VSn-3 catalyst shows tentative vanadium content (14.5 wt%) that is significantly higher than nominal content (10 wt%) with a 4.5 difference. The difference between the tentative and nominal vanadium content for the rest of the catalyst ranges from 0.2 (VSn-1) to 2.5 (VSn-6). The EDX elemental mappings of the heterostructure VO_x-SnO_2 catalysts (**Fig. A-3**) indicated good dispersion/distribution of the V_2O_5 on the SnO_2 matrix. The images showed the V_2O_5 to be distributed evenly within the SnO_2 nanoparticles as inter-metal oxide dispersion.

4.2.4 Transmission electron microscopy (TEM) analysis

The TEM micrograph images of SnO_2 (**Fig. 4-6**) showed to comprise of agglomerations made of small NPs with diameter size in a range of 7 - 15 nm while that of V_2O_5 displayed

to compose of platelets with large particles size. The TEM results of SnO_2 and V_2O_5 catalysts were in agreement with the trend observed in the SEM images.
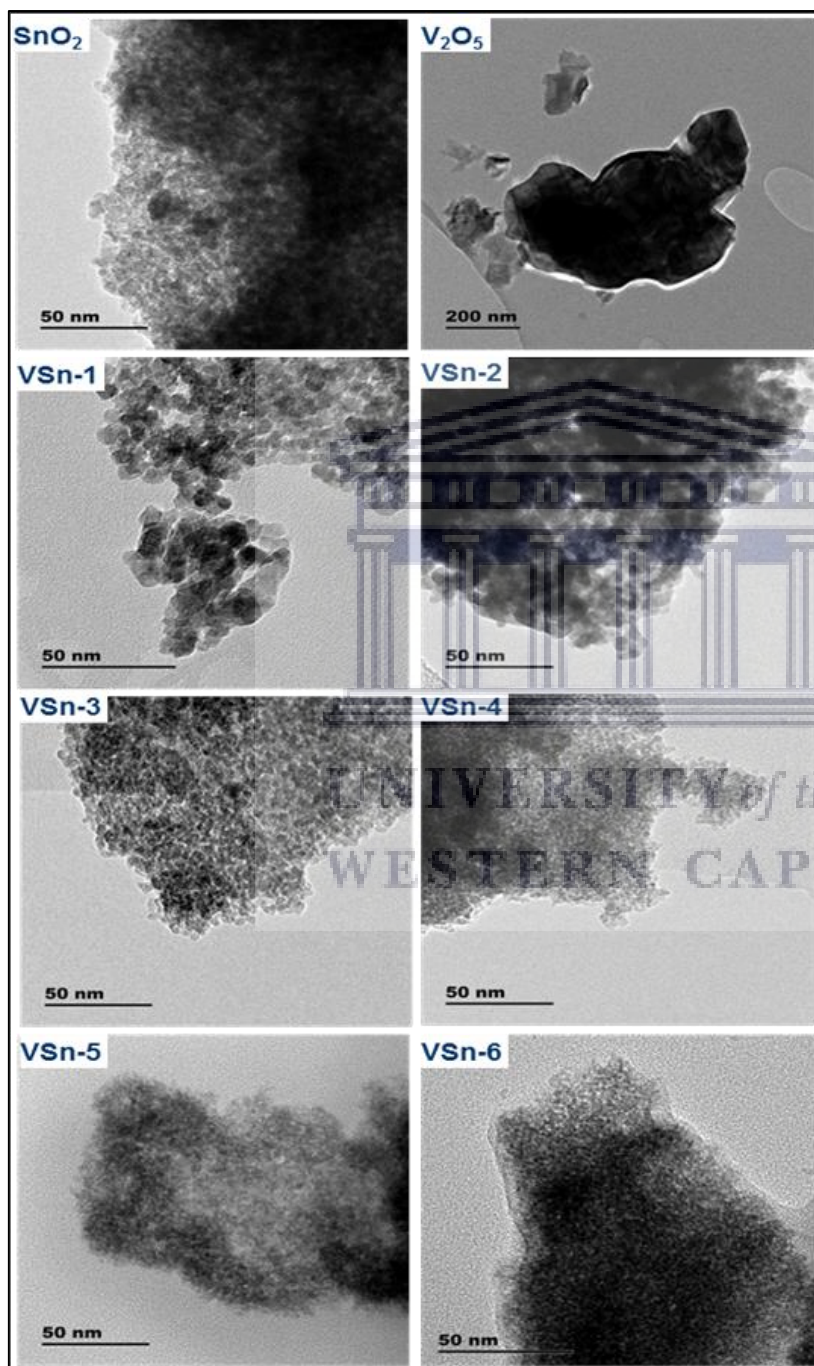
Fig. 4-6: TEM micrograph images of the heterostructured VO_x-SnO_2 catalysts.

For the heterostructure VO_x-SnO_2 catalysts, the morphology of SnO_2 NPs was relatively retained whereas the platelet morphology of V_2O_5 disappeared to adopt the overall heterostructured VO_x-SnO_2 catalysts morphologies of uniform spherical NPs similar to those of pure SnO_2. With the VSn-2 catalyst showing the highest surface area amongst all the heterostructured VO_x-SnO_2 catalysts, it was chosen a representative sample to carry out the high resolution (HR) TEM analysis and the results are presented in **Fig. 4-7**. The HRTEM analysis carried out was the selected area electron diffraction (SAED), high-angle annular dark-field scanning transmission electron microscopy (HAADF-STEM) and EDX elemental mapping. The SAED patterns of the bare SnO_2 and V_2O_5 are also included for comparison. The SnO_2 SAED pattern (**Fig. 4-7a**) is characterized by discrete spots arranged in rings indicating the crystallinity of the catalyst whereas that of V_2O_5 (**Fig. 4-7b**) is characterized by orderly arranged discrete spots typical of platelet morphology materials.

As shown in **Fig 4-7d**, the VSn-2 NPs showed to agglomerate and thus resulting into a variety of non-uniform shapes and size measured to be within the wide range of 5-15 nm. The measured lattice spacing in **Fig. 4-7d** was found to be equal to 0.33 nm, which correspond to the (110) plane of SnO_2 oxide. Also, the presence of V_2O_5 NPs in the VSn-2 catalyst was difficult to confirm with SAED due to the d-spacing of the (110) plane of V_2O_5 (0.34 nm) being similar to that of SnO_2 (110) plane (0.33 nm). The SAED pattern of VSn-2 was characterized by the diffraction rings with discrete spots which indicated the polycrystalline nature of the heterostructured VO_x-SnO_2 catalyst (**Fig. 4-7c**). The indicated SAED rings for VSn-2 and SnO_2 corresponded to the respective (110), (101), (211) (301), and (112) planes of the tetragonal phase of SnO_2 NPs, which are in agreement with the obtained XRD data showing predominantly the SnO_2 reflections with negligible peaks due to V_2O_5 (**Fig. 4-2**). The HAADF-STEM image and TEM-EDX elemental mapping (**Figs. 4-**

7e and **4-7f**) indicated good dispersion/distribution of V_2O_5 within the SnO_2 matrix, which is also in agreement with the SEM-EDX results (**Fig. A-2**). The SnO_2 NPs appeared as bright and V_2O_5 as grey on the HAADF-STEM image.
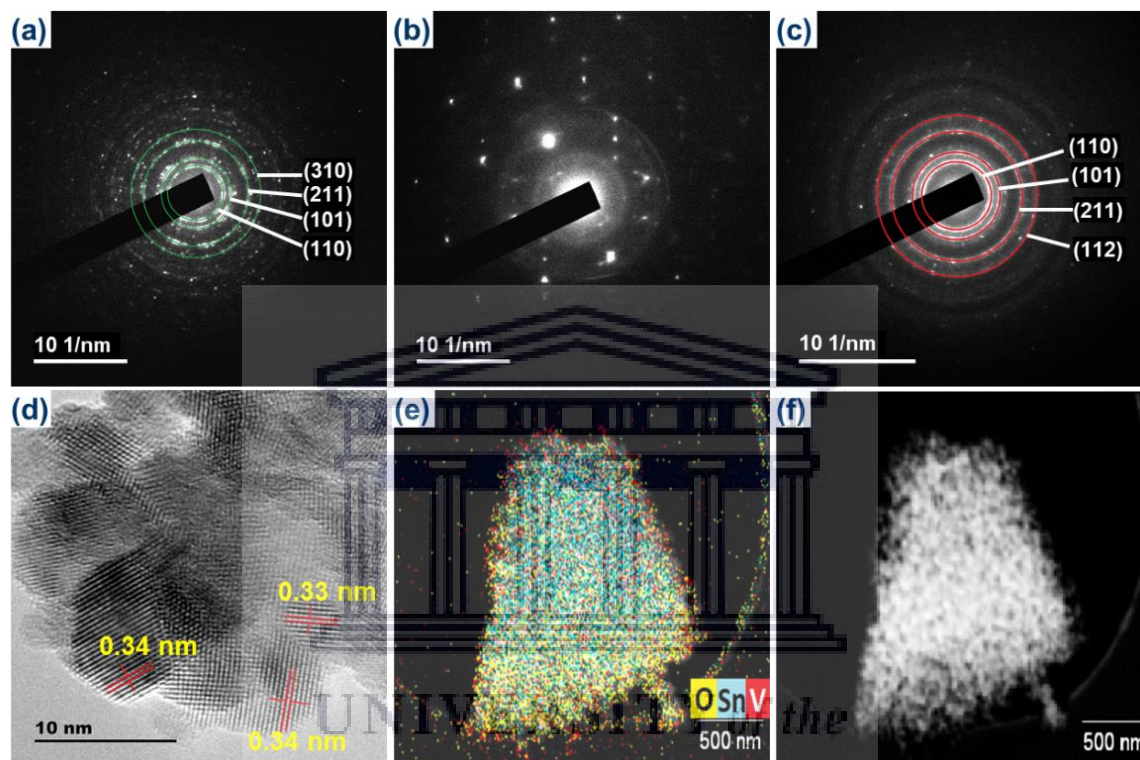
Fig. 4-7: Selected area electron diffraction (SAED) patterns of; (a) SnO_2, (b) V_2O_5 and (c) VSn-2 catalysts; (d) HRTEM micrograph of VSn-2, (e) TEM-EDX of VSn-2 and (f) the HAADF-STEM image of VSn-2.

4.2.5 X-ray photoelectron spectroscopy (XPS) analysis

To study the nature of interactions, elemental chemical state and electronic structure of the heterostructured catalysts of V_2O_5 and SnO_2 nano-oxides, XPS measurements were carried out and the overall obtained results are presented in **Fig. 4-8**. In addition, the electron binding energies (BE) of Sn3d, V2p and O1s are summarized in **Table 4-2**. The overall XPS survey profiles of the catalysts are presented in **Fig. 4-8** showing the presence of V and Sn oxide metals. The Sn profile peaks appeared as a spin-orbit doublet at around 486.6 eV ($3d_{5/2}$) and 495.0 eV ($3d_{3/2}$), which indicated that the Sn species is

predominantly in the 4+ oxidation state. The obtained Sn XPS structure information is corroborated by previously reported data.[43,44]
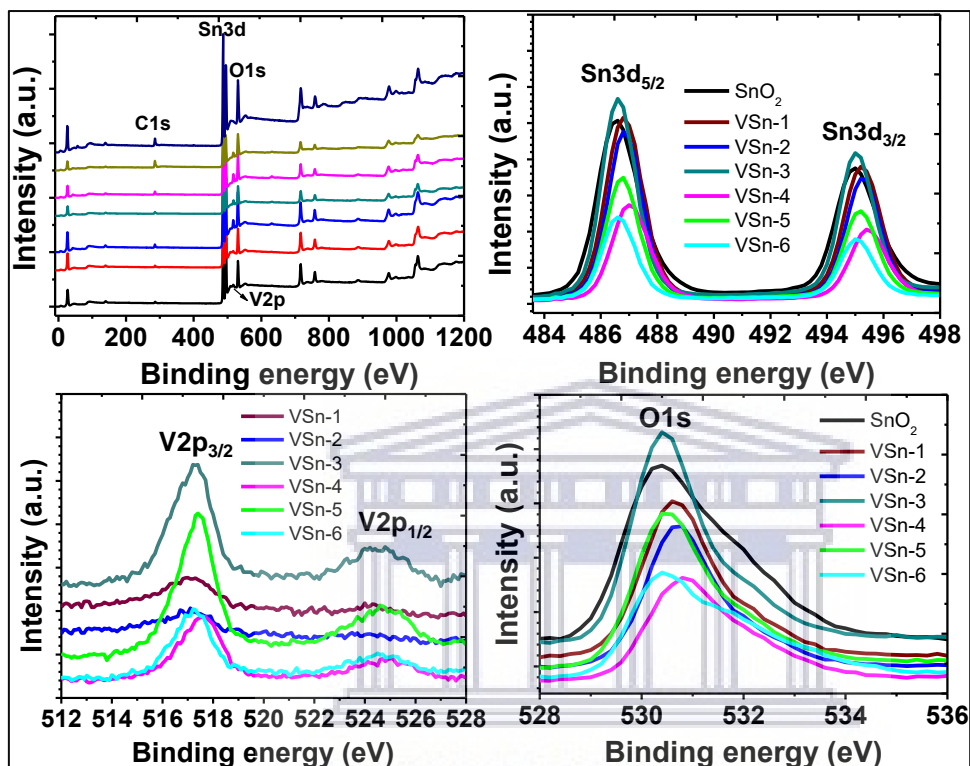
Fig. 4-8: XPS peaks profiles data of the VO_x-SnO_2 catalysts showing the respective tin, vanadium and oxygen electronic structure information.

With respect to the SnO_2 $Sn3d_{5/2}$ peak, the BE for the $Sn3d_{5/2}$ profile peak was the same for VSn-3 and VSn-6 with the peaks for the VSn-1, VSn-2, VSn-4 and VSn-5 catalysts shifted to slightly higher BEs by 0.2 - 0.4 eV. The intensity and broadness of this peak decreases with increasing vanadium content for all the heterostructure VO_x-SnO_2 catalysts with the exception of VSn-3 which had the highest intensity and broadness of all the VO_x-SnO_2 catalysts. The shift in BE of core-level peaks has been reported to be a result of the collective contribution of electrostatic and electronic effects which in some instances cancel out.[45-48] As a result, the observed BE shift (or lack thereof) of the

Sn3d$_{5/2}$ peaks in the heterostructured VO$_x$-SnO$_2$ catalysts would be related to the crystalline structure and phase composition changes observed in the XRD and FTIR, respectively. These structure changes are correlated to the changes in the vanadia species (i.e. phases, oxidation state and interaction with SnO$_2$) as the V-metal loadings increased from the mono-layer to above mono-layer and crystalline, thus inducing varying electronic and oxidation state structure properties of the respective Sn and V oxide metals. This is evident by the increasing surface V-metal content which increased with the nomimal V-metal loadings (**Table 4-1**).

Table 4-2: XPS binding energy data values of the VO$_x$-SnO$_2$ catalysts.

Entry	Catalyst	Core line binding energy (eV)					V^{4+}/V^{5+}	O$_V$/O$_L$
		Sn3d$_{5/2}$	Sn3d$_{3/2}$	V2p$_{3/2}$	V2p$_{1/2}$	O1s		
1	SnO$_2$	486.6	495.0	N/A	N/A	530.4	N/A	0.86
2	VSn-1	486.8	495.3	517.0	524.0	530.6	0.25*	0.61
3	VSn-2	486.8	495.3	517.0	-	530.7	0.60	0.15
4	VSn-3	486.6	495.0	517.5	524.9	530.4	0.32	0.34
5	VSn-4	487.0	495.4	517.5	525.0	530.7	0.24	1.47
6	VSn-5	486.8	495.3	517.5	525.0	530.5	0.19	0.22
7	VSn-6	486.6	495.0	517.2	525.0	530.4	0.24	0.51

*ratio of V^{3+}/V^{5+}

The O 1s profile peak has an average BE around 530.5 eV for the VO$_x$-SnO$_2$ catalysts indicating that the oxygen atoms exist as the O^{2-} species (**Fig. 4-8**).[49] As is the case for the Sn 3d peaks, the O 1s BE peaks profiles exhibited shifting to slightly higher binding energy regions for the VSn-1, VSn-2, VSn-4 and VSn-5 catalysts. The high-resolution fitted profiles (obtained with the Gaussian fitting method) for the O1s peaks in **Fig. 4-9** showed three peaks at BEs around 530 eV (O$_L$), 531-532 eV (O$_V$) and 532-534 eV (O$_A$). The peaks at 530 eV are attributed to the lattice O^{2-} species, those at 531-532 eV to

oxygen vacancies or surface adsorbed oxygen species and the peaks between 532-534 eV are attributed to oxygen from surface adsorbed water molecules.[49,50] The V 2p profile peaks appeared as the spin-orbit doublet at around 517.3 eV ($2p_{3/2}$) and 525 eV ($2p_{1/2}$), which are associated with V^{5+} oxidation state.[51-52] The presence of peaks for both V $2p_{3/2}$ and V $2p_{1/2}$ indicated that the VO_x-SnO_2 catalysts were predominantly in the high vanadium metal oxidation state.
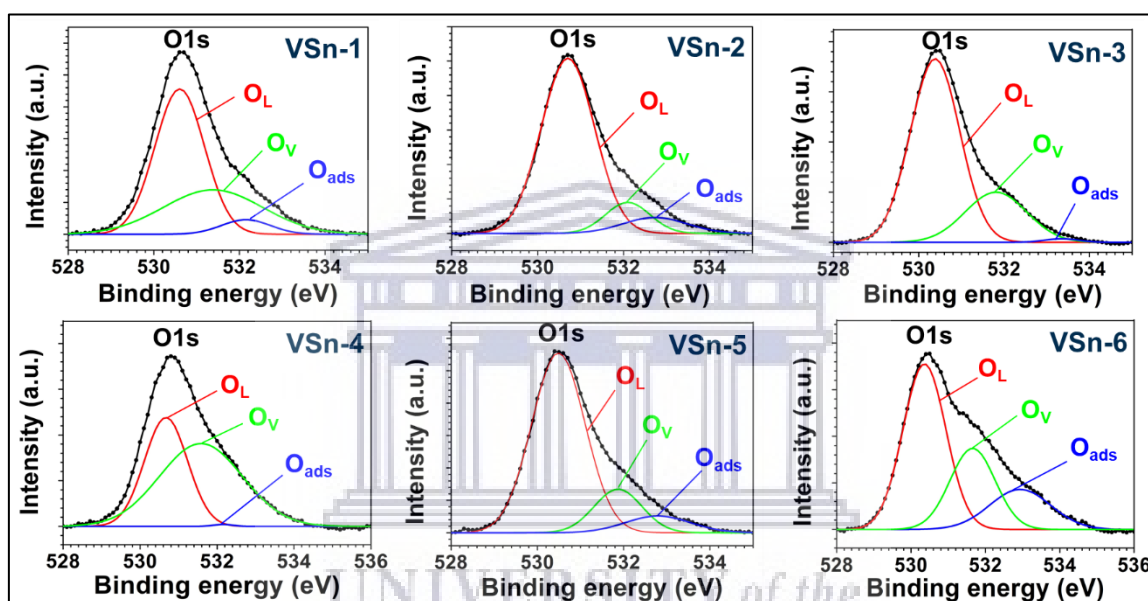
Fig. 4-9: XPS fitted O 1s peak profiles of the heterostructure VO_x-SnO_2 catalysts.

All the heterostructure VO_x-SnO_2 catalysts showed the presence of the $2p_{3/2}$ profile peaks with varying intensity and shapes. Further, the $2p_{1/2}$ profile peaks were observed for all heterostructured VO_x-SnO_2 catalysts with its intensity very small for the VSn-1 and VSn-2 catalysts (**Fig. 4-8**). In fact, the $2p_{1/2}$ profile peaks for these catalysts became more apparent on the fitted profile peaks (**Fig. 4-10**). Overall, the intensity of the $2p_{1/2}$ profiles appearing at around BE of 525.0 eV were very low for all the catalysts compared to high intense $2p_{3/2}$ peaks. The V $2p_{3/2}$ deconvoluted peak profiles showed two peaks at around 516 eV and 517 eV and these peaks are attributed to the V^{4+} and V^{5+} species,

respectively, with the exception of the VSn-1 catalyst which showed the lower BE peak at 515 eV corresponding to V^{3+} species.[53]
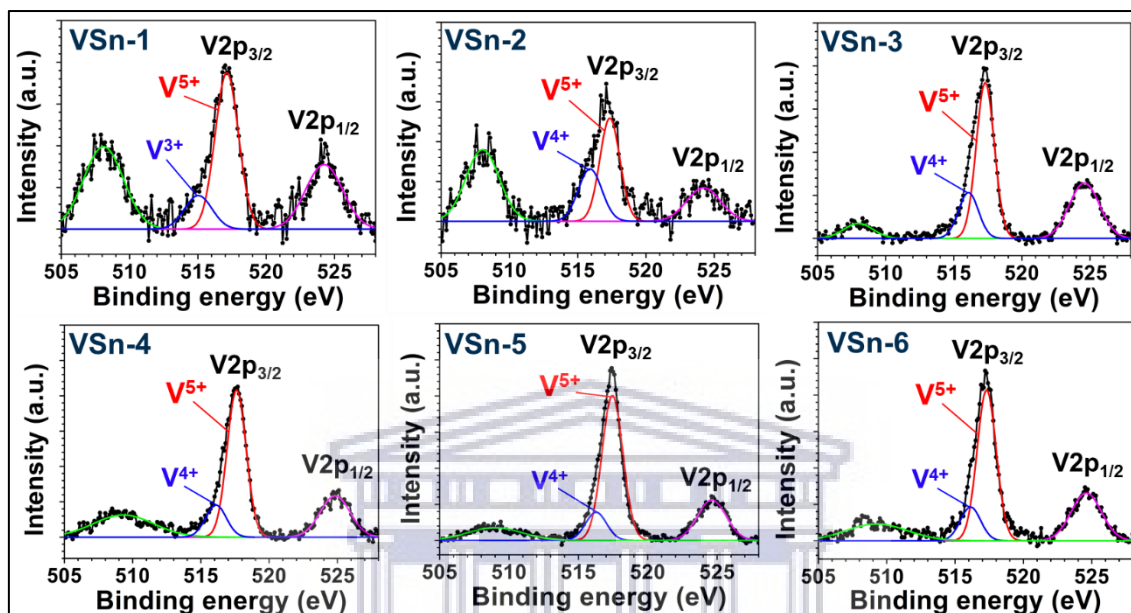
Fig. 4-10: XPS fitted V 2p peak profiles of the heterostructure VO_x-SnO_2 catalysts.

The V^{4+} peak at 516 eV indicates the presence of monomeric and polymeric VO_x phases which have been proven to enhance catalytic activity for certain reactions.[22] The calculated V^{4+}/V^{5+} peak area ratios (**Table 4-2**) shows the V^{4+} species to predominantly exist on the VSn-2 catalyst. The fitted V2p profiles further showed a satellite peak at around 508.0 eV in addition to the V $2p_{3/2}$ and V $2p_{1/2}$ profile fits. The intensity of this satellite was broader and more intense for the VSn-1 and VSn-2 catalysts. The BE of the peak is lower than those of lower vanadium oxidation states, V^0 (512.4 eV), V^{3+} (515.7 eV) and V^{4+} (516.2 eV),[54] and therefore cannot be attributed to any of these vanadium species. The satellite peaks have been postulated to be caused by the strong hybridization between the electronic structure of the V $2p_{3/2}$ and the O 1s levels and this has been shown both experimentally and theoretically to exist for the V_2O_5, VO_2 and V_2O_3

vanadia phases.[55,56] Overall, the XPS data for heterostructured VO_x-SnO_2 catalysts confirmed the vanadium in the predominant V^{5+} oxidation state and tin in the Sn^{4+} oxidation state, which confirm the formation of highly oxidized redox catalysts.

4.2.6 Electron paramagnetic resonance (EPR) analysis

The EPR spectra of the heterostructured VO_x-SnO_2 catalysts are presented in **Fig. 4-11**, along with those of V_2O_5 and SnO_2. The V_2O_5 EPR spectra showed anisotropic resonance lines at g = 2.098 and g = 1.928 which are characteristic of quasi isolated V^{4+} ions in highly distorted octahedron environment of oxygen atoms with short V-O bonds. The spin-spin dipolar interactions occurring between neighbouring V^{4+} ions within the V_2O_5 structure leads to broadened Lorentzian lines and thus a not well-resolved hyperfine structure. This indicates the presence of VO_x monomeric and polymeric species formed by VO_x sites connected by oxygen bridges.[57,58]

The spectra of SnO_2 also showed anisotropic resonance lines at g =2.097, g = 1.966 and g = 1.949. Since both Sn^{4+} and Sn^{2+} ions are EPR silent, these signals are attributed to V_O^- paramagnetic centres created by the single-electron trapped inside the oxygen vacancies (V_O).[59-61] The spectra of the heterostructured VO_x-SnO_2 catalysts appeared as complex well-resolved hyperfine structures. The spin-spin interactions were not observed for the catalysts, instead the hyperfine structures were present due to the interaction of the unpaired electron (d^1) of V^{4+} with the nuclear magnetic moment of ^{51}V (*I* = 7/2). This indicates the presence of V^{4+} ions.[62,63] The signal observed at g = 2.007 for the VSn-1 catalyst indicates the presence of superoxide ions and was not observed for the other catalysts.[64]
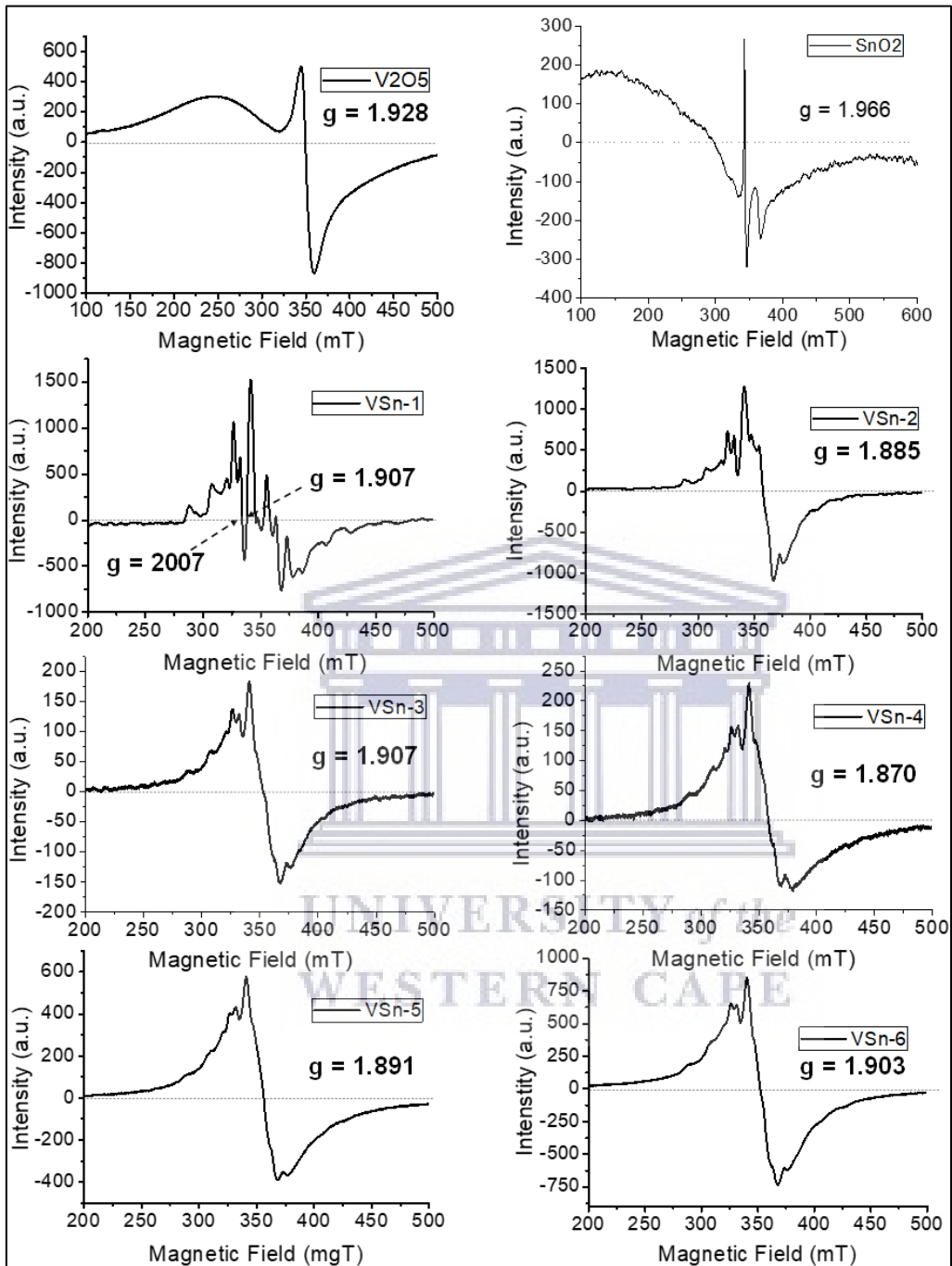
Fig. 4-11: EPR spectra of the heterostructured VO_x-SnO_2 catalysts.

4.3. Catalytic activity evaluation

4.3.1 Catalytic oxidation of furfural

4.3.1.1 Screening activity of catalysts for furfural oxidation

The catalytic activity of the heterostructured VO_x-SnO_2 catalysts were evaluated in terms of conversion, selectivity and yield toward maleic acid in the oxidation of furfural using $50\%_{(aq)}$ H_2O_2 as an oxidant. The detailed oxidation procedure and products analysis methods are described in **chapter 3**. The obtained catalytic performance results of the different VO_x-SnO_2 catalysts are summarized in **Table 4-3**. The furfural oxidation reaction that was carried out without a catalyst (**Table 4-3**, entry 1) gave a low yield of less than 2.8% for maleic acid formation at 5.2% furfural conversion. Also, SnO_2 afforded a low yield of 4.7% for maleic acid at furfural conversion of 7.8%. A furfural conversion of 11.3% and yields of 6.2% for maleic acid and 2.7% for oxalic acid were achieved when using V_2O_5 as the oxidation catalyst.

Table 4-3: Catalytic activity screening performance of heterostructured VO_x-SnO_2 catalysts in the oxidation reaction of furfural.

Entry	Catalysts	Conversion (%)	Yield (%)		
			Maleic acid	Oxalic acid	[a] Others
1	Blank	5.2	1.6	1.2	2.4
2	SnO_2	7.8	4.7	1.9	1.2
3	V_2O_5	11.3	6.2	2.7	2.4
4	VSn-1	39.2	22.0	3.8	13.4
5	VSn-2	74.4	38.9	9.8	25.7
6	VSn-3	27.1	10.3	4.2	12.6
7	VSn-4	21.4	8.5	3.6	9.3
8	VSn-5	19.3	6.7	3.6	9.0
9	VSn-6	18.5	5.9	2.4	10.2

[a] Side products such as 2-furanone, fumaric, succinic, formic acid and furoic acids. Reaction conditions: 1 mmol furfural, 50 mg catalyst, 4 mmol 50% (aq) H_2O_2 in H_2O, 5 mL solvent, T = 65 °C and t = 20 h.

The VSn-1 catalyst with low nominal vanadium metal loading content of 3.8 wt% also showed an improved yield of maleic acid (22.0%). The highest yield of 38.9% for maleic acid at furfural conversion of 74.4% was achieved with the VSn-2 catalyst containing about 9.3 wt% vanadium metal loading. With further increase of vanadium content beyond 9.3 wt% in the VO_x-SnO_2 catalysts, the catalytic activity for furfural conversion decreased significantly (**Table 4-3**, entries 6-9). The VSn-6 catalyst showed low furfural conversion and the least efficiency in terms of the yield of maleic acid (5.9%). Correlation of the catalytic and BET surface area results showed that the most active VSn-2 catalyst did not possess the highest surface area amongst all the catalysts thus indicating that surface area alone does not enhance catalytic activity for oxidation reaction of furfural and other properties are important. Correlation of the obtained catalytic performances of the different VO_x-SnO_2 catalysts with changes in the crystalline structure showed that there were possible modifications of the electronic and metal oxide interaction structures that probably induced varying catalytic active sites. This was observed in the XPS results of the VO_x-SnO_2 catalysts where the peak profiles of both the V 2p and O 1s showed to be significantly modified relative to the increasing amount of the V-metal loading. Although all the heterostructured VO_x-SnO_2 catalysts showed to possess the high oxidation state of Sn^{4+} and V^{5+}, the presence of populated V^{4+} and V^{5+} for the VSn-2 catalyst sample indicated a profound catalytic activity influence due to both low vanadia loading structure phases and the formation of various vanadium oxidation state which was effective to facilitate the required co-occurrence of V^{5+}/V^{4+} and V^{4+}/V^{3+} redox pairs for effective catalytic activity in the oxidation of furfural. Further, the low content of the V^{4+} species (**Table 4-2**) for high vanadium loading content catalysts, VSn-4 to VSn-6 correlated well with their significant decrease in catalytic activity conversions of the furfural. Accordingly, the V^{4+}/V^{5+} redox pair has been proposed as the most active and selective catalytic sites

in the vanadia based catalysts with the high concentration of V^{4+} on the catalyst surface enhancing the activity as observed for VSn-2. The easily exchangeable V^{4+}/V^{5+} redox pair is important for accelerating the electron transfer processed and facilitating the C-C bond cleavage of the substrate for an efficient oxidation reaction. In addition, at low vanadia loading, VO_4 species are formed which are postulated as the most active species in the vanadium supported catalytic systems. Such catalytic activity dependence of vanadium supported catalysts on loading amount have been reported previously.[65,66] Moreover, the VSn-2 catalyst possessed the lowest concentration of surface oxygen defects with a low ratio of O_V/O_L (**Table 4-2**) and larger concentrations of these defects showed to be ineffective on enhancing the catalytic activity. This indicates a large concentration of lattice oxygen atoms necessary for facilitating the electron transfer process. **Table 4-2** also shows the VSn-2 catalyst to possess the highest number of exposed surface V atoms as evident by the high surface V/actual V ratio. The high number of surface V atoms is crucial for maximising the exposed surface V^{4+} active sites.

4.3.1.2 Effect of solvent on VO_x-SnO_2 catalyst performance

The first reaction parameter investigated was the effect of different solvents on catalytic activity of VSn-2 catalyst for furfural oxidation (**Fig. 4-12**). Amongst the different solvents evaluated, water afforded the best catalytic performance with furfural conversion of 74% at yields of 39% for maleic acid and 10% for oxalic acid. The reaction conducted in isobutanol as a solvent appeared to be the least efficient as demonstrated by the very low maleic acid yield (1%) and furfural conversion (15%), respectively. The low activity of VSn-2 in isobutanol indicated that the solvent could be competing significantly with the furfural substrate to be oxidized where isobutanol could saturate or cover up the active sites of the catalyst surface for furfural access. The polar protic solvents of formic and

acetic acids were also not efficient with maleic acid and oxalic acid yields of 10% and 8%, respectively. The polar aprotic solvents (DMF, 1,4-dioxane, THF, ethyl acetate and acetonitrile) were also inefficient. Although considerable conversions of up to 45% were achieved in THF and 1,4-dioxane, the two solvents appeared to favour the formation of high amounts of by-products with their total combined yields exceeding 40% (**Fig. 4-12**). The non-polar toluene solvent afforded the total yield of 2% for both maleic acid and oxalic acid at low furfural conversion of 25%. Ultimately, with water affording the best catalytic performance results of VSn-2 catalyst, it was then selected as the solvent of choice for the subsequent optimization of furfural oxidation reaction process.
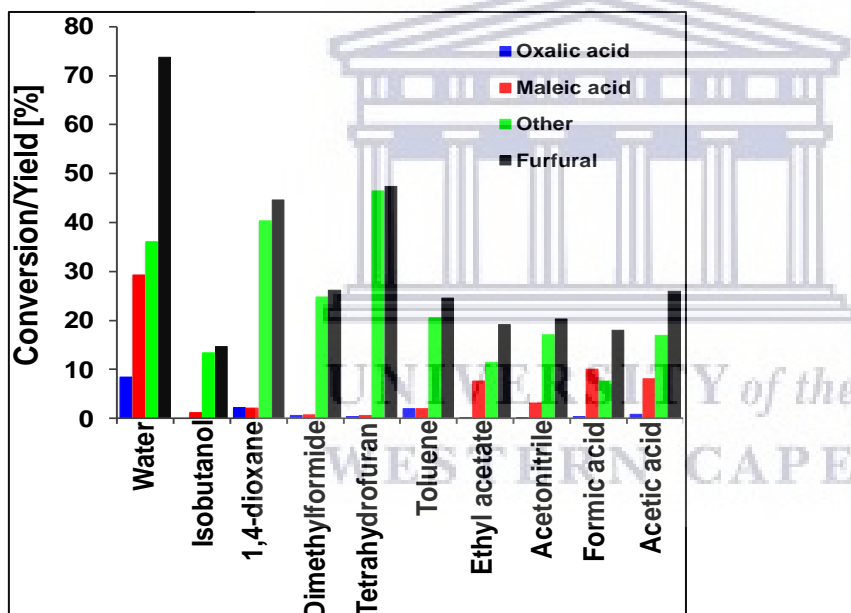
Fig. 4-12: Effect of different solvents on furfural oxidation reaction. Reaction conditions: 1 mmol furfural, 50 mg catalyst, 4 mmol 50% aq. H_2O_2 , 5 mL solvent, T = 70 °C and t = 20 h.

4.3.1.3 Comparison of 30% and 50% aqueous H_2O_2 concentration

The effects of the different concentrations of H_2O_2 oxidant (i.e. 50% and 30% in water) were evaluated for the catalytic activity influence on VSn-2 catalyst in the oxidation of furfural (**Fig. 4-13**). Although the same amount of H_2O_2 (4 mmol) was utilized, the less concentrated 30% H_2O_2 solution led to improved catalytic activity results compared to the

more concentrated 50% H_2O_2 solution. The low efficiency of the 50% H_2O_2 could be related to its rapid decomposition rate accelerated by the catalyst effect, thus reducing its oxygen atom utilization efficiency in the conversion of furfural when compared to 30% H_2O_2. The slightly higher volume of water solvent in 30% H_2O_2 could also play a significant role of inducing its slow decomposition rates relatively to the progression of the reaction, which could be beneficial to improve its efficiency and furfural conversion. The yields improved from 30% to 42% (maleic acid) and 8% to 10% (oxalic acid) when the concentration of H_2O_2 was changed from 50%$_{(aq)}$ to 30%$_{(aq)}$, respectively. Similarly, the concentration of 30%$_{(aq)}$ H_2O_2 also resulted in an improvement of furfural conversion from 74% to 88% for 50% H_2O_2 and 30% H_2O_2, respectively. Also, the 50%$_{(aq)}$ H_2O_2 showed to lead to slightly high formation of by-products.
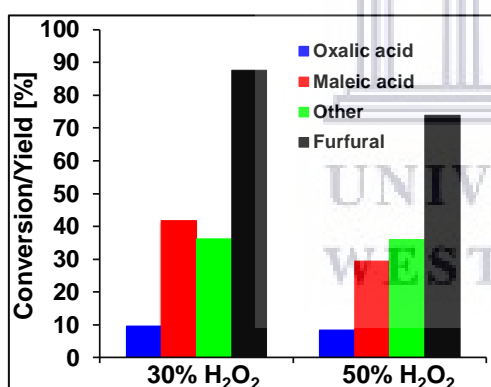
Fig. 4-13: Effect of 30% H_2O_2 vs 50% H_2O_2 concentration on furfural oxidation reaction. Reaction conditions: furfural (1 mmol), VSn-2 catalyst (50 mg), H_2O_2 oxidant (4 mmol), water solvent (5 mL), T = 70 °C and t = 20 h.

4.3.1.4 Effect of H_2O_2 molar ratio concentration

Next, the effect of furfural/H_2O_2 ratio on the oxidation rates of furfural and its products distribution was evaluated. **Fig. 4-14** illustrate the results of five different furfural/H_2O_2 ratio of 1:4, 1:5, 1:6, 1:7 and 1:8 (mol/mol) tested for the furfural oxidation reaction. When

the ratio was increased from 1:4 to 1:5 the furfural conversion improved from 88% to 100%. However, the yield of maleic acid decreased from 42% to 33% and that of oxalic acid decreased from 10% to 2% while the yield of the by-products increased from 36% to 65%. With further increase of furfural/H_2O_2 ratio to 1:6 improved yields of 53% for maleic acid and 16% for oxalic acid were achieved at a furfural conversion of 97%. Increasing the furfural/H_2O_2 ratio beyond 1:6 showed a significant decrease in the yields of maleic acid and oxalic acid respectively (**Fig. 4-14**). An increase in the yields of the by-products was also noticeable while the furfural conversion remained at 100%. As a result, the optimum ratio of furfural/H_2O_2 of 1:6 was found to be adequate to give the stoichiometric amount required for an efficient furfural oxidation reaction process.
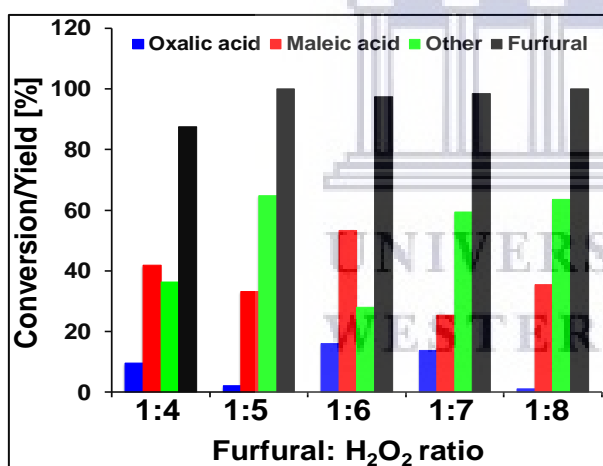
Fig. 4-14: Effect of furfural/H_2O_2 ratios on furfural oxidation reaction. Reaction conditions: furfural (1 mmol), catalyst (50 mg), water solvent (5 mL), VSn-2 catalyst (50 mg), oxidant (30% aq. H_2O_2), T = 70 °C and t = 20 h.

4.3.1.5 Effect of catalyst dosage amount

To further improve on the oxidation rates of furfural and product selectivity, the reaction was optimized by varying the amount of the catalyst dosage. **Fig. 4-15** illustrates the oxidation results for the VSn-2 catalyst dosage varied between 5 and 50 mg. The yield of maleic acid improved to 57% when 5 mg of catalyst was used compared to 53% when 50

mg was used. However, the furfural conversion was only up to 89% for 5 mg catalyst dosage. The best results were achieved with 10 mg of catalyst dosage affording yields of 60% maleic acid at furfural conversion of 99%. Further increase in catalyst dosage beyond 10 mg resulted in complete furfural conversion but significantly low yields of maleic acid, while the yields of the by-products increased relatively.
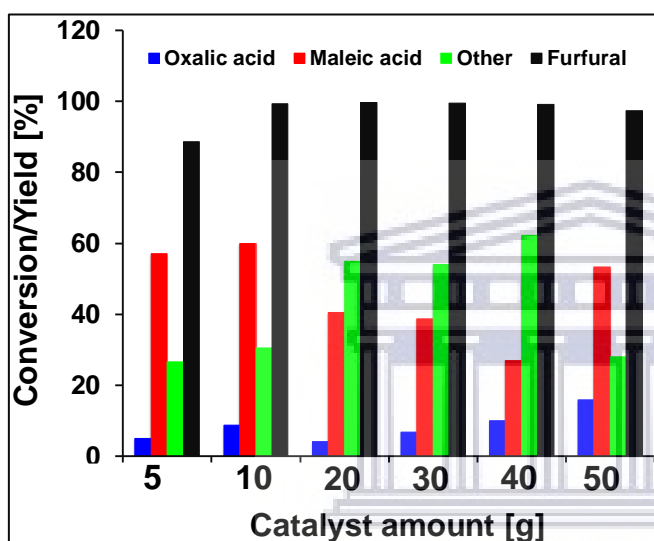
Fig. 4-15: Effect of catalyst amount on furfural oxidation reaction rates. Reaction conditions: Furfural (1 mmol), 30% aq. H_2O_2 oxidant (6 mmol), water solvent (5 mL), T = 70 °C and t = 20 h.

4.3.1.6 Catalyst recyclability and leaching test

The reusability performance of VSn-2 catalyst was evaluated and the obtained results are shown in **Fig. 4-16**. In the typical test reaction, the catalyst was recovered by centrifugation after reaction, thereafter washed with ethanol/water solution and dried in an oven at 100 °C for 5 h before it was used in the next recyclability cycle. The conversion of furfural showed the gradual decline with the subsequent usage of the recovered catalyst material over three recycling runs. In the first recycle use, furfural conversion was 99.6%, and in the second and third recycling it decreased significantly to 81.3 and 63.7%, respectively. The observed decline in furfural conversion amount could most probably be

related to the nature of the reaction content acidity as the reaction progress, where carboxylic acid products such as fumaric acid, maleic acid, oxalic acid are formed. The influence of these products could practically make the reaction mixture to be acidic during the course of the reaction, which could promote the catalyst metal leaching.
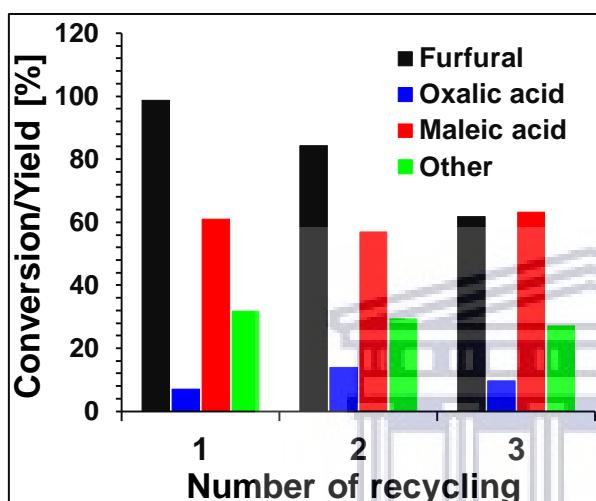
Fig. 4-16: Recyclability results of the VSn-2 catalyst during furfural oxidation reaction. Reaction conditions: furfural (1 mmol), water solvent (5 mL), catalyst (50 mg), oxidant (30% aq. H_2O_2), T = 70 °C and t = 20 h.
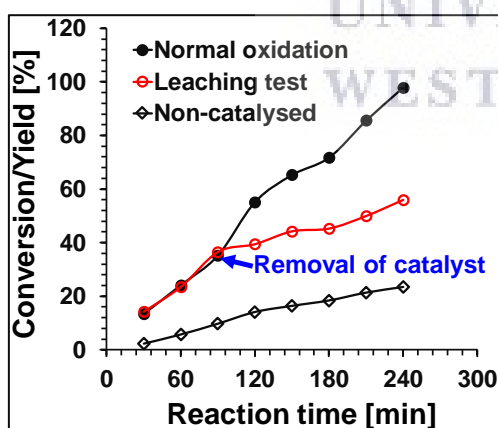
Fig. 4-17: Leaching test of VO_x-SnO_2 catalyst in the furfural oxidation reaction. Reaction conditions: furfural (1 mmol), catalyst (50 mg), water solvent (5 mL), VSn-2 catalyst (50 mg), oxidant (30% aq. H_2O_2), T = 70 °C and t = 4 h.

As a result, we evaluated the susceptibility of leaching, particularly vanadium in the VO_x-SnO_2 catalyst under the furfural oxidation reaction (**Fig. 4-17**). The conversion of furfural before the separation of VSn-2 catalyst from the reaction mixture solution after 90 min (1.5 h) was 36.5%. By allowing the reaction to proceed further for 2.5 h after the catalyst removal the conversion of furfural increased slightly to 48.9%. For the catalyzed reaction without catalyst removal, the conversion of furfural reached up to 97.9% while the non-catalyzed reaction could only achieve 23.4% furfural conversion. This demonstrated possible leaching of the metal catalyst that was accountable for the slightly increase in furfural conversion after the catalyst removal. The presence of the leached vanadium metal was confirmed by ICP analysis but with no detectable SnO_2. The confirmed vanadium metal leaching could explain the observed significant decrease in the VSn-2 catalyst activity upon its recyclability test (**Fig. 4-17**). The comparison of the present V-metal leaching in the furfural oxidation reaction indicate that the formed carboxylic acids were the main cause of the catalyst deactivation since the previous studies showed VO_x-SnO_2 catalyst to be stable under benzene oxidation reaction to phenol, which do not present acidic reaction medium content.[67] Further, the characterization of the spent catalyst by XRD, FTIR and TEM (**Figs. 4-18 and 4-1**) showed changes in structure of SnO_2 indicated by the disappearance of certain FTIR and XRD peaks. The crystallinity of the catalyst also decreased as shown by changes in NP structure (**Fig. 4-18c**) and in the XRD peak shape and intensity.
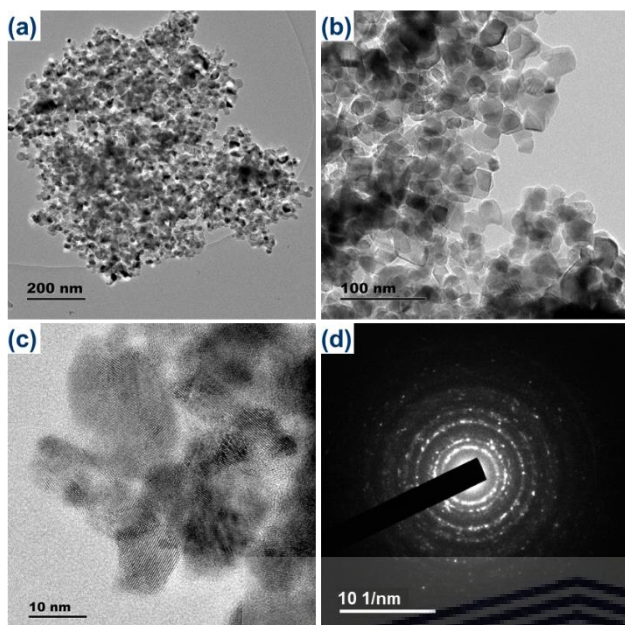
Fig. 4-18: TEM (a-c) and SAED (d) images of re-used VSn-2 catalyst.
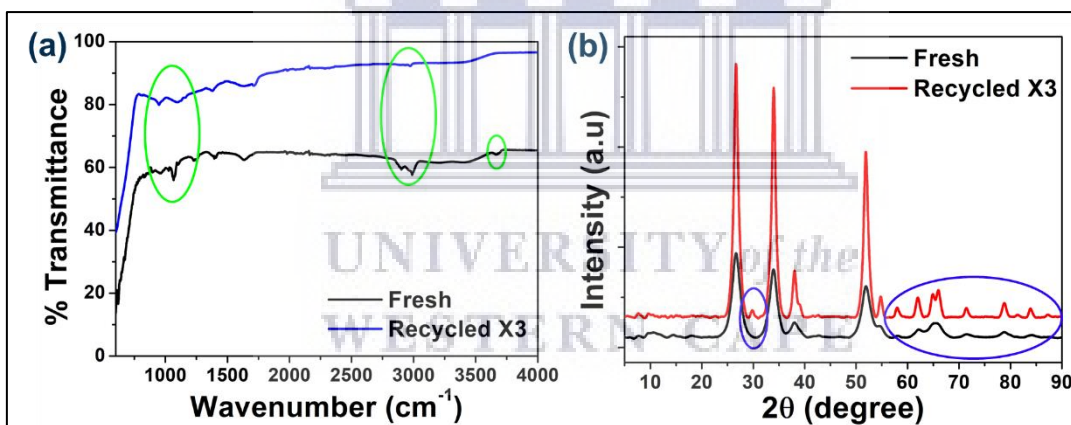
Fig. 4-19: FTIR spectrum (a) and XRD pattern (b) of the re-used VSn-2 catalyst.

4.3.2 Oxidation of 5-hydroxymethylfurfural to maleic acid

4.3.2.1 Catalysts activity screening for HMF oxidation

The catalytic oxidation properties of the VO_x-SnO_2 catalysts were also evaluated in the conversion of 5-hydroxymethylfurfural to maleic acid using H_2O_2 as oxidant. **Table 4-4** and **Fig. 4-20** summarizes the catalytic results obtained expressed in terms of conversion, selectivity and yield toward maleic acid and other products. The reaction was carried out

in the absence of a catalyst (**Table 4-4,** entry 1) and a maleic acid yield of 12.3% was achieved with a remarkable 5-hydroxymethylfurfural conversion of 96.6% being achieved. Interestingly, 2.5-diformylfuran was produced as the main product with a yield of 45.0% along with 5-hydroxymethyl-2-furandicarboxylic acid with a yield of 25.4%. Further, 2.5-furandicarboxylic acid was also produced with a 5.0% yield. The yield of maleic acid decreased to just 5.6% when SnO_2 was used as a catalyst. The yields of 2.5-diformylfuran and 5-formyl-2-furancarboxylic acid were increased to 53.5% and 5.7%, respectively, while that of 5-hydroxymethyl-2-furandicarboxylic acid decreased to 20.5%. The yield of 2.5-furandicarboxylic acid remained unchanged (4.9%) and that of the by-products was significantly decreased to just 1.7%.

Table 4-4. Activity results of the heterostructure VO_x-SnO_2 catalysts in 5-hydroxymethylfurfural oxidation.

Entry	Catalyst	Conv. (%)	Yield (%)						
			MA	OA	FFCA	FDCA	HMFCA	DFF	[1] Other
1	Blank	96.6	12.3	1.1	1.8	5.0	25.4	45.0	6.1
2	SnO_2	93.0	5.6	1.1	5.7	4.9	20.5	53.5	1.7
3	V_2O_5	99.0	59.7	19.3	5.7	0.4	2.6	0.5	10.9
4	VSn-1	98.1	49.7	34.6	3.9	0.3	0.2	1.5	6.4
5	VSn-2	99.8	52.2	31.7	3.8	1.7	0.3	0.0	10.2
6	VSn-3	99.8	35.7	55.1	2.9	1.2	1.3	0.5	3.3
7	VSn-4	99.0	39.0	50.2	2.6	1.0	1.2	0.4	4.6
8	VSn-5	98.3	44.9	43.3	2.4	0.8	1.3	0.7	5.0
9	VSn-6	98.4	27.6	47.4	1.3	0.0	0.4	13.2	8.6

[1] Side products such as formic acid, fumaric acid and furoic acid. Symbol: MA = maleic acid, OA = oxalic acid, FFCA = 5-formyl-2-furancarboxylic acid, FDCA = 2.5-furandicarboxylic acid, HMFCA = 5-hydroxymethyl-2-furandicarboxylic acid, DFF = 2.5-diformylfuran. Reaction conditions: 1 mmol HMF, 10 mg catalyst, 6 mmol 30% $_{(aq)}$ H_2O_2, 5 mL deionised water, T = 70 °C and t = 20 h.
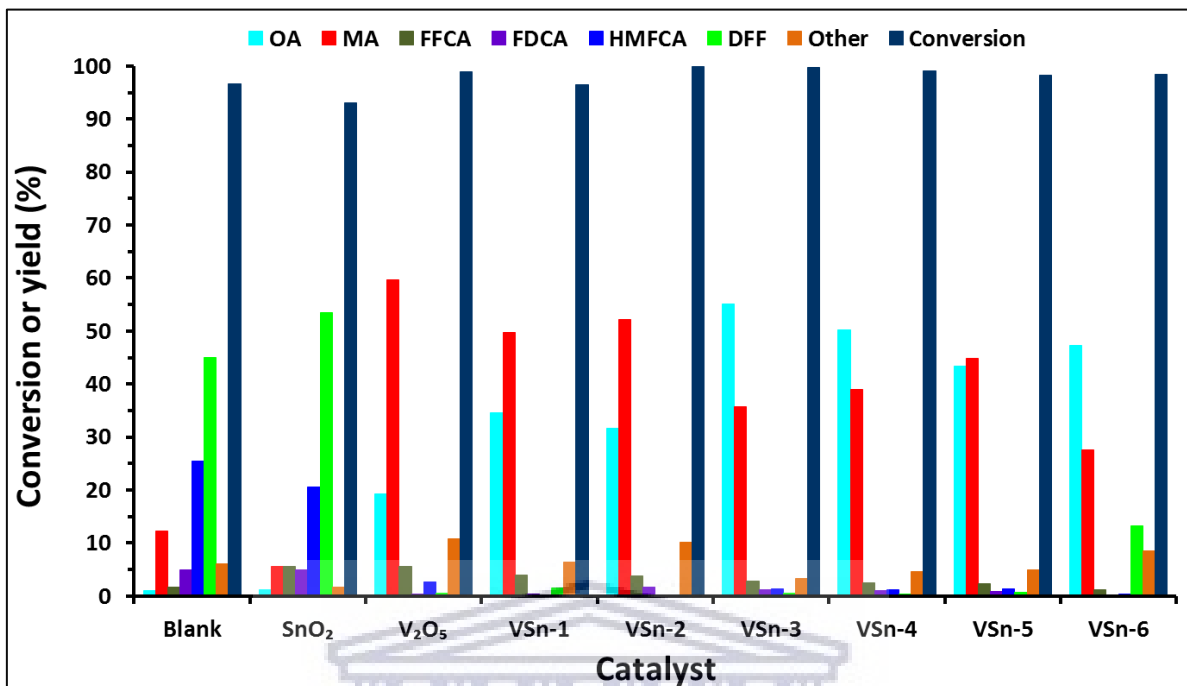
Fig. 4-20: Catalytic activity screening results of heterostructure VO_x-SnO_2 catalysts in 5-hydroxymethylfurfural oxidation. Reaction conditions: 1 mmol HMF, 10 mg catalyst, 6 mmol 30% (aq) H_2O_2, 5 mL deionised water, T = 70 °C and t = 20 h.

A high conversion of 5-hydroxymethylfurfural (93.0%) was also achieved with SnO_2 as a catalyst. In fact, over 90% 5-hydroxymethylfurfural conversion was achieved for all the catalysts used with the VSn-2, VSn-3, VSn-4 and V_2O_5 catalysts showing the highest conversion of 99% and above. The V_2O_5 catalyst proved to be significantly more active and selective as a catalyst than SnO_2 towards maleic acid and oxalic acid with yields of 59.7% and 19.3%, respectively. The combined yields of 5-hydroxymethyl-2-furandicarboxylic acid, 2.5-furandicarboxylic acid and 2.5-diformylfuran were notably reduced to a total of 3.5% whereas that of 5-formyl-2-furancarboxylic acid remained unchanged (5.7%). These results are hardly surprising since V_2O_5 is known to be more catalytically active than SnO_2 due to its redox character and moderate Lewis acidity. However, despite the high activity of V_2O_5 in this instance its main drawback was the

catalyst dissolving in the reaction mixture (forming a homogeneous solution), thus rendering it unstable and its recoverability difficult.

For the heterostructured VO_x-SnO_2 catalysts, the reaction conducted with the VSn-1 catalyst produced maleic acid with a yield of 49.7% and 34.6% for oxalic acid. The yields of 5-formyl-2-furancarboxylic acid, 2.5-furandicarboxylic acid, 5-hydroxymethyl-2-furandicarboxylic acid and 2.5-diformylfuran were very low with a total combined of 5.9% and that of the by-products was 6.4%. The VSn-2 produced the highest yield of maleic acid (52.2%) amongst all VO_x-SnO_2 catalysts. The yield of oxalic acid achieved with the catalyst was 18.4% while the total combined of 5-formyl-2-furancarboxylic acid, 2,5-furandicarboxylic acid, 5-hydroxymethyl-2-furandicarboxylic acid and 2.5-diformylfuran was 5.8% and of the by-products was 10.2%. The VO_x-SnO_2 catalysts with a higher vanadium loading above 10 wt%, VSn-3 to VSn-6 (**Table 4-4**, entries 6-9) produced lower yields of maleic acid and appeared to be more selective towards oxalic acid with yields in the range 43.3% - 55.1%. However, it should be noted that the high yields of oxalic acid produced by these catalysts are believed to be as a result of the over-oxidation of the C_4 carboxylic acid products as will be demonstrated in **Chapter 5**. Amidst the selectivity towards oxalic acid, the VSn-5 was able to produce maleic acid with a yield of 44.9%. The production of by-products was suppressed by these catalysts reaching a low yield of 3.3% with the VSn-3 catalyst. The highest yield for 2.5-diformylfuran of 13.2% was achieved with the VSn-6 catalyst and the highest yield of 5-formyl-2-furancarboxylic acid achieved was 3.9% and 3.8% obtained with the VSn-1 and VSn-2 catalysts, respectively. 2.5-Furandicarboxylic acid and 5-hydroxymethyl-2-furandicarboxylic acid were always produced in trace amounts when the VO_x-SnO_2 catalysts were utilized (**Table 4-4**).

Although the VO_x-SnO_2 heterostructured catalysts showed a lower activity for 5-hydroxymethylfurfural conversion to maleic acid than V_2O_5 (~ 52% yield of maleic acid compared to ~60%), dispersing V_2O_5 over SnO_2 as a support provides better stability for the catalyst because all the VO_x-SnO_2 catalysts were easily recovered by centrifuge. The comparable results between 5-hydroxymethylfurfural and furfural oxidation under the same reaction conditions suggest that the maximum exposed surface active V^{4+} species on the VSn-2 catalyst active for furfural oxidation are also effective for 5-hydroxymethylfurfural oxidation. This suggestion is supported in the literature where it has been demonstrated that at low loading content, vanadium is present as monomeric to polymeric VO_x species on metal oxide supports and as crystalline V_2O_5 at higher surface vanadia coverage.[32,37] These literature results lead to the conclusion that the surface VO_x species exposed at low vanadia coverage are the active phase for furfural and 5-hydroxymethyl oxidation while the crystalline V_2O_5 formed at high vanadia coverage are not as efficient.

4.3.2.2 Effect of nature of solvent

The effect of various solvents on the catalytic activity of the VSn-2 catalyst for oxidation of 5-hydroxymethylfurfural to maleic acid was investigated (**Fig. 4-21**). Similar to furfural oxidation, deionised water afforded the best catalytic performance results of VSn-2 catalyst achieving a 5-hydroxymethylfurfural conversion of 99.8% at yields of 52.2% for maleic acid and 31.7% for oxalic acid. The reaction conducted in dimethylformide, 1,4-dioxane and acetonitrile appeared to produce 5-hydroxymethyl-2-furandicarboxylic acid as the main product with respective yields of 19.6%, 30.1% and 24.4% at 5-hydroxymethylfurfural conversion rates of 49.9%, 57.8% and 60.1%. The yields of maleic

acid achieved were very low with 3.4% obtained in dimethylformide, 7.0% in 1,4-dioxane and 14.2% in acetonitrile. When toluene was used as a solvent, a maleic acid yield of 18.5% was achieved at an improved 5-hydroxymethylfurfural conversion of 89.1%. While a 15.8% yield of 2.5-furandicarboxylic acid was obtained, the solvent led to formation of high yield of by-products (46.6%). The main side product formed was 2-furoic acid with a yield of 38.0%.
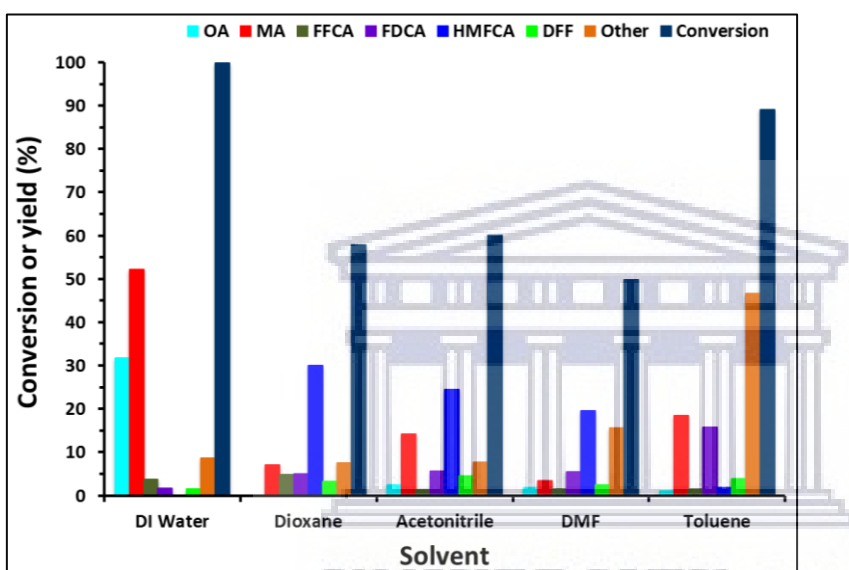
Fig. 4-21: Effect of different solvents on 5-hydroxymethylfurfural oxidation. Reaction conditions: 1 mmol substrate, 10 mg catalyst, 6 mmol 30% $_{(aq)}$ H_2O_2 in H_2O, 5 mL solvent, T = 70 °C and t = 20 h.

4.4 Concluding remarks

In summary, we have demonstrated the synthesis of heterostructured VO_x-SnO_2 catalysts using a surfactant-free polyol method. This method afforded the formation of 7-10 nm size of indistinguishable nanoparticles of V and Sn metal oxides. The VO_x-SnO_2 catalyst loaded with 9.3 wt% V-metal presented a highly active catalyst for the oxidation of both furfural and 5-hydroxymethylfurfural with H_2O_2 to maleic acid. Under optimized conditions, complete furfural and 5-hydroxymethylfurfural conversions were achieved with 60% maleic acid yield from furfural and 52% yield from 5-hydroxymethylfurfural being obtained.

Characterization results showed the active catalysts to consist of low vanadium loading, which exhibited to compose of VO_x mono- and polymeric active sites populated with the balanced V^{5+}/V^{4+} redox pairs as evidenced by the XPS results. This demonstrated the low V-metal loadings on SnO_2 to provide suitable solid phase interface of the two metal oxides, which induced highly active sites amenable for oxidation of furfural and 5-hydroxymethylfurfural with complete conversion and preserved selectivity towards targeted maleic acid. Based on the XPS and EPR results such hetero-mixed oxides interfaces resulted in modified electronic structure interactions and exposure of surface superoxide species, which were active for the furfural and 5-hydroxymethylfurfural oxidation reactions. Both the catalyst leaching and recyclability test demonstrated the gradual decrease of catalytic activity for furfural oxidation, which exhibited to be due to the leaching of the V-metal. Further studies that could re-design the catalyst to improve on its recyclability and selectivity will present heterostructured VO_x-SnO_2 as a cheap catalyst for the production of renewable maleic acid from sustainable biomass-derived furfural.
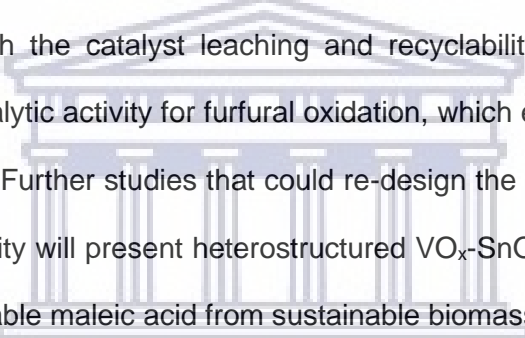
4.5 References

[1] A.S. Mamman, J. Lee, Y. Kim, I.T. Hwang, N. Park, Y.K. Hwang, J. Chang, J. Hwang, Furfural: Hemicellulose/xylose derived biochemical. Biofuels, Bioproducts and Biorefining: Innovation for a sustainable economy, **2008**, 2, pp. 438-454.

[2] P. Gallezot, Conversion of biomass to selected chemical products. Chemical Society Reviews, **2012**, 41, pp. 1538-1558.

[3] L.T. Mika, E. Cséfalvay, Á. Németh, Catalytic conversion of carbohydrates to initial platform chemicals: chemistry and sustainability. Chemical Reviews, **2018**, 118, pp. 505-613.

[4] X. Li, P. Jia, T. Wang, Furfural: A promising platform compound for sustainable production of C4 and C5 chemicals. ACS Catalysis, **2016**, 6, pp. 7621-7640.

[5] R. Mariscal, P. Maireles-Torres, M. Ojeda, I. Sádaba, M.L. Granados, Furfural: A renewable and versatile platform molecule for the synthesis of chemicals and fuels. Energy & Environmental Science, **2016**, 9, pp. 1144-1189.

[6] A.E. Eseyin, P.H. Steele, An overview of the applications of furfural and its derivatives, International Journal of Advanced Chemistry, **2015**, 3(2), pp. 42-47.

[7] L. Zhang, G. Xi, K. Yu, H. Yu, X. Wang, Furfural production from biomass-derived carbohydrates and lignocellulosic residues via heterogeneous acid catalysts. Industrial Crops and Products, **2017**, 98, pp. 68-75.

[8] F. Trifirò, R. Grasselli, How the yield of maleic anhydride in n-butane oxidation, using VPO catalysts, was improved over the years. Topics in Catalysis, **2014**, 57, pp. 1188-1195.

[9] D.K. Hood, O.M. Musa, Progress in maleic anhydride production. In: O.M. Musa (Ed.), Handbook of maleic anhydride based materials: Syntheses, properties and applications. Springer International Publishing, Cham, Switzerland, **2016**, pp. 3-35.

[10] T.R. Felthouse, J.C. Burnett, B. Horrell, M.J. Mummey, Y.J. Kuo. Maleic anhydride, maleic acid, and fumaric acid. 4th ed. In: J. Kroschwitz, M. Home-Grant (Ed.), Kirk-Othmer Encyclopedia of Chemical Technology. New York, John Wiley and Sons, **2001**, Vol 19, pp. 1-58.

[11] B.C. Trivedi, B.M. Culbertson, Maleic anhydride, Springer, Boston, USA, 1**982**, p.17.

[12] J. Lan, Z. Chen, J. Lin, G. Yin, Catalytic aerobic oxidation of renewable furfural to maleic anhydride and furanone derivatives with their mechanistic studies. Green Chemistry, **2014**, 16, pp. 4351-4358.

[13] T. Soták, M. Hronec, M. Gál, E. Dobročka, J. Škriniarová, Aqueous-phase oxidation of furfural to maleic acid catalyzed by copper phosphate catalysts. Catalysis Letters, **2017**, 147, pp. 2714-2723.

[14] S. Shi, H. Guo, G. Yin, Synthesis of maleic acid from renewable resources: catalytic oxidation of furfural in liquid media with dioxygen. Catalysis Communications, **2011**, 12, pp. 731-733.

[15] H. Guo, G. Yin, Catalytic aerobic oxidation of renewable furfural with phosphomolybdic acid catalyst: an alternative route to maleic acid. The Journal of Physical Chemistry C, **2011**, 115, pp. 17516-17522.

[16] N. Alonso-Fagúndez, I. Agirrezabal-Telleria, P.L. Arias, J.L.G. Fierro, R. Mariscal, M.L. Granados, Aqueous-phase catalytic oxidation of furfural with H_2O_2: high yield of maleic acid by using titanium silicalite-1. RSC Advances, **2014**, 4, pp. 54960-54972.

[17] R. Wojcieszak, F. Santarelli, S. Paul, F. Dumeignil, F. Cavani, R. Gonçalves, Recent developments in maleic acid synthesis from bio-based chemicals. Sustainable Chemical Processes, **2015**, 3, pp. 1-11.

[18] N. Alonso-Fagúndez, M.L. Granados, R. Mariscal, M. Ojeda, Selective conversion of furfural to maleic anhydride and furan with VO_x/Al_2O_3 catalysts. ChemSusChem, **2012**, 5, pp. 1984-1990.

[19] N. Alonso-Fagúndez, M. Ojeda, R. Mariscal, J.L.G. Fierro, M. López, M.L. Granados, Gas phase oxidation of furfural to maleic anhydride on $V_2O_5/\gamma\text{-}Al_2O_3$ catalysts: reaction conditions to slow down the deactivation. Journal of Catalysis, **2017**, 348, pp. 265-275.

[20] X. Li, B. Ho, Y. Zhang, Selective aerobic oxidation of furfural to maleic anhydride with heterogeneous Mo–V–O catalysts. Green Chemistry, **2016**, 18, pp. 2976-2980.

[21] J. Lan, J. Lin, Z. Chen, G. Yin, Transformation of 5-hydroxymethylfurfural (HMF) to maleic anhydride by aerobic oxidation with heteropolyacid catalysts. ACS Catalysis, **2015**, 5, pp. 2035-2041.

[22] I.E. Wachs, Catalysis science of supported vanadium oxide catalysts. Dalton Transactions, **2013**, 42, pp. 11762-11769.

[23] Z. Zhu, Z. Liu, S. Liu, H. Niu, A novel carbon-supported vanadium oxide catalyst for NO reduction with NH_3 at low temperatures. Applied Catalysis B: Environmental, **1999**, 23, pp. L229-L233.

[24] M. Ai, The oxidation activity and acid-base properties of SnO_2-based binary catalysts: I. The $SnO_2\text{-}V_2O_5$ system. Journal of Catalysis, **1975**, 40, pp. 318-326.

[25] K. Sekizawa, H. Widjaja, S. Maeda, S. Ozawa, Y.K. Eguchi, Low temperature oxidation of methane over Pd/SnO_2 catalyst. Applied Catalysis A: General, **2000**, 200, pp. 211-217.

[26] X. Wang, Y. Xie, Preparation and characterization of SnO_2-based composite metal oxides: active and thermally stable catalysts for CH_4 oxidation. Catalysis Letters, **2001**, 75, pp. 73-80.

[27] S. Wang, J. Huang, Y. Zhao, S. Wang, X. Wang, T. Zhang, S. Wu, S. Zhang, W. Huang, Preparation, characterization and catalytic behavior of SnO_2 supported Au catalysts for low-temperature CO oxidation. J Journal of Molecular Catalysis A: Chemical, **2006**, 259, pp. 245-252.

[28] T. Matthias, K. Katsumi, A.V. Neimark, J.P. Olivier, Rodriguez-Reinoso Francisco, R. Jean, K.S. Sing, Physisorption of gases, with special reference to the evaluation of surface area and pore size distribution (IUPAC Technical Report). Pure and Applied Chemistry, **2015**, 87, pp. 1051.

[29] R. Adnan, N.A. Razana, I.A. Rahman, M.A. Farrukh, Synthesis and characterization of high surface area tin oxide nanoparticles via the sol-gel method as a catalyst for the hydrogenation of styrene. Journal of the Chinese Chemical Society, **2010**, 57, pp. 222-229.

[30] L. Xi, D. Qian, X. Tang, C. Chen, High surface area SnO_2 nanoparticles: Synthesis and gas sensing properties. Materials Chemistry and Physics, **2008**, 108, pp. 232-236.

[31] K. Sakaushi, Y. Oaki, H. Uchiyama, E. Hosono, H. Zhou, H. Imai, Aqueous solution synthesis of SnO nanostructures with tuned optical absorption behavior and photoelectrochemical properties through morphological evolution. Nanoscale, **2010**, 2, pp. 2424-2430.

[32] A. Khodakov, J. Yang, S. Su, E. Iglesia, A. T. Bell, Structure and properties of vanadium oxide-zirconia catalysts for propane oxidative dehydrogenation. Journal of Catalysis, **1998**, 177, pp. 343-351.

[33] A.A. Lemonidou, L. Nalbandian, I.A. Vasalos, Oxidative dehydrogenation of propane over vanadium oxide based catalysts: effect of support and alkali promoter. Catalysis Today **2000**, 61, pp. 333-341.

[34] S. Loridant, Determination of the maximum vanadium oxide coverage on SnO_2 with a high surface area by Raman spectroscopy. The Journal of Physical Chemistry B, **2002**, 106, pp. 13273-13279.

[35] B. Solsona, A. Dejoz, T. Garcia, P. Concepción, J.M.L. Nieto, M.I. Vázquez, M.T. Navarro, Molybdenum–vanadium supported on mesoporous alumina catalysts for the oxidative dehydrogenation of ethane. Catalysis Today, **2006**, 117, pp. 228-233.

[36] S. Gnanam, V. Rajendran, Synthesis of tin oxide nanoparticles by sol-gel process: effect of solvents on the optical properties. Journal of Sol-Gel Science and Technology, **2010**, 53, pp. 555-559.

[37] A. Gaber, A.Y. Abdel-Latief, M.A. Abdel-Rahim, M.N. Abdel-Salam, Thermally induced structural changes and optical properties of tin dioxide nanoparticles synthesized by a conventional precipitation method. Materials Science in Semiconductor Processing, **2013**, 16, pp. 1784-1790.

[38] V.C. Reddy, B. Babu, P.S.V. Ravikumar, R.V.S.S.N Ravikumar, J. Shim, Structural and optical properties of vanadium doped SnO_2 nanoparticles with high photocatalytic activities. Journal of Luminescence, **2016**, 179, pp. 26-34.

[39] A. Ungureanu, O. Oprea, B. Vasile, C. Andronescu, G. Voicu, I. Jitaru, Temperature effect over structure and photochemical properties of nanostructured SnO_2 powders. Central European Journal of Chemistry, **2014**, 12, pp. 909-917.

[40] L. Jiang, G. Sun, Z. Zhou, S. Sun, Q. Wang, S. Yan, H. Li, J. Tian, J. Guo, B. Zhou, Q. Xin, Size-controllable synthesis of monodispersed SnO_2 nanoparticles and application in electrocatalysts. The Journal of Physical Chemistry B, **2005**, 109, pp. 8774-8778.

[41] S.K. Pillai, O. Gheevarghese, S. Sugunan, Catalytic properties of V_2O_5/SnO_2 towards vapour-phase Beckmann rearrangement of cyclohexanone oxime. Applied Catalysis A: General, **2009**, 353, pp. 130-136.

[42] M.M. Margoni, S. Mathuri, K. Ramamurthi, R.R. Babu, K. Sethuraman, Sprayed vanadium pentoxide thin films: Influence of substrate temperature and role of HNO_3 on the structural, optical, morphological and electrical properties. Applied Surface Science, **2017**, 418, pp. 280-290.

[43] Z. Li, W. Shen, X. Zhang, L. Fang, X. Zu, Controllable growth of SnO_2 nanoparticles by citric acid assisted hydrothermal process. Colloids and Surfaces A: Physicochemical and Engineering Aspects, **2008**, 327, pp. 17-20.

[44] Q. Zhao, Controllable synthesis and catalytic activity of SnO_2 nanostructures at room temperature. Transactions of Nonferrous Metals Society of China, **2009**, 19, pp. 1227-1231.

[45] P.S. Bagus, E.S. Ilton, C.J. Nelin, The interpretation of XPS spectra: Insights into materials properties. Surface Science Reports, **2013**, 68, pp. 273-304.

[46] G. Greczynski, L. Hultman, X-ray photoelectron spectroscopy: Towards reliable binding energy referencing. Progress in Materials Science, **2020**, 107, pp. 100591.

[47] T.C. Taucher, I. Hehn, O.T. Hofmann, M. Zharnikov, E. Zojer, Understanding chemical versus electrostatic shifts in X-ray photoelectron spectra of organic self-assembled monolayers. The Journal of Physical Chemistry C, **2016**, 120, pp. 3428-3437.

[48] T.J. McCue, J.Y. Ying, SnO_2-In_2O_3 nanocomposites as semiconductor gas sensors for CO and NO_x detection. Chemistry of Materials, **2007**, 19, pp. 1009-1015.

[49] V.P. Santos, M.F.R. Pereira, J.J.M. Órfão, J.L. Figueiredo, The role of lattice oxygen on the activity of manganese oxides towards the oxidation of volatile organic compounds. Applied Catalysis B: Environmental, **2010**, 99, pp. 353-363.

[50] N. Asim, S. Radiman, M.A. Yarmo, M.S.B. Golriz, Vanadium pentoxide: synthesis and characterization of nanorod and nanoparticle V_2O_5 using CTAB micelle solution. Microporous and Mesoporous Materials, **2009**, 120, pp. 397-401.

[51] M. Shahid, I. Shakir, S. Yang, D.J. Kang, Facile synthesis of core–shell SnO_2/V_2O_5 nanowires and their efficient photocatalytic property. Materials Chemistry and Physics, **2010**, 124, pp. 619-622.

[52] J. Mendialdua, R. Casanova, Y. Barbaux, XPS studies of V_2O_5, V_6O_{13}, VO_2 and V_2O_3. Journal of Electron Spectroscopy and Related Phenomena, **1995**, 71, pp. 249-261.

[53] M. Demeter, M. Neumann, W. Reichelt, Mixed-valence vanadium oxides studied by XPS. Surface Science, **2000**, 454, pp. 41-44.

[54] G. Silversmit, D. Depla, H. Poelman, G.B. Marin, R. De Gryse, Determination of the V2p XPS binding energies for different vanadium oxidation states (V^{5+} to V^{0+}). Journal of Electron Spectroscopy and Related Phenomena, **2004**, 135, pp. 167-175.

[55] G.A. Sawatzky, D. Post, X-ray photoelectron and Auger spectroscopy study of some vanadium oxides, Physical Review B, **1979**, 20, pp. 1546-1555.

[56] R. Zimmermann, R. Claessen, F. Reinert, P. Steiner, S. Hüfner, Strong hybridization in vanadium oxides: evidence from photoemission and absorption spectroscopy. Journal of Physics: Condensed Matter, **1998**, 10, pp. 5697-5716.

[57] K. Dyrek, M. Łabanowska, H. Rembertowicz, E. Bidzińska, Electron paramagnetic resonance study of V_2O_5 deactivation in the course of catalytic oxidation of SO_2 to SO_3. Spectrochimica Acta Part A: Molecular and Biomolecular Spectroscopy, **2000**, 56, pp. 309-318.

[58] Z. Strassberger, E. Ramos-Fernandez, A. Boonstra, R. Jorna, S. Tanase, G. Rothenberg, Synthesis, characterization and testing of a new V_2O_5/Al_2O_3-MgO

catalyst for butane dehydrogenation and limonene oxidation. Dalton Transactions, **2013**, 42, pp. 5546-5553.

[59] F. Morazzoni, C. Canevali, N. Chiodini, C. Mari, R. Ruffo, R. Scotti, L. Armelao, E. Tondello, L.E. Depero, E. Bontempi, Nanostructured Pt-doped tin oxide films: Sol-gel preparation, spectroscopic and electrical characterization. Chemistry of Materials, **2001**, 13, pp. 4355-4361.

[60] X. Chen, L. Li, Y. Xu, Y. Zhang, G. Li, Electron competitive migration regulating for dual maxima of water photolysis, RSC Advances, **2016**, 6, pp. 995-1003.

[61] D. Gulevich, M. Rumyantseva, A. Marikutsa, T. Shatalova, E. Konstantinova, E. Gerasimov, A. Gaskov, Nanocomposites SnO_2/SiO_2: SiO_2 impact on the active centers and conductivity mechanism. Materials, 2019, 12, pp. 3618.

[62] S. Zhang, Q. Zhong, Promotional effect of WO_3 on O_2^- over V_2O_5/TiO_2 catalyst for selective catalytic reduction of NO with NH_3. Journal of Molecular Catalysis A: Chemical, **2013**, 373, pp. 108-113.

[63] C.B. Rodella, P.A. Nascente, V.R. Mastelaro, M. Zucchi, R.W.A. Franco, C.J. Magon, P. Donoso, A.O. Florentino, Chemical and structural characterization of V_2O_5/TiO_2 catalysts. Journal of Vacuum Science & Technology A: Vacuum, Surfaces, and Films, **2001**, 19, pp. 1158-1163.

[64] P. Chetri, B. Choudhury, Room temperature ferromagnetism in SnO_2 nanoparticles: An experimental and density functional study. Journal of Materials Chemistry C, **2014**, 2, pp. 9294-9302.

[65] M.S. Rigutto, H. van Bekkum, Vanadium site in VAPO-5: characterization and catalytic properties in liquid-phase alkene epoxidation and benzylic oxidation. Journal of Molecular Catalysis, **1993**, 81, pp. 77-98

[66] K. Lemke, H. Ehrich, U. Lohse, H. Berndt, K. Jähnisch, Selective hydroxylation of benzene to phenol over supported vanadium oxide catalysts. Applied Catalysis A: General, **2003**, 243, pp. 41-51.

[67] P.R. Makgwane, S.S. Ray, Development of a high-performance nanostructured V_2O_5/SnO_2 catalyst for efficient benzene hydroxylation. Applied Catalysis A: General, **2015**, 492, pp. 10-22.

CHAPTER 5

Heterostructure SnO₂ interfaced Co, Cu, Mn and Ni nano-oxide catalysts for selective oxidation of furfural to maleic acid

5.1 Introduction

The development of bifunctional heterogeneous catalysts for mediating efficient catalytic conversion of biomass into commodity, specialty and functional performance chemicals still remains one of the main challenges in attaining green and sustainable chemistry processing.[1,2] The utilization of transition metal oxide based heterogeneous catalysts with adequate acidic, basic or redox active sites have long been exploited in catalysis.[3-5] In particular, the use of cheap heterogeneous catalysts consisting of cheap metal oxides of Co, Cu, Mn, and Ni coupled to support materials with tunable basic/acidic sites as bifunctional catalysts has been successfully demostrated in the oxidation reactions of 5-hydroxymethylfurfural to 2,5-diformylfuran[6,7], 5-formyl-2-furancarboxylic acid[8], and 2,5-furandicarboxylic acid.[9-11]

The conversion of lignocellulose derived furans, furfural and 5-hydroxymethylfurfural to a plethora of value-added chemicals has received considerable research attention as prominent substitutes or supplements to some of the petroleum-based chemical.[12-14] Amongst the many routes for the conversional upgrade of these biomass-derived platform chemicals, the liquid-phase oxidation reaction of furfural, a key chemical compound derived from the dehydration of xylose, with molecular O_2 or H_2O_2 oxidants presents a direct route for the synthesis of renewable maleic acid as an alternative to the industrial gas phase butane oxidation process. Commercially, maleic acid is synthesized by hydrolysis of maleic anhydride, which is produced from the gas-phase oxidation process

of butane or benzene.[15] However, the industrial process for maleic anhydride production is fossil resource-based, which is associated with several energy intensive steps and also produces green house gases such as CO_2 and CO, thus rendering the process economically costly and environmentally unfriendly.[16]

Recently, there has been a growing interest to produce renewable maleic acid from sustainable biomass derived carbon sources. Furthermore, the liquid-phase oxidation of furfural and 5-hydroxymethylfurfural over different catalysts to produce bio-based maleic acid and maleic anhydride has been successfully demonstrated at the laboratory scale.[17-25] The successful use of H_2O_2 as an atom efficient oxidant presents an attractive route to develop a green protocol for the synthesis of bio-based maleic acid from furfural oxidation reaction (**Scheme 5-1**). Araji and co-workers[26] demonstrated the furfural oxidation reaction using H_2O_2 under aqueous solution of betaine hydrochloride (BHC, a quaternary ammonium salt) as homogeneous catalyst to achieve a 61% yield of maleic acid. Unfortunately, the recycling usage of BHC catalyst required an extra step to recover it by dehydration reaction, which could incur complications and costs to the product isolation and purification processes. Alonso-Fagúndez et.al[27] used a waste-derived poly-(styrene sulphonic acid) designed bifunctional catalyst possessing both redox and acidic active sites for the furfural oxidation with H_2O_2 to achieve maleic acid yield of 34%. Furthermore, the same group investigated the catalytic activity of bifunctional titanium-silicate (TS-1) molecular sieve catalyst for the furfural oxidation reaction with H_2O_2.[28] A maleic acid yield of 78% at reaction temperature of 50 °C was achieved. Unfortunately, the TS-1 catalyst experienced significant leaching of the Ti active sites, which resulted in catalyst deactivation upon recycling. Yang et.al[29] recently explored the oxidation of furfural with a series of K-doped graphitic carbon nitride with H_2O_2 and obtained a maleic acid yield of

70.4% at 100 °C. Based on the catalytic results achieved to date in the furfural oxidation reaction, there is a need for developing an effective catalyst that is chemically and structurally stable, active and reusable to improve on low furfural substrate conversion or yield, including catalyst leaching without the use of additives or co-catalysts. Ideally, the development of the furfural oxidation reaction with H_2O_2 to maleic acid based on heterogeneous metal oxide catalysts consisting of Co, Cu, Mn and Ni oxides could present an attractive and economical process. As a result, from a sustainable chemistry viewpoint, it would be interesting to exploit the redox properties of these low cost and abundant metal oxides for developing an efficient oxidation reaction conversion of furfural to maleic acid under mild reaction conditions. More importantly, the combination of these base metal oxides with an acidic oxide such as tin dioxide (SnO_2) could render the design of heterostructured composite catalysts with the required bifunctional reactive sites for mediating the selective furfural oxidation reaction to targeted maleic acid. These active sites are crucial for the furfural oxidation reaction were the Lewis acid sites are required to accelerate the electron transfer steps and the metal redox centres to facilitate the C–C bond cleavage process of the furfural substrate. Although SnO_2 on its own is a poor redox oxidation catalyst, however its synergistic coupling with another active metal will undoubtedly provide a dynamic approach to enhanced metal cationic effect arising from the SnO_2 Lewis acid reactive center that could induce the bifunctional coupling activity amenable for catalytic oxidation reaction of furfural as reported previously.[30-32]
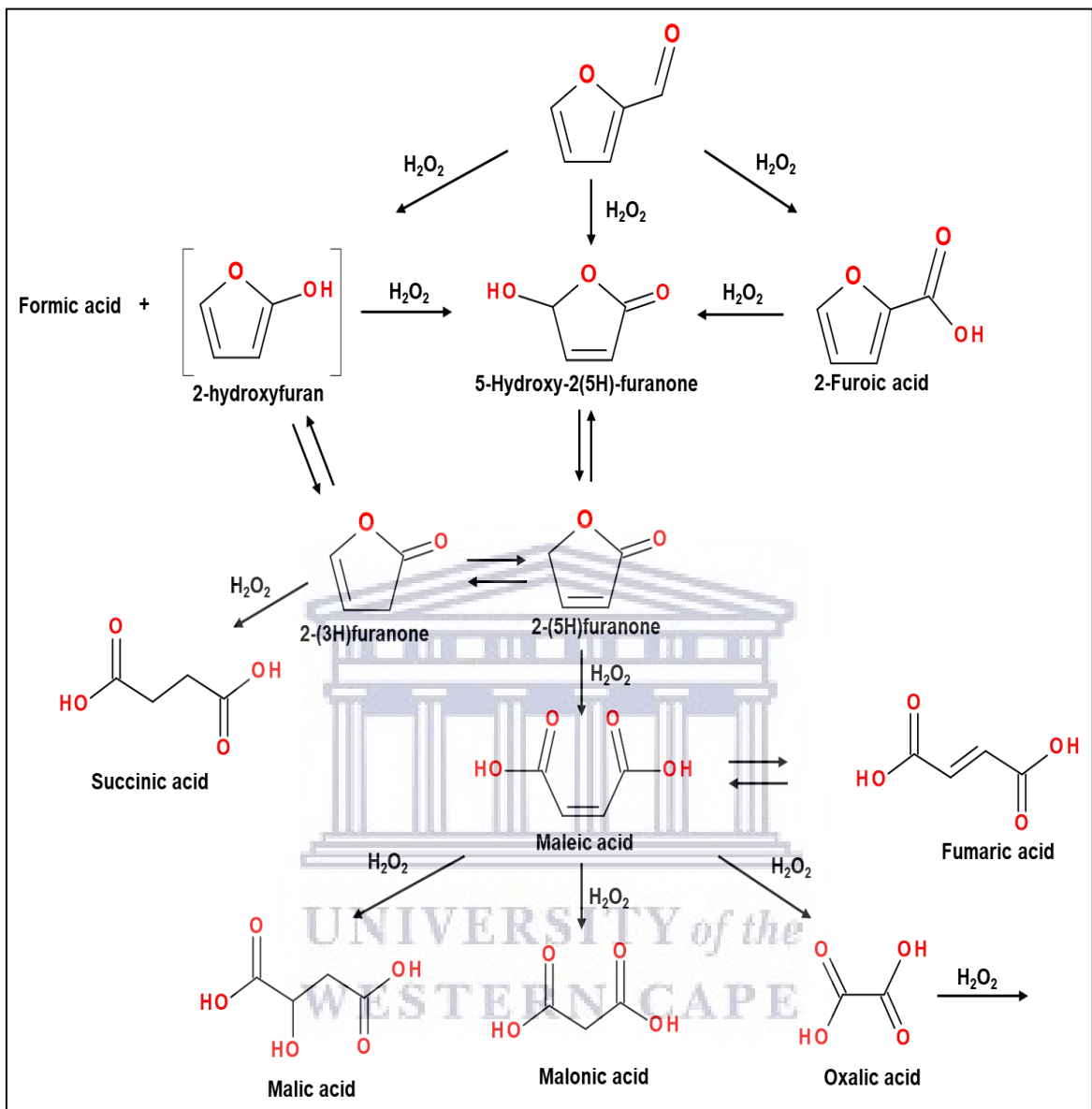
Scheme 5-1. Furfural oxidation reaction pathways to various products and intermediates.

This chapter details the synthesis of active heterostructure SnO_2 interfaced catalysts consisting of Co, Cu, Mn and Ni nano-oxide metals. The catalytic oxidation activity of the catalysts was evaluated in the oxidation reaction of furfural to maleic acid using H_2O_2 oxidant. In order to establish the baseline catalytic activity effect of the respective SnO_2 interfaced metal oxides, the structure properties of the catalysts were studied by using XRD, BET, H_2-TPR, HRTEM, and XPS.

5.2 Catalysts structure characterisation

5.2.1 Nitrogen sorption analysis

The BET surface areas (S_{BET}) and porosity analysis results of the SnO_2 heterostructure catalysts are summarized in **Table 5-1**. SnO_2 shows a surface area of 85.8 m^2/g with pore volume (V_p) and pore size (D_p) of 0.20 cm^3/g and 9.2 nm, respectively. For the SnO_2 heterostructure catalysts, their S_{BET}, V_p and D_p varied respectively according to the base metal oxide used. The NiO_x-SnO_2 catalyst obtained the lowest S_{BET} of 26.6 m^2/g with the D_p of 18.5 nm corresponding to the V_p of 0.12 cm^3/g. Both CoO_x-SnO_2 and CuO_x-SnO_2 catalysts showed a decrease in their S_{BET} to 60.6 m^2/g and 64.3 m^2/g, respectively, when compared to 85.8 m^2/g of SnO_2. Further, the respective D_p of 14.8 nm and 10.2 nm were determined for CoO_x-SnO_2 and CuO_x-SnO_2 with V_p of 0.23 cm^3/g (CuO_x-SnO_2) and 0.16 cm^3/g (CoO_x-SnO_2). The MnO_x-SnO_2 catalyst obtained the highest S_{BET} of 92.4 m^2/g and V_p of 0.33 cm^3/g at D_p of 14.4 nm. The isotherms of the catalysts showed to be type IV with classified H1 hysteresis loops, which is characteristic of materials with mesoporous pore structure (**Fig. 5-1**).[33] The mesoporous structure character of the catalysts is confirmed by their pore size distribution, which range between 4 - 64 nm (**Fig. B-1**).

Table 5-2: N_2 sorption, crystallite size and elemental analysis results of the heterostructured SnO_2 catalysts

Catalysts	SnO_2	CuO_x-SnO_2	CoO_x-SnO_2	MnO_x-SnO_2	NiO_x-SnO_2
S_{BET} (m^2/g)	85.8	60.6	64.3	92.4	26.6
D_p (nm)	9.2	14.8	10.2	14.4	18.5
V_p (cm^3/g)	0.20	0.23	0.16	0.33	0.12
[a] Crystallite size (nm)	11.8	7.5	7.4	8.1	17.4
[b] Metal loading (wt%)	N/A	17.9	19.1	18.9	18.4
[c] Surface metal atomic %	-	5.1	3.0	4.8	3.2
[c] Surface Sn atomic %	21.5	17.6	23.9	21.1	22.0
[c] Surface O atomic %	78.5	77.3	73.1	74.1	74.8
Surface metal/actual metal	-	0.28	0.16	0.25	0.17

[a] For SnO_2 phase determined by XRD using Scherrer equation, [b] ICP analysis; [c] XPS analysis.
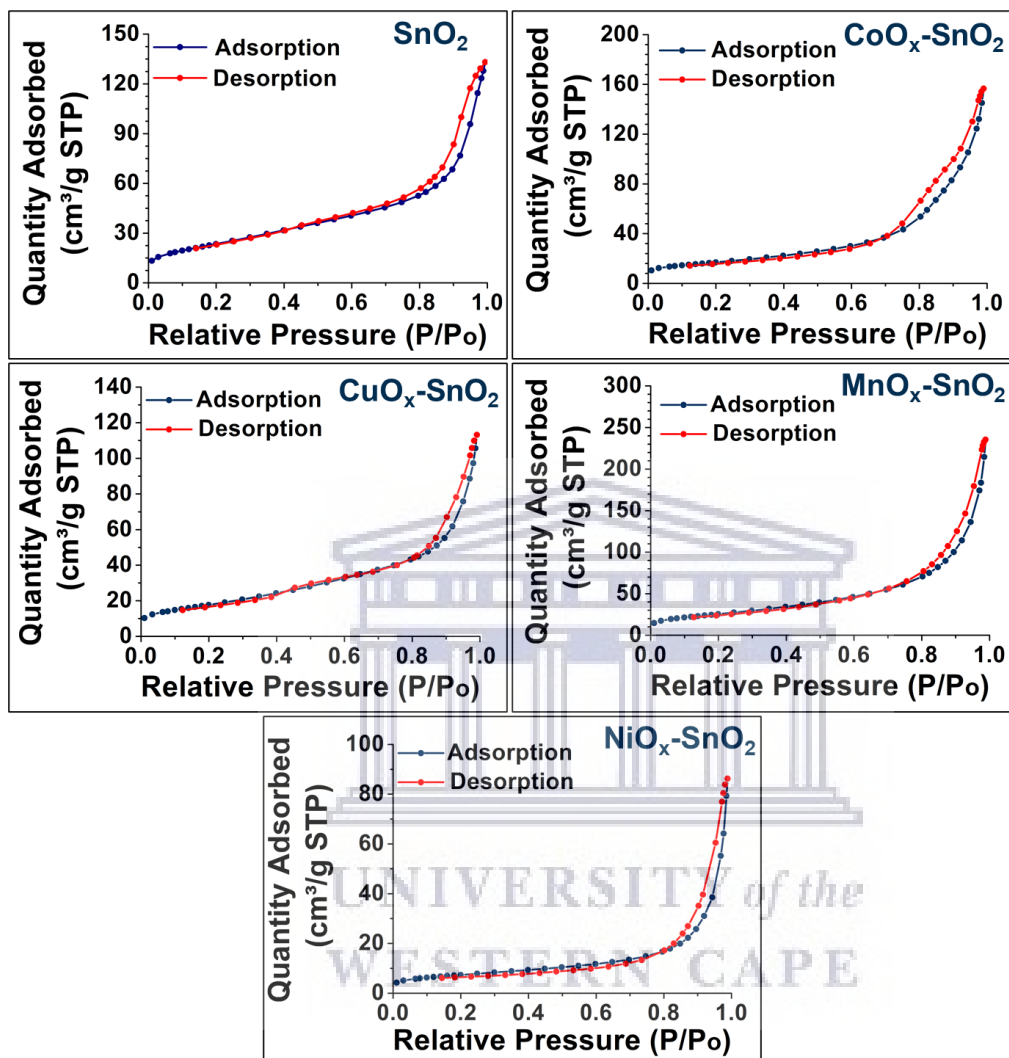
Fig. 5-1: Nitrogen sorption isotherms of the heterostructured SnO_2 catalysts.

5.2.2 X-ray diffraction (XRD) analysis

Fig. 5-2 shows the XRD of the SnO_2 heterostructure oxide catalysts. The peaks at 2θ of 26.6°, 33.9°, 38.0°, 51.8° and 54.7° are all indexed to (110), (101), (200), (211) and (220) crystallographic planes of SnO_2 with a tetragonal rutile structure (JCPDS no. 41-1445). Further, SnO_2 also shows two additional peaks at 2θ of 29.6° and 35.8°, which are due to the (101) and (002) planes of SnO (JCPDS no. 55-0837). The XRD of CoO_x-SnO_2 shows

additional four peaks at 2θ of 18.9°, 31.2°, 44.7° and 59.3° , which are due to the respective (111), (022), (004) and (115) planes of Co_3O_4 (JCPDS no. 42-1467).
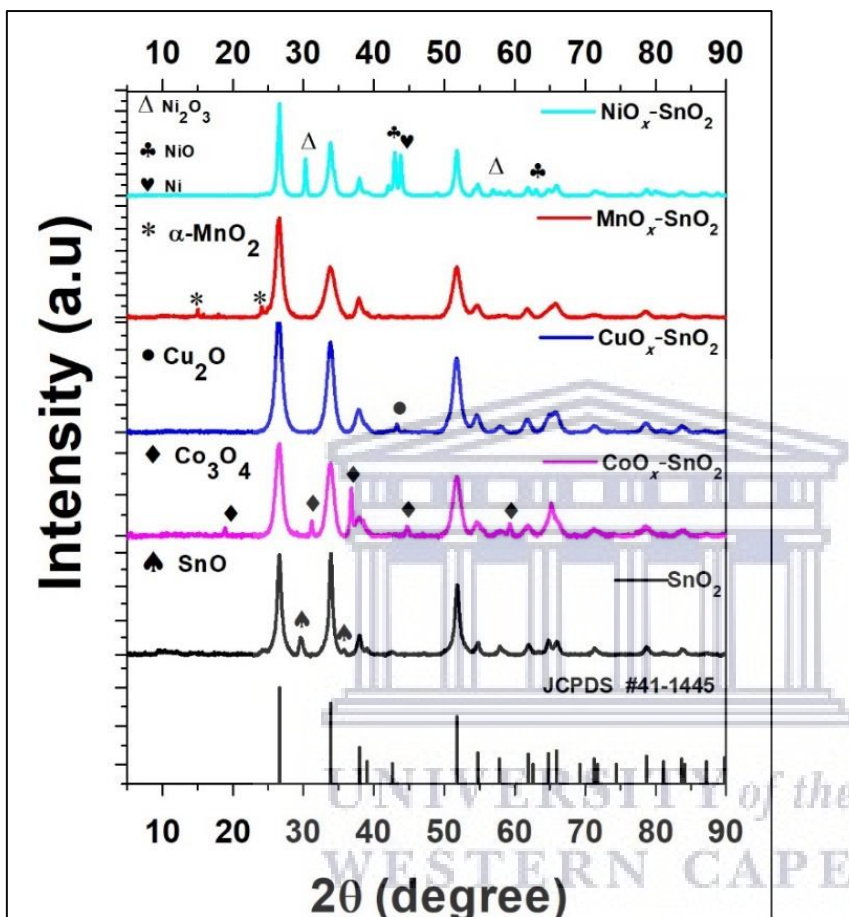
Fig. 5-2: XRD patterns of SnO_2 heterostructure oxide catalysts.

The XRD of CuO_x-SnO_2 shows one peak at 43.2° corresponding to (200) plane of Cu_2O (JCPDS no. 35-1091). MnO_x-SnO_2 shows the three XRD peaks at 2θ of 15.0°, 18.7° and 40.7° which are assigned to (110), (200) and (301) planes of α-MnO_2 (JCPDS no. 44-0141). For NiO_x-SnO_2 catalyst, a total of five peaks in addition to those of SnO_2 were observed. The peaks at 2θ of 30.3° and 56.9°, which are indexed respectively to the (002) and (202) planes of the Ni_2O_3 phase (JCPDS no. 14-0481) while those at 42.9° and 63.0° are indexed to the (200) and (220) planes of the NiO phase (JCPDS no. 47-1049). The

peak at 2θ of 43.8° is assigned to the (111) plane of metallic Ni (JCPDS no. 04-0850). The average crystallite sizes of the catalysts determined using the Scherrer equation and the SnO_2 (110) peak are in **Table 5-1**, which indicate the changes in the crystallite sizes of SnO_2 with respect to the interfaced metal oxides. SnO_2 showed the average crystallite size of 11.8 nm while the SnO_2 interfaced Co, Cu and Mn metal oxide catalysts show decreased crystallite sizes with the exception of the NiO_x-SnO_2, which showed the largest of 17.4 nm.

5.2.3 Morphological analysis

The scanning electron microscopy (SEM) micrograph images of SnO_2 showed the sample to compose of an agglomeration of densely packed nanoparticles (NPs) with non-uniform shapes and sizes (**Fig. 5-3**). The introduction of Co and Cu oxides onto SnO_2 showed to maintain the NPs morphology similar to that of the SnO_2. MnO_x-SnO_2 catalyst showed to form NPs arranged into platelet, flake-like morphology. Similarly, NiO_x-SnO_2 showed the formation of self-assembled NPs into arrays of sharp rod-like morphology with some wide pores.
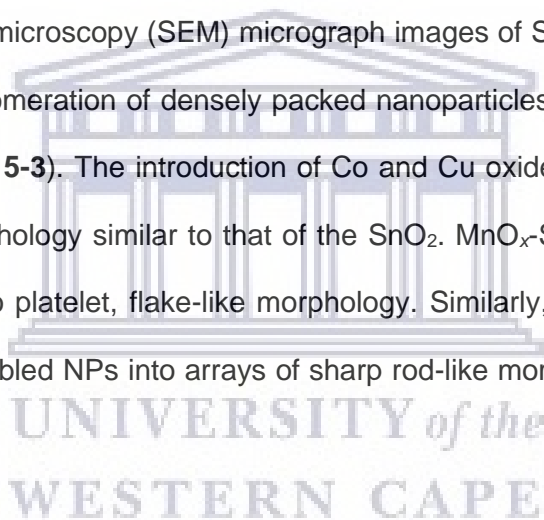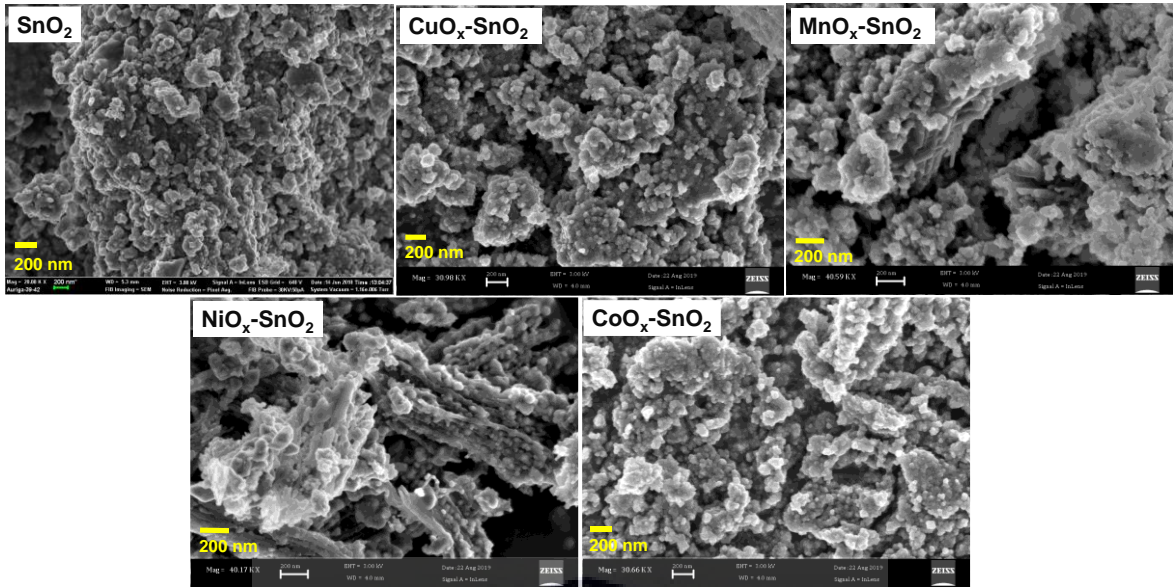
Fig. 5-3: SEM images of the heterostructure SnO_2 metal oxide catalysts.
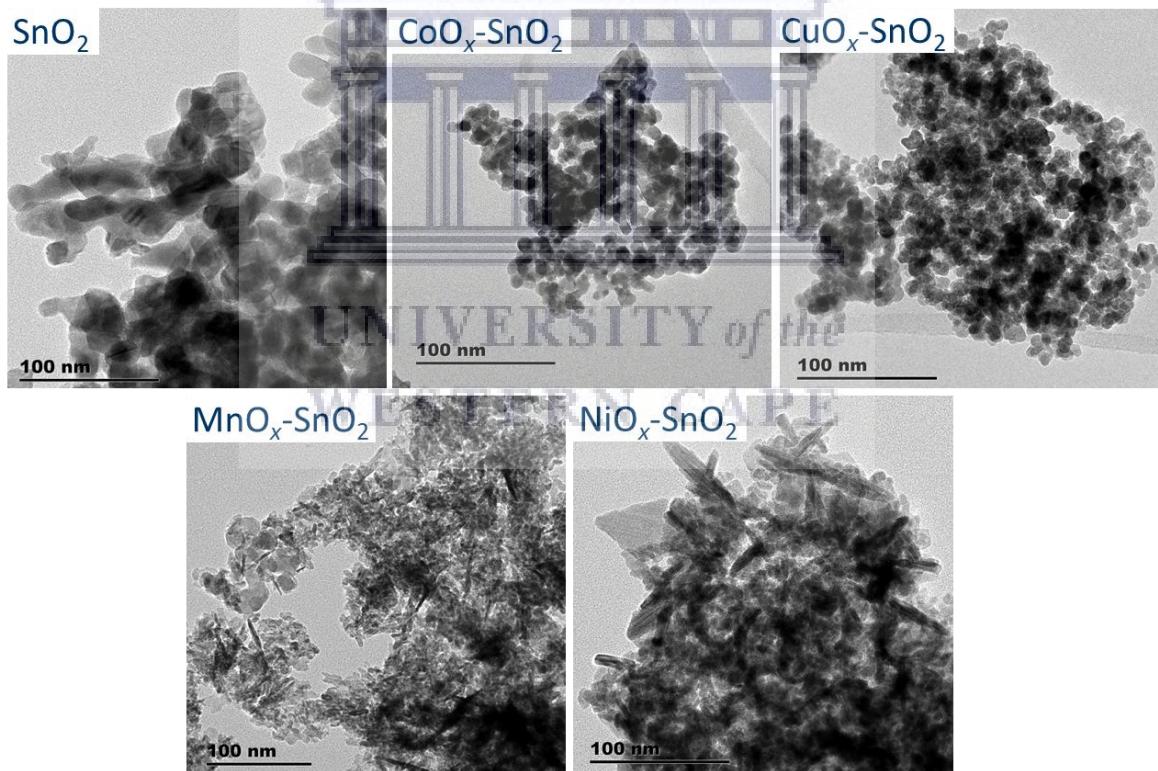
Fig. 5-4: TEM micrograph images of the heterostructured SnO_2-based catalysts.

The TEM micrograph images shown in **Fig. 5-4** show SnO_2 to comprise of an agglomeration of densely packed NPs of variable shapes and sizes with the CoO_x-SnO_2

and CuO_x-SnO_2 showing similar morphology. The MnO_x-SnO_2 oxide displayed densely packed NPs with populated flake-like morphology while the NiO_x-SnO_2 oxide showed a composition of short, densely packed NPs with nano-rod morphology. These results are in agreement with the morphologies observed from SEM analysis. The HRTEM micrographs of the catalysts (**Fig. 5-5**) are characterized by well-defined lattice fringes indicating the crystalline nature of the catalysts. The measured d-spacing on all the micrographs are equal to 0.33 nm which correspond to the (110) crystallographic plane of SnO_2 (tetragonal). A d-spacing of 0.26 nm was measured for the CuO_x-SnO_2 and NiO_x-SnO_2 catalysts which correspond to the (101) crystallographic plane of tetragonal SnO_2.
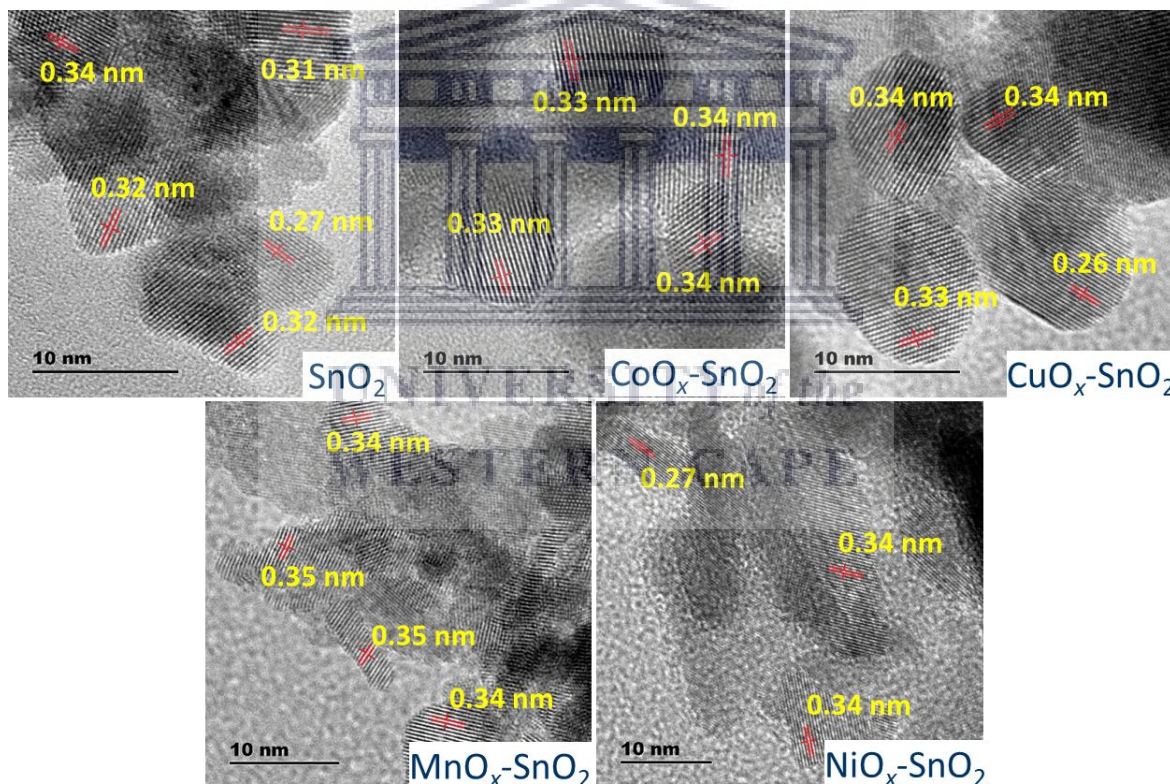
Fig. 5-5: HRTEM micrograph images of the heterostructured SnO_2-based catalysts.

The SAED patterns of the catalysts (**Fig. 5-6**) were characterized by the concentric diffraction rings with discrete spots, which confirmed the polycrystalline nature of the SnO_2

heterostructure catalysts. The three most inner SAED rings were all indexed to the respective (110), (101) and (211) planes of the tetragonal phase of SnO_2 NPs. In addition to the three rings, a fourth concentric ring is also observed for the CoO_x-SnO_2, CuO_x-SnO_2 and MnO_x-SnO_2 catalysts corresponding to the SnO_2 (112) plane. The fourth ring observed for the NiO_x-SnO_2 catalyst corresponds to the SnO_2 (301) plane. These results along with those from the measured interplanar spacing (HRTEM) are in agreement with the obtained XRD data showing predominantly the SnO_2 reflections.
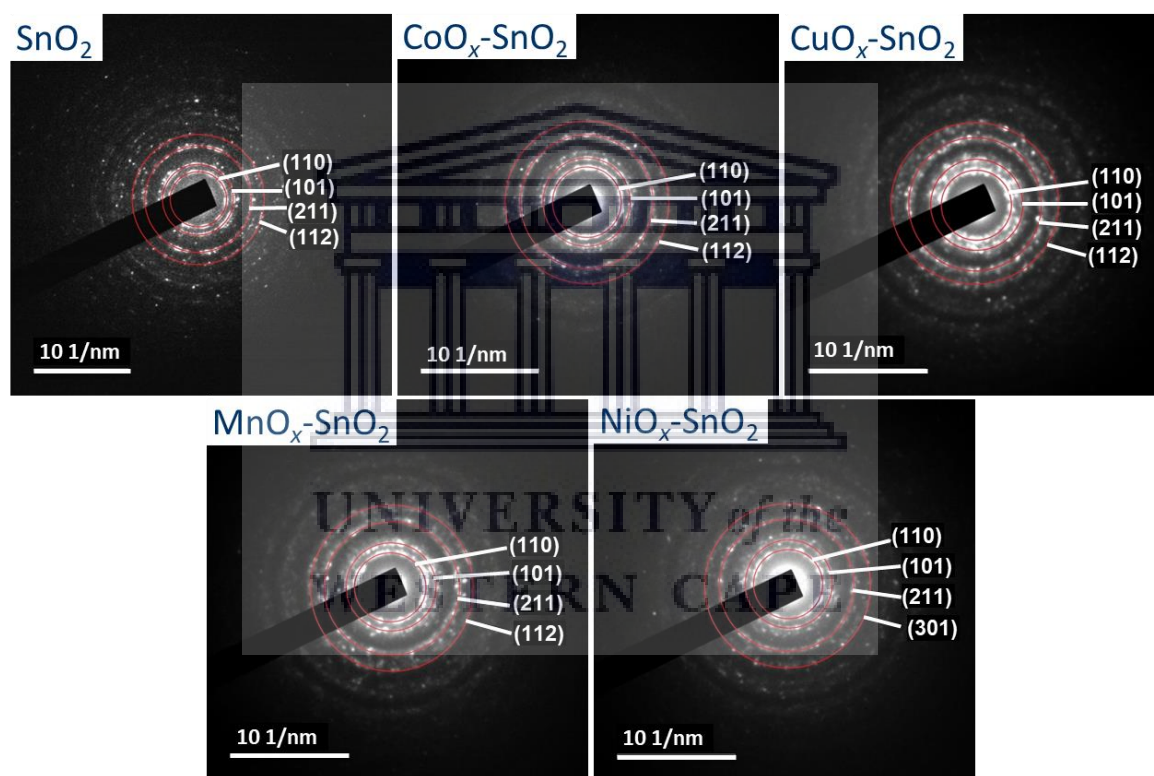
Fig. 5-6: SAED patterns of the heterostructured SnO_2-based catalysts.

5.2.4 X-ray photoelectron spectroscopy (XPS) analysis

XPS analysis was used to evaluate the surface chemical state and the electronic structure interactions of the heterostructured SnO_2 catalysts. **Fig. 5-7** shows the survey scans, Sn3d and O 1s profile peaks of SnO_2 and the heterostructure SnO_2 catalysts, respectively. The Sn3d peaks showed to appear as a spin-orbit doublet. The respective Sn 3d peaks of

SnO$_2$ corresponding to the 3d$_{5/2}$ and 3d$_{3/2}$ orbitals were observed at 486.6 eV and 495.0 eV. The obtained Sn XPS structure information is consistent with previously reported data that showed Sn with the predominant 4+ oxidation state.[34-36] The Sn 3d peaks of the respective heterostructure SnO$_2$ catalysts showed shifting to higher and lower binding energies with the exception of CuO$_x$-SnO$_2$. For example, MnO$_x$-SnO$_2$ and CoO$_x$-SnO$_2$ exhibited peak shift to lower binding energies, and NiO$_x$-SnO$_2$ to higher binding energy. The shifts in the Sn 3d peaks binding energy were induced by the varying electronic structure interaction of the base metals with SnO$_2$, which could infer various catalytic activity performances. The O 1s peak of SnO$_2$ at 530.4 eV indicate the existence of the lattice oxygen atoms to be mainly as the O^{2-} species.[37,38] The asymmetrical shape of the O 1s profile peaks indicate that they are due to the contribution of more than one metal oxide species.
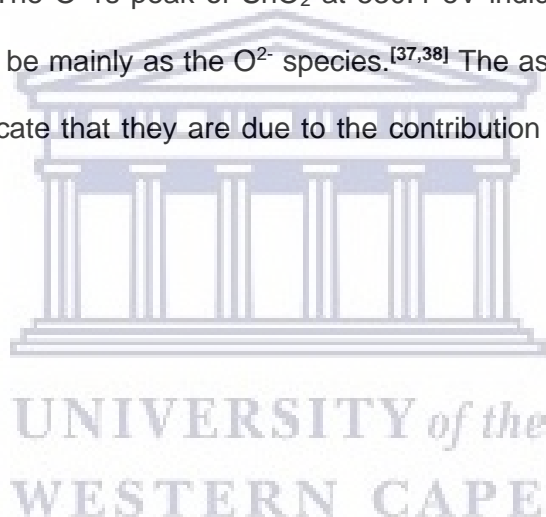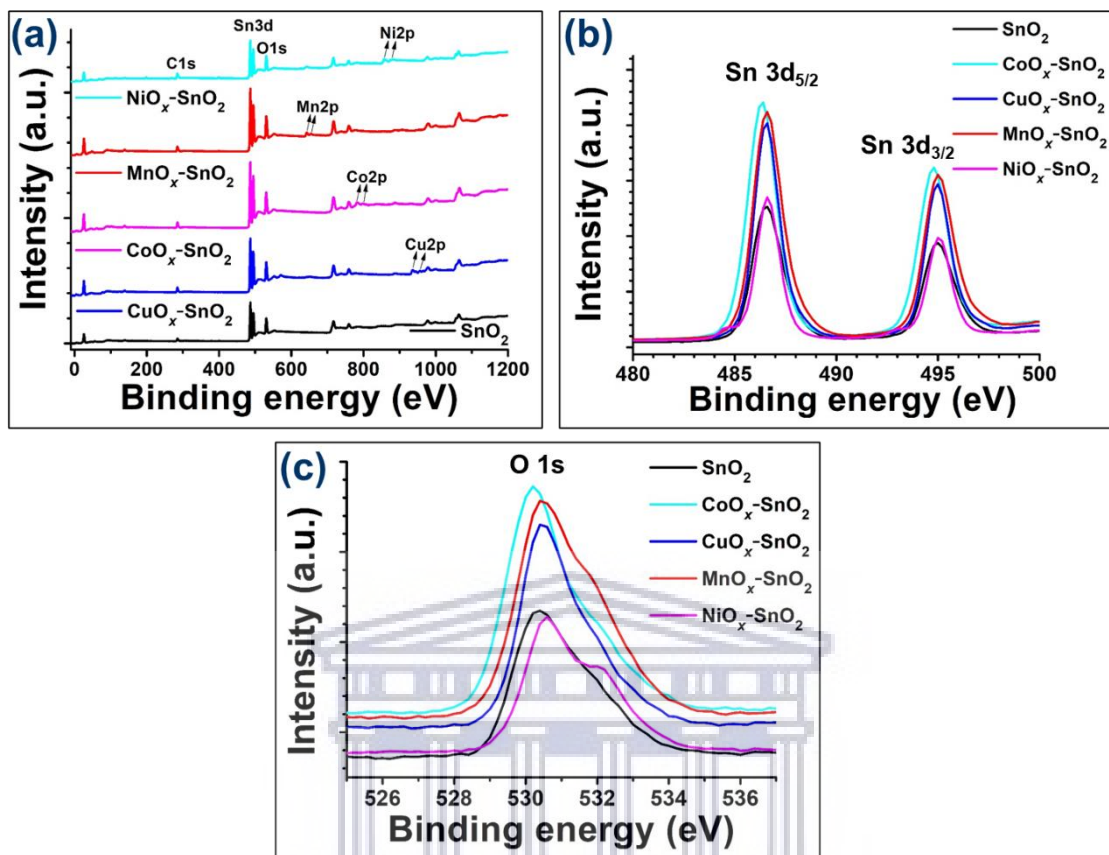
Fig. 5-7: XPS spectra of the heterostructured SnO_2 catalysts showing (a) survey scans, (b) Sn 3d, and (c) O 1s peaks.

Fig. 5-8 shows the 2p electronic structure of the Co, Cu, Mn and Ni oxides interfaced SnO_2 catalysts. The Co 2p consist of peaks at 780.8 eV ($2p_{3/2}$) and 797.7 eV ($2p_{1/2}$), while for Cu 2p the peaks are at 934.4 eV ($2p_{3/2}$) and 955.1 eV ($2p_{1/2}$). The Cu 2p further shows two satellite peaks at 944.9 eV and 962.7 eV, which indicate the presence of Cu in the 2+ oxidation state. The Mn 2p peaks of MnO_x-SnO_2 are at 641.7 eV ($2p_{3/2}$) and 653.7 eV ($2p_{1/2}$), while for Ni 2p are observed at 856.6 eV ($2p_{3/2}$) and 874.2 eV ($2p_{1/2}$) with two additional satellite peaks at 862.5 eV and 881.6 eV. The base metal XPS electronic information obtained is corroborated by previously reported data.[39-43]
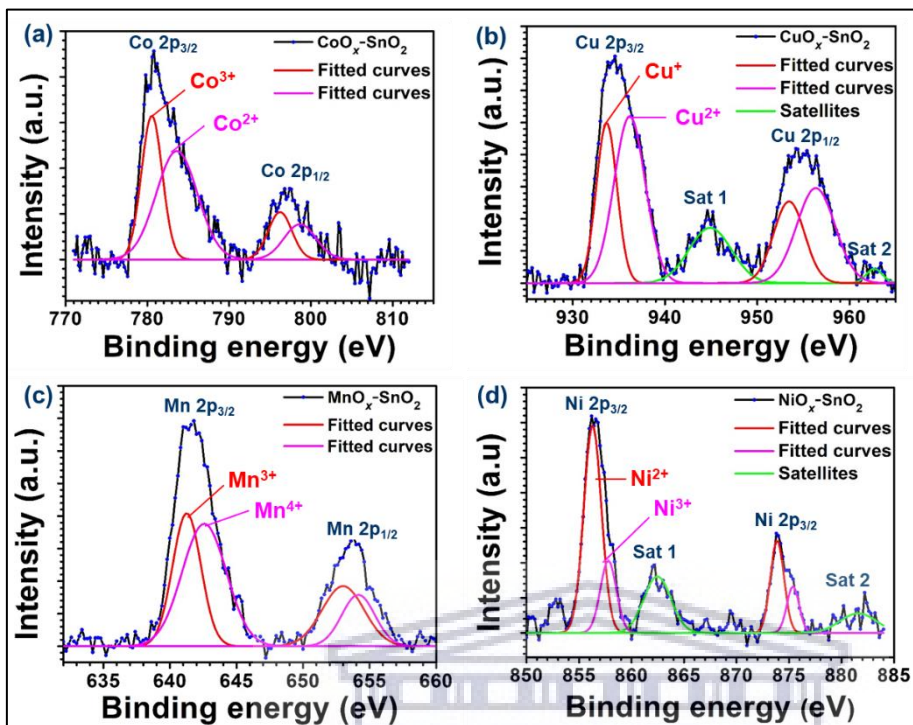
Fig. 5-8: High resolution XPS 2p peak profiles of (a) CoO_x-SnO_2; (b) CuO_x-SnO_2; (c) MnO_x-SnO_2; and (d) NiO_x-SnO_2 catalysts.

The fitted XPS 2p peaks of the catalysts presented in **Fig. 5-8** show both the $2p_{3/2}$ and $2p_{1/2}$ peaks. The fitted peaks of Co $2p_{3/2}$ are at 780.5 eV and 783.6 eV, which are assigned to Co^{3+} and Co^{2+}, respectively.[43,44] The peak area ratio of Co^{2+}/Co^{3+} is 1.49 (**Table 5-2**), indicating cobalt to exist predominantly in 2+ oxidation state. For CuO_x-SnO_2, the peaks of Cu $2p_{3/2}$ are at 933.7 eV and 936.2 eV, which confirms the presence of both Cu^+ and Cu^{2+} oxidation state.[45,46] The peak area ratio Cu^+/Cu^{2+} is 0.63 showing copper to exist more in the 2+ oxidation state. The Mn $2p_{3/2}$ of MnO_x-SnO_2 catalyst is fitted with peaks at 641.3 eV and 642.6 eV, which correspond respectively to Mn^{3+} and Mn^{4+}.[47,48] The peak area ratio of Mn^{3+}/Mn^{4+} peaks is 0.70, which indicate the existence of manganese to be slightly more in the 4+ oxidation state. The fitted Ni $2p_{3/2}$ peaks at 856.3 eV and 857.8 eV confirm the presence of Ni^{2+} and Ni^{3+} in the NiO_x-SnO_2 catalyst, respectively.[49,50] The peak area ratio of Ni^{2+}/Ni^{3+} is 3.16, which shows the existence of

132

nickel in Ni^{2+} oxidation state. Further, the percentage amounts of Mn and Mn-1 surface oxidation state compositions are summarized in **Table 5-2** while surface enriched amounts of the various heterostructured MOx-SnO$_2$ interface metal oxides catalysts are in **Table 5-1**.

Table 5-2. XPS surface compositions data of the heterostructured SnO$_2$ metal oxide catalysts.							
Catalyst	Metal 2p$_{3/2}$				O1s		
	Fitted	Metal	%	M^{n-1}/M^n	Fitted	Oxygen	O_V/O_L
SnO$_2$	N/A				530.2	O_L	0.86
					531.2	O_V	
					532.2	O_{ads}	
CoO$_x$-SnO$_2$	780.5	Co^{3+}	59.9	1.49	530.0	O_L	1.64
	783.6	Co^{2+}	40.1		531.2	O_V	
					533.9	O_{ads}	
CuO$_x$-SnO$_2$	933.7	Cu^+	38.3	0.63	530.3	O_L	1.75
	936.2	Cu^{2+}	61.3		531.0	O_V	
					532.3	O_{ads}	
MnO$_x$-SnO$_2$	641.3	Mn^{3+}	58.9	1.43	530.4	O_L	0.46
	642.6	Mn^{4+}	41.1		532.0	O_V	
					533.2	O_{ads}	
NiO$_x$-SnO$_2$	856.3	Ni^{2+}	76.0	3.16	530.5	O_L	2.11
	857.8	Ni^{3+}	24.0		531.6	O_V	
					532.2	O_{ads}	

Fig. 5-9 shows the fitted O1s profile peaks of all the SnO$_2$ heterostructure catalysts. The O1s profiles are fitted into three distinctive peaks, which are assigned to lattice oxygen atoms (O_L, ~530 eV), oxygen vacancies or surface adsorbed oxygen (O_V, ~531 eV) and adsorbed water (O_{ads}, ~532-533 eV).[51,52] A number of literature studies have reported the intimate relation of surface oxygen vacancies on oxide surfaces and their catalytic activity, and high concentrations amount of surface oxygen vacancies in the oxides structure have been demonstrated to be beneficial for certain catalytic oxidation reactions.[53,54] The

concentration of surface oxygen vacancies was estimated by calculating the peak area ratios of the O_L and O_V peaks (**Table 5-2**).
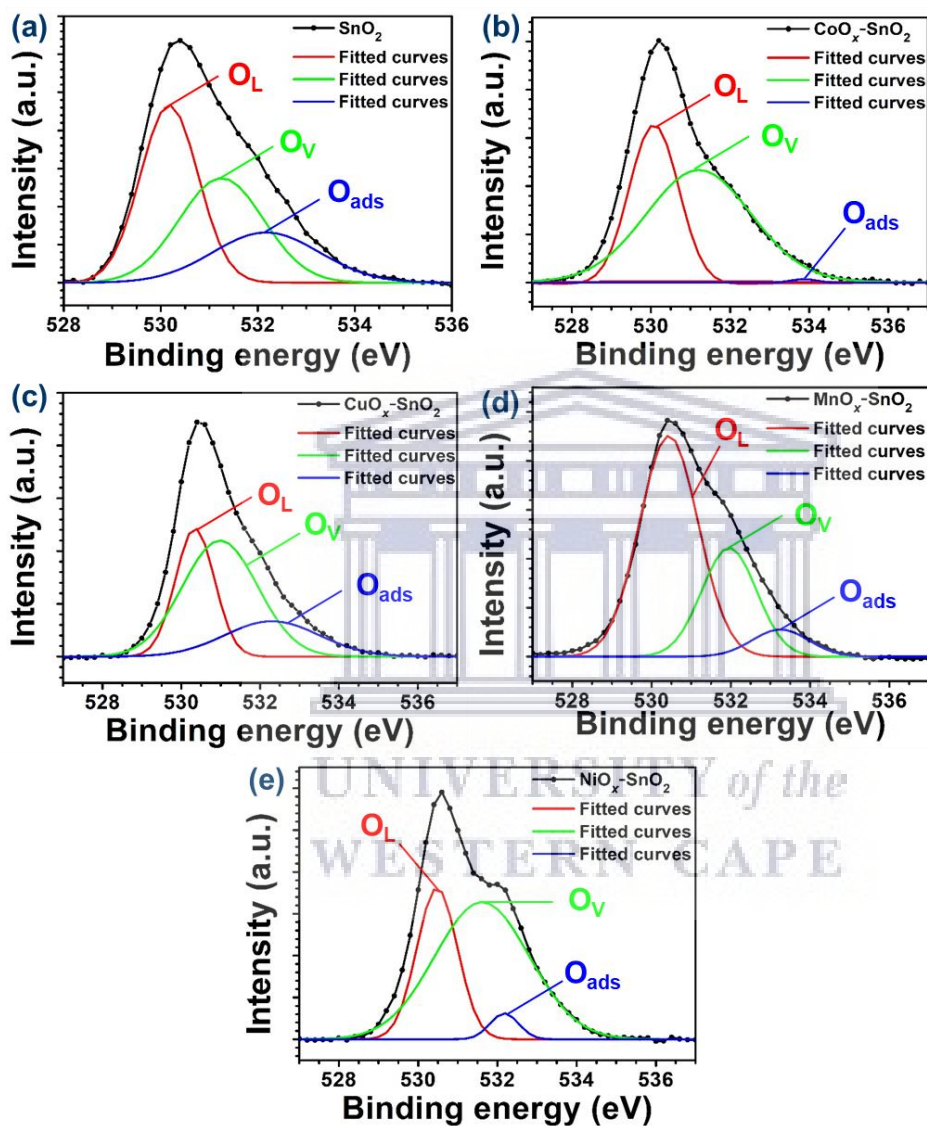
Fig. 5-9: High resolution XPS O 1s peak profiles of SnO_2 heterostructure catalysts.

The calculated O_V/O_L peak area ratios were as follows: 0.86 (SnO_2), 1.64 (CoO_x-SnO_2), 1.75 (CuO_x-SnO_2), 0.46 (MnO_x-SnO_2) and 2.11 (NiO_x-SnO_2). These results show the NiO_x-SnO_2 catalyst to possess large concentration amount of surface oxygen vacancies and MnO_x-SnO_2 catalyst the least. The varying O_V/O_L ratios are correlated to the observed

shifts of the O1s peaks in SnO_2 heterostructure catalysts, which signify the different modified electronic structure interactions of SnO_2 with the respective base metals (**Fig. 5-7**). The O1s peak of CoO_x-SnO_2 is shifted to low BE while both CuO_x-SnO_2 and NiO_x-SnO_2 catalysts are shifted to high BE and the MnO_x-SnO_2 catalyst O 1s peak is not shifted.

5.2.5 Hydrogen-Temperature programmed reduction (H_2-TPR) analysis

Fig. 5-10 shows the H_2-TPR profiles of the Co, Cu, Mn and Ni oxides heterostructured SnO_2 catalysts. All the catalysts showed the high intensity low reduction temperature peak at 130-150 °C. The respective reduction temperatures of this peak are as follows, CuO_x-SnO_2 (126.6 °C), CoO_x-SnO_2 (135.6 °C); MnO_x-SnO_2 (138.1 °C), and NiO_x-SnO_2 (143.1 °C) with CuO_x-SnO_2 showing the lowest temperature for the removal of the surface oxygen atoms. Moreover, CuO_x-SnO_2 shows an additional peak at 227.9 °C, which indicates the two-stage reduction of CuO via the Cu^{2+} to Cu^+ and then to Cu^0.[55,56] Also, the CoO_x-SnO_2 catalyst is showing the two additional reduction peaks at 201.4 °C and 291.3 °C, which indicate the multiple stage reduction patterns of Co oxide via its Co^{3+}, Co^{2+}, Co^+ and Co^0 oxidation states.[57,58]

The high reduction temperature peaks stretching from 340 °C to 540 °C in both CuO_x-SnO_2 and CoO_x-SnO_2 is assigned to SnO_2.[59,60] Both MnO_x-SnO_2 and NiO_x-SnO_2 catalysts shows shoulder reduction peaks at around 180 - 220 °C, which connects continuously with the reduction peaks in the region of SnO_2. This is attributed to the multiple reduction temperature stages of the catalysts and their strong interactions with the SnO_2, which showed to lower its reduction temperatures slightly.[61-64]
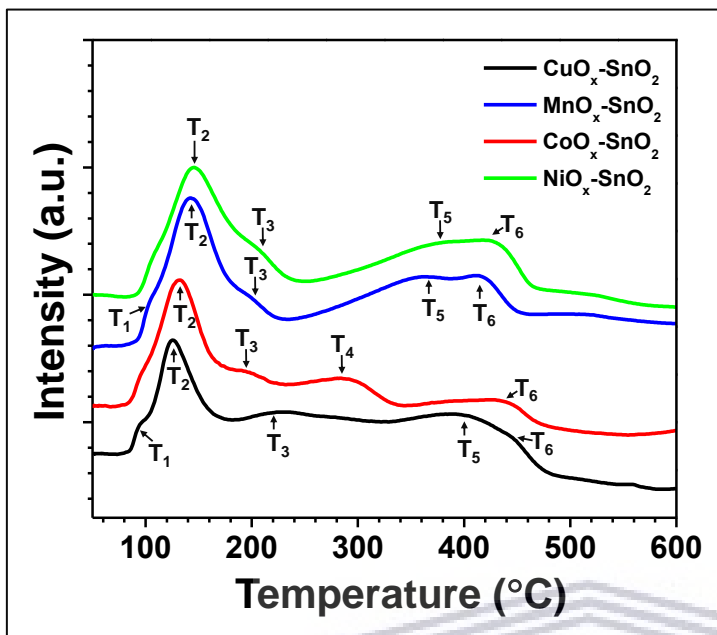
Fig. 5-10: H_2-TPR profiles of the heterostructured SnO_2 catalysts.

Table 5-3: Analysis amount of H_2 consumption of the various heterostructured MO_x-SnO_2 catalysts

	Total H_2 uptake μmol.$(g_{cat})^{-1}$						Total H_2 uptake
Catalysts	T_1	T_2	T_3	T_4	T_5	T_6	μmol.$(g_{cat})^{-1}$
CuO_x-SnO_2	33.7	229.6	93.9	–	98.1	106.6	561.9
CoO_x-SnO_2	–	237.8	45.4	102.1	–	137.2	522.5
NiO_x-SnO_2	–	264.3	58.2	–	141.7	119.3	583.5
MnO_x-SnO_2	22.4	258.1	60.9	–	155.8	104.8	602.0

Table 5-3 summarizes the tentative H_2 consumption amounts at various reduction temperatures of the heterostructured MO_x-SnO_2 catalysts. Both CuO_x-SnO_2 and MnO_x-SnO_2 start with low reduction temperature H_2 consumption, which indicate the presence of some isolated surface oxygen atoms compared to the other catalysts. Further, at high reduction temperatures of 350 °C both MnOx-SnO_2 and NiOx-SnO_2 shows the high amount uptake of H_2 due the broadness of their reductions overlapping to higher

temperature, which indicate the strong metal support interaction leading to possible spill over to SnO_2 support to promote the mobility of sub-surface to surface removal.

5.3 Catalytic activity results

5.3.1 Effect of catalyst amount on furfural oxidation rates and product evolution

The catalytic activity performance of the different heterostructure SnO_2 base metal oxide catalysts were evaluated in the oxidation of furfural using H_2O_2. However, the catalytic oxidation reaction was optimized first with the CuO_x-SnO_2 catalyst before screening of the catalysts. The first parameter investigated was the effect of catalyst dosage on the rate and product distribution and the activity results obtained in terms of conversion and yield of maleic acid are respectively summarized in **Table 5-4** and **Fig. 5-11**. The conversion of furfural showed to increase from 89.6% to 96.2% with the increase in CuO_x-SnO_2 catalyst dosages from 10 mg to 40 mg, while at 50 mg it showed to decrease slightly to 93.4%. The selectivity of maleic acid decreased significantly from 41.3% at 10 mg to 16.1% at 50 mg. The yield of maleic acid showed slight increase from 37.0% at 10 mg to 39.4% at 20 mg, while it decreased relatively for catalyst dosages of 30 - 50 mg to achieve the least amount of 15.1% at 50 mg.

Table 5-4: Effect of catalyst dosage on furfural oxidation rates with the CuO_x-SnO_2 catalyst.

Amount (mg)	Conversion (%)	Yield (%)					
		MA	OA	FMA	SA	FA	[a] Others
10	89.6	37.0	33.9	7.9	1.3	4.3	5.2
20	93.9	39.4	33.9	9.1	0.0	1.3	10.2
30	94.4	34.3	42.3	9.1	0.6	2.6	5.5
40	96.2	17.1	68.1	6.7	0.2	0.8	3.3
50	93.4	15.1	57.0	0.0	0.0	14.8	6.5

[a] Side products such as 2-(5H)-furanone, formic acid and malic acid. Symbols: MA = maleic acid, OA = oxalic acid, FMA = fumaric acid, SA = succinic acid, FA = 2-furoic acid. Reaction conditions: furfural (1 mmol); 30% aq. H_2O_2 (5 mmol); H_2O solvent (2 mL); T= 60°C and t = 3 h.

The most noticeable by-product with the high amount increase was oxalic acid, which increased from the yield of 33.9% at 10 mg to 68.1% at 40 mg, then decreased to 57.0% at 50 mg. Other by-products included the formation of fumaric acid and 2-furoic acid with practical yields of less than 15% (**Table 5-4**). Overall, the use of small quantities of the catalyst (10 and 20 mg) showed to present sufficient active sites for the furfural conversion while high amounts (≥ 30 mg) were detrimental to promote the over-oxidation reactions of the products. The 20 mg catalyst dosage was then selected as the best performing to give both reasonable conversion and highest maleic acid selectivity (41.9%) for further optimization of furfural reaction conditions.
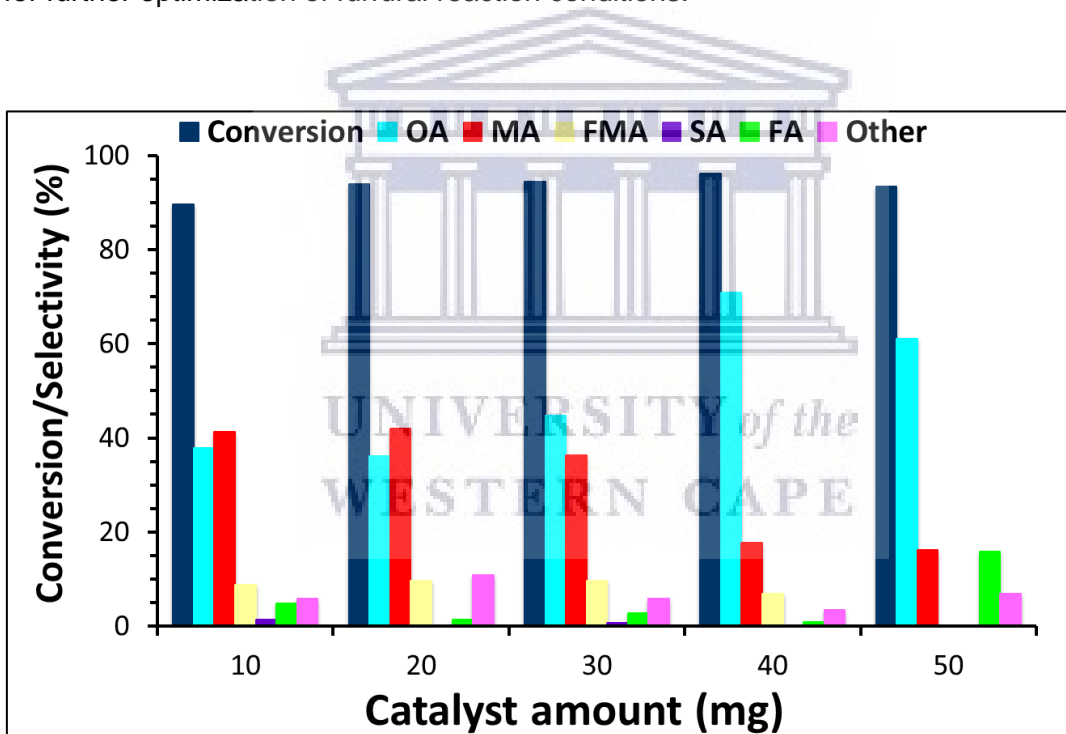
Fig. 5-11: Influence of catalysts dosage on the furfural oxidation rate and product selectivity. Reaction conditions: furfural (1 mmol); 30% aq. H_2O_2 (5 mmol); H_2O solvent (2 mL); T= 60°C and t = 3 h.

5.3.2 Effect of reaction temperature on furfural oxidation rates

The effect of temperature in a range of 40 - 80 °C on catalytic performance of CuO$_x$-SnO$_2$ catalyst for oxidation of furfural was investigated and the results obtained are presented in

Fig. 5-12 and **Table 5-5**. At 40 °C, the conversion of furfural was 59.1% and this amount increased to 82.7% at 50 °C. Further increase of reaction temperature to a range of 60 - 80 °C showed the conversion of furfural to remain within 88.0 - 94.0%. The effect of temperature was more influential on both selectivity and yield of maleic acid. Better yields of maleic acid, 32.6% and 39.4% at respective selectivity of 39.5% and 41.9% were attained for the reaction temperatures of 50 °C and 60 °C, respectively. The yield of oxalic showed to increase significantly from 2.5% at 40 °C to 76.3% at 80 °C. Another noted by-product was furoic acid, which formed mostly at low temperatures of 40 and 50 °C with the respective yields of 32.5% and 16.8%.

Table 5-5: Effect of reaction temperature on furfural oxidation rates with the CuO_x-SnO_2 catalyst.

Temperature (°C)	Conversion (%)	Yield (%)					
		MA	OA	FMA	SA	FA	Others
40	59.1	18.2	2.5	2.9	0.4	32.5	2.6
50	82.7	32.6	18.2	8.0	1.0	16.8	6.1
60	93.9	39.4	33.9	9.1	0.0	1.3	10.2
70	88.0	4.2	74.2	2.6	0.0	1.0	6.0
80	93.1	1.7	76.3	0.0	0.0	0.5	14.6

Reaction conditions: furfural (1 mmol); 30% aq. H_2O_2 (5 mmol); H_2O solvent (2 mL); catalyst (20 mg) and t = 3 h.

The results obtained suggests that for oxidation reactions carried out low temperatures (i.e. 50 °C and 60 °C), the thermal decomposition of H_2O_2 proceeds at a slow rate, thus favoring the formation of maleic acid with better yields. Inversely, the H_2O_2 decomposition occurs rapidly at higher temperatures (i.e. > 60 °C) and this leads to over-oxidation reactions that favour the formation of oxalic acid with high yields at the expense of reduced selectivity of maleic acid. Consequently, the reaction temperature of 60 °C was determined to afford the maximum yield and selectivity toward maleic acid at reasonable

furfural conversion of 93.9%, therefore it then was selected to be used in the subsequent reaction parameters optimization.
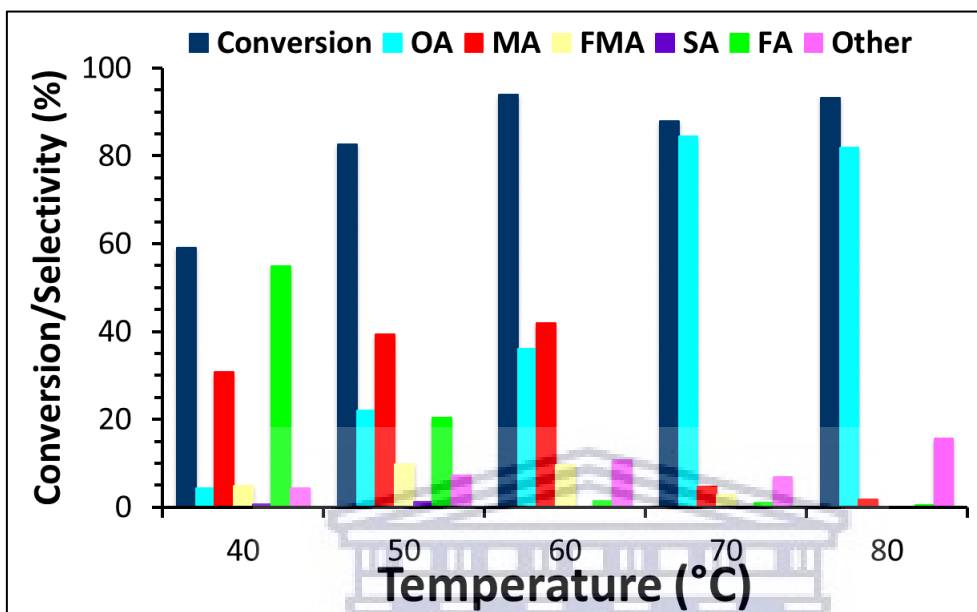
Fig. 5-12: Effect of reaction temperature on furfural oxidation products over the CuO$_x$-SnO$_2$ catalyst. Reaction conditions: furfural (1 mmol); 30% aq. H$_2$O$_2$ (5 mmol); DI H$_2$O solvent (2 mL); catalyst (20 mg) and t = 3 h.

5.3.3 Influence of solvent composition on furfural oxidation rates

Previous studies in furfural oxidation have shown that the choice of solvent composition is critical as it can affect conversion and products distribution selectivity, thus yield.[28]. As a result, we evaluated the performance of three different co-solvent systems, namely; (1) acetonitrile (MeCN)-H$_2$O, (2) acetic acid (AcOH)-H$_2$O and (3) γ-valerolactone (GVL)-H$_2$O, and H$_2$O alone using CuO$_x$-SnO$_2$ catalyst at 60 °C in oxidation reaction of furfural. The results obtained are summarized in **Fig. 5-13** and **Table 5-6**. The reaction performed in H$_2$O solvent reached near complete furfural conversion of 93.4% and the yield of maleic acid achieved was 39.4% at 41.9% selectivity. In addition, the yields of 33.9% and 9.1% were achieved for oxalic acid and fumaric acid, respectively. The reaction performed in MeCN-H$_2$O co-solvent afforded a furfural conversion of 74.9% and a slightly lower maleic acid yield of 31.6% while fumaric acid yield was 4.1%. Interestingly, the yield of oxalic acid

significantly decreased to just 1.1%, thus indicating the effectiveness of acetonitrile in minimizing or inhibiting the over-oxidation reaction path accountable for its formation. The catalyst was markedly more selective towards furoic acid with a 29.1% yield at 38.8% selectivity in acetonitrile-H_2O co-solvent with the yield of the side-products slightly lowered to 9.1%. For the reaction carried out in the AcOH-H_2O co-solvent, a furfural conversion of 82.9% was obtained with improved yield of maleic acid to 60.3% at 72.7% selectivity. Under the AcOH-H_2O co-solvent, the yield of fumaric acid and oxalic acid were 2.8% and 4.7%, respectively, which demonstrated the effect of acetic acid in inhibiting the formation rate of oxalic acid compared to H_2O solvent. The reaction performed in GVL-H_2O co-solvent afforded a furfural conversion of 32.5% and a low maleic acid yield of 3.7% while 2-furoic acid was the main product with a yield of 26.9% at 82.7% selectivity.

Table 5-6: Effect of solvent composition on furfural oxidation rates with the CuO_x-SnO_2 catalyst.

Solvent	Conversion (%)	Yield (%)					
		MA	OA	FMA	SA	FA	Others
H_2O	93.9	39.4	33.9	9.1	0.0	1.3	10.2
Acetonitrile-H_2O	74.9	31.6	1.1	4.1	0.0	29.1	9.0
Acetic acid-H_2O	82.9	60.3	4.7	2.8	1.5	12.5	1.1
GVL-H_2O	32.5	3.7	0.0	1.0	0.0	26.9	0.9

Reaction conditions: furfural (1 mmol); 30% aq. H_2O_2 (5 mmol); solvent (2 mL); catalyst (20 mg) T = 60 °C and t = 3 h.

The results obtained indicate that while the reaction carried out in H_2O solvent afforded very a good furfural conversion of 93.4%, the rate of over-oxidation of products to form oxalic acid was accelerated in H_2O solvent. The over-oxidation to oxalic acid was significantly mitigated by introducing acetonitrile and acetic acid as co-solvents into the reaction mixture. The improved results achieved when acetonitrile and acetic acid are utilized respectively together with H_2O as co-solvents are attributed to the ability of acetonitrile to assist the activation of H_2O_2 by forming a peroxy hydroxyl anion (OOH$^-$)

which reacts with acetonitrile resulting in a peroxy carboximidic acid complex, while acetic acid reacts with H_2O_2 to form a peracetic acid complex.[65,66] Both these complexes are stronger and more selective oxidizing agents than H_2O_2. These results together demonstrate the optimization of the co-solvent for furfural oxidation reaction is key under the catalytic effect of CuO_x-SnO_2 to obtain the maximized yield of maleic acid with high selectivity while also limiting the over-oxidation of products and production of unwanted by-products. The use of acetic acid resulted in an increased maleic acid yield while also minimizing the production of side products. As a result, the effect of the catalyst on the stability of the reaction products and intermediates was next investigated with the reactions conducted in H_2O solvent and the AcOH-H_2O co-solvent.
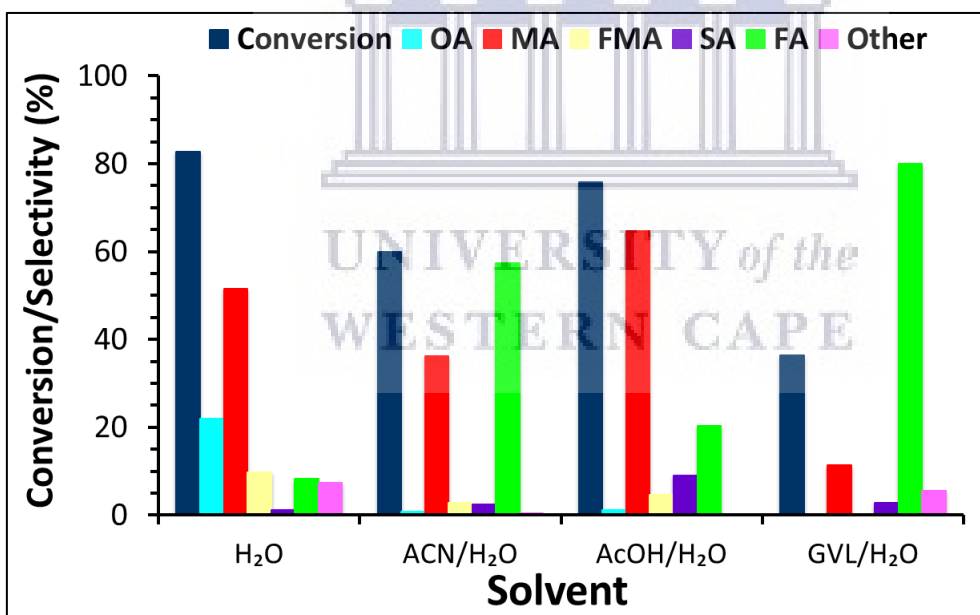
Fig. 5-13: Influence of solvent composition on furfural oxidation products over the CuO_x-SnO_2 catalyst. Reaction conditions: furfural (1 mmol); 30% aq. H_2O_2 (5 mmol); solvent (2 mL); catalyst (20 mg), T = 60 °C and t = 3 h.

5.3.4 Effect of catalyst on stability of the oxidation intermediates

To investigate the catalytic effect of CuO_x-SnO_2 on the stability of different furfural oxidation reaction intermediates and final stable desired products in the presence of H_2O_2, 1 mmol of the intermediates and products (2-furoic acid, 2-(5H)-Furanone, maleic acid, succinic acid and fumaric acid) were oxidised as substrates under the furfural oxidation reaction conditions described in **section 5.3.3** and the results obtained are summarised in **Table 5-7**. The oxidation of 2-furoic acid over CuO_x-SnO_2 catalyst in H_2O solvent resulted in 99.3% conversion achieved with oxalic acid produced exclusively as the major product at 98.4% yield. Trace amounts of fumaric and succinic acids were detected. In AcOH-H_2O co-solvent, the conversion of 2-furoic acid was reduced to 29.3% with oxalic acid produced in trace amounts. The main reaction products were maleic acid (10.7% yield) and 2-(5H)-furanone (9.6% yield).

Table 5-7: Influence of the CuO_x-SnO_2 catalyst on the stability of oxidation intermediates and products.

Substrate	Solvent	Conversion (%)	Yield (%)				
			MA	OA	FMA	SA	FOA
FA	H_2O	99.3	0.0	98.4	0.7	0.2	0.0
	AcOH-H_2O	[1] 29.3	10.7	0.1	1.2	5.9	1.8
2-Furanone	H_2O	87.8	10.3	20.9	0.0	0.0	56.6
	AcOH-H_2O	47.0	26.4	9.7	0.0	0.0	10.9
MA	H_2O	20.2	-	5.3	0.7	0.0	14.2
	AcOH-H_2O	7.5	-	0.0	0.0	0.0	7.5
FMA	H_2O	21.3	2.0	0.3	-	0.0	19.0
	AcOH-H_2O	10.4	0.0	0.2	-	1.1	9.1
SA	H_2O	96.2	0.0	7.5	0.0	-	88.7
	AcOH-H_2O	22.2	0.0	22.2	0.0	-	0.0

[1] Only side product was 2-(5H)-furanone. Symbols: MA = maleic acid, OA = oxalic acid, FMA = fumaric acid, SA = succinic acid, FA = 2-furoic acid and FOA = formic acid. Reaction conditions: Substrate (1 mmol); 30% aq. H_2O_2 (5 mmol); solvent (2 mL); catalyst (20 mg); T = 60 °C and t = 3 h.

The oxidation of 2-(5H)-furanone intermediate in H_2O solvent showed to proceed with high rates to afford 87.8% conversion with selectivity favouring high formation yields towards oxalic acid (20.9%) and formic acid (56.6%). The maleic acid was also produced at 10.3% yield confirming 2-(5H)-furanone as a possible intermediate in the furfural oxidation which is consistent with the results reported previously.[63] The conversion of 2-(5H)-furanone in $AcOH$-H_2O co-solvent was reduced to 47.0% with oxalic acid and formic produced with reduced yields of 9.7% and 10.9%, respectively. The main reaction product was maleic acid with an improved yield of 26.4%. The conversions of maleic acid and fumaric acid in the stability test oxidation reaction were low, giving respective conversions of 20.2% and 21.2% in H_2O solvent. The products of maleic acid oxidation were oxalic acid with 5.3% yield, formic acid with 14.2% yield while those of fumaric acid were maleic acid (by isomerisation) with 2.0% yield and formic acid with 19.0% yield. The conversion of maleic acid and fumaric acid and yields of their conversion products were also significantly reduced in $AcOH$-H_2O co-solvent. The same trend was observed for the conversion of succinic acid, with the yield of formic acid reduced from 88.7 in H_2O solvent to 0.0% in $AcOH$-H_2O co-solvent and conversion also decreasing from 96.2% to 22.2%.

The results of these experiments show that the excess H_2O_2 in H_2O solvent is detrimental to the stability of furfural oxidation products and intermediates in the presence of the CuO_x-SnO_2 catalyst with most of the products and intermediates being oxidized to mainly either formic acid or oxalic acid or both. Maleic acid and its isomer fumaric acid are the only products that showed to undergo slow over-oxidation reactions, thus excellent stability under H_2O_2/CuO_x-SnO_2 catalytic system once they are formed. The presence of oxalic acid as a product in the oxidation of all the tested substrates supports the suggestion made earlier that its increased yield is due to over-oxidation of the furfural

oxidation intermediates products. The extent of over-oxidation of the furfural oxidation products and intermediates was significantly reduced when acetic acid and H_2O were utilized as a co-solvent. These results would prove insightful for optimising the catalyst active sites structure design to efficiently improve on the selectivity of maleic acid where oxalic acid showed to be the predominant stable oxidation by-product.

5.3.5 Catalysts activity screening of BMO-SnO$_2$ catalysts

The catalytic activity performance of the heterostructured SnO_2 catalysts were evaluated in the oxidation reaction of furfural using H_2O_2 as oxidant under the optimized reaction conditions. **Fig. 5-14** and **Table 5-8** summarizes the catalytic activity screening results of the heterostructured SnO_2 catalysts expressed in terms of furfural conversion amounts, yield and selectivity towards the different products, including the targeted maleic acid. The oxidation reaction of furfural carried out with SnO_2 resulted in 8.5 % conversion of furfural to afford 2-furoic acid as the only major product with a 6.8 % yield at 80.5 % selectivity. The interface of Co oxide with SnO_2 showed to perform poorly compared to the bare SnO_2 in terms of furfural conversion, resulting in a low substrate conversion of 8.6 %. Again, similar to SnO_2 the CoO_x-SnO_2 catalyst produced 2-furoic acid as the main oxidation product with a yield of 6.4 % at 74.0 % selectivity.

In the case of MnO_x-SnO_2 catalyst, the yields of maleic acid and 2-furoic acid of 2.7% and 17.8%, respectively, were achieved at furfural conversion of 21.4%. The selectivity towards 2-furoic acid was 83.1% with the MnO_x-SnO_2 catalyst. Oxalic acid, fumaric acid, succinic acid and other by-products were once again produced with a combined yield of less than 1%. The NiO_x-SnO_2 catalyst showed an increased furfural conversion of 26.5% relative to the one obtained with SnO_2 (8.5%). 2-Furoic acid was also produced as the major product with the NiO_x-SnO_2 catalyst at a yield of 23.5% and 88.8% selectivity.

Table 5-8: Catalytic activity screening the BMO-SnO$_2$ catalysts under optimized reaction conditions.

Catalyst	Conversion (%)	Yield (%)					
		MA	OA	FMA	SA	FA	Other
SnO$_2$	8.5	0.2	0.1	0.0	0.0	6.8	1.4
CoO$_x$-SnO$_2$	8.6	1.5	0.1	0.3	0.2	6.4	0.1
CuO$_x$-SnO$_2$	82.9	60.3	4.7	2.8	1.5	12.5	1.1
MnO$_x$-SnO$_2$	21.4	2.7	0.0	0.3	0.5	17.8	0.1
NiO$_x$-SnO$_2$	26.5	1.8	0.2	0.3	0.2	23.5	0.5

Reaction conditions: furfural (1 mmol); 30% aq. H$_2$O$_2$ (5 mmol); acetic acid-H$_2$O solvent (2 mL); catalyst (20 mg); T = 60 °C and t = 3 h.
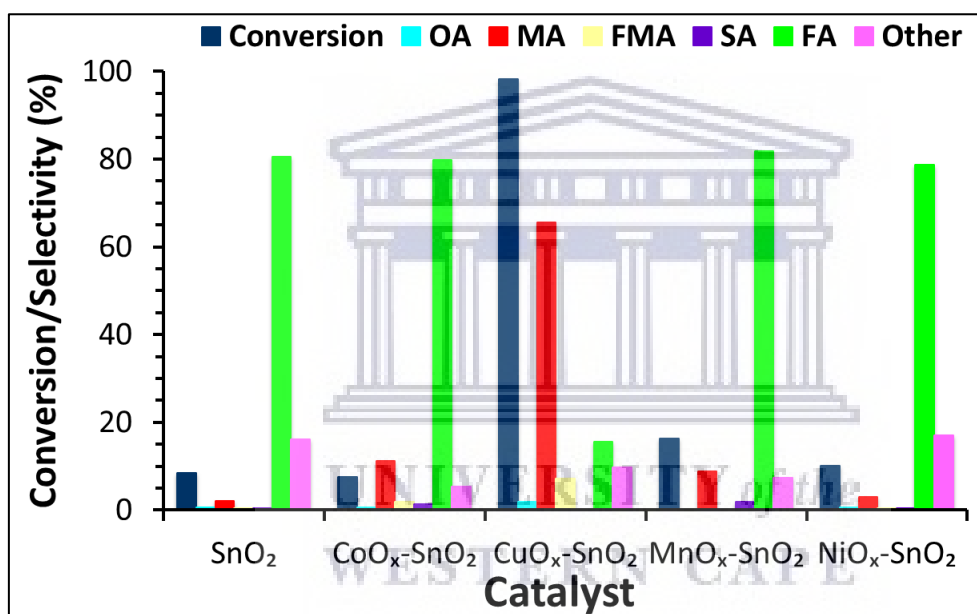
Fig. 5-14: Products distribution from the catalytic activity screening results of the heterostructured SnO$_2$ catalysts. Reaction conditions: furfural (1 mmol); 30% aq. H$_2$O$_2$ (5 mmol); acetic acid-H$_2$O solvent (2 mL); catalyst (20 mg); T = 60 °C and t = 3 h.

The best catalytic results for maleic acid production were obtained with the CuO$_x$-SnO$_2$ catalyst. The CuO$_x$-SnO$_2$ catalyst afforded a markedly increased furfural conversion of 82.9% producing 60.3% maleic acid yield at 72.7% selectivity. Moreover, CuO$_x$-SnO$_2$ catalyst showed an increased yield of 2.8% towards fumaric acid formation compared to the other hetero-mixed SnO$_2$ metal oxides catalysts. 2-Furoic acid was produced with a

yield 12.5% at 15.0% selectivity when the CuO$_x$-SnO$_2$ catalyst was employed in the furfural oxidation reaction.

In terms of selectivity, SnO$_2$ and the heterostructured SnO$_2$ metal oxides catalysts with the exception of CuO$_x$-SnO$_2$ which showed to favour the formation of 2-furoic acid with high selectivity of up to 92.3% (**Fig. 5-14**). For selectivity towards maleic acid formation, the CuO$_x$-SnO$_2$ catalyst showed the highest of 72.7% followed by CoO$_x$-SnO$_2$ (17.6%) and MnO$_x$-SnO$_2$ (12.6%), respectively. Interestingly, the MnO$_x$-SnO$_2$ oxide catalyst with the highest surface area showed maleic acid yield of 2.7% compared to CuO$_x$-SnO$_2$ of 60.3%. Also, the 21.4% furfural conversion obtained for MnO$_x$-SnO$_2$ with high surface area was low when compared to 82.9% for CuO$_x$-SnO$_2$ catalyst. As a result, the high catalytic activity of CuO$_x$-SnO$_2$ was not based on the effect of surface area or porosity nature of the designed catalysts materials, thus other factors contributed significantly.

The XPS analysis showed the SnO$_2$ interfaced base metal oxides catalysts of Mn, Co and Ni to exist more in their lower oxidation states (i.e. Mn^{3+}, Co^{2+} and Ni^{2+}) with the exception of CuO$_x$-SnO$_2$ which showed an even distribution of Cu^{2+}/Cu$^+$ oxidation states (**Fig. 5-8** and **Table 5-2**). As a result, the low oxidation states of the SnO$_2$ interfaced metal oxides catalysts could have contributed negatively on their redox reactivity to facilitate the required free radical driven oxidation redox electron-transfer mechanism to create reactive oxygen species (ROS) effective for the efficient conversion of furfural substrate. In addition, the CuO$_x$-SnO$_2$ catalyst also showed the highest surface metal content (**Table 5-1,** surface metal/actual metal ratio) thus exhibiting maximised exposure of surface active sites. For MnO$_x$-SnO$_2$ and NiO$_x$-SnO$_2$ heterostructured catalysts, similar to SnO$_2$ they showed to possess a large concentration of surface oxygen defects. However, these

surface oxygen defects did not prove to be effective on enhancing the catalytic activity. Again, SnO_2 showed poor furfural conversion which somehow could be correlated to both its poor redox reactivity and low available number of surface lattice oxygen species due the high concentration of oxygen defects based on the XPS analysis results. Also, the CoO_x-SnO_2 showed a small fraction of surface oxygen defects concentration and low surface area compared to CuO_x-SnO_2 (**Table 5-1** and **Table 5-2**), but still showed poor catalytic activity as a result of its reduced redox ability which consisted predominantly of the Co^{2+} oxidation state. The poor catalytic activity of the NiO_x-SnO_2 is attributed to its low surface area, and generally poor oxidizing ability in selective oxidation reactions. In this case, the presence of multiple phases including the formation of metallic Ni as evidenced by XRD analysis could have contributed significantly to the NiO_x-SnO_2 low catalytic activity to activate the furfural oxidation reaction.

According to the TPR results, the CuO_x-SnO_2 showed the lowest reduction temperature, which is correlated to the degree of reactivity for the removal of the surface oxygen species. The results for TPR correlates well with the XPS data, which indicated that the CuO_X-SnO_2 possessed the oxygen surface rich reactive sites compared to the others. As a result, the concomitant presence of balanced redox oxidation state of the Cu^{2+}/Cu^+ and the availability of enriched reactive surface oxygen are proposed as the main contributing factors of better catalytic activity performance of CuO_x-SnO_2 in the oxidation reaction of furfural. The simplified effective redox cycle of Cu^{2+}/Cu^+ in activating the H_2O_2 catalyzed reaction can be described by the free-radicals driven catalytic cycle depicted in **Scheme 5-2**. The copper metal redox cycle initiates the redox free-radicals oxidation mechanism where the metal is partially reduced due to electron-transfer upon its interaction with the H_2O_2 oxidant and re-oxidize after the abstraction of H^+ of the reacting organic substrate

molecule. During this stage of the reaction, H_2O_2 is dissociated into reactive oxygen species such as hydroxyl (OH^-), O_2, O_2^-, and O_2^{2-} following the free-radicals driven (i) initiation, then oxygen atom insertion into the organic carbocation free radical molecule via the (ii) propagation and (iii) termination to form stable products.
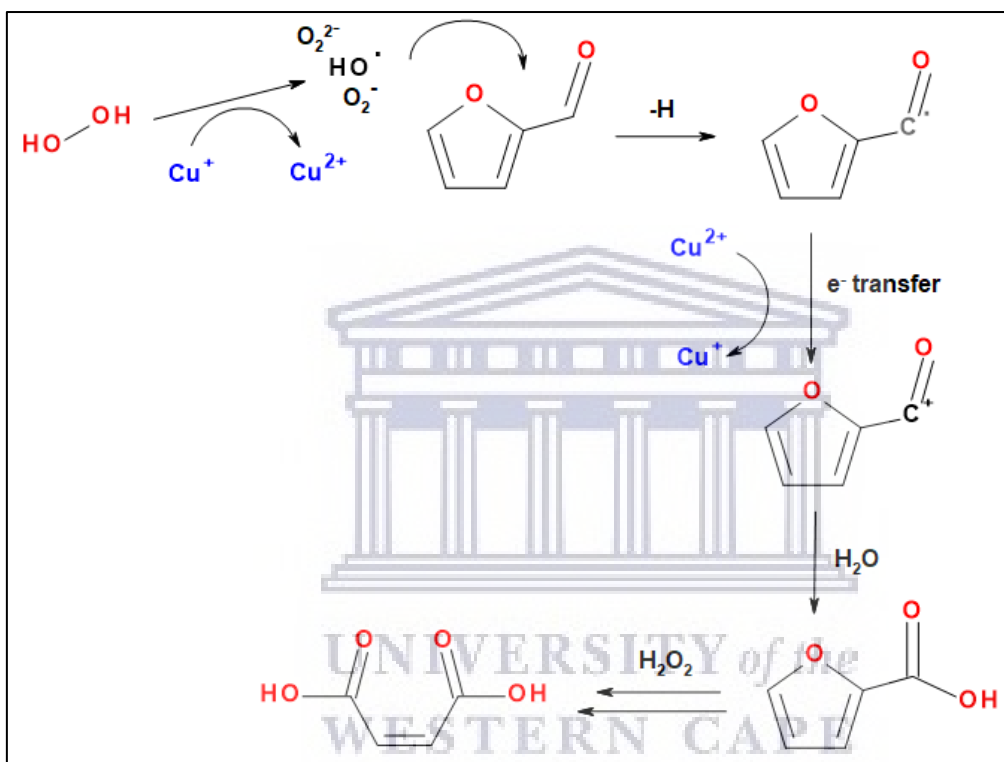
Scheme 5-2: Plausible redox oxidation mechanism of copper-tin oxide catalysts in the oxidation of furfural to maleic acid using H_2O_2 as oxidation.
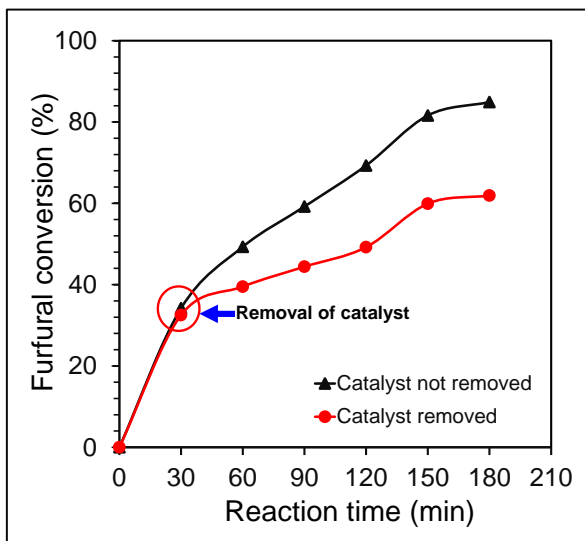
Fig. 5-15: Evaluation of metal leaching during furfural conversion. Reaction conditions: furfural (1 mmol); 30 % aq. H_2O_2 (5 mmol); acetic acid-H_2O solvent (2 mL); catalyst (20 mg); T = 60 °C and t = 3 h.

5.3.6 Catalyst leaching tests

The test experiments for possible metal catalyst leaching were carried out in order to establish the extend of its effect on conversion of furfural. As shown in **Fig. 5-15**, the CuO_x-SnO_2 catalyst showed some possible metal leaching based on the amount of furfural converted after the catalyst removal. After the removal of the catalyst solid sample by hot filtration, the conversion of furfural was determined to be 30.3 % while allowing the filtrate solution to react further for total reaction time of 3 h, the furfural conversion of 61.9 % was achieved. The normal catalysed reaction without the catalyst removal obtained the conversion of 84.7 % after 3 h. This showed that after the removal of the catalyst, there was a possible metal catalyst leaching that contributed to the increase in furfural conversion of 31.6 % to achieve 61.9 % compared to 84.7 %. However, further experimental testing and characterization of the spent catalyst is required to confirm this phenomenon. The leaching of the metal catalyst (i.e. Ti species of TS-1) was previously demonstrated by Alonso-Fagúndez et al.[28] based on the nature of solvent used in the furfural oxidation using H_2O_2 oxidant. In the different study, it was shown that changing of

solvent/solvent composition could improve on both maleic acid selectivity and catalyst stability, thus solving the problem of leaching.[65]

5.4 Concluding remarks

A series of heterostructure SnO_2 interfaced oxide catalysts consisting of Co, Cu, Mn, and Ni metals were synthesized by surfactant-free method using alcohol solvent. The catalytic activity of the catalysts was evaluated in the liquid-phase oxidation of furfural to maleic acid using H_2O_2 oxidant. Among the heterostructured SnO_2 catalysts, CuO_x-SnO_2 gave the best catalytic performance to afford maleic acid yield of 60.3 % in 3 h at furfural conversion of 82.9 % under optimized conditions. According to characterization results, the TPR of CuO_x-SnO_2 showed the lowest reduction temperature, which is correlated to the high degree of reactivity for the removal of the surface oxygen species. The TPR correlated well with the XPS, which showed CuO_X-SnO_2 to possess the oxygen surface rich reactive sites compared to other heterostructure SnO_2 interfaced oxide catalysts in addition to the highest exposed surface metal content. Overall, based on catalysts structure characterization results the concomitant presence of balanced redox oxidation state of the Cu^{2+}/Cu^+, high surface presence of Cu and the availability of enriched surface reactive surface oxygen are proposed as the main contributing factors for the better catalytic activity performance of CuO_x-SnO_2 in the oxidation reaction of furfural. Furthermore, the use of co-solvents, especially acetic acid and water mixture showed to improve yield and selectivity maleic acid. The catalyst showed some metal leaching which would affect its catalyst stability for prolonged usage. Overall, the heteromixing of Cu oxide onto SnO_2 support afforded an efficient catalyst for the conversion of biomass furfural to high-value chemicals (maleic and fumaric acids) under mild conditions.

5.5 References

[1]   J.C. Serrano-Ruiz, R. Luque, A. Sepúlveda-Escribano, Transformations of biomass derived platform molecules: from high added-value chemicals to fuels via aqueous-phase processing, Chemical Society Reviews, **2011**, 40, pp. 5266-5281.

[2]   M. Wang, J. Ma, H. Liu, N. Luo, Z. Zhao, F. Wang, Sustainable productions of organic acids and their derivatives from biomass via selective oxidative cleavage of C–C bond, ACS Catalysis, **2018**, 8, pp. 2129-2165.

[3]   P. Gallezot, Chapter 1: Metal catalysts for the conversion of biomass to chemicals, new and future developments in catalysis, In: S.L. Suib (Ed.), New and future developments in catalysis: Catalytic biomass conversion. Newnes, **2013**, pp. 1-27.

[4]   R.K. Grasselli, Fundamental principles of selective heterogeneous oxidation catalysis. Topics in Catalysis, **2002**, 21, pp. 79-88.

[5]   J.C. Védrine, I. Fechete, Heterogeneous partial oxidation catalysis on metal oxides, Comptes Rendus Chimie, **2016**, 19, pp. 1203-1225.

[6]   B. Liu, Z. Zhang, K. Lv, K. Deng, H. Duan, Efficient aerobic oxidation of biomass-derived 5-hydroxymethylfurfural to 2,5-diformylfuran catalyzed by magnetic nanoparticle supported manganese oxide, Applied Catalysis A: General, **2014**, 472, pp. 64-71.

[7]   L. Ding, W. Yang, L. Chen, H. Cheng, Z. Qi, Fabrication of spinel $CoMn_2O_4$ hollow spheres for highly selective aerobic oxidation of 5-hydroxymethylfurfural to 2,5-diformylfuran, Catalysis Today, **2018**.

[8]   M. Ventura, M. Aresta, A. Dibenedetto, Selective aerobic oxidation of 5-hydroxymethylfurfural to 5-formyl-2-furancarboxylic acid in water, ChemSusChem **2016**, 9, pp. 1096-1100.

[9]   S. Wang, Z. Zhang, B. Liu, Catalytic conversion of fructose and 5-hydroxymethylfurfural into 2,5-furandicarboxylic acid over a recyclable Fe_3O_4–CoO_x magnetite nanocatalyst, ACS Sustainable Chemistry & Engineering, **2015**, 3, pp. 406-412.

[10] X. Han, C. Li, X. Liu, Q. Xia, Y. Wang, Selective oxidation of 5-hydroxymethylfurfural to 2,5-furandicarboxylic acid over MnO_x–CeO_2 composite catalysts, Green Chemsitry, **2017**, 19, pp. 996-1004.

[11] A. Jain, S.C. Jonnalagadda, K.V. Ramanujachary, A. Mugweru, Selective oxidation of 5-hydroxymethyl-2-furfural to furan-2,5-dicarboxylic acid over spinel mixed metal oxide catalyst, Catalysis Communications, **2015**, 58, pp. 179-182.

[12] X. Kong, Y. Zhu, Z. Fang, J.A. Kozinski, I.S. Butler, L. Xu, H. Song, X. Wei, Catalytic conversion of 5-hydroxymethylfurfural to some value-added derivatives, Green Chemistry, **2018**, 20, pp. 3657-3682.

[13] K. Gupta, R.K. Rai, S.K. Singh, Metal catalysts for the efficient transformation of biomass derived HMF and furfural to value added chemicals, ChemCatChem, **2018**, 10, pp. 2326-2349.

[14] R. Mariscal, P. Maireles-Torres, M. Ojeda, I. Sádaba, M.L. Granados, Furfural: A renewable and versatile platform molecule for the synthesis of chemicals and fuels, Energy & Environmental Science, **2016**, 9, pp. 1144-1189.

[15] T.R. Felthouse, J.C. Burnett, B. Horrell, M.J. Mummey, Y. Kuo, Maleic anhydride, maleic acid, and fumaric acid, in: Kirk-Othmer Encyclopedia of Chemical Technology, American Cancer Society, **2001**.

[16] O.M. Musa, Handbook of maleic anhydride based materials: Syntheses, properties and applications, Springer International Publishing, Cham, **2016**.

[17] R. Wojcieszak, F. Santarelli, S. Paul, F. Dumeignil, F. Cavani, R.V. Gonçalves, Recent developments in maleic acid synthesis from bio-based chemicals, Sustainable Chemical Processes, **2015**, 3, pp. 9.

[18] S. Shi, H. Guo, G. Yin, Synthesis of maleic acid from renewable resources: Catalytic oxidation of furfural in liquid media with dioxygen, Catalysis Communications **2011**, 12, pp. 731-733.

[19] H. Guo, G. Yin, Catalytic aerobic oxidation of renewable furfural with phosphomolybdic acid catalyst: an alternative route to maleic acid, The Journal of Physical Chemistry C **2011**, 115, pp. 17516-17522.

[20] J. Lan, Z. Chen, J. Lin, G. Yin, Catalytic aerobic oxidation of renewable furfural to maleic anhydride and furanone derivatives with their mechanistic studies, Green Chemistry, **2014**, 16, pp. 4351-4358.

[21] T. Soták, M. Hronec, M. Gál, E. Dobročka, J. Škriniarová, Aqueous-Phase Oxidation of Furfural to Maleic Acid Catalyzed by Copper Phosphate Catalysts, Catalysis Letters, **2017**, 147, pp. 2714-2723.

[22] X. Li, Y. Zhang, The conversion of 5-hydroxymethyl furfural (HMF) to maleic anhydride with vanadium-based heterogeneous catalysts, Green Chemistry, **2016**, 18, pp. 643-647.

[23] Z. Du, J. Ma, F. Wang, J. Liu, J. Xu, Oxidation of 5-hydroxymethylfurfural to maleic anhydride with molecular oxygen, Green Chemistry, **2011**, 13, pp. 554.

[24] J. Lan, J. Lin, Z. Chen, G. Yin, Transformation of 5-hydroxymethylfurfural (HMF) to maleic anhydride by aerobic oxidation with heteropolyacid catalysts, ACS Catalysis, **2015**, 5, pp. 2035-2041.

[25] A. Tirsoaga, M. El Fergani, V.I. Parvulescu, S.M. Coman, Upgrade of 5-hydroxymethylfurfural to dicarboxylic acids onto multifunctional-based $Fe_3O_4@SiO_2$ magnetic catalysts, ACS Sustainable Chemistry & Engineering, **2018**, 6, pp. 14292-14301.

[26] N. Araji, D.D. Madjinza, G. Chatel, A. Moores, F. Jérôme, K.D.O. Vigier, Synthesis of maleic and fumaric acids from furfural in the presence of betaine hydrochloride and hydrogen peroxide, Green Chemistry, **2017**, 19, pp. 98-101.

[27] N. Alonso-Fagúndez, V. Laserna, A.C. Alba-Rubio, M. Mengibar, A. Heras, R. Mariscal, M.L. Granados, Poly-(styrene sulphonic acid): An acid catalyst from polystyrene waste for reactions of interest in biomass valorization, Catalysis Today, **2014**, 234, pp. 285-294.

[28] N. Alonso-Fagúndez, I. Agirrezabal-Telleria, P.L. Arias, J.L.G. Fierro, R. Mariscal, M.L. Granados, Aqueous-phase catalytic oxidation of furfural with H_2O_2: high yield of maleic acid by using titanium silicalite-1, RSC Advances, **2014**, 4, pp. 54960-54972.

[29] T. Yang, W. Li, Q. Liu, M. Su, T. Zhang, J. Ma, Synthesis of maleic acid from biomass-derived furfural in the presence of KBr/graphitic carbon nitride (g-C_3N_4) catalyst and hydrogen peroxide, Bioresources, **2019**, 14, pp. 5025-5044.

[30] K. Sekizawa, H. Widjaja, S. Maeda, Y. Ozawa, K. Eguchi, Low temperature oxidation of methane over Pd/SnO_2 catalyst, Applied Catalysis A: General, **2000**, 200, pp. 211-217.

[31] K. Yu, Z. Wu, Q. Zhao, B. Li, Y. Xie, High-temperature-stable Au@SnO_2 core/shell supported catalyst for CO oxidation, The Journal of Physical Chemistry C, **2008**, 112, pp. 2244-2247.

[32] F. Gonçalves, P.R.S. Medeiros, J.G. Eon, L.G. Appel, Active sites for ethanol oxidation over SnO_2-supported molybdenum oxides, Applied Catalysis A: General, **2000**, 193, pp. 195-202.

[33] T. Matthias, K. Katsumi, A.V. Neimark, J.P. Olivier, F. Rodriguez-Reinoso, R. Jean, K.S. Sing, Physisorption of gases, with special reference to the evaluation of surface area and pore size distribution (IUPAC Technical Report). Pure and Applied Chemistry, **2015**, 87, pp. 1051.

[34] M.A. Stranick, A. Moskwa, SnO_2 by XPS. Surface Science Spectra, **1993**, 2, pp. 50-54.

[35] F.A. Akgul, C. Gumus, A.O. Er, A.H. Farha, G. Akgul, Y. Ufuktepe, Z. Liu, Structural and electronic properties of SnO_2. Journal of Alloys and Compounds, **2013**, 579, pp. 50-56.

[36] Q. Zhao, Controllable synthesis and catalytic activity of SnO_2 nanostructures at room temperature. Transactions of Nonferrous Metals Society of China, **2009**, 19, pp. 1227-1231.

[37] J. Dupin, D. Gonbeau, P. Vinatier, A. Levasseur, Systematic XPS studies of metal oxides, hydroxides and peroxides. Physical Chemistry Chemical Physics, **2000**, 2, pp. 1319-1324.

[38] L.Q. Wu, Y.C. Li, S.Q. Li, Z.Z. Li, G.D. Tang, W.H. Qi, L.C. Xue, X.S. Ge, L.L. Ding, Method for estimating ionicities of oxides using O1s photoelectron spectra. AIP Advances, **2015**, 5, pp. 9721-9727.

[39] J. Yang, H. Liu, W.N. Martens, R.L. Frost, Synthesis and Characterization of Cobalt Hydroxide, Cobalt oxyhydroxide, and cobalt oxide nanodiscs. The Journal of Physical Chemistry C, **2010**, 114, pp. 111-119.

[40] M.C. Biesinger, Advanced analysis of copper X-ray photoelectron spectra. Surface and Interface Analysis, **2017**, 49, pp. 1325-1334.

[41] A.P. Grosvenor, M.C. Biesinger, R.S.C. Smart, N.S. McIntyre, New interpretations of XPS spectra of nickel metal and oxides. Surface Science, **2006**, 600, pp. 1771-1779.

[42] M.C. Biesinger, L.W.M. Lau, A.R. Gerson, R.S.C. Smart, Resolving surface chemical states in XPS analysis of first row transition metals, oxides and hydroxides: Sc, Ti, V, Cu and Zn. Applied Surface Science, **2010**, 257, pp. 887-898.

[43] C. Shang, S. Dong, P. Hu, J. Guan, D. Xiao, X. Chen, L. Zhang, L. Gu, G. Cui, L. Chen, Compatible interface design of CoO-based Li-O_2 battery cathodes with long-cycling stability. Scientific Reports, **2015**, 5, pp. 8335.

[44] X. Li, F. She, D. Shen, C. Liu, L. Chen, Y. Li, Z. Deng, Z. Chen, H. Wang, Coherent nanoscale cobalt/cobalt oxide heterostructures embedded in porous carbon for the oxygen reduction reaction. RSC Advances, **2018**, 8, pp. 28625-28631.

[45] J. Luo, Y. Liu, Y. Niu, Q. Jiang, R. Huang, B. Zhang, D. Su, Insight into the chemical adsorption properties of CO molecules supported on Au or Cu and hybridized Au–CuO nanoparticles. Nanoscale, **2017**, 9, pp. 15033-15043.

[46] D. Gao, J. Zhang, J. Zhu, J. Qi, Z. Zhang, W. Sui, H. Shi, D. Xue, Vacancy-mediated magnetism in pure copper oxide nanoparticles. Nanoscale Research Letters, **2010**, 5, pp. 769.

[47] X. Han, C. Li, X. Liu, Q. Xia, Y. Wang, Selective oxidation of 5-hydroxymethylfurfural to 2,5-furandicarboxylic acid over MnO_x-CeO_2 composite catalysts. Green Chemistry, **2017**, 19, pp. 996-1004.

[48] H. Liu, X. Cao, J. Wei, W. Jia, M. Li, X. Tang, X. Zeng, Y. Sun, T. Lei, S. Liu, L. Lin, Efficient aerobic oxidation of 5-hydroxymethylfurfural to 2,5-diformylfuran over Fe_2O_3 promoted MnO_2 catalyst. ACS Sustainable Chemistry & Engineering, **2019**, 7, pp. 7812-7822.

[49] T. Zhou, Z. Cao, P. Zhang, H. Ma, Z. Gao, H. Wang, Y. Lu, J. He, Y. Zhao, Transition metal ions regulated oxygen evolution reaction performance of Ni-based hydroxides hierarchical nanoarrays. Scientific Reports, **2017**, 7, pp. 46154.

[50] P. Dubey, N. Kaurav, R.S. Devan, G.S. Okram, Y.K. Kuo, The effect of stoichiometry on the structural, thermal and electronic properties of thermally decomposed nickel oxide. RSC Advances, **2018**, 8, pp. 5882-5890.

[51] W. Zhang, J. Xie, W. Hou, Y. Liu, Y. Zhou, J. Wang, One-pot template-free synthesis of Cu-MOR zeolite toward efficient catalyst support for aerobic oxidation of 5-hydroxymethyl furfural under ambient pressure. ACS Applied Materials & Interfaces, **2016**, 8, pp. 23122-23132.

[52] E. Hayashi, Y. Yamaguchi, K. Kamata, N. Tsunoda, Y. Kumagai, F. Oba, M. Hara, Effect of MnO_2 crystal structure on aerobic oxidation of 5-hydroxymethylfurfural to 2,5-furan dicarboxylic acid. Journal of the American Chemical Society, **2019**, 141, pp. 890-900.

[53] S. Saha, S.B. Abd Hamid, $CuZrO_3$ nanoparticles catalyst in aerobic oxidation of vanillyl alcohol. RSC Advances, **2017**, 7, pp. 9914-9925.

[54] R. Behling, G. Chatel, S. Valange, Sonochemical oxidation of vanillyl alcohol to vanillin in the presence of a cobalt oxide catalyst under mild conditions. Ultrasonics Sonochemistry, **2017**, 36, pp. 27-35.

[55]   G. Fierro, M. Lojacono, M. Inversi, P. Porta, R. Lavecchia, F. Cioci, A study of anomalous temperature-programmed reduction profiles of Cu_2O, CuO, and CuO-ZnO catalysts. Journal of Catalysis, **1994**, 148, pp. 709-721.

[56]   M. Luo, Y. Zhong, X. Yuan, X. Zheng, TPR and TPD studies of CuO-CeO_2 catalysts for low temperature CO oxidation. Applied Catalysis A: General, **1997**, 162, pp. 121-131.

[57]   C. Tang, C. Wang, S. Chien, Characterization of cobalt oxides studied by FT-IR, Raman, TPR and TG-MS. Thermochimica Acta, **2008**, 473, pp. 68-73.

[58]   G. Fierro, M. Lo Jacono, M. Inversi, R. Dragone, P. Porta, TPR and XPS study of cobalt–copper mixed oxide catalysts: evidence of a strong Co–Cu interaction. Topics in Catalysis, **2000**, 10, pp. 39-48.

[59]   F. Lan, X. Wang, X. Xu, R. Zhang, N. Zhang, Preparation and characterization of SnO_2 catalysts for CO and CH4 oxidation . Reaction Kinetics, Mechanisms and Catalysis, **2011**, 106, pp. 113-125.

[60]   K. Li, Y. Wang, S. Wang, B. Zhu, S. Zhang, W. Huang, S. Wu, A comparative study of CuO/TiO_2-SnO_2, CuO/TiO_2 and CuO/SnO_2 catalysts for low-temperature CO oxidation. Journal of Natural Gas Chemistry, **2009**, 18, pp. 449-452.

[61]   K. Ramesh, L. Chen, F. Chen, Y. Liu, Z. Wang, Y. Han, Re-investigating the CO oxidation mechanism over unsupported MnO, Mn_2O_3 and MnO_2 catalysts. Catalysis Today, **2008**, 131, pp. 477-482.

[62]   H. Liang, H. Sun, A. Patel, P. Shukla, Z.H. Zhu, S. Wang, Excellent performance of mesoporous Co_3O_4/MnO_2 nanoparticles in heterogeneous activation of peroxymonosulfate for phenol degradation in aqueous solutions. Applied Catalysis B: Environmental, **2012**, 127, pp. 330-335.

[63]   N.K. Kotsev, L.I. Ilieva, Determination of non-stoichiometric oxygen in NiO by temperature-programmed reduction. Catalysis Letters, **1993**, 18, pp. 173-176.

[64]   A. Parmaliana, F. Arena, F. Frusteri, N. Giordano, Temperature-programmed reduction study of NiO–MgO interactions in magnesia-supported Ni catalysts and NiO–MgO physical mixture. Journal of the Chemical Society, Faraday Transactions, **1990**, 86, pp. 2663-26693.

[65]   U.R. Pillai, E. Sahle-Demessie, Selective oxidation of alcohols over vanadium phosphorus oxide catalyst using hydrogen peroxide. Applied Catalysis A: General, **2004**, 276, pp. 139-144.

[66]   Y. Lou, S. Marinkovic, B. Estrine, W. Qiang, G. Enderlin, Oxidation of furfural and furan derivatives to maleic acid in the presence of a simple catalyst system based on acetic acid and TS-1 and hydrogen peroxide. ACS Omega, **2020**, 5, pp. 2561-2568.

[67]   C. Choudhary, S. Nishimura, K. Ebitani, Highly efficient aqueous oxidation of furfural to succinic acid using reusable heterogeneous acid catalyst with hydrogen heroxide, Chemistry Letters, **2012**, 41, pp. 409-411.

[68]   C. Van Nguyen, J.R. Boo, C.H. Liu, T. Ahamad, S.M. Alshehri, B.M. Matsagar, K.C.W. Wu, Oxidation of biomass-derived furans to maleic acid over nitrogen-doped

carbon catalysts under acid-free condition, Catalysis Science & Technology, **2020**, 10, pp. 1498-1506.

CHAPTER 6

Bifunctional SnO₂-TiO₂ Catalyst for Maleic Acid Synthesis

6.1 Introduction

Selective oxidation of furfural to maleic acid and maleic anhydride is one of the important industrial processes in the production of bio-based chemicals from renewable biomass.[1] Both maleic acid and maleic anhydride can be converted to bio-succinic acid, which is the precursor to 1,4-butanediol and the synthesis of numerous biodegradable polymers.[2-4] In the context of producing renewable bio-based chemicals, there is a continuing interest in catalysts development to achieve an efficient oxidation process of furfural to maleic acid with high selectivity, yields and catalyst re-usability. Based on the previsously reported catalytic activity of TiO_2 and SnO_2 based catalysts in the oxidation reactions,[5-7] the design of heterostructured TiO_2-SnO_2 interfaced nano-oxide and the use of H_2O_2 could provide an access to an economical synthesis route to bio-based maleic acid from furfural and 5-hydroxymethylfurfural oxidation. The use of TiO_2-SnO_2 could take the advantages of Lewis acidic sites associated with both TiO_2 and SnO_2, including the redox reactivity of Ti^{4+}/Ti^{3+} and oxygen vacancies for the enhanced catalytic effect.

In this chapter, the synthesis of heterostructured TiO_2-SnO_2 oxide composite catalysts consisting of relatively cheap and abundant using the microwave-assisted heating method is described. The catalyst synthesis procedure is described in **section 3.2.3**. The heterostructure catalysts were evaluated for their catalytic performance in the liquid-phase oxidation of furfural and 5-hydroxymethylfurfural to maleic acid as described in **section 3.4.1**. Furthermore, the study investigated the effect of several oxidation reaction parameters such as solvents compositions, reaction temperature and time on the

evolution and stability of the furfural oxidation products with the aim to optimize the maleic acid yield and selectivity. The reusability of the catalyst and possible leaching of the metal catalyst active sites were also investigated.
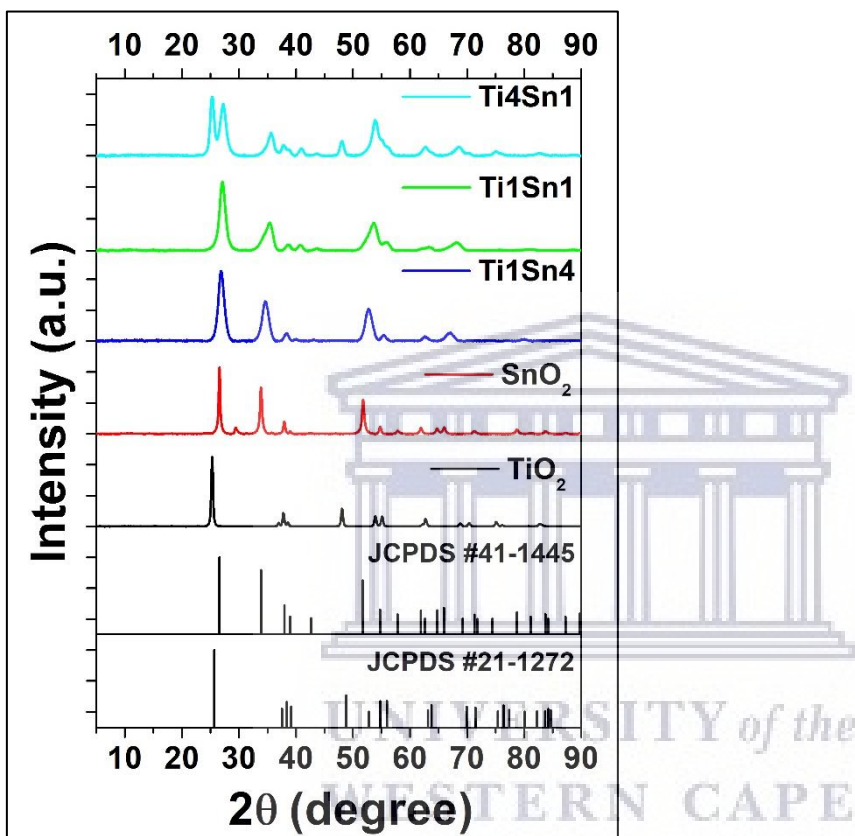
Fig. 6-1: Powder XRD patterns of the heterostructure TiO_2-SnO_2 catalysts.

6.2 Catalyst structure characterization

6.2.1 X-ray diffraction (XRD) analysis

Fig. 6-1 shows the XRD patterns measured in order to determine the crystal structure and phase compositions of the heterostructure TiO_2-SnO_2 catalysts. The SnO_2 pattern shows main peaks at 2θ values of 26.9°, 34.2°, 38.0°, 51.8° and 54.7° which are all indexed to the (110), (101), (200), (211) and (220) crystallographic planes of SnO_2 with a tetragonal

rutile structure (JCPDS no. 41-1445). The pattern also shows additional peaks at 2θ values of 29.3° and 36.3° which are respectively due to the (101) and (002) planes of the SnO phase (JCPDS no. 55-0837). The rest of the peaks are due to the SnO_2 phase. The XRD pattern of the synthesised TiO_2 displays peaks, which are all due to anatase phase of TiO_2. The peaks associated with the anatase phase are found at 25.3°, 38.6°, 48.1°, 53.9° and 55.1° and these peaks are indexed to the (101), (112), (200), (105) and (211) planes (JCPDS no. 21-1272).
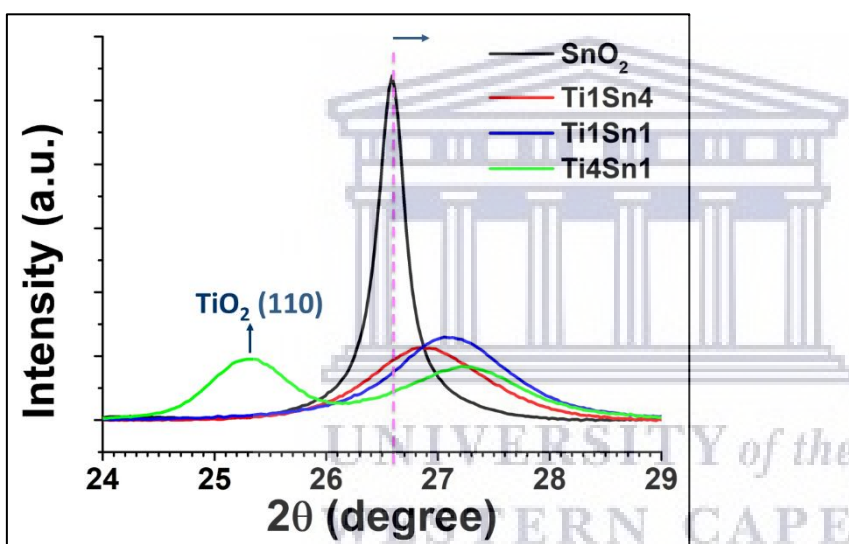
Fig. 6-2: The observed shift of the SnO_2 (110) peak for the heterostructure TiO_2-SnO_2 catalysts.

The XRD patterns of the heterostructure TiO_2-SnO_2 catalysts all shows mainly strong intense SnO_2 peaks without any of the peaks due to the SnO phase observed thus indicating the structural influence of TiO_2 in growing phase pure SnO_2. However, it should be noted that the SnO_2 peaks observed are shifted to slightly higher 2θ values (**Fig. 6-2**). The shift is a result of micro-strains in the SnO_2 lattice introduced by heterostructuring strong interface with TiO_2 and increases with increasing TiO_2 loading, and which is indicative of lattice contraction due to TiO_2.[8,9] This result is typically observed in the case

of doping a foreign ion into the host matrix in substitutional or interstitial mode and has been previously evoked in TiO_2-SnO_2 heterostructures.[10-12] The SnO_2 peaks were also broadened and their intensity decreased consequence to heterostructuring with TiO_2, indicating a decrease in crystallinity for the heterostructure TiO_2-SnO_2 catalysts compared to pure SnO_2. The peaks due to TiO_2 are less resolved for the heterostructure TiO_2-SnO_2 catalysts with the main anatase (101) and (200) TiO_2 peaks only observed for the Ti4Sn1 catalyst with the highest TiO_2 loading. The average crystallite sizes of the heterostructure catalysts shown in **Table 6-1** were determined by using the Scherrer equation and the broadening effect of the SnO_2 (110) peak, and the anatase (101) peak for TiO_2. These changes in crystallite sizes indicate varying structural modifications and different interactions of the TiO_2-SnO_2 catalyst nanomaterials and could impose varying degrees of catalytic activity of the overall heterostructured catalysts.

6.2.2 Nitrogen sorption analysis

The physical and textural properties of the heterostructure TiO_2-SnO_2 catalysts were determined using N_2 sorption analysis. As shown in **Table 6-1**, low S_{BET} of 13.2 m^2/g and 19.9 m^2/g were obtained for the pristine SnO_2 and TiO_2 oxides, respectively. The heterostructuring of TiO_2 and SnO_2 resulted in an increase in the S_{BET}, V_p and D_p with the Ti1Sn4 catalyst displaying the highest S_{BET} of 100.9 m^2/g. However, S_{BET} decreases systematically with increasing TiO_2 loading content reaching 72.6 m^2/g and 62.5 m^2/g for the Ti1Sn1 and Ti4Sn1 catalysts, respectively. The D_p of the heterostructure catalysts increases with TiO_2 loading from 10.9 nm for the Ti1Sn4 catalyst to 14.7 nm for the Ti4Sn1 catalyst, while the V_p of the catalysts is relatively similar (0.20 - 0.27 cm^3/g).

Table 6-1: N_2 sorption, crystallite size and elemental analysis results of the heterostructured TiO_2-SnO_2 catalysts

Catalysts	SnO_2	TiO_2	Ti1Sn4	Ti1Sn1	Ti4Sn1
S_{BET} (m²/g)	13.2	19.9	100.9	72.6	62.5
D_p (nm)	9.5	7.6	10.9	11.0	14.7
V_p (cm³/g)	0.031	0.037	0.27	0.20	0.23
[a] Crystallite size (nm)	6.1	33.3	7.7	5.9	[b]13.1
[c] Surface Ti atomic %	-	15.9	16.8	20.6	27.4
[c] Surface Sn atomic %	23.7	-	13.4	7.9	3.5
[c] Surface O atomic %	76.3	84.1	69.8	71.5	69.1

[a] For SnO_2 phase by XRD analysis. [b] average determined with both the SnO_2 (110) and TiO_2 (101) peaks. [c] XPS analysis.

The N_2 adsorption/desorption isotherms of the prepared catalysts are presented in **Fig. 6-3**. The isotherms of all the catalysts present as type IV with classified H2 hysteresis loops characteristic of mesoporous materials according to the IUPAC physisorption isotherms classification.[13] This type of isotherm is indicative of agglomerates arranged in a fairly uniform way that have pores with narrow mouths and relatively uniform channel-like pores. The mesoporous character of the heterostructure catalysts and TiO_2 is further confirmed by the pore size distribution plots, which all showed a narrow and uniform distribution in the range 4 - 18 nm. The individual SnO_2 had a much broader pore size distribution of 3 – 128 nm (**Fig. C-1**).
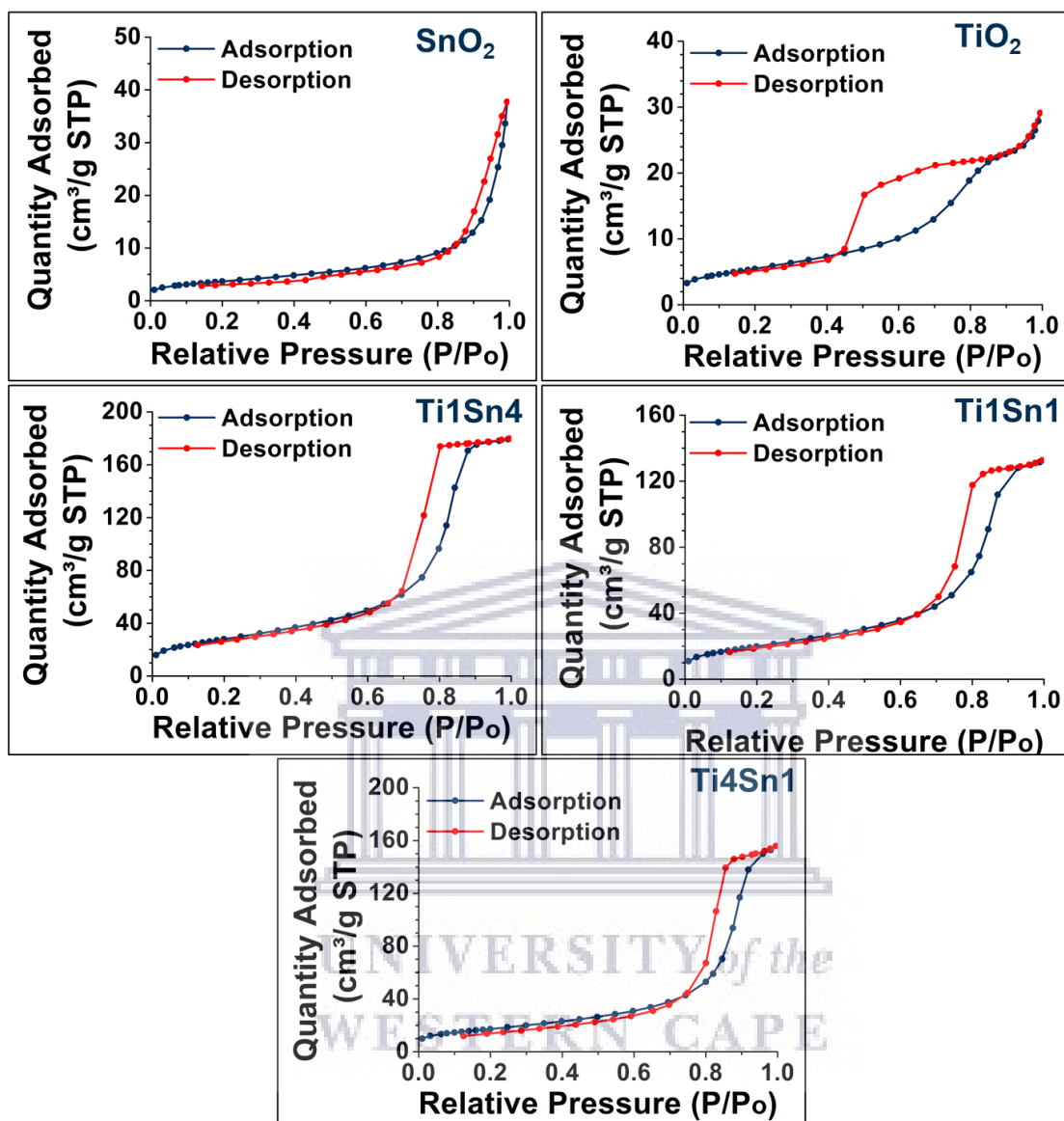
Fig. 6-3: BET sorption isotherms of the TiO_2-SnO_2 heterostructure catalysts.

6.2.3 Fourier-transform infrared (FTIR) spectroscopy analysis

To identify the functional groups present on the catalysts, FTIR analysis was conducted.

The FTIR spectrum of SnO_2 presented in **Fig. 6-4** shows the presence of a sharp band at

602 cm^{-1} and a broad band at 956 cm^{-1} which are due to the antisymmetric Sn–O–Sn and

O–Sn–O stretching vibrations of SnO_2, respectively.[14-16] The spectrum of TiO_2 shows a

single band at 832 cm^{-1} which is attributed to the Ti–O vibration mode of TiO_2.[17,18] The

spectra of the heterostructure TiO$_2$-SnO$_2$ catalysts only shows a single band at 652 cm^{-1} due to overlapping of the Sn–O–Sn and Ti–O–Ti vibrational bands with the O–Sn–O stretching band not observed. The Ti–O vibration band is only observed for the Ti4Sn1 catalyst with low intensity and is shifted to 800 cm^{-1}.
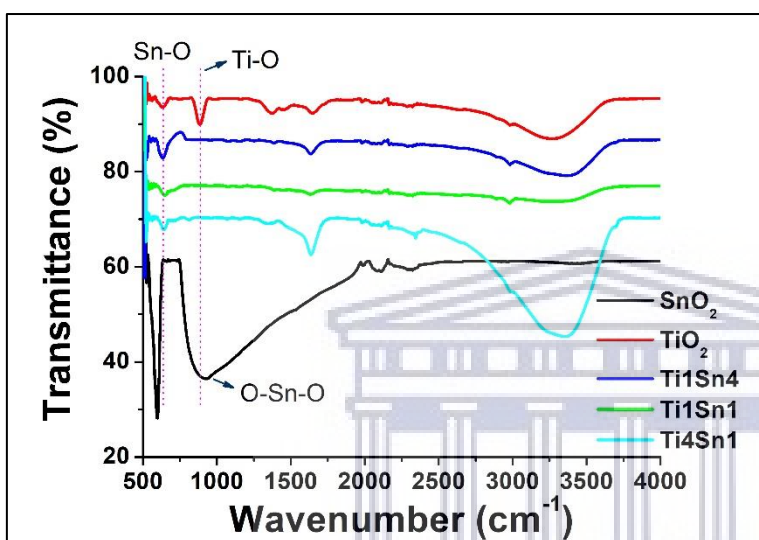
Fig. 6-4: FTIR spectra of the heterostructure TiO$_2$-SnO$_2$ catalysts.

The broad band observed at 3000 - 3500 cm^{-1} and the small band at 1660 cm^{-1} are due to the vibration of hydrogen bonded –OH and water molecules adsorbed on the catalyst surface, respectively.[16,19] The intensity of these bands is highest for the Ti4Sn1 catalyst and lowest for Ti1Sn4 catalyst. The band at 1660 cm^{-1} was observed as a shoulder on the SnO$_2$ spectrum while the intensity of the band at 3000 - 3500 cm^{-1} was very small for SnO$_2$. The additional bands observed at 1374 and 1462 are attributed to the C-OH and C-C stretching vibrations.[17] The changes in the observed bands for the heterostructure TiO$_2$-SnO$_2$ catalysts compared to individual TiO$_2$ and SnO$_2$ are a result of changes in the local environment of TiO$_2$ and SnO$_2$ which are indicative of the inherent changes in the chemical structure of the catalyst due to heterostructuring.

6.2.4 Morphological and particles dimensions analysis

The microstructure morphology of the catalysts was investigated with SEM and the resultant micrographs are presented in **Fig. 6-5**. The results show the catalysts to be made up of porous agglomerates of nanoparticles with varying sizes. The TEM and HRTEM micrographs presented in **Fig. 6-6** and **Fig. 6-7** show the pristine SnO_2 catalyst to be composed of agglomerates of densely packed nanoparticles (NPs) with non-uniform shapes and sizes. The pristine TiO_2 catalyst is made up of a densely packed agglomerate of very short amorphous rod-like particles. From the HRTEM micrograph of the catalyst, the rods are about 4 nm in diameter and the length ranges between 8 -10 nm. The heterostructure TiO_2-SnO_2 nanocatalysts possess morphology close to that of pristine SnO_2 of densely packed nanoparticles with the rod-like growth of TiO_2 diminished. However, the catalysts are less agglomerated than SnO_2 and the Ti4Sn1 is the less agglomerated of all the catalysts.
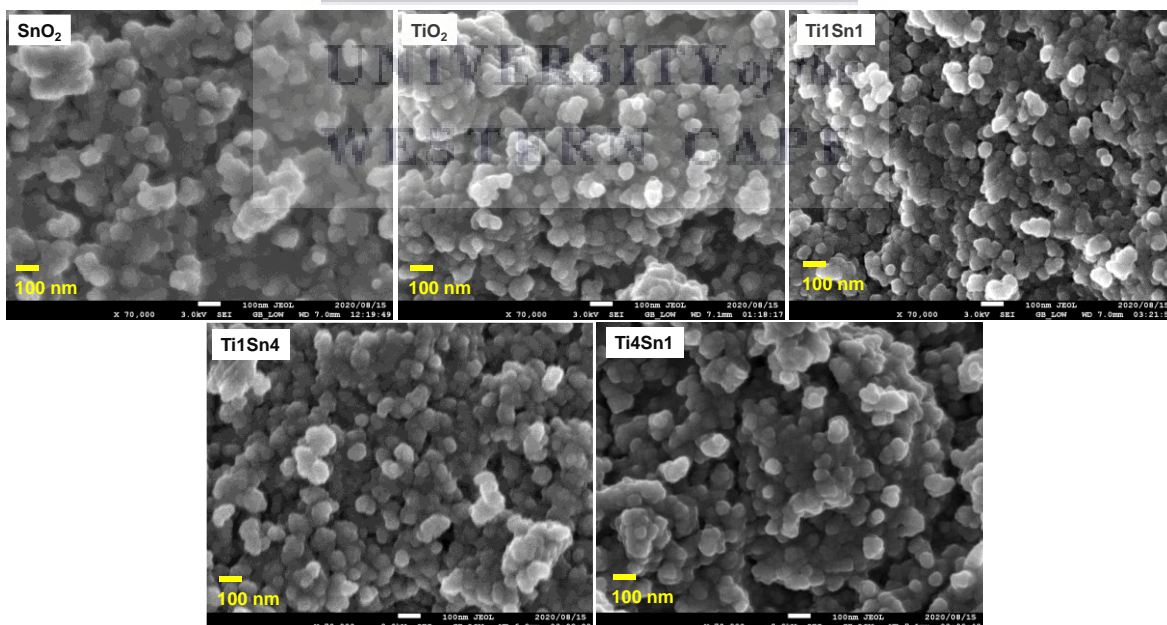
Fig. 6-5: SEM micrograph images of the heterostructure TiO_2-SnO_2 catalysts.

Fig. 6-8 shows the SAED patterns of the catalysts. The SAED patterns were characterized by the diffraction rings which indicated the polycrystalline nature of the heterostructure catalysts. The diffraction rings of SnO_2 and the heterostructure TiO_2-SnO_2 catalysts comprise of discrete spots whereas those of TiO_2 are more diffused.
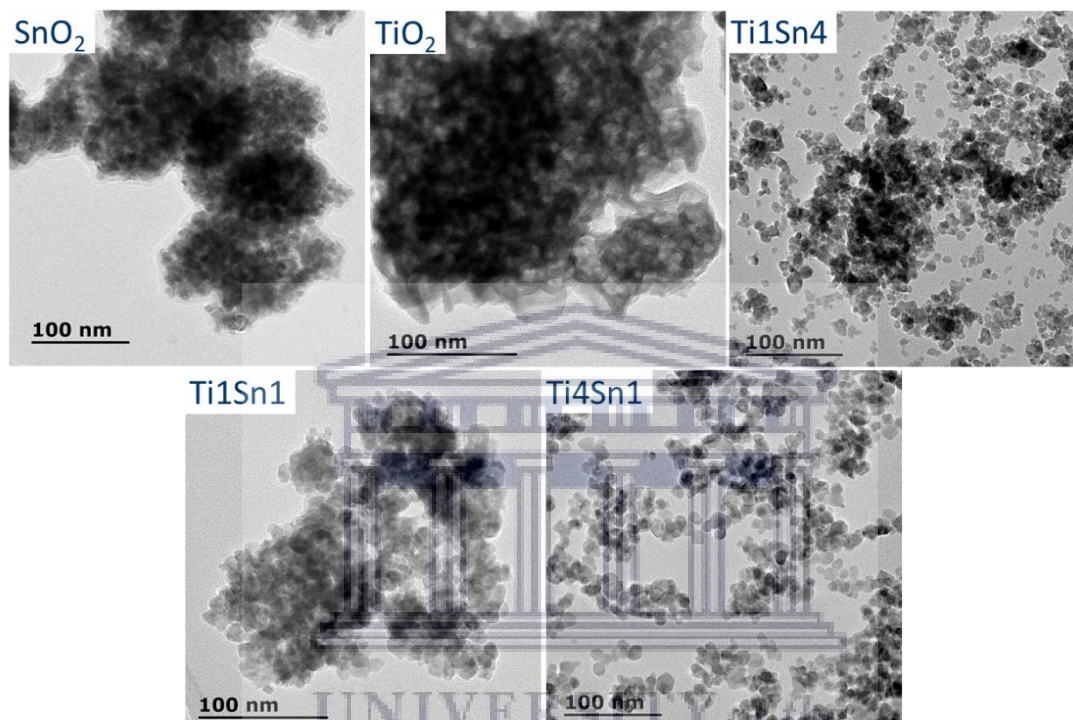
Fig. 6-6: TEM micrograph images heterostructure TiO_2-SnO_2 catalysts.
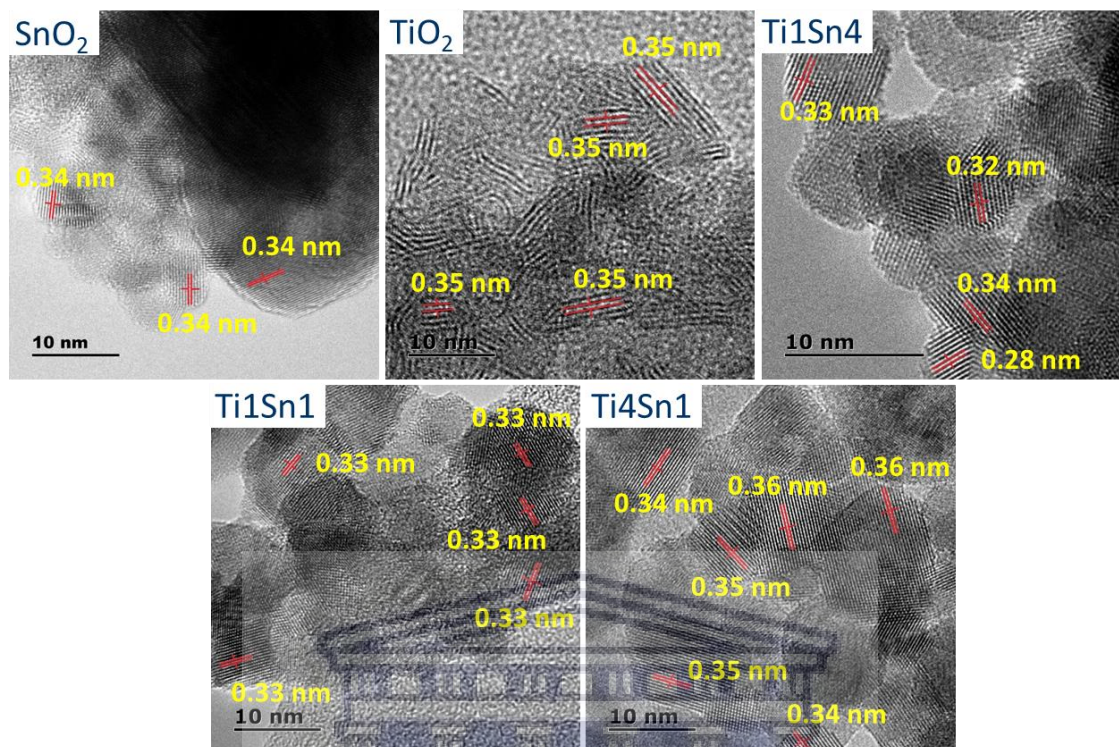
Fig. 6-7: HRTEM micrograph images of the heterostructure TiO_2-SnO_2 catalysts.

The two most inner indicated SAED rings for SnO_2 and the TiO_2-SnO_2 catalysts correspond to the respective (110) and (101) planes of the tetragonal phase of SnO_2 NPs. A SAED ring corresponding to the (211) plane was also observed for SnO_2 and the TiO_2-SnO_2 catalysts. While the (112) ring was observed for SnO_2, the SnO_2 (301) ring was observed instead for the TiO_2-SnO_2 catalysts. These results are in agreement with the obtained XRD data (**Fig. 6-1**) showing predominantly the SnO_2 reflections. In addition to the four SnO_2 rings, one more ring was also observed for Ti1Sn1 corresponding to the (112) plane of anatase TiO_2 and two more rings corresponding to the (112) and (204) planes of anatase were observed for the Ti4Sn1 catalyst. The indexed rings for the TiO_2 catalyst correspond to the respective (200), (204) and (215) planes of the anatase phase.
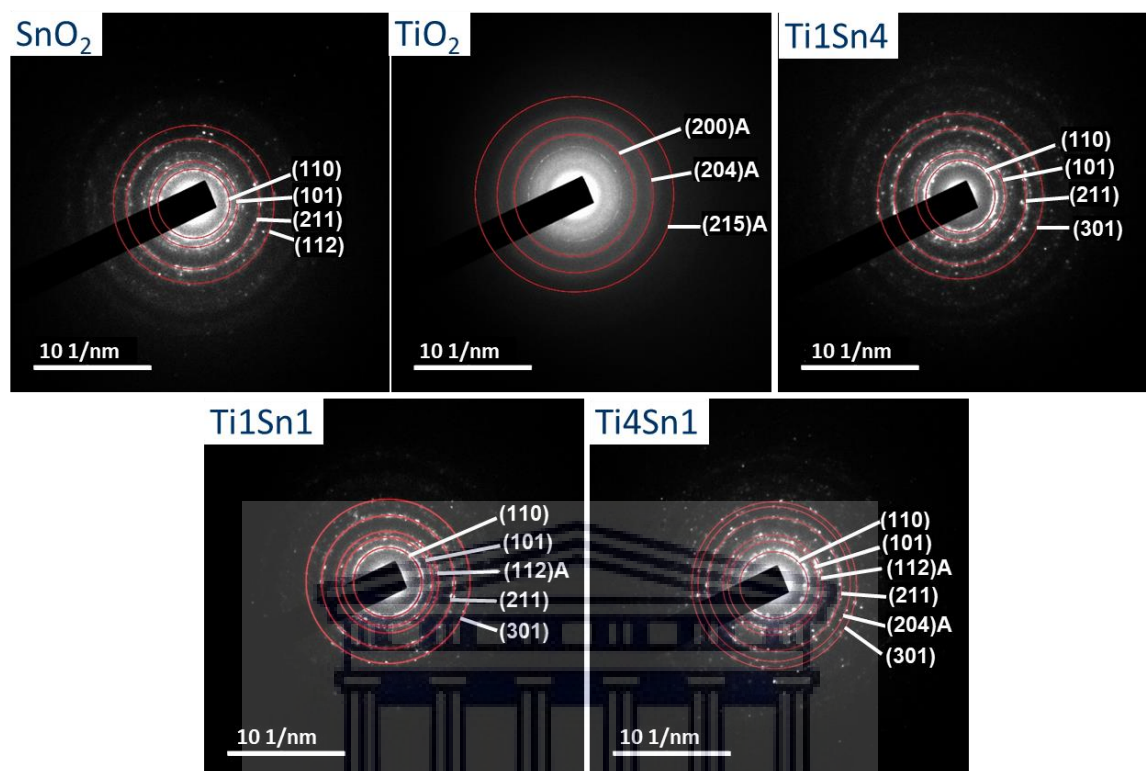
Fig. 6-8: SAED patterns of heterostructure TiO_2-SnO_2 catalysts.

To confirm the elemental composition of the catalysts, SEM–EDX mappings and spectra were recorded and are presented in the **Appendix** (**Figs. C-2** and **C-3**), which showed the nanocatalyst to comprise of only Ti, Sn and O with no presence of impurities.

6.2.5 X-ray photoelectron spectroscopy (XPS) analysis

To investigate the surface elemental composition, chemical and electronic states of the heterostructure TiO_2-SnO_2 catalysts, XPS analysis was performed and the obtained spectra and core electron binding energies (BE) of Sn3d, Ti 2p and O 1s peaks are presented in **Fig. 6-9** and **Table 6-2**. The broad survey scan spectrum presented in **Fig. 6-9a** shows the nanocatalysts' surface to contain only Ti, Sn and O with no impurities detected in agreement with the SEM-EDX results (**Appendix**, **Fig.s' C-2** and **C-3**). **Fig. 6-**

9 (b-d) shows the Sn 3d, Ti 2p and O 1s high resolution core level spectra of the pristine SnO$_2$, TiO$_2$ and those of the heterostructured TiO$_2$-SnO$_2$ catalysts, respectively. The Sn 3d peaks (**Fig. 6-9b**) of pristine SnO$_2$ corresponding to the respective 3d$_{5/2}$ and 3d$_{3/2}$ orbitals were as a spin-orbit doublet observed at 486.6 eV and 495.0 eV, and these values are consistent with the literature data showing the Sn ions to be predominantly in the 4+ oxidation state.[20,21] The Sn 3d peaks were shifted slightly to lower BE for the heterostructured TiO$_2$-SnO$_2$ nanocatalysts by 0.4 eV for the Ti1Sn4 catalyst with low TiO$_2$ loading and by 0.6 eV for the Ti1Sn1 and Ti4Sn1 catalysts with high TiO$_2$ loading. These peak shifts are brought about by the lesser electron withdrawing strength (lower electronegativity) of Ti compared to Sn and are indicative of electronic interactions of the two elements. The chemical shifts are due to changes in the local chemical and physical environment due to extra Coulombic interactions between the photo-emitted electron and the ion core induced by the incorporation of Ti oxide onto the SnO$_2$ matrix. The O 1s core level spectrum (**Fig. 6-9d**) of pristine SnO$_2$ catalyst show the O 1s peak was observed at 530.4 eV indicating that the lattice oxygen atoms exist mainly as the O^{2-} species.[22] The O 1s peaks of TiO$_2$ and the TiO$_2$-SnO$_2$ catalysts were also shifted slightly to lower BE by 0.4 – 0.8 eV.

Table 6-2: XPS binding energy data values of the TiO$_2$-SnO$_2$ catalysts.

Catalysts	Core line binding energy (eV)					O$_V$/O$_L$
	Sn3d$_{5/2}$	Sn3d$_{3/2}$	Ti2p$_{3/2}$	Ti2p$_{1/2}$	O1s	
SnO$_2$	486.6	495.1	N/A	N/A	530.4	0.85
TiO$_2$	N/A	N/A	458.2	464.1	529.8	1.48
Ti1Sn4	486.2	494.6	458.4	464.4	530.0	0.21
Ti1Sn1	486.0	494.4	458.2	464.0	529.7	0.49
Ti4Sn1	486.0	495.4	458.3	464.0	529.6	0.35
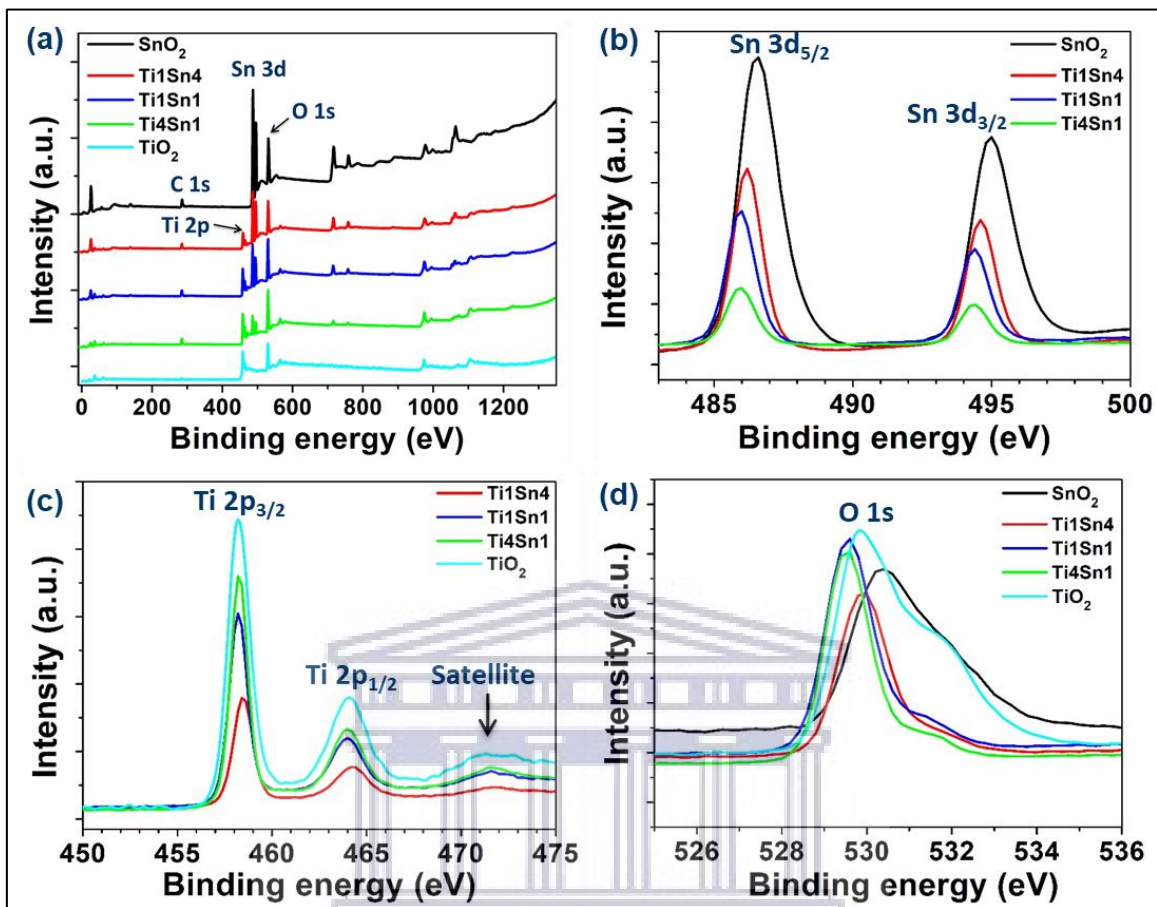
Fig. 6-9: XPS spectra of the heterostructure TiO₂-SnO₂ catalysts showing (a) survey scans, high resolution (b) Sn 3d, (c) Ti 2p, and (d) O 1s profiles.

The Ti 2p core level spectrum (**Fig. 6-9c**) of pristine TiO_2 show as a spin-orbit doublet of peaks corresponding to the respective $2p_{3/2}$ and $2p_{1/2}$ orbitals located at 458.2 eV and 464.1 eV. The TiO_2 2p spectrum also showed a satellite peak centred at 472.2 eV. The Ti 2p peaks BE values which are consistent with the literature data and the presence of the satellite peak indicate the Ti ions to exist predominantly in the 4+ oxidation state.[23-25] The Ti 2p peaks of the heterostructure TiO_2-SnO_2 catalysts were also shifted slightly to lower BE by 0.1 – 0.3 eV as explained above. Comparison of the surface Ti atomic content with nominal Ti loading showed the Ti1Sn4 catalyst to possess the highest amount of surface exposed Ti atoms with 16.8% at a nominal Ti loading of 25% (**Table 6-1**). The surface Ti

atomic content was lower for the other TiO_2-SnO_2 catalysts at 20.6% for Ti1Sn1 (50% nominal Ti loading) and 27.4% for Ti4Sn1 (75% nominal Ti loading).

The asymmetry of the O 1s peaks indicate the contribution of more than one oxygen species and were thus deconvoluted using the Gaussian fitting method. The O 1s peaks could be fittted into three peaks centred at BE around 530 eV, 531-532 eV and 532-534 eV (**Fig. 6-10**). The peaks at 530 eV are assigned to the lattice O^{2-} species (O_L), those at 531-532 eV to surface defects such as oxygen vacancies or surface adsorbed oxygen species (O_V) and the peaks between 532-534 eV are attributed to oxygen from surface adsorbed water molecules (O_A).[26] The calculated O_V/O_L peak area ratios (**Table 6-2**) show pristine SnO_2 to contain a high density of surface defects (O_V) and the Ti1Sn4 catalyst to contain the least.
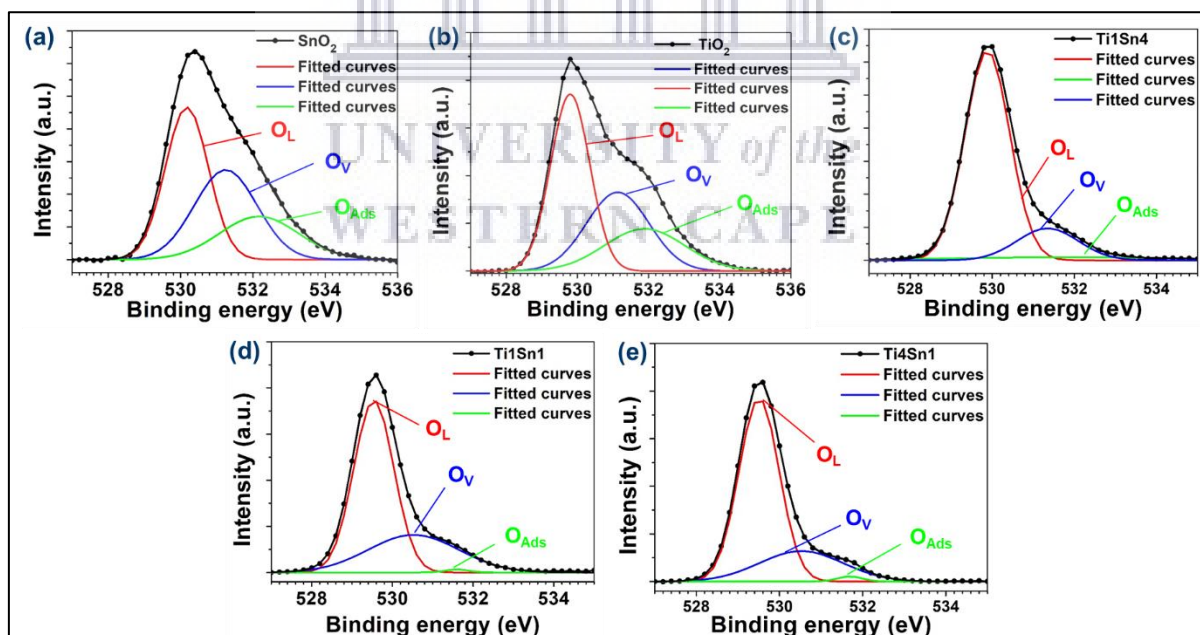
Fig. 6-10: Deconvoluted O1s XPS spectral profiles of the heterostructure TiO_2-SnO_2 catalysts.

Overall, the XPS data confirmed both the Ti and Sn to exist predominantly in the 4+ oxidation state for the heterostructure TiO_2-SnO_2 catalysts indicating the formation of highly oxidized catalysts. In addition, the observed chemical shift of the Sn3d, Ti2p and O1s core level binding energies for the different titania loadings also showed varying electronic structure interaction of Ti and Sn in the heterostructure metal oxide catalysts that could affect the catalytic activity to varying degrees. Furthermore, the varying density of surface defects on the nanocatalysts could also induce different catalytic active sites, thus activities.

6.2.6 Structure defects and oxygen vacancies analysis

To study the nature of the defect states of the heterostructure TiO_2-SnO_2 catalysts, room temperature photoluminescence (PL) analysis was performed and the obtained spectra is shown in **Fig. 6-11**. The spectra of the catalysts show two broad emission bands; the blue band centred around 405 nm and the near-infrared band centred at 810 nm. The intensity of these bands is highest for pristine SnO_2 followed by pristine TiO_2. In contrast, the intensity of emission bands for the heterostructure TiO_2-SnO_2 catalysts decreased with decreasing TiO_2 loading with the Ti1Sn4 catalyst showing the lowest intensity. Since the number of defects present is directly related to the relative intensity of the bands, these results are in agreement with the XPS analysis showing pristine SnO_2 possesses the highest density of defects and the Ti1Sn4 catalyst the lowest. The high density of defects (oxygen vacancies) interacts with interstitial metal ions leading to the formation of a considerable amounts of trapped states within the band gap of the metal oxide, which in turn give rise to high intensity PL emission bands.
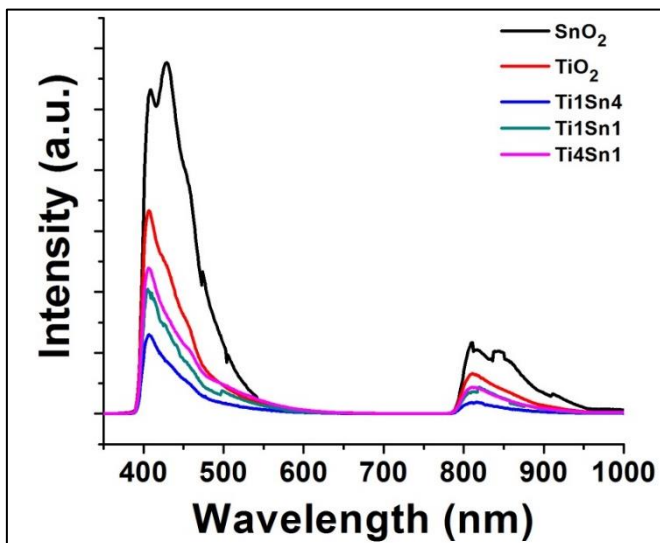
Fig. 6-11: PL spectra of the heterostructure TiO_2-SnO_2 catalysts.

The blue emission band of the catalysts was deconvoluted using the Gaussian fitting method and could be fitted into multiple peaks as shown in **Fig. 6-12**. The pristine SnO_2 spectra was deconvoluted to six emission peaks at 402 nm (P_1), 409 nm (P_2), 426 nm (P_3), 450 nm (P_4), 468 nm (P_5) and 501 nm (P_6). P_1, P_2 and P_6 originate from oxygen vacancies (O_v) and P_3 is attributed to Sn interstitials (Sn_i).[27,28] P_4 and P_5 are caused by the transition of excited electrons from the Sn_i level to the valence band.[29] The pristine TiO_2 spectra was also deconvoluted to six emission peaks at 401 nm (P_1), 409 nm (P_2), 424 nm (P_3), 445 nm (P_4), 475 nm (P_5) and 489 nm (P_6). P_1-P_4 are caused by the self-trapped excitons located at the TiO_6 octahedra.[30,31] P_5 originate from shallow trapped oxygen vacancies and P_6 is caused by an electron transition from an F^+ centre to an acceptor level above the valence band. The F^+ centre is formed by an electron pair left behind in a vacancy cavity created by the loss of an oxygen atom.[32]
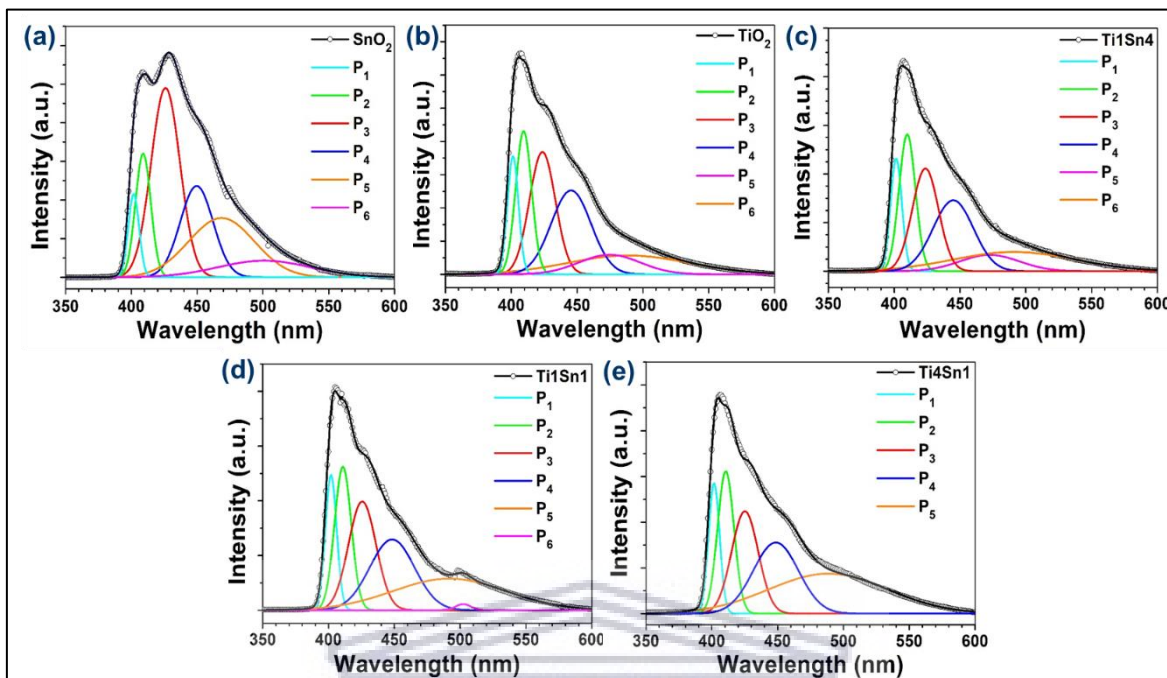
Fig. 6-12: The deconvoluted blue emission band PL spectra of the heterostructure TiO_2-SnO_2 catalysts.

6.3 Catalytic activity evaluation for maleic acid synthesis

6.3.1 Catalyst screening for furfural oxidation

To evaluate the catalytic activity of the heterostructure TiO_2-SnO_2 catalysts, the catalysts were assessed in terms of conversion, selectivity and yield toward maleic acid in the oxidation of furfural using H_2O_2 as an oxidant. The oxidation of furfural was carried out for 24 h under the following conditions; 5 mmol of furfural, 100 mg catalyst, 5 mL each of H_2O and acetonitrile solvent, at 60 °C, and 25 mmol of H_2O_2 oxidant with 5 mmol added at the start of the reaction, then 5 mmol added every 3 h for four times. The obtained catalytic performance results of the different catalysts are comparatively summarized in **Table 6-3** and presented graphically in **Fig. 6-13**, respectively. **Table 6-3** shows the conversion of furfural and products yield for the oxidation reaction with the different catalysts. The pristine SnO_2 gave a furfural conversion of 18.4% while producing maleic acid with a yield 2.6% and fumaric acid with just 0.1% yield. 2-Furoic acid (FA), the reaction intermediate,

was produced with a 15.3% yield while the other side products (which include 2-(5H)-furanone, malic acid, formic acid and possibly 2-hydroxy-2-(5H)-furanone) were produced in trace amounts. The yield of maleic acid and furfural conversion were improved respectively to 15.0% and 23.7% when pristine TiO_2 was employed as the reaction catalyst. The yield of 2-furoic acid was also improved to 4.9% while oxalic acid, fumaric acid and succinic acid were detected in trace amounts. However, the yield of the side products was slightly increased to 2.5%.

Table 6-3: Catalytic conversion results of the heterostructure TiO_2-SnO_2 catalysts for furfural oxidation with H_2O_2 oxidant.

Catalyst	Conversion (%)	Yield (%)					
		MA	OA	FMA	SA	FA	[1] Others
SnO_2	18.4	2.6	0.4	0.1	0.0	15.3	0.0
TiO_2	23.7	15.0	0.3	0.8	0.2	4.9	2.5
Ti1Sn4	94.9	63.7	0.7	1.4	1.4	7.2	20.5
Ti1Sn1	96.3	63.8	1.3	4.1	1.4	5.0	20.7
Ti4Sn1	87.6	59.3	0.5	2.0	1.2	6.2	18.4

[1] Side products such as 2-(5H)-furanone, malic and formic acids. Symbol: MA = maleic acid, OA = oxalic acid, FMA = fumaric acid, SA = succinic acid, FA = 2-furoic acid. Reaction conditions: 5 mmol furfural, 25 mmol 30% (aq) H_2O_2 (5 mmol of H_2O_2 oxidant was added initially at the beginning of the reaction, then added periodically at 3 h intervals four times), 5 mL H_2O and 5 mL MeCN solvent, 100 mg catalyst, T = 60 °C and t = 24 h.

The catalytic activity results were remarkably improved when utilizing the heterostructure TiO_2-SnO_2 catalysts with the furfural conversion reaching reaching 94.9% for the Ti1Sn4 catalyst with lowest TiO_2 loading (25 wt%). The catalyst produced maleic acid with 63.7% yield and 67.2% selectivity. Increasing the TiO_2 loading to 50 wt% (Ti1Sn1) and 75 wt% (Ti4Sn1) resulted in respective furfural conversions of 96.3% and 87.6%. The yield of maleic acid produced was 63.8% for the Ti1Sn1 catalyst and 59.3% for the Ti4Sn1 catalyst.
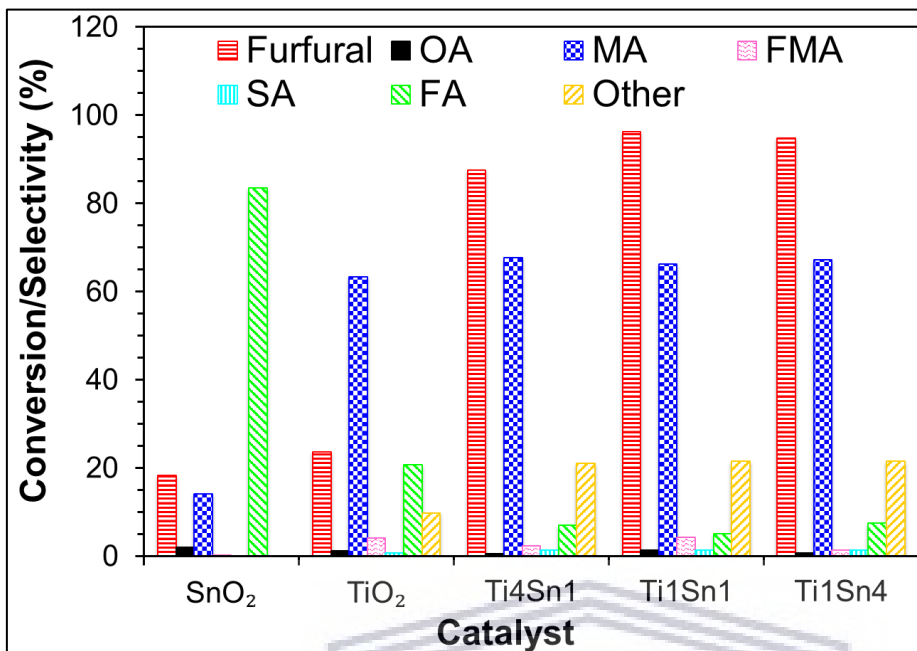
Fig. 6-13: Selectivity results for the oxidation of furfural with TiO_2-SnO_2 catalysts. Reaction conditions: 5 mmol furfural, 25 mmol 30% (aq) H_2O_2 (5 mmol of H_2O_2 oxidant was added initially at the beginning of the reaction, then added periodically at 3 h intervals four times), 5 mL H_2O and 5 mL MeCN solvent, 100 mg catalyst, T = 60 °C and t = 24 h.

The catalytic screening results in terms of selectivity presented in **Fig. 6-13** show that the while low furfural conversions were achieved with both the individual SnO_2 and TiO_2 metal oxides, SnO_2 was highly selective towards 2-furoic acid (83.5%) and TiO_2 very selective towards maleic acid (63.4%). Although heterostructuring of TiO_2 with SnO_2 leads to a large improvement of furfural conversion, the increase in selectivity is minimal with maleic acid selectivity reaching 67.7% for Ti1Sn4 catalyst with 25 wt% TiO_2 loading. Further increase of TiO_2 loading to 50 wt% (Ti1Sn1) and 75 wt% (Ti4Sn1) led to respective maleic acid selectivity of 66.3% and 67.2%. Also, the high selectivity of SnO_2 towards 2-furoic acid is also decreased following the heterostructuring with TiO_2 with the highest 2-furoic acid selectivity for the heterostructure TiO_2-SnO_2 catalysts achieved being 7.6% with the Ti1Sn4 catalyst (least TiO_2 loading). It should also be noted that while the selectivity towards the other side products was low with pristine SnO_2 (0.1%) and TiO_2 (9.7%), the

selectivity towards the side products was increased to 18 - 21 % with the heterostructure TiO_2-SnO_2 catalysts.

The XPS analysis revealed the SnO_2 interfaced TiO_2 mixed metal oxides catalysts to exist more in both their higher (4+) oxidation states thus presenting fully oxidized nanocatalysts. As a result, the mixed metal oxides synergistically contributed positively on their redox reactivity to facilitate the required electron-transfer mechanism to create reactive oxygen species effective for the efficient conversion of furfural while also showing high selectivity towards maleic acid. Comparison of the XPS surface and nominal Ti loading showed the Ti1Sn4 catalyst to possess the highest amount of surface exposed Ti atoms. The XPS results coupled with PL analysis also revealed that a high density of surface oxygen defects is detrimental for maleic acid selectivity with the Ti1Sn4 catalyst, which possessed the least density of surface defects affording the best catalytic performance. The surface area measurements also showed that the most active Ti1Sn4 catalyst possessed the highest surface area amongst all the catalysts. This high surface area of Ti1Sn4 catalyst and the high amount of surface exposed Ti atoms makes available the maximized number of exposed surface active sites, thus enhancing catalytic activity for furfural oxidation. Furthermore, the Ti1Sn4 catalyst also diplays the largest pore volume thus improving the adsorption/desorption of the furfural substrate to and from the catalyst active sites. When considering the combination of conversion, yield, selectivity towards maleic acid and the stability of the products in terms of over-oxidation to oxalic acid, the high surface area Ti1Sn4 catalyst afforded the best catalytic performance and was thus selected for further catalytic experiments in order to optimize the oxidation process.

6.3.2 Effect of solvent composition on furfural oxidation rates

The solvent composition can influence the catalyst activity in terms of substrate conversion, products distribution, and yields and is thus a critical component to consider for optimizing a chemical reaction process. The effect of different solvent compositions such as; (1) deionized water (H_2O), and co-solvents of (2) γ-valerolactone and H_2O (GVL-H_2O), (3) acetic acid and H_2O (AcOH-H_2O), and (4) acetonitrile and H_2O (MeCN-H_2O), were evaluated for furfural oxidation with the Ti1Sn4 catalyst (**Table 6-4** and **Fig. 6-14**). Compared to the reaction conducted in the co-solvent of MeCN-H_2O, the reaction carried out in H_2O afforded poor catalytic results with just 9.3% furfural conversion and 2.5% maleic acid yield. The H_2O solvent favoured the formation of 2-furoic acid with 3.9% yield and 42.4% selectivity while oxalic acid, fumaric acid and succinic acid were formed in trace amounts. Rodenas et.al.[33] recently demonstrated the effect of GVL in stabilizing the TS-1 catalyst from leaching while also improving the yield of maleic acid in furfural oxidation with H_2O_2 in a GVL-H_2O solvent mixture. However, the reaction carried out in the GVL-H_2O mixture in this study proved to impact negatively (compared to MeCN-H_2O) on the catalytic activity of the Ti1Sn4 catalyst with furfural conversion reaching 33.2% while producing maleic acid with 19.8% yield (**Table 6-4**). The best catalytic results were obtained with AcOH-H_2O solvent mixture with 99.2% furfural conversion obtained and a maleic acid yield of 80.5% at 81.1% selectivity (**Fig. 6-14**). The solvent mixture also afforded fumaric acid with a yield of 6.1%, while trace amounts of oxalic acid and succinic acid were produced and 2-furoic acid was not detected.

Table 6-4: Effect of solvent composition on furfural oxidation rates with the Ti1Sn4 catalyst.

Solvent	Conversion (%)	Yield (%)					
		MA	OA	FMA	SA	FA	Others
H_2O	9.3	2.5	0.7	0.2	0.0	3.9	2.0
GVL-H_2O	33.2	19.8	1.4	1.5	0.5	3.8	6.2
AcOH-H_2O	99.2	80.5	0.9	6.1	1.0	0.0	10.7
MeCN-H_2O	94.9	63.7	0.7	1.4	1.4	7.2	20.5

Reaction conditions: 5 mmol furfural, 25 mmol 30% (aq) H_2O_2 (5 mmol of H_2O_2 oxidant was added initially at the beginning of the reaction, then added periodically at 3 h intervals four times), 10 mL solvent, 100 mg catalyst, T = 60 °C and t = 24 h.
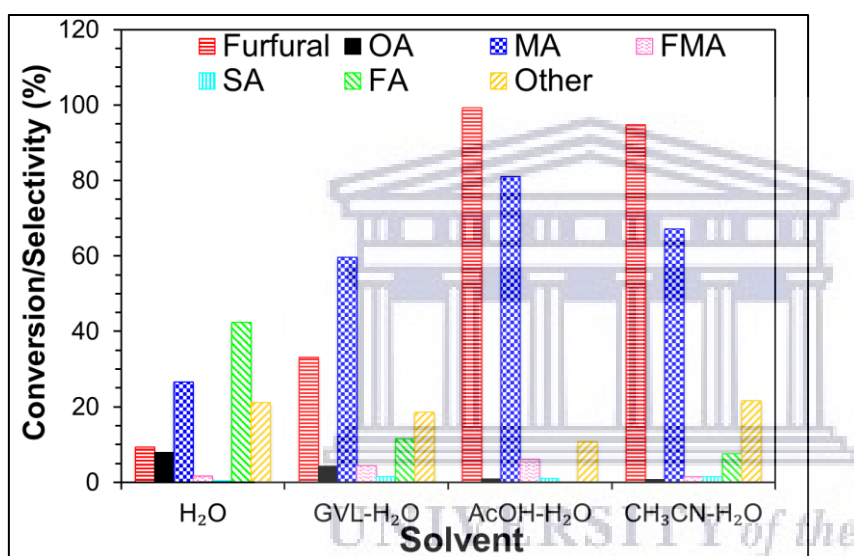
Fig. 6-14: Selectivity results for the oxidation of furfural with Ti1Sn4 catalyst in different solvent mixtures. Reaction conditions: 5 mmol furfural, 25 mmol 30% (aq) H_2O_2 (5 mmol of H_2O_2 oxidant was added initially at the beginning of the reaction, then added periodically at 3 h intervals four times), 10 mL solvent, 100 mg catalyst, T = 60 °C and t = 24 h.

In terms of selectivity, the reaction carried out in the AcOH-H_2O solvent mixture showed to be less selective towards the side products with 10.8% selectivity, which was the lowest of all the solvent mixtures, investigated. To study the promotional effect of acetonitrile and acetic acid on the furfural oxidation rates and products distribution, the reaction was carried out without the catalyst in both the MeCN-H_2O and AcOH-H_2O co-solvents (**Table 6-5**). Excellent conversion of furfural was achieved in both solvent systems, 94.4% in

MeCN-H_2O and 99.9% in AcOH-H_2O. However, the yield of maleic acid was significantly decreased in the absence of a catalyst reaching 11.2% in MeCN-H_2O and 40.0% in AcOH-H_2O compared to the catalysed reaction (63.7% in MeCN-H_2O and 80.5% in AcOH-H_2O). The non-catalysed reactions in both solvent systems showed high formation of 2-furoic acid with yields of 36.2% in MeCN-H_2O and 68.1% in AcOH-H_2O.

Table 6-5: Effect of solvent composition on non-catalysed furfural oxidation rates and products distribution.

Solvent	Conversion (%)	Yield (%)					
		MA	OA	FMA	SA	FA	Others
AcOH-H_2O	99.9	40.0	1.0	2.4	0.0	36.2	20.3
MeCN-H_2O	94.4	11.2	0.3	1.3	0.4	68.1	13.1

Reaction conditions: 5 mmol furfural, 25 mmol 30% $_{(aq)}$ H_2O_2 (5 mmol of H_2O_2 oxidant was added initially at the beginning of the reaction, then added periodically at 3 h intervals four times), 10 mL solvent, T = 60 °C and t = 24 h.

The excellent conversion of furfural achieved in both solvent systems is attributed to the ability of acetonitrile to assist the activation of H_2O_2 by forming a peroxy hydroxyl anion (OOH^-) which reacts with acetonitrile resulting in a peroxy carboximidic acid complex, while acetic acid reacts with H_2O_2 to form a peracetic acid complex.[34,35] These complexes are capable of oxidising certain organic substrates and show a stronger oxidizing strength than aqueous H_2O_2 alone as demonstrated by Pillai and Sahle-Demessie,[34] and Lou et.al.[35] for the respective oxidation of cyclic alkanes and alcohols, and furfural. The decreased yield of maleic acid for the non-catalysed reactions illustrated the critical role of the Ti1Sn4 catalyst in enhancing the yield and selectivity towards maleic acid from furfural oxidation. For further investigating other reaction parameters, the AcOH-H_2O was utilized as it yielded superior catalytic results.

6.3.3 Effect of reaction temperature

The next reaction parameter investigated was the effect of temperature on the distribution of products and oxidation rates. The role played by temperature is also critical as it affects the rate at which H_2O_2 dissociates into O_2 and H_2O, and thus the overall oxidation rate and the stability of the products. Only three sets of temperature were investigated; 60, 70, and 80 °C the reasoning being that higher temperatures (> 80 °C) lead to fast dissociation of H_2O_2 and over-oxidation of the products to oxalic acid (**chapter 5, section 5.3.2**) and lower temperatures (< 60 °C) lead to slow dissociation of H_2O_2 and slow oxidation rate. To study the effect of temperature, the oxidation reaction was carried as outlined in **section 6.3.1**, with two slight modifications; the 5 mmol of H_2O_2 were added every one hour instead of three and reaction products sampled and analysed after 6, 8 and 24 h. The catalytic performance results of the study are comparatively summarised in **Table 6-6** and presented graphically in **Fig. 6-15**.

Table 6-6: Effect of reaction temperature on furfural oxidation rates with the Ti1Sn4 catalyst in AcOH-H_2O solvent.

Temperature (°C)	Time (h)	Conversion (%)	Yield (%)					
			MA	OA	FMA	SA	FA	Others
60	6	93.3	70.1	1.4	5.3	0.0	1.9	14.6
	8	96.4	79.6	0.9	3.3	0.2	0.2	12.2
	24	99.1	74.8	0.0	3.1	1.4	0.0	19.8
70	6	96.4	74.1	0.6	4.4	1.1	2.9	16.3
	8	98.2	71.9	0.4	4.8	1.5	2.5	17.1
	24	99.0	68.0	0.0	3.9	1.5	1.9	23.7
80	6	94.0	53.0	32.3	1.3	0.0	0.0	7.4
	8	95.2	26.1	49.3	3.2	1.2	0.0	15.4
	24	100	0.5	63.9	3.9	1.7	0.0	30.0

Reaction conditions: 5 mmol furfural, 25 mmol 30% (aq) H_2O_2 (5 mmol of H_2O_2 oxidant was added initially at the beginning of the reaction, then added periodically at 1 h intervals four times), 5 mL H_2O and 5 mL AcOH solvent, 100 mg catalyst, t = 24 h.

For the reaction conducted at 60 °C, after 6 h reaction time a furfural conversion of 93.3% was achieved with 70.1% maleic acid yield. The yield of fumaric acid at this time was 5.3% and that of 2-furoic acid was 1.9%. The yield of the side products was 14.6%. After 8 h of reaction time, the yield of maleic acid was increased to 79.6% and that of fumaric acid was decreased to 3.3%. The conversion was also increased to 96.4% with the yield 2-furoic acid decreasing to 0.2%.
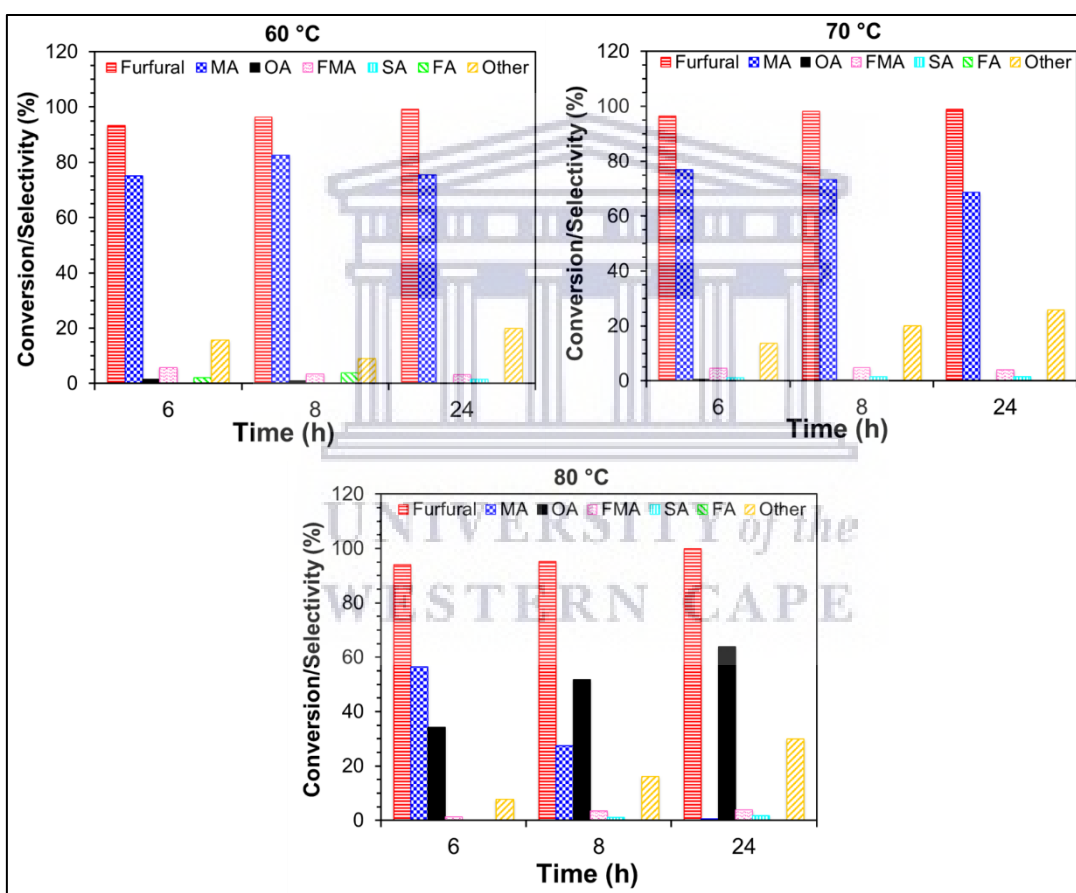
Fig. 6-15: Furfural oxidation products selectivity at various temperatures with Ti1Sn4 catalyst in AcOH-H_2O solvent. Reaction conditions: 5 mmol furfural, 25 mmol 30% $_{(aq)}$ H_2O_2 (5 mmol of H_2O_2 oxidant was added initially at the beginning of the reaction, then added periodically at 1 h intervals four times), 5 mL and 5 mL AcOH solvent, 100 mg catalyst, t = 24 h.

At 24 h reaction, while furfural conversion increased further to 99.1% the yield of maleic acid was decreased to 74.8% and that of fumaric acid slightly decreased to 3.1%. On the other hand, oxalic acid and 2-furoic acid were not detected. The decrease in the yields of oxalic acid and maleic acid is attributed to the over-oxidation of these products to CO_2 (not quantifiable by HPLC) and formic acid as indicated by the increase in yield of side products to 19.8% after 24 h. The presence of CO_2 gas was evidenced visually by the increase in pressure of the balloon used to seal reaction mixture after 24 h. The reaction performed at 70 °C resulted in 74.1% yield of maleic acid after 6 h at 96.4% furfural conversion. The yield of fumaric acid at this time was 4.4% with that of 2-furoic acid at 2.9% and the side products were produced with 16.3% yield. With furfural conversion increased to 98.2% after 8 h, the yield of maleic acid decreased to 71.9% and further decreased to 68.0% after 24 h of reaction time as a result of over-oxidation. The yield of 2-furoic acid decreased gradually to 2.5% and 1.9% after 8 and 24 h, respectively. The yield of fumaric acid increased to 4.4% after 8 h, and thereafter decreased to 3.9% after 24 h. The yield of the side products was increased consequence to the over-oxidation of the products and reached 23.7% at the end of the reaction. The oxidation reaction performed at 80 °C obtained a 53.0% yield of maleic acid after 6 h at 94.0% furfural conversion and resulted in large increase in oxalic acid yield to 32.3%, which increased further to 49.3% after 8 h. The yield of maleic acid was decreased to 26.1% after 8 h, then to 0.5% after 24 h. The conversion of furfural reached 100% after 24 h. The large decrease in maleic acid yield at a higher temperature (80 °C) is due to over-oxidation to oxalic acid, which increased in yield to 63.9% after 24 h. The extent of over-oxidation at larger temperatures is further substantiated by the increased yield of side products to 30.0% after 24 h.

6.3.4 Effect of reaction time

Next, the progression of furfural oxidation and evolution of the products with time was studied. The reaction was performed as described in **section 6.3.3** with the products analysed every hour prior to the addition of H_2O_2. As shown in **Table 6-7** and **Fig. 6-16**, during the first 3 h of the reaction the oxidation of furfural proceeded very slowly with conversion reaching 20.1% after 3 h. The yield of maleic acid during the 3 h reached just 4.7% while 2-furoic acid was produced as the main product with 81.2% selectivity after 1 h which decreased as the reaction progressed to 63.4% after 3 h. The conversion of furfural increased sharply to reach 59.9% after 4 h (addition of final portion of H_2O_2) and thereafter continued to increase to 92.5% after 5 h. The yield of maleic acid followed the same trend increasing to 33.5% after 4 h and to 67.9% after 5 h. The selectivity towards 2-furoic acid continued to decrease to reach 19.4% after 4 h and 1.4% after 5 h. The yield of the side products increased as the reaction progressed to reach 20.7% after 5 h.

Table 6-7: Evolution of products with reaction time with the Ti1Sn4 catalyst in AcOH-H_2O solvent.

Time (h)	Conversion (%)	Yield (%)					
		MA	OA	FMA	SA	FA	Others
1	1.9	0.1	0.0	0.0	0.0	1.6	0.2
2	6.0	0.6	0.1	0.0	0.0	4.7	0.6
3	20.1	4.7	0.1	0.1	0.2	12.7	2.3
4	59.9	33.5	0.4	0.0	1.4	11.8	12.8
5	92.5	67.9	0.6	0.0	2.0	1.3	20.7
6	96.4	74.1	0.6	4.4	1.1	0.0	16.2
8	98.2	71.9	0.4	4.8	1.5	0.0	19.6
24	99.0	68.0	0.0	3.9	1.5	0.0	25.6

Reaction conditions: 5 mmol furfural, 25 mmol 30% (aq) H_2O_2 (5 mmol of H_2O_2 oxidant was added initially at the beginning of the reaction, then added periodically at 1 h intervals four times), 5 mL H_2O and 5 mL AcOH solvent, 100 mg catalyst, T = 60 °C and t = 24 h.

The conversion of furfural continued to increase to 96.4% after 6 h with the yield of maleic acid increasing to 74.1% at 76.9% selectivity and the yield of fumaric acid increased to

4.4%. 2-Furoic acid was not detected after 6 h while the yield of the side products decreased to 16.2%. The decrease in the yield of side products is attributed to the oxidation of 2-(5H)-furanone to maleic acid and fumaric acid as evidenced by the increase in the yield of these products. After 8 h, the conversion of furfural increased further to 98.2%. However, the yield of maleic acid began to decrease because of over-oxidation. The yield of fumaric acid increased slightly to 4.8% and 2-furoic acid was again not detected. When the reaction was stopped after 24 h, the yield of maleic acid decreased even further to 68.0% with furfural conversion slightly increased to 99.0%. The yield of fumaric acid also decreased to 3.9%. As a result of over-oxidation of maleic acid and fumaric acid, the yield of the side products increased to 25.6%. After 24 h, oxalic acid and 2-furoic acid were not detected in the reaction mixture. The results obtained above indicate that a reaction time of 6 h is sufficient to produce maleic acid with an optimum yield 74.1% at 76.9% selectivity. Running the reaction beyond this time exposes the products (particularly maleic acid and fumaric acid) to excess H_2O_2, which leads to deep oxidation of the products to form CO_2 and formic acid.
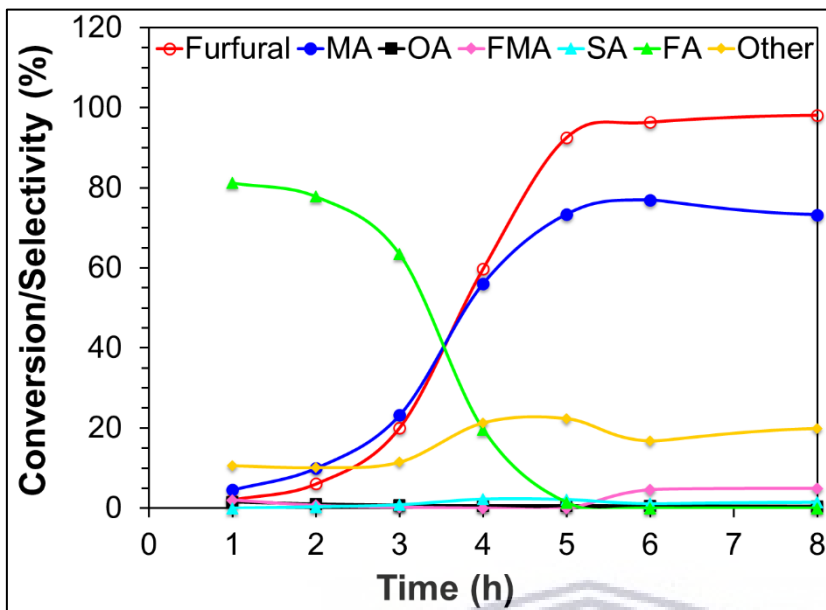
Fig. 6-16: Products selectivity with time for the oxidation of furfural with Ti1Sn4 catalyst in AcOH-H_2O solvent. Reaction conditions: 5 mmol furfural, 25 mmol 30% $_{(aq)}$ H_2O_2 (5 mmol of H_2O_2 oxidant was added initially at the beginning of the reaction, then added periodically at 1 h intervals four times), 5 mL H_2O and 5 mL AcOH solvent, 100 mg catalyst, T = 60 °C and t = 24 h.

6.3.5 Catalyst recyclability performance test

The stability of the catalyst was also investigated by conducting successive reutilization runs with the experiments conducted as in **section 6.3.4** but ran for a 6 h duration. The difficulty of powder catalyst mass loss during handling is always encountered when conducting catalyst recyclability investigations. To compensate for the loss of catalyst; the amount of catalyst used and the amounts of furfural, aqueous H_2O_2, and solvent were all increased by a factor of three for the first reaction cycle and by a factor of 2.5 for the second cycle {i.e. 15 mmol furfural, 75 mmol 30% $_{(aq)}$ H_2O_2, 15 mL (H_2O) and 15 mL (AcOH) co-solvent, and 300 mg catalyst} for the first cycle and {12.5 mmol furfural, 62.5 mmol 30% $_{(aq)}$ H_2O_2, 12.5 mL (H_2O) and 12.5 mL (AcOH) co-solvent, and 250 mg catalyst} for the second cycle). After the first reaction cycle, the catalyst was collected and washed

by centrifuge three times with a mixture of ethanol, acetone and H_2O (1:1:2, vol/vol) and thereafter dried in an oven at 60 °C overnight.

Table 6-8: Recyclability performance test of the Ti1Sn4 catalyst.

Cycle	Conversion (%)	Yield (%)					
		MA	OA	FMA	SA	FA	Others
1	76.2	42.2	1.1	5.2	0.2	13.2	14.3
2	22.2	3.2	0.1	0.5	0.1	9.1	9.2

Reaction conditions: T = 60 °C and t = 6 h, Cycle 1 = 15 mmol furfural, 75 mmol 30% (aq) H_2O_2 , 15 mL H_2O and 15 mL AcOH solvent, and 300 mg catalyst. Cycle 2 = 12.5 mmol furfural, 62.5 mmol 30% (aq) H_2O_2, 12.5 mL H_2O and 12.5 mL AcOH solvent, and 250 mg catalyst.

After the first reaction cycle, 76.2% furfural conversion was achieved and a maleic acid yield of 42.2% at 55.3% selectivity. 2-Furoic acid and fumaric acid were produced with yields of 13.2% and 5.2%. These results were poor compared to those obtained in **section 6.3.4** where maleic acid was produced with 74.1% yield at 76.9% selectivity and 96.4% furfural conversion after 6 h. This could be a result of up scaling the reaction in a small reaction vessel (50 mL flask) which amplified the negative effects of mass transfer limitations. The obtained results were even poorer after the second reaction cycle with just 22.2% furfural conversion and a 3.2% maleic acid yield achieved. The yield of 2-furoic acid was 9.1% while fumaric acid was produced in trace amounts. The poor activity of the catalyst after the second reaction cycle is indicative of leaching of the catalyst active sites, which was probed next.
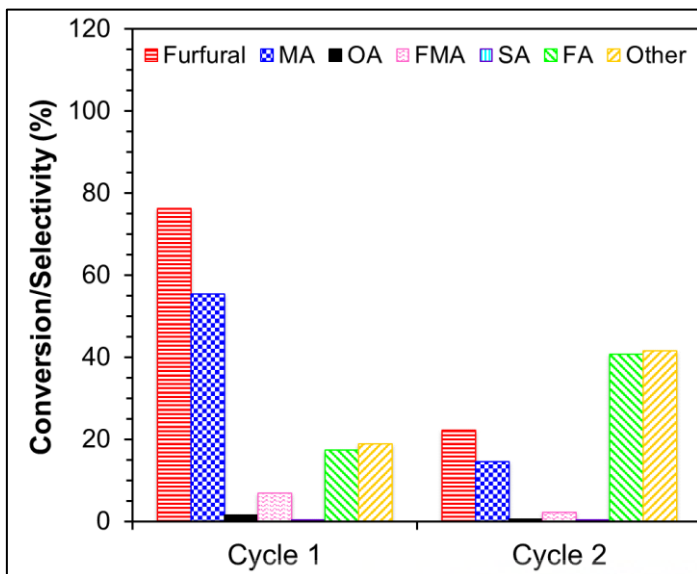
Fig. 6-17: Products selectivity for the catalyst reutilization test with Ti1Sn4 nanocatalyst in AcOH-H_2O co-solvent. Reaction conditions: T= 60 °C and t = 6 h, Cycle 1 = 15 mmol furfural, 75 mmol 30% $_{(aq)}$ H_2O_2 , 15 mL H_2O and 15 mL AcOH co-solvent, and 300 mg catalyst. Cycle 2 = 12.5 mmol furfural, 62.5 mmol 30% $_{(aq)}$ H_2O_2, 12.5 mL H_2O and 12.5 mL AcOH co-solvent, and 250 mg catalyst.

6.3.6 Investigation of the catalyst leaching effect

To investigate leaching of the catalyst active sites indicated by the catalyst reutilization test, two sets of experimental leaching tests were conducted in H_2O and AcOH-H_2O solvents, respectively. The two sets of experiments were set-up as described in **section 6.3.3** with one modification; for the leach tests after 2.5 h of reaction time, the catalyst was removed by hot-filtration and the filtrate solutions were allowed to react for a further 3.5 h (6 h in total) under the same conditions without the catalyst. The non-catalysed oxidation reactions (blank) were also performed for 6 h under the same conditions for comparison. The results from these experiments are displayed in **Table 6-9** and **Fig. 6-18**.

Table 6-9: Catalyst active site leaching test with the Ti1Sn4 catalyst.

Solvent	Cycle	Conversion (%)	Yield (%)					
			MA	OA	FMA	SA	FA	[1] Others
DI H_2O	Blank	14.3	0.1	0.1	0.0	0.0	11.7	2.4
	Leach test	37.9	1.8	0.2	0.4	0.0	29.2	6.3
AcOH-H_2O	Blank	99.8	8.5	0.6	0.3	0.0	72.5	17.9
	Leach test	99.2	65.2	1.6	3.9	0.0	1.4	27.1

Reaction conditions: 5 mmol furfural, 25 mmol 30% (aq) H_2O_2 (5 mmol of H_2O_2 oxidant was added initially at the beginning of the reaction, then added periodically at 1 h intervals four times), 10 mL solvent, 100 mg catalyst, T = 60 °C and t = 6 h.
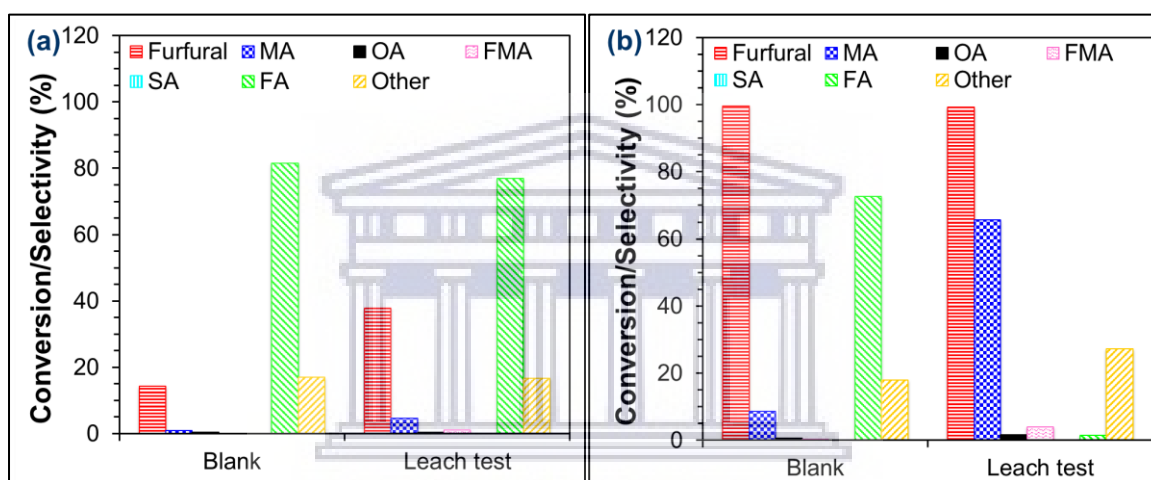
Fig. 6-18: Products selectivity for the catalyst active site leaching test with Ti1Sn4 catalyst in (a) H_2O and (b) AcOH-H_2O solvents. Reaction conditions: 5 mmol furfural, 25 mmol 30% (aq) H_2O_2 (5 mmol of H_2O_2 oxidant was added initially at the beginning of the reaction, then added periodically at 1 h intervals four times), 10 mL solvent, 100 mg catalyst, T = 60 °C and t = 6 h.

The non-catalysed reaction showed a furfural conversion of just 14.3% was achieved in H_2O solvent with trace amounts of maleic acid and oxalic acid detected while 2-furoic acid was produced as the main product with 11.7% yield at 81.5% selectivity. In contrast, the non-catalysed reaction conducted in AcOH-H_2O solvent showed full conversion of furfural (99.8%). However, 2-furoic acid was also produced as the main product with 72.5% yield (72.7% selectivity) and trace amounts of fumaric acid and oxalic acid were detected. The catalytic leaching test performed in H_2O solvent showed an increase in furfural conversion

to 37.9% while 99.2% conversion for the AcOH-H_2O solvent was achieved. Both sets of catalytic leaching experiments showed an increase in the yield of maleic acid to 1.8% in H_2O solvent and to 65.2% in AcOH-H_2O solvent. The yields of oxalic acid, fumaric acid and side products were also increased in both solvent systems. The leaching experiment conducted in H_2O still showed high selectivity towards 2-furoic acid (77.0%) while the experiment conducted in AcOH-H_2O showed high selectivity towards maleic acid (65.7%). The results of these experiments and of the catalyst reutilization test indicate the leaching of the TiO_2 active sites. The active site leaching is further confirmed by comparison of the non-catalysed experiment conducted in AcOH-H_2O solvent with the catalysed reaction affording high selectivity towards maleic acid (65.7%) after removal of the catalyst and the non-catalysed (blank) reaction affording just 8.5% selectivity.

6.3.7 Catalytic evaluation for maleic acid synthesis from 5-hydroxymethylfurfural

The effectiveness of the heterostructure TiO_2-SnO_2 catalysts for the synthesis of maleic acid from 5-hydroxymethylfurfural (HMF) oxidation was also evaluated using aqueous H_2O_2 and the results thereof are presented in **Table 6-10** and **Fig. 6-19**. The catalytic activity of the catalysts was evaluated under the reaction conditions for furfural oxidation in **section 6.3.1** (i.e. 5 mmol of HMF, 100 mg catalyst, 5 mL each of DI water and acetonitrile solvent, at 60 °C, and 25 mmol of H_2O_2 oxidant with 5 mmol added at the start of the reaction, then 5 mmol added every 3 h for four times). When the reaction was carried out with pristine SnO_2 as a catalyst, respective yields of maleic acid and fumaric acid of just 1.7% and 2.0% were achieved with an excellent HMF conversion of 98.7% being achieved. 2.5-Diformylfuran was produced as the main product with a higher yield of 71.7% at 72.7% selectivity. However, 5-formyl-2-furancarboxylic acid was produced with notable 20.3% yield. The yields of maleic acid and fumaric acid increased to 9.1% and

9.0%, respectively, at 18% selectivity when pristine TiO_2 was employed as a catalyst. The respective yields of 2.5-diformylfuran and 5-formyl-2-furancarboxylic acid were decreased to 7.5% and 5.2% while that of 5-hydroxymethyl-2-furandicarboxylic acid increased to 13.1%. However, compared to SnO_2 the use of TiO_2 resulted in a lower HMF conversion of 50.4% and an increase to 6.5% in yield of the by-products.

Table 6-10: Catalytic activity screening results of the heterostructure TiO_2-SnO_2 catalysts for HMF oxidation with H_2O_2 oxidant.

Catalyst	Conversion (%)	Yield (%)						
		MA	FMA	FFCA	FDCA	HMFCA	DFF	[1] Other
SnO_2	98.7	1.7	2.0	20.3	2.0	0.0	71.7	3.0
TiO_2	50.4	9.1	9.0	5.2	0.0	13.1	7.5	6.5
Ti4Sn1	95.8	13.3	7.1	1.1	0.2	0.0	67.9	6.2
Ti1Sn1	99.3	51.7	6.4	16.4	1.7	1.5	13.8	9.5
Ti1Sn4	98.3	56.6	27.2	0.9	0.0	0.0	2.9	10.7

[1] Side products such as oxalic, malic and formic acids. Symbol: MA = maleic acid, FMA = fumaric acid, FFCA = 5-formyl-2-furancarboxylic acid, FDCA = 2.5-furandicarboxylic acid, HMFCA = 5-hydroxymethyl-2-furandicarboxylic acid, DFF = 2.5-diformylfuran. Reaction conditions: 5 mmol HMF, 25 mmol 30% $_{(aq)}$ H_2O_2 (5 mmol of H_2O_2 oxidant was added initially at the beginning of the reaction, then added periodically at 3 h intervals four times), 5 mL H_2O and 5 mL MeCN solvent, 100 mg catalyst, T = 60 °C and t = 24 h.

The yield of maleic acid was increased when the heterostructure TiO_2-SnO_2 catalysts were employed with HMF conversions of 95.8 – 99.3% being achieved. The Ti4Sn1 catalyst with the highest TiO_2 loading produced maleic acid with a 13.3% yield at 95.8% HMF conversion while proving to be more selective towards 2.5-diformylfuran with a 67.9% yield at 71.0% selectivity. The catalyst also resulted in a fumaric acid yield of 7.1% with 5-formyl-2-furancarboxylic acid and 2.5-furandicarboxylic acid produced in trace amounts and 5-hydroxymethyl-2-furandicarboxylic acid was not detected. The use of the Ti1Sn1 catalyst led to the best HMF conversion (99.3%) and an increase in the yields of maleic acid (51.7%) and 5-formyl-2-furancarboxylic acid (16.4%), and a decrease in the yields of 2.5-diformylfuran and fumaric acid to 13.8% and 6.4%, respectively. An increase

in the yield of the side products to 9.5% was observed with the Ti1Sn1 catalyst. The best catalytic results were observed with the Ti1Sn4 catalyst. At 98.3% HMF conversion, a combined total yield of 83.8% for maleic acid and its isomer fumaric acid was achieved at selectivity of 57.6% towards maleic acid and 27.7% toward fumaric acid. 2.5-furandicarboxylic acid and 5-hydroxymethyl-2-furandicarboxylic acid were not produced and trace amounts of 5-formyl-2-furancarboxylic acid were detected, the yield of 2.5-diformylfuran was also significantly decreased to juts 2.9%. However, a slight increase in the yield of the side products to 10.7% was also observed for the Ti1Sn4 catalyst.
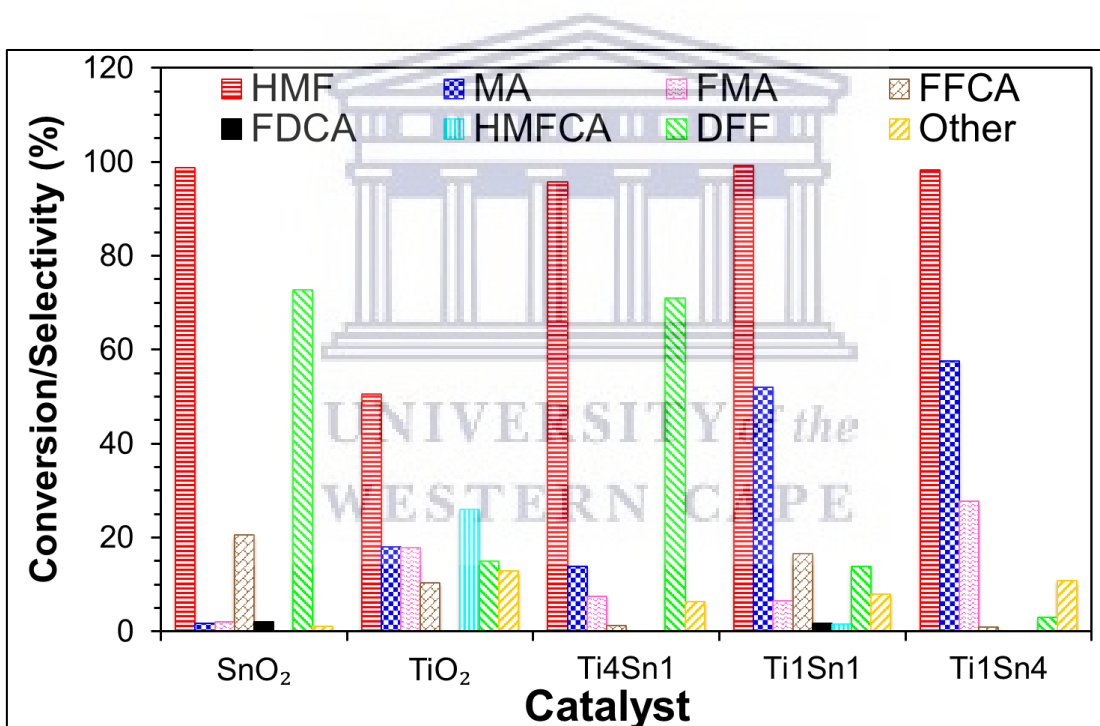
Fig. 6-19: Selectivity results for the oxidation of HMF with TiO_2-SnO_2 catalysts. Reaction conditions: 5 mmol HMF, 25 mmol 30% (aq) H_2O_2 (5 mmol of H_2O_2 was added initially at the beginning of the reaction, then added periodically at 3 h intervals four times), 5 mL H_2O and 5 mL MeCN solvent, 100 mg catalyst, T = 60 °C and t = 24 h.

The least density of surface defects observed by XPS and PL analysis for the Ti1Sn4 catalyst along with the highest surface area and pore volume proved to be beneficial for

HMF oxidation affording the best catalytic performance results, as was the case for furfural oxidation. It should be noted that a similar result was observed with the heterostructure VO_x-SnO_2 catalysts (**Chapter 4**), where the 10VSn catalyst resulted in the highest yield of maleic acid from both furfural and HMF. However, the maleic acid yield produced from HMF oxidation (56.6%) was lower compared to furfural (63.7%) under the same reaction conditions as a possible result of the isomerisation of maleic acid to fumaric acid as evidenced by the increased yield of fumaric acid (27.2%). Lou et.al.[35] reported the need of at least two additional equivalents of H_2O_2 in order to oxidize HMF to maleic acid due to the extra C–C bond present in the HMF structure that has to be broken. However, this was not case with near full conversion of HMF being achieved with SnO_2 and the heterostructure TiO_2-SnO_2 catalysts.

6.4 Concluding remarks

In conclusion, a series of heterostructure TiO_2-SnO_2 catalysts were synthesised by a simple microwave-assisted method characterized by 7-10 nm indistinguishable nanosized particles of Ti and Sn metal oxides. The heterostructure TiO_2-SnO_2 catalyst with a high surface area composing of Ti1Sn4 ratio presented a highly active catalyst for oxidation of furfural with H_2O_2 to maleic acid. The Ti1Sn4 catalyst afforded total yield of 74.1% for maleic acid and 4.4% for its isomer fumaric acid from furfural under optimal reaction conditions. Moreover, the Ti1Sn4 catalyst afforded a 56.6% yield for maleic acid and 27.2% for its isomer fumaric acid from HMF oxidation. The correlation of catalytic testing and characterization results showed the most active catalyst to possess the highest surface area and pore volume with maximized surface exposed Ti active sites. XPS analysis revealed the induced structural modifications due to various TiO_2 loadings, which in effect result in different electronic interactions of Ti and Sn thus varying catalytic

influence contributions with the most active Ti1Sn4 catalyst showing the highest amount of surface exposed Ti atoms. In particular, the presence of a high density of surface oxygen defects proved detrimental to the catalytic activity. Furthermore, the use of a co-solvent of water and acetic acid proved to enhance product selectivity, yield, and overall catalytic performance by forming a peracetic acid intermediate with stronger oxidizing strength. However, the catalyst suffered severe leaching of the Ti active site under these conditions.

6.5 References

[1] T.R. Felthouse, J.C. Burnett, B. Horrell, M.J. Mummey, Y.J. Kuo. Maleic anhydride, maleic acid, and fumaric acid. 4th ed. In: J. Kroschwitz, M. Home-Grant (Ed.), Kirk-Othmer Encyclopedia of Chemical Technology. New York, John Wiley and Sons, **2001**, Vol 19, pp. 1-58.

[2] M.L. Granados, J. Moreno, A.C. Alba-Rubio, J. Iglesias, D.M. Alonso, R. Mariscal, Catalytic transfer hydrogenation of maleic acid with stoichiometric amounts of formic acid in aqueous phase: paving the way for more sustainable succinic acid production. Green Chemistry ,2020, 22, pp. 1859-1872.

[3] M.Y. Byun, J.S. Kim, J.H. Baek, D.W. Park, M.S. Lee, Liquid-phase hydrogenation of maleic acid over Pd/Al_2O_3 catalysts prepared via deposition–precipitation method. Energies, **2019**, 12, pp. 284.

[4] D.K. Hood, O.M. Musa, Progress in maleic anhydride production. In: O.M. Musa (Ed.), Handbook of maleic anhydride based materials: Syntheses, properties and applications. Springer International Publishing, Cham, Switzerland, 2016, pp. 3-35.

[5] A.C. Alba-Rubio, J.L.G. Fierro, L. León-Reina, R. Mariscal, J.A. Dumesic, M.L. Granados, Oxidation of furfural in aqueous H_2O_2 catalysed by titanium silicalite: deactivation processes and role of extraframework Ti oxides. Applied Catalysis B: Environmental, **2017**, 202, pp. 269-280.

[6] S.K. Pillai, O. Gheevarghese, S. Sugunan, Catalytic properties of V_2O_5/SnO_2 towards vapour-phase Beckmann rearrangement of cyclohexanone oxime. Applied Catalysis A: General, **2009**, 353, pp. 130-136.

[7] P.R. Makgwane, S.S. Ray, Development of a high-performance nanostructured V_2O_5/SnO_2 catalyst for efficient benzene hydroxylation. Applied Catalysis A: General, **2015**, 492, pp. 10-22.

[8] B. Cheng, J. Jiao, W. Sun, B. Tian, Y. Xiao, S. Lei, Lattice variation and Raman spectroscopy in hierarchical heterostructures of zinc antimonate nanoislands on ZnO nanobelts. Nanotechnology, **2009**, 21, pp. 025704.

[9] T.P. Mokoena, E.C. Linganiso, V. Kumar, H.C. Swart, S.H. Cho, O.M. Ntwaeaborwa, Up-conversion luminescence in Yb^{3+}-Er^{3+}/Tm^{3+} co-doped Al_2O_3-TiO_2 nano-composites. Journal of Colloid and Interface Science, **2017**, 496, pp. 87-99.

[10] H. Cao, S. Huang, Y. Yu, Y. Yan, Y. Lv, Y. Cao, Synthesis of TiO_2-N/SnO_2 heterostructure photocatalyst and its photocatalytic mechanism. Journal of Colloid and Interface Science, **2017**, 486, pp. 176-183.

[11] X. Wang, Y. Sang, D. Wang, S. Ji, H. Liu, Enhanced gas sensing property of SnO_2 nanoparticles by constructing the SnO_2–TiO_2 nanobelt heterostructure. Journal of Alloys and Compounds, **2015**, 639, pp. 571-576

[12] L. Zhang, W. Yu, C. Han, J. Guo, Q. Zhang, H. Xie, Q. Shao, Z. Sun, Z. Guo, Large scaled synthesis of heterostructured electrospun TiO_2/SnO_2 nanofibers with an enhanced photocatalytic activity. Journal of the Electrochemical Society, **2017**, 164, pp. H651.

[13] T. Matthias, K. Katsumi, A.V. Neimark, J.P. Olivier, F. Rodriguez-Reinoso, R. Jean, K.S. Sing, Physisorption of gases, with special reference to the evaluation of surface area and pore size distribution (IUPAC Technical Report). Pure and Applied Chemistry, **2015**, 87, pp. 1051.

[14] A. Ungureanu, O. Oprea, B. Vasile, C. Andronescu, G. Voicu, I. Jitaru, Temperature effect over structure and photochemical properties of nanostructured SnO_2 powders. Central European Journal of Chemistry, 2014, 12, pp. 909-917.

[15] L. Jiang, G. Sun, Z. Zhou, S. Sun, Q. Wang, S. Yan, H. Li, J. Tian, J. Guo, B. Zhou, Q. Xin, Size-controllable synthesis of monodispersed SnO_2 nanoparticles and application in electrocatalysts. The Journal of Physical Chemistry B, **2005**, 109, pp. 8774.

[16] S. Gnanam, V. Rajendran, Synthesis of tin oxide nanoparticles by sol–gel process: effect of solvents on the optical properties. Journal of Sol-Gel Science and Technology, **2010**, 53, pp. 555-559.

[17] M.P. Palacio, P.I. Villabrille, G.P. Romanelli, P.G. Vázquez, C.V. Cáceres, Preparation, characterization and use of V_2O_5-TiO_2 mixed xerogels as catalysts for sustainable oxidation with hydrogen peroxide. Applied Catalysis A: General, **2012**, 417-418, pp. 273-280.

[18] S.J. Mofokeng, V. Kumar, R.E. Kroon, O. M. Ntwaeaborwa, Structure and optical properties of Dy^{3+} activated sol-gel ZnO-TiO_2 composites. Journal of Alloys and Compounds, **2017**, 711, pp. 121-131.

[19] A. Gaber, A.Y. Abdel-Latief, M.A. Abdel-Rahim, M.N. Abdel-Salam, Thermally induced structural changes and optical properties of tin dioxide nanoparticles synthesized by a conventional precipitation method. Materials Science in Semiconductor Processing, **2013**, 16, pp. 1784-1790.

[20] Z. Li, W. Shen, X. Zhang, L. Fang, X. Zu, Controllable growth of SnO_2 nanoparticles by citric acid assisted hydrothermal process. Colloids and Surfaces A: Physicochemical and Engineering Aspects, **2008**, 327, pp. 17-20.

[21] R.G. Motshoeneng, I. Kortidis, S.S. Ray, D.E. Motaung, Designing SnO_2 nanostructure-based sensors with tailored selectivity toward propanol and ethanol vapors. ACS Omega, **2019**, 4, pp. 13696-13709.

[22] N. Kruse, S. Chenakin, XPS characterization of Au/TiO_2 catalysts: Binding energy assessment and irradiation effects. Applied Catalysis A: General, **2011**, 391, pp. 367-376.

[23] L. Huang, F. Peng, F.S. Ohuchi, "In situ" XPS study of band structures at Cu_2O/TiO_2 heterojunctions interface. Surface Science, **2009**, 603, pp. 2825-2834.

[24] B. Erdem, R.A. Hunsicker, G.W. Simmons, E.D. Sudol, V.L. Dimonie, M.S. El-Aasser, XPS and FTIR surface characterization of TiO_2 particles used in polymer encapsulation. Langmuir, **2001**, 17, pp. 2664-2669.

[25] S. Watanabe, X. Ma, C. Song, Characterization of structural and surface properties of nanocrystalline TiO_2-CeO_2 mixed oxides by XRD, XPS, TPR, and TPD. The Journal of Physical Chemistry C, **2009**, 113, pp. 14249-14257.

[26] C. Wang, C. Shao, X. Zhang, Y. Liu, SnO_2 nanostructures-TiO_2 nanofibers heterostructures: controlled fabrication and high photocatalytic properties. Inorganic Chemistry, **2009**, 48, pp. 7261-7268.

[27] H. Sefardjella, B. Boudjema, A. Kabir, G. Schmerber, Structural and photoluminescence properties of SnO_2 obtained by thermal oxidation of evaporated Sn thin films. Current Applied Physics, **2013**, 13, pp. 1971-1974.

[28] D.E. Motaung, G.H. Mhlongo, P.R. Makgwane, B.P. Dhonge, F.R. Cummings, H.C. Swart, S.S. Ray, Ultra-high sensitive and selective H_2 gas sensor manifested by interface of n-n heterostructure of CeO_2-SnO_2 nanoparticles. Sensors and Actuators B, **2018**, 254, pp. 984-995.

[29] S. Marković, A. Stanković, J. Dostanić, L. Veselinović, L. Mančić, S.D. Škapin, G. Dražič, I. Janković-Častvan, D. Uskoković, Simultaneous enhancement of natural sunlight- and artificial UV-driven photocatalytic activity of a mechanically activated ZnO/SnO_2 composite. RSC Advances, **2017**, 7, pp. 42725-42737.

[30] Y.X. Zhang, G. H. Li, Y.X. Jin, Y. Zhang, J. Zhang, L.D. Zhang, Hydrothermal synthesis and photoluminescence of TiO_2 nanowires. Chemical Physics Letters, **2002**, 365, pp. 300-304.

[31] J. Shi, J. Chen, Z. Feng, T. Chen, Y. Lian, X. Wang, C. Li, Photoluminescence characteristics of TiO_2 and their relationship to the photoassisted reaction of water/methanol mixture. The Journal of Physical Chemistry C, **2007**, 111, pp. 693-699.

[32] Z.P. Tshabalala, D.E. Motaung, G.H. Mhlongo, O.M. Ntwaeaborwa, Facile synthesis of improved room temperature gas sensing properties of TiO_2 nanostructures: Effect of acid treatment. Sensors and Actuators B, **2016**, 224, pp. 841-856.

[33] Y. Rodenas, R. Mariscal, J.L.G. Fierro, D.M. Alonso, J.A. Dumesic, M.L. Granados, Improving the production of maleic acid from biomass: TS-1 catalysed aqueous phase oxidation of furfural in the presence of γ -valerolactone. Green Chemistry, **2018**, 20, pp. 2845-2856.

[34] U.R. Pillai, E. Sahle-Demessie, Selective oxidation of alcohols over vanadium phosphorus oxide catalyst using hydrogen peroxide. Applied Catalysis A: General, **2004**, 276, pp. 139-144.

[35] Y. Lou, S. Marinkovic, B. Estrine, W. Qiang, G. Enderlin, Oxidation of furfural and furan derivatives to maleic acid in the presence of a simple catalyst system based on acetic acid and TS-1 and hydrogen peroxide. ACS Omega, **2020**, 5, pp. 2561-2568.

CHAPTER 7

Transferance of the furfural oxidation process from flask to a batch reactor

7.1 Introduction

Process up-scaling present a very important route for transferring any chemical technology from laboratory scale to pilot/mass production scale and remains a challenge for the commercialization of many chemical processes.[1,2] The main limitations are related to issues such as catalyst activity and stability, heat and mass transfer effects which tend to be very different compared to laboratory-scale, product yield and reaction mass efficiency, formation of by-products, product separation and purification, all of which contribute to the overall process efficiency, economic feasibility and the likelihood of implementation of a process design at larger scale.[3,4] The two main approaches for process up-scaling are (1) increasing the batch reactor size and (2) transforming the reaction to a continuous process. The issues of mass and energy transfer limitations still persist when utilizing large batch reactor but are significantly eliminated in continuous flow reactors due to improved interfacial mass transfer dynamics of reactant contacts and tailored residue times.[5]

In the context of bio-based maleic acid synthesis, the current ongoing research still is almost exclusively focused on laboratory experiments. Comparatively little effort has been devoted to the design and realization of large scale or at least scalable laboratory bench top oxidation reaction prior to pilot demonstration. As a result, this chapter is aimed at developing a scalable furfural oxidation process by transferring the laboratory flask (25 mL) reaction to a bench-top stirred glass batch reactor 100 mL using the catalysts

developed in **Chapters 4 - 6.** In order to identify important parameters for catalyst activity and stability, a glass batch reactor of 100 mL working volume was utilized.

7.2 Batch furfural oxidation using TiO_2-SnO_2 catalyst

The feasibility of up-scaling the oxidation reaction was investigated using a lab-scale glass batch reactor as outlined in **section 3.4.2**. The aqueous H_2O_2 was added in three portions at 30 min intervals from the start of the reaction and the reaction products were sampled and analysed every 1 h thereafter. With the Ti1Sn4 catalyst affording in the best catalytic activity results among the all the heterostructured SnO_2-based catalysts, it was therefore employed first for the up-scaling process and the obtained results of the process with the catalyst are summarised in **Table 7-1** and **Fig. 7-1**.

Table 7-1: Catalytic conversion results for the batch oxidation of furfural with the Ti1Sn4 catalyst.

Time (h)	Conversion (%)	Yield (%)				
		MA	FMA	FA	FOA	[1] Other
1	1.8	0.2	0.1	1.5	0.0	0.0
2	6.8	0.8	0.1	5.9	0.0	0.0
3	13.6	2.0	0.3	11.0	0.0	0.3
4	27.1	5.9	0.7	19.5	0.1	0.9
5	44.0	14.5	1.1	26.6	0.4	1.4
6	62.9	33.5	1.9	24.5	0.9	2.1
7	83.8	63.4	2.3	12.9	2.3	2.9
8	93.6	76.0	2.1	6.9	4.6	4.0
9	97.6	84.8	1.8	1.2	5.3	4.5
10	99.1	87.1	1.4	0.0	6.2	4.4

[1] Side products such as 2-(5H)-furanone; succinic, malic and oxalic acids. Symbol: MA = maleic acid, FOA = formic acid, FMA = fumaric acid, FA = 2-furoic acid. Reaction conditions: 25 mmol furfural, 697 mmol 30% (aq) H_2O_2 (232 mmol of H_2O_2 oxidant was added initially at the beginning of the reaction, then added periodically at 30 min intervals two times), 5 mL H_2O and 34.4 mL MeCN solvent, 250 mg catalyst, T = 75 °C and t = 10 h.

As was the case with the small-scale flask oxidation reaction, the oxidation of furfural proceeded very slowly during the first 3 h of the reaction with conversion reaching 13.6% after 3 h. 2-Furoic acid was produced as the main product with 82.8% selectivity after 1 h which increased to 85.4% after 2 h, and thereafter started to decrease to reach 81.2% after 3 h at 11.0% yield. The selectivity towards maleic acid was also slowly increasing from 11.1% during the 1 h of reaction to 14.9% after 3 h with 2.0% yield. The side products were produced in trace amounts up to a reaction time of 5 h. Only 0.3% yield of fumaric acid was obtained after 3 h at 2.4% selectivity.
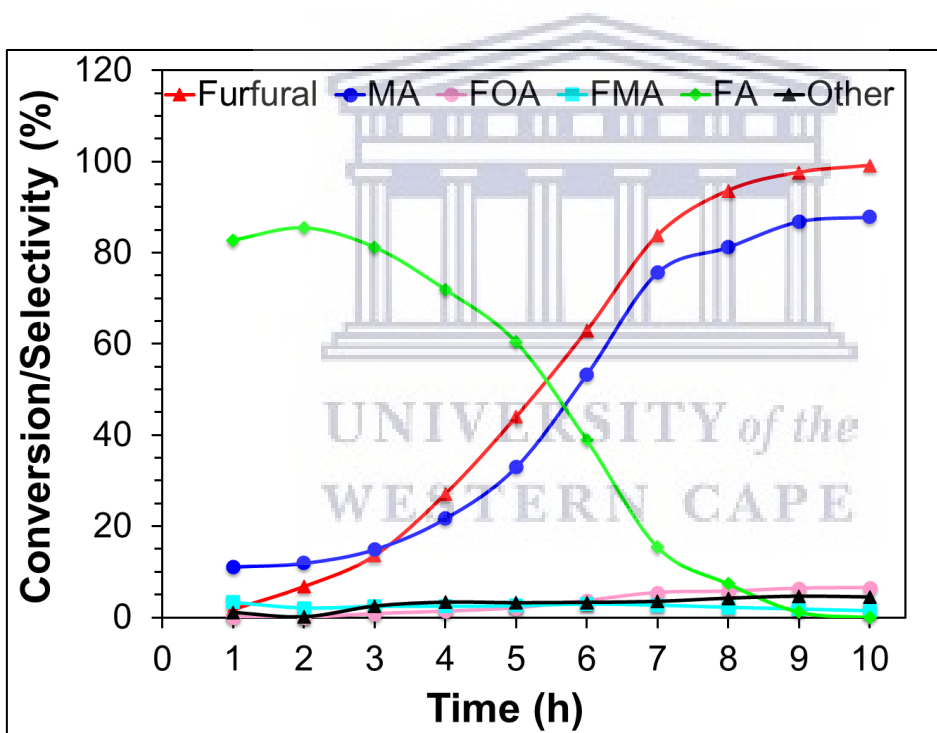
Fig. 7-1: Products selectivity for the batch oxidation of furfural with Ti1Sn4 catalyst in MeCN-H_2O solvent. Reaction conditions: 25 mmol furfural, 697 mmol 30% (aq) H_2O_2 (232 mmol of H_2O_2 oxidant was added initially at the beginning of the reaction, then added periodically at 30 min intervals two times), 5 mL H_2O and 34.4 mL MeCN solvent, 250 mg catalyst, T = 75 °C and t = 10 h.

Up to the reaction time of 7 h, furfural conversion increased sharply to reach 83.8% and the yield of maleic acid also increased rapidly to reach 63.4% at 75.6% selectivity after 7

h. During that period, the yield of 2-furoic acid intermediate continued to increase reaching a maximum of 26.6% after 5 h and thereafter began to decrease reaching 12.9% after 7 h. The yield of fumaric acid reached 1.9% after 7 h. With furfural conversion continuing to increase reaching 99.1% when the reaction was stopped after 10 h, the yield of maleic acid also continued to increase to a maximum of 87.1% at 87.9% selectivity. The yield of 2-furoic acid continued to decrease with the progression of the reaction until there was none detected at the end of the reaction. Only 1.4% of fumaric acid was produced at the end of the reaction and the yield of the side products was at 4.5%. The main by-product produced was formic acid with a yield of 6.2% after 10 h.

Table 7-2: Catalytic conversion results for the batch oxidation of furfural with the CuO_x-SnO_2 catalyst.

Time (h)	Conversion (%)	Yield (%)					
		MA	FMA	FA	FOA	OA	[1] Other
0.5	47.4	2.5	0.3	26.4	0.2	0.3	17.7
1	78.3	23.8	3.7	38.7	5.1	2.1	4.9
2	97.4	22.6	6.6	3.4	17.0	8.7	39.1
3	99.5	11.5	3.7	1.0	10.6	4.8	67.9
4	99.6	7.0	2.1	0.7	6.4	3.1	80.3

[1] Side products such as 2-(5H)-furanone; succinic and malic acids. Symbol: MA = maleic acid, FOA = formic acid, FMA = fumaric acid, FA = 2-furoic acid, OA = oxalic acid. Reaction conditions: 25 mmol furfural, 697 mmol 30% (aq) H_2O_2 (232 mmol of H_2O_2 oxidant was added initially at the beginning of the reaction, then added periodically at 30 min intervals two times), 5 mL H_2O and 34.4 mL MeCN solvent, 250 mg catalyst, T = 75 °C and t = 4 h.

7.3 Batch furfural oxidation using CuO_x-SnO_2 catalyst

The batch furfural oxidation process was also investigated with the CuO_x-SnO_2 catalyst developed in **Chapter 5** under the reaction conditions described above but for 4 h reaction time instead of 10 h. After 30 min of reaction time, a remarkable 47.4% furfural conversion was achieved with the CuO_x-SnO_2 catalyst. However, during that time the yield of maleic acid was just 2.5% at 5.3% selectivity with 2-furioc acid produced as the main product at a

yield of 26.4% and 55.6% selectivity. The yield of the side products was 17.7% after 30 min with the main side product detected being the intermediate 2-(5H)-furanone at 14.7% yield. 2-(5H)-furanone was later converted to maleic and fumaric acids as evidenced by the decrease in its yield to 2.7% and the increase in the yields of the two isomers after 1 h of reaction to 23.8% (maleic acid) and 3.7% (fumaric acid). The yield of 2-furoic acid also increased after 1 h to 38.7% at 49.4% selectivity. An increase in the yields of oxalic acid and formic acid to 2.1% and 5.1%, respectively, was also observed after 1 h while the conversion of furfural was 78.3%.
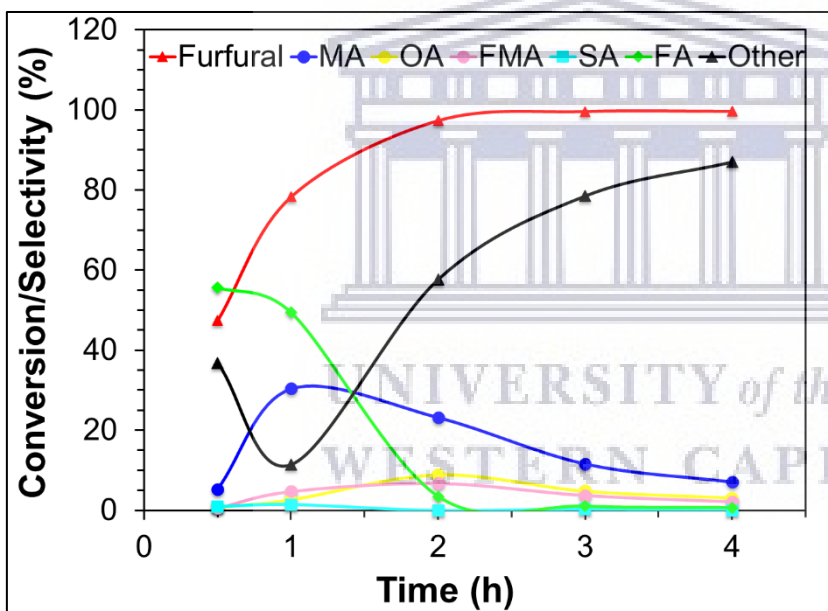
Fig. 7-2: Products selectivity for the batch oxidation of furfural with CuO_x-SnO_2 catalyst in MeCN-H_2O solvent. Reaction conditions: 25 mmol furfural, 697 mmol 30% (aq) H_2O_2 (232 mmol of H_2O_2 oxidant was added initially at the beginning of the reaction, then added periodically at 30 min intervals two times), 5 mL H_2O and 34.4 mL MeCN solvent, 250 mg catalyst, T = 75 °C and t = 4 h.

The conversion of furfural continued to increase after 2 h to reach 97.4% while the yield of maleic acid decreased to 22.6% at 23.2% selectivity. The decrease in maleic acid yield was a result of over-oxidation to oxalic acid and formic acid the yield for which increased

to 8.7% and 17.0%, respectively, after 2 h. The yield of 2-furoic acid also decreased drastically to just 3.4% after 2 h due to oxidation to side products as evidenced by the large increase in yield of the side products from 8.9% to 56.1% at 57.7% selectivity. The yield of fumaric increased to 6.6% with selectivity at 6.8%. The conversion of furfural increased slightly after 3 h to 99.5% and remained unchanged at the end of the reaction (99.6%). The yield of maleic acid continued to decrease after 2 h to reach 11.5% at 3 h and 7.0% at 4 h. The yield of fumaric acid also began to decrease after 3 h to 3.7% and to 2.1% at the end of the reaction while the yield of 2-furoic acid also decreased further to just 0.7% after 4 h. The respective yields of oxalic acid and formic acid also began decreasing to 4.8% and 10.6% after 3 h and further to 3.1% and 6.4% after 4 h. The decrease in yield of these acids was a result of deep-oxidation of the products with H_2O_2 to CO_2 and H_2O with CO_2 not detectable by HPLC. However, there were other unidentified side products produced as well with the combined yield of the side products reaching 67.9% after 3 h and 80.3% after 4 h. It is worth noting the extent of deep-oxidation of the products becomes more severe after 1 h of reaction when all the reacting H_2O_2 has been added to reaction mixture. The deep-oxidation of products was investigated in **Chapter 5**.

7.4 Batch furfural oxidation using VO$_x$-SnO$_2$ catalyst

The VO$_x$-SnO$_2$ (VSn-2) catalyst developed in **Chapter 4** was also employed for the batch furfural oxidation process and investigated under the same reaction conditions as above. After 30 min of reaction time, the conversion of furfural was at 13.4% while the respective yields of maleic acid and fumaric acid were 2.7% and 0.6% respectively. The reaction intermediate, 2-furoic acid, was once again produced as the main product at this time with a yield of 8.7% and 65.1% selectivity. The yield of the side products was 1.2%. Furfural conversion increased after 1 h of reaction to reach 55.0% and the yield of maleic acid

produced amounted to 32.2%. The yields of fumaric acid and 2-furoic acid also increased to 6.0% and 9.8%, respectively. The respective yield of formic acid and the side products also increased to 3.4% and 5.1%. After 2 h, the conversion of furfural reached 98.2% with the yield of 2-furoic acid decreasing to just 0.2%. At the same time, maleic acid yield increased to 73.3% at 74.6% selectivity and that of fumaric acid increased to 10.5%. The yields of formic acid and the side products also increased to 7.7% and 6.5%, respectively.

Table 7-3: Catalytic conversion results for the batch oxidation of furfural with the VSn-2 catalyst.						
Time	Conversion	Yield (%)				
(h)	(%)	MA	FMA	FA	FOA	[1] Other
0.5	13.4	2.7	0.6	8.7	0.2	1.3
1	55.0	32.2	6.0	9.8	3.4	3.6
2	98.2	73.3	10.5	0.2	7.7	6.5
3	99.3	71.3	9.7	0.0	8.9	9.4
4	99.3	66.4	9.3	0.0	9.1	14.5

[1] Side products such as 2-(5H)-furanone; succinic, malic and oxalic acids. Symbol: MA = maleic acid, FOA = formic acid, FMA = fumaric acid, FA = 2-furoic acid. Reaction conditions: 25 mmol furfural, 697 mmol 30% (aq) H_2O_2 (232 mmol of H_2O_2 oxidant was added initially at the beginning of the reaction, then added periodically at 30 min intervals two times), 5 mL H_2O and 34.4 mL MeCN solvent, 250 mg catalyst, T = 75 °C and t = 4 h.

The yield of maleic acid began to decrease after 3 h to 71.3% and continued to decrease to 66.4% after 4 h, along with that of fumaric acid which decreased slightly to 9.7% at 3 h and further to 9.3% at the end of the reaction. The furfural conversion increased to 99.2% and remained relatively unchanged at the end of the reaction while 2-furioc acid was not detected for the remainder of the reaction. The continued decrease in the yields of maleic acid and fumaric acid as a result of over-oxidation was accompanied by an increase in the yields of the side products to 9.3% after 3 h and to 14.5% after 4 h. The yield of formic acid also increased to 8.9% after 3 h and to 9.1% after 4 h due to deep-oxidation of the products. The main side product generated was formic acid which was not the main side product with the CuO_x-SnO_2 catalyst.
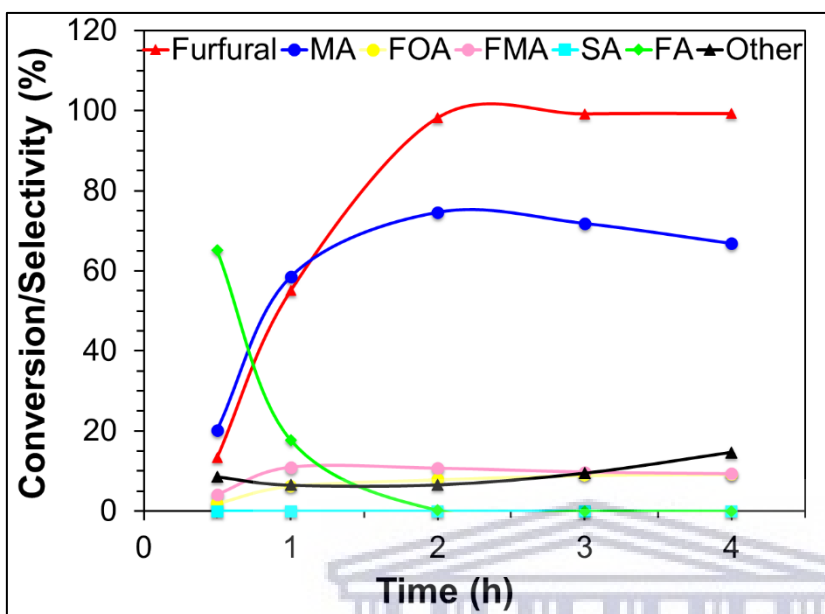
**Fig. 7-3**: Products selectivity for the batch oxidation of furfural with VSn-2 catalyst in MeCN-H$_2$O solvent. Reaction conditions: 25 mmol furfural, 697 mmol 30% $_{(aq)}$ H$_2$O$_2$ (232 mmol of H$_2$O$_2$ oxidant was added initially at the beginning of the reaction, then added periodically at 30 min intervals two times), 5 mL H$_2$O and 34.4 mL MeCN solvent, 250 mg catalyst, T = 75 °C and t = 4 h.

7.5 Effect of H$_2$O$_2$ addition method

In an attempt to further improve the catalytic results, the effect of H$_2$O$_2$ addition method on the up-scaled furfural oxidation was studied with the Ti1Sn4 catalyst. The two methods investigated were; (1) periodic addition of H$_2$O$_2$ and (2) all the H$_2$O$_2$ was added at the start of the reaction. The catalytic results for the reaction conducted with H$_2$O$_2$ added periodically every 1 h are presented in **Table 7-5** and **Fig. 7-4b**. For comparison, the results of the oxidation reaction conducted with all the H$_2$O$_2$ oxidant added at the start of the reaction are shown **Table** in **7-4** and **Fig. 7-4a**. The results from both experiments showed that 2-furoic acid was the main product produced during the early stages of the reaction (1 – 4 h) with selectivity decreasing from 90% to 55% during that time. Thus,

indicating the same reaction path was followed regardless of the method of H_2O_2 addition applied.

Table 7-4: Catalytic conversion results for the batch oxidation of furfural with the Ti1Sn4 catalyst with aqueous H_2O_2 all added at the start of the reaction.

Time (h)	Conversion (%)	Yield (%)				
		MA	FMA	FA	FOA	[1] Other
1	4.8	0.5	0.2	3.8	0.0	0.3
2	14.1	1.7	0.4	11.7	0.0	0.3
3	26.9	4.7	0.5	21.1	0.3	0.3
4	46.9	14.3	1.0	29.7	1.0	0.9
5	63.9	37.6	1.3	21.8	1.2	2.0
6	93.0	75.2	2.9	6.8	4.7	3.4
7	98.5	87.7	2.0	0.7	5.2	2.9
8	100	90.2	1.4	0.4	5.1	2.9

[1] Side products such as 2-(5H)-furanone; succinic, malic and oxalic acids. Symbol: MA = maleic acid, FOA = formic acid, FMA = fumaric acid, FA = 2-furoic acid. Reaction conditions: 25 mmol furfural, 697 mmol 30% (aq) H_2O_2, 5 mL H_2O and 34.4 mL MeCN solvent, 250 mg catalyst, T = 75 °C and t = 8 h.

Table 7-5: Catalytic conversion results for the batch oxidation of furfural with the Ti1Sn4 catalyst with aqueous H_2O_2 added every 1 h.

Time (h)	Conversion (%)	Yield (%)				
		MA	FMA	FA	FOA	[1] Other
1	1.8	0.1	0.1	1.6	0.0	0.0
2	7.9	0.8	0.2	6.7	0.0	0.2
3	46.3	8.2	0.8	35.9	0.5	0.9
4	89.6	34.9	1.9	49.6	2.0	1.2
5	98.9	84.5	2.1	7.7	4.5	0.1
6	99.9	91.4	1.2	0.2	4.8	2.3
7	99.9	93.2	0.0	0.0	3.9	2.8
8	100	93.1	0.0	0.0	4.5	2.4

Reaction conditions: 25 mmol furfural, 697 mmol 30% (aq) H_2O_2 (232 mmol of H_2O_2 oxidant was added initially at the beginning of the reaction, then added periodically at 1 h intervals two times), 5 mL H_2O and 34.4 mL MeCN solvent, 250 mg catalyst, T = 75 °C and t = 8 h.

The reaction carried out with H_2O_2 added periodically every 1 h provided better catalytic results in that it took only 5 h to obtain a maleic acid yield of 84.5% at 84.5% selectivity

with furfural conversion of 99%. At the same time, the reaction performed with all the H_2O_2 oxidant added at the start of the reaction produced 37.6% yield of maleic acid with furfural conversion of 63.9%. It required 7 h to achieve the same furfural conversion (99%) when all the H_2O_2 oxidant was added at the start of the reaction, and the yield and selectivity toward maleic acid were 87.7% and 88.9%, respectively, after 7 h. The yield of side products was also slightly lower when H_2O_2 oxidant was added periodically with a maximum of 2.8% after 7 h compared to 3.4% after 6 h when all H_2O_2 was added at the start of the reaction. In both experiments, formic acid was the major by-product with respective yields of 4.5% and 5.1% after 8 h.

The maximum yield of fumaric acid obtained when all the H_2O_2 oxidant was added at the start of the reaction was 2.9% after 6 h compared 2.1% after 5 h when H_2O_2 was added periodically. The yield of this product decreased to 1.4% for when all H_2O_2 was added at the beginning and decreased to 0% when H_2O_2 was added periodically possibly due to isomerization to maleic acid which experienced an increase in yield to 93.2% after 7 h (**Table 7-5**) when the 2-furoic acid intermediate was no longer produced and was all consumed. In terms of conversion, the reaction performed with H_2O_2 added periodically achieved total consumption of the furfural substrate in 6 h whereas it took 8 h to achieve the same result when H_2O_2 was added at the beginning. The maximum yield of maleic acid produced was also higher (93.2% after 7 h) when H_2O_2 was added periodically compared to when H_2O_2 was added at the start of the reaction (90.2% after 8 h).
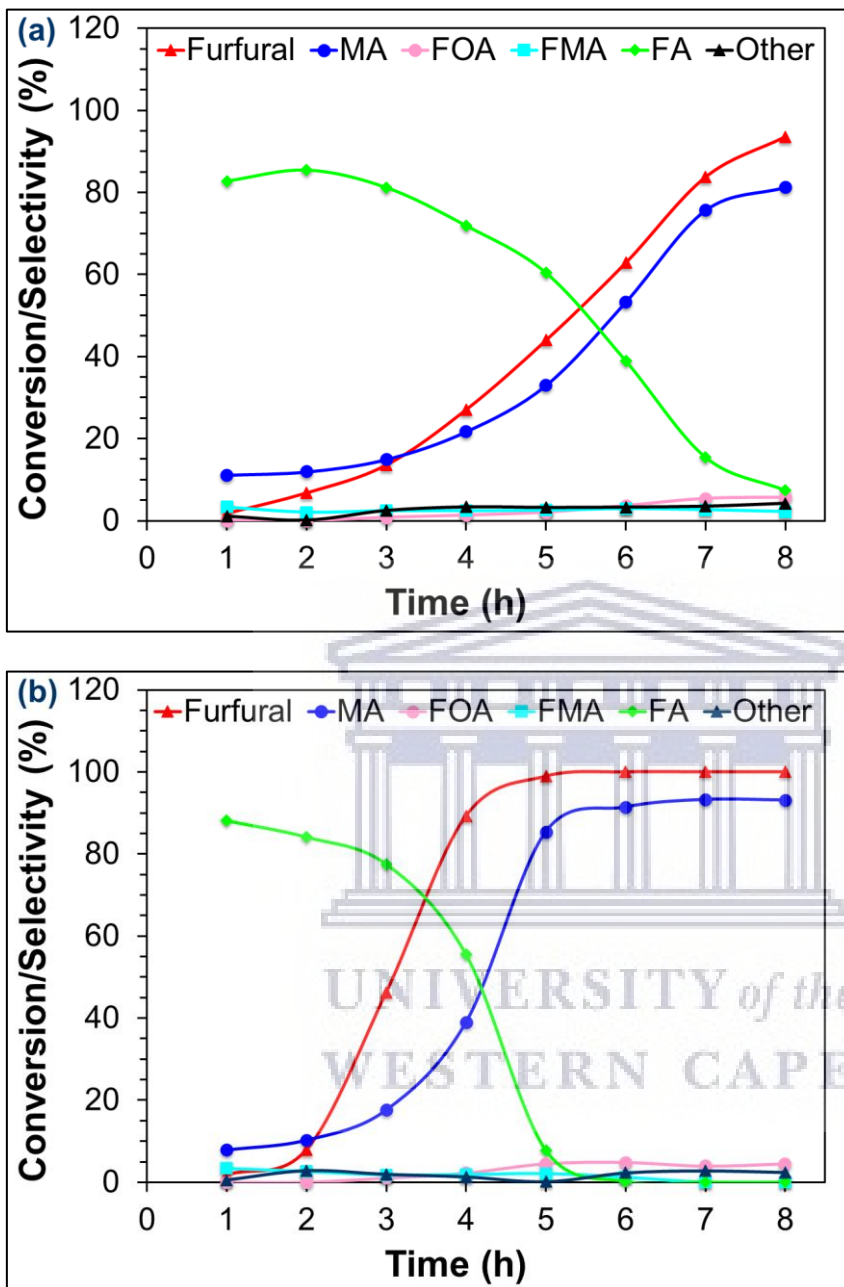
Fig. 7-4: Products selectivity with time for the batch oxidation of furfural with TiO_2-SnO_2 catalyst in MeCN-H_2O solvent. Reaction conditions: 25 mmol furfural, 697 mmol 30% (aq) H_2O_2, 5 mL H_2O and 34.4 mL MeCN solvent, 250 mg catalyst, T = 75 °C and t = 8 h. (a) Results obtained with all the H_2O_2 added at the start of the reaction, and (b) 232 mmol of H_2O_2 oxidant was added initially at the beginning of the reaction, then added periodically at 1 h intervals two times.

A graphic comparison of the three H_2O_2 addition methods is presented in **Fig. 7-5**. In terms of conversion, the periodical addition of H_2O_2 every 1 h showed to be more efficient

with full conversion of furfural achieved in 6 h and compared to 8 h when all the H_2O_2 was added at the start of the reaction and to the 10 h required to achieve the same result when H_2O_2 was added every 30 min (**Fig. 7-5a)**. Selectivity towards maleic acid was higher when H_2O_2 was added every 1 h reaching 85.4% in 5 h compared to 33.0% (H_2O_2 was added every 30 min) and 58.8% (all H_2O_2 added at the start of the reaction) achieved at the same reaction time under the other two methods. The highest selectivity of 93.3% was obtained after 7 h when H_2O_2 was added every 1 h while the highest obtained when H_2O_2 was added every 30 min was 87.9% after 10 h and 90.2% after 8 h when all the H_2O_2 was added at the start of the reaction (**Fig. 7-5b**).
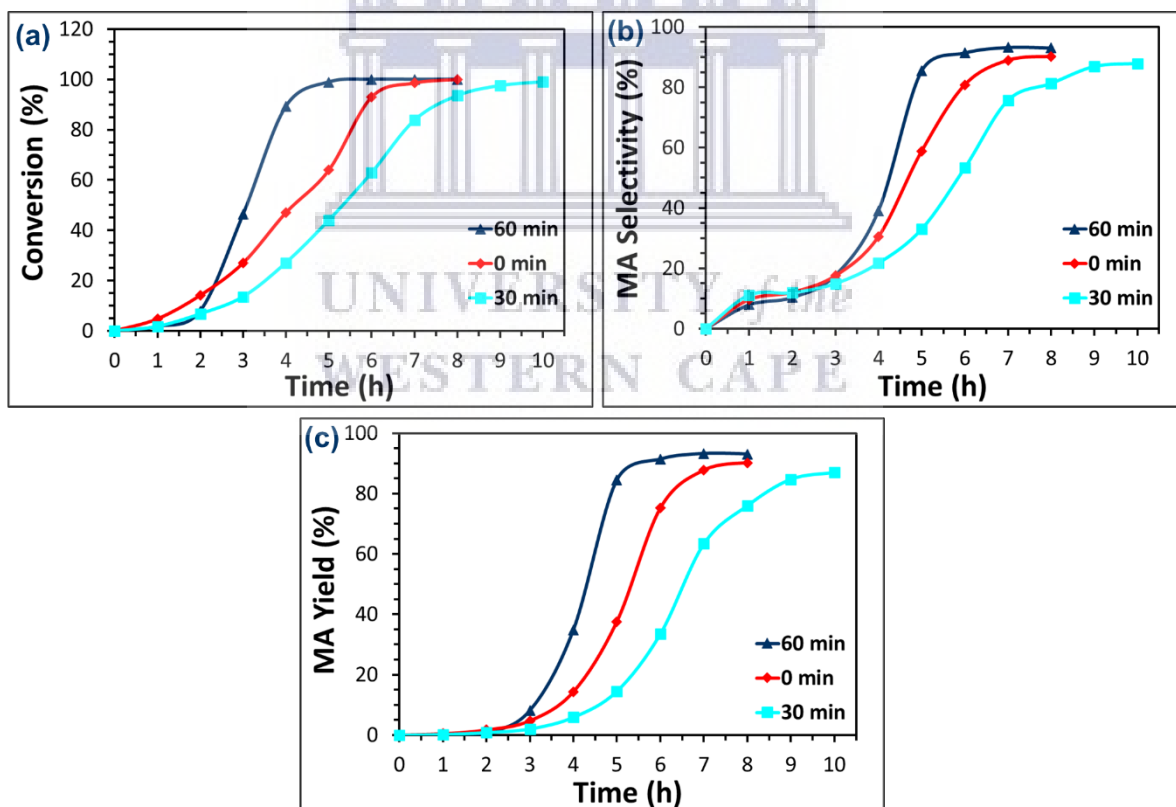
Fig. 7-5: Catalytic (a) conversion, (b) maleic acid selectivity and (c) yield results obtained under different H_2O_2 addition procedures for the batch oxidation of furfural with the TiO_2-SnO_2 catalyst.

Similarly, the yield of maleic acid was higher when H_2O_2 was added every 1 h reaching 85.4% in 5 h compared to respective yields of 37.6% and 14.5% achieved at the same reaction time when all the H_2O_2 was added at the start of the reaction and when added every 30 min (**Fig. 7-5c**). The yield of maleic acid produced was also highest under the periodical addition of H_2O_2 every 1 h reaching a maximum of 93.1% after 8 h. Maleic acid yields of 90.2% and 87.1% were achieved after 8 h and 10 h when all the H_2O_2 was added at the start of the reaction and when added every 30 min, respectively. The different results obtained under the three H_2O_2 addition methods can be explained in terms of the rate of decomposition of H_2O_2. H_2O_2 decomposes in the presence of supported metal oxides generating hydroxyl (OH·) and ·HO_2 radicals, hydroxyl (OH^-) and superoxide (O_2^-) anions in the process (**Equations 1-6**).[6,7]

$$M + H_2O_2 \rightarrow M^+ + OH^- + OH^· \tag{1}$$

$$H_2O_2 + OH^· \rightarrow H_2O + ·HO_2 \tag{2}$$

$$·HO_2 \rightleftarrows O_2^- + H^+ \tag{3}$$

$$O_2^- + M^+ \rightarrow O_2 + M \tag{4}$$

$$O_2^- + H_2O_2 \rightarrow O_2 + OH^- + OH^· \tag{5}$$

$$OH^· + H_2O_2 \rightarrow H_2O + H^+ + O_2^- \tag{6}$$

The rate with which H_2O_2 decomposes appears dependent on the method of H_2O_2 addition as evidenced by the rate of conversion of furfural (**Fig. 7-5a**). The slow addition of H_2O_2 in 1 h intervals leads to a controlled decomposition of H_2O_2 to produce OH· radicals, which are strong oxidants involved in the oxidation reaction, resulting in improved reaction rates and better maleic acid selectivity. The slightly more rapid addition of H_2O_2 in 30 min

intervals leads to the reaction of the added H_2O_2 with the generated superoxide anion and $OH^.$ radicals forming oxygen and water (**Equations 5** and **6**), respectively, and results in a slightly slower reaction rate and maleic acid selectivity with the furfural substrate now oxidized by the generated oxygen instead of the $OH^.$ radicals.

7.6 Concluding remarks

In summary, the development of a scalable maleic acid synthesis process by furfural oxidation with a bench top stirred glass batch reactor was successfully demonstrated with heterostructured SnO_2 catalysts. Improved maleic acid yields to those obtained with the laboratory flask reaction were realised with the VSn-2 and Ti1Sn4 catalysts. A maleic acid yield of 73.3% was obtained in 2 h with the VSn-2 catalyst compared to a 60 % maleic acid yield achieved in 20 h for the laboratory flask reaction. Similarly, for the Ti1Sn4 catalyst, a yield of 93.2% for maleic acid was obtained in 7 h compared to a 74.1 % maleic acid yield achieved in 6 h for the laboratory flask reaction. The issue of over-oxidation of the products was intensified when the CuO_x-SnO_2 catalyst was employed with a yield of 86.7% for side products obtained. Furthermore, the method of aqueous H_2O_2 addition showed to affect the furfural oxidation rate and yield of maleic acid. The maximum yield of maleic acid produced was higher (93.2% after 7 h) when H_2O_2 was added periodically every 1 h compared to when H_2O_2 was added periodically every 30 min (87.3% after 10 h) and when H_2O_2 was added at the start of the reaction (90.2% after 8 h).

7.7 References

[1] V. Inglezakis, S. Poulopoulos, Adsorption, ion exchange and catalysis. Elsevier, Amsterdam, **2006**.

[2] E. Cooreman, T. Vangeel, K. Van Aelst, J. Van Aelst, J. Lauwaert, J.W. Thybaut, S. Van den Bosch, B.F. Sels, Perspective on overcoming scale-up hurdles for the reductive catalytic fractionation of lignocellulose biomass. Industrial & Engineering Chemistry Research, **2020**, 59, pp. 17035-17045.

[3] S.T. Kolaczkowski, S. Serbetcioglu, Development of combustion catalysts for monolith reactors: a consideration of transport limitations. Applied Catalysis A: General, **1996**, 138, pp. 199-214.

[4] D.D. Vanhove, Catalyst testing at a lab scale in mild oxidation: Can you control the reaction temperature?. Applied Catalysis A: General, **1996**, 138, pp. 215-234.

[5] S. Lomel, L. Falk, J.M. Commenge, J.L. Houzelot, K. Ramdani, The microreactor: a systematic and efficient tool for the transition from batch to continuous process?. Chemical Engineering Research and Design, **2006**, 84, pp. 363-369.

[6] N. Kitajima, S. Fukuzumi, Y. Ono, Formation of superoxide ion during the decomposition of hydrogen peroxide on supported metal oxides, The Journal of Physical Chemistry, **1978**, 82, pp. 1505-1509.

[7] B.R. Petigara, N.V. Blough, A.C. Mignerey, Mechanisms of hydrogen peroxide decomposition in soils. Environmental Science & Technology, **2002**, 36, pp.639-645.

CHAPTER 8

Process Intensification for Maleic Acid Synthesis: Batch and Microwave

8.1 Introduction

The development of new resources for the chemical industry often leads to the need for new and/or improved technology processes which are cleaner, safer and more efficient. Process intensification is a viable and attractive approach that enables the establishment of these economical processes.[1] Process intensification is referred to as an ensemble of creative innovations applied in process and equipment design for the development of smaller, cleaner and more energy efficient process technologies.[1,2] The innovation is achieved by following the main principles of process intensification as described by van Gerven and Stankiwiez[3], which are as follows: (**i**) maximise the effectiveness of intra- and inter-molecular events, (**ii**) give each molecule the same processing experience, (**iii**) optimize the driving forces and associated surface areas, and (**iv**) maximise synergistic effects between processes. There are two main approached to process intensification that enable the realisation of these principles, namely through process intensification equipment and process intensification methods.[4,5] Among the process intensification methods, the use of alternative energy sources such as microwave, solar, electric and magnetic centrifugal fields is highly important.

The use of microwave irradiation to accelerate chemicals reactions has been known for many years. However, it wasn't until during the first decade of the 21st century that its application on biomass processing was recognised.[6] Some examples of the use of microwave irradiation for accelerated biomass valorisation processes include synthesis of furfural and 5-hydroxymethylfurfural from untreated biomass[7,8], furfural synthesis from

xylose/xylan[9,10], and 5-hydroxymethylfurfural synthesis from fructose[11,12]. The microwave-assisted oxidation of 5-hydroxymethylfurfural to produce 5-formyl-2-furancarboxylic acid[13], 2,5-furandicarboxylic acid[13,14] and 5-hydroxymethyl-furancarboxylic acid[15] has been recently studied. However, there are currently no literature reports on the microwave-assisted oxidation of furfural.

Process intensification through the use of microwave irradiation in chemical reactions is made possible by the efficiency of microwaves as an energy source. The microwave heating process is made efficient due to microwaves acting directly on materials in comparison to the conventional heating method which relies on conduction and convection. The direct interaction of molecules with the microwave electromagnetic field leads to rapid and volumetric heating with most solvents reaching and bypassing their boiling point within seconds.[16,17] In addition, microwave irradiation can lead to superheating of the solid catalyst by selective heating and the generation of localized hot-spots thus resulting in drastically increased reaction rates.[18] In this context, the work conducted in this chapter was aimed at intensifying the maleic acid synthesis process by conducting and optimizing the furfural oxidation reaction under microwave irradiation with the Ti1Sn4 catalyt.

8.2 Optimization of process conversion and products distribution

8.2.1 Effect of reaction solvents

The choice of solvent is a critical component to consider for a chemical synthesis process as the solvent can influence the catalyst activity in terms of substrate conversion, products distribution, and yields. The solvent becomes even more imperative for microwave-assisted reactions as the nature and dielectric properties of the solvent determine the

efficiency with which microwave energy is converted to thermal energy.[17] The furfural oxidation under microwave irradiation was performed as outlined in **Sub-section 3.4.3** and thus the first reaction parameter to be investigated was the effect of different solvents on furfural oxidation rates and products distribution. In total, nine solvents were used for the furfural oxidation process and the results obtained are shown in **Fig. 8-1** and **Table 8-1.** The reaction carried out in deionized water and acetic acid as polar protic solvents showed to be the most efficient in terms of maleic acid yield, affording respective yields of 5.9% and 8.1%. The selectivity towards maleic acid was highest with deionized water and acetic acid solvents at 49.1% and 56.0%, respectively. The conversion of furfural was 12.0% conversion in water and 14.5% in acetic acid. Another polar protic solvent, methanol proved to be less efficient producing trace amounts of maleic acid at furfural conversion of 4.8%. 2-Furoic acid was the main product in methanol with a yield of 4.2% at 87.4% selectivity.

Table 8-1: Effect of different solvents on furfural oxidation rates with the Ti1Sn4 catalyst.

Solvent	Conversion (%)	Yield (%)				
		MA	FMA	FA	FOA	[1] Other
DI H2O	12.0	5.9	2.1	1.8	1.9	0.3
Acetonitrile	2.6	0.3	0.1	2.1	0.0	0.1
Acetic acid	14.5	8.1	0.4	4.2	0.4	1.4
Methanol	4.8	0.2	0.4	4.2	0.0	0.0
1,4-Dioxane	4.5	0.1	0.1	4.2	0.0	0.0
DMF	3.6	0.2	0.0	3.4	0.0	0.0
Toluene	1.8	0.0	1.8	0	0.0	0.0
DMSO	2.1	0.0	0.0	1.8	0.0	0.3
THF	16.1	0.8	0.1	15.1	0.0	0.1

[1] Side products such as 2-(5H)-furanone; succinic, malic and oxalic acids. Symbol: MA = maleic acid, FOA = formic acid, FMA = fumaric acid, FA = 2-furoic acid. Reaction conditions: 3 mmol furfural, 15 mmol 30% (aq) H_2O_2 (H_2O_2/furfural = 5), 60 mg catalyst, 15 mL solvent, T = 100 °C and t = 20 min.

The polar aprotic solvents (DMF, 1,4-dioxane, THF, DMSO and acetonitrile) also proved to be inefficient for maleic acid synthesis. Maleic acid was produced in trace amounts and the conversion achieved in these solvents was 2.1 – 4.5% while the highest furfural conversion of 16.1% was achieved with THF solvent. However, THF appeared to favour the formation of the 2-furoic acid intermediate with a yield of 15.1% at 94.0% selectivity. In fact, all the other polar aprotic solvents showed high selectivity towards 2-furoic acid (82.3 – 94.4%) with yields in the range 1.8 – 4.2%. The non-polar toluene showed the least efficiency affording a very low conversion of 1.8% for while producing fumaric acid as the sole product with a 1.8% yield.
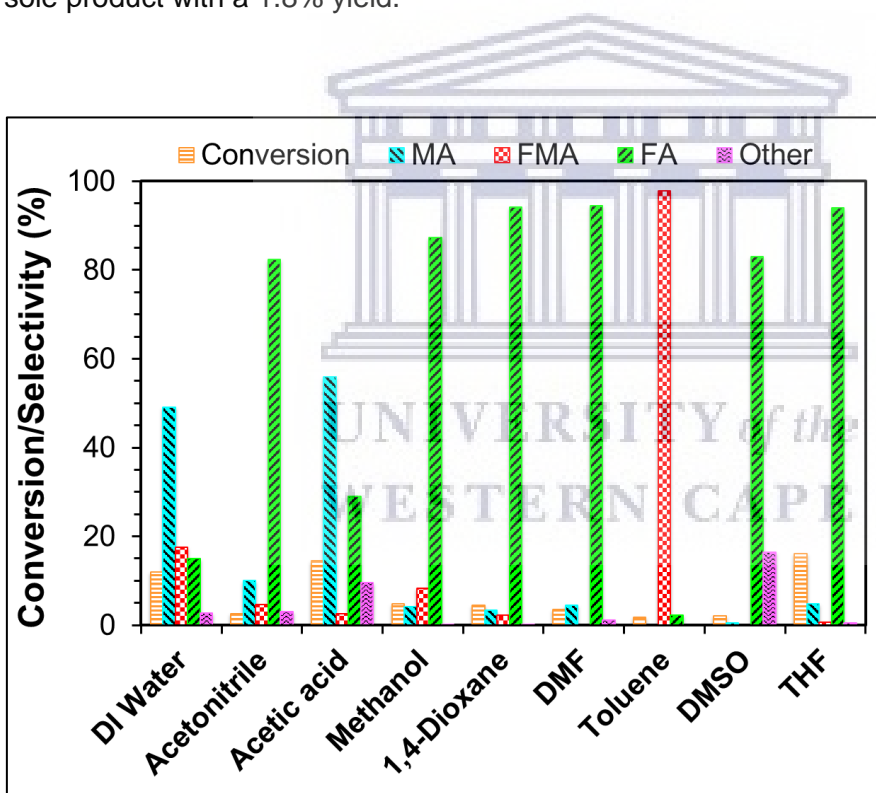
Fig. 8-1: Products selectivity for the microwave-assisted batch oxidation of furfural with Ti1Sn4 catalyst in different solvents. Reaction conditions: 3 mmol furfural, 15 mmol 30% (aq) H_2O_2 (H_2O_2/furfural = 5), 60 mg catalyst, 15 mL solvent, T = 100 °C and t = 20 min.

The efficiency of a solvent in microwave-assisted reactions is determined by its loss tangent (tangent delta, tan δ), which is a measure of the solvent's ability to convert

electromagnetic energy into heat.[17] Another dielectric parameter used to determine the effectiveness of a solvent is the dielectric loss (ε''), which indicates the rate at which the solvent will reach its desired temperature. Thus, a high ε'' number represents a quickly-heating solvent in a microwave reactor and vice versa. The solvents employed herein and their respective tan δ and ε'' numbers are presented in **Table 8-2** and colour-coded as high microwave absorbers (green), medium absorbers (yellow) and low absorbers (purple). In this context, DMSO and methanol which are high microwave absorbers afforded poor catalytic results with low conversion (2.1% and 4.8%, respectively) and produced 2-furoic acid as the major product. The low microwave absorbers (THF, 1,4-dioxane and toluene) also resulted in poor catalytic results with 2-furoic acid as the major product once again even though THF afforded the best furfural conversion (16.1%). Two of the medium microwave absorbers, DMF and acetonitrile, also resulted in 2-furoic acid as the major product with low furfural conversions. The best catalytic results were obtained with the other two medium microwave absorbers, deionised water and acetic acid, producing maleic acid at 49.1% and 56.0% selectivity, respectively. Thus, for the subsequent optimization reactions a co-solvent of deionised water and acetic acid was employed.

Table 8-2: Dielectric properties of different solvents employed in furfural oxidation.

Solvent	SnO_2	TiO_2
DMSO	0.825	37.125
Methanol	0.659	21.483
Water	0.123	9.889
DMF	0.161	6.070
Acetonitrile	0.062	2.325
Acetic acid	0.174	1.079
THF	0.047	0.348
1,4-Dioxane	0.05	0.112
Toluene	0.04	0.096

8.2.2 Effect of reaction temperature

The next reaction parameter to be investigated was the effect of different temperatures on products distribution and furfural oxidation rates. Three different temperatures were investigated and the results displayed in **Fig. 8-2** and **Table 8-3** indicate the negative effect of employing high temperatures for the oxidation reaction. The reaction performed at 100 °C resulted in a furfural conversion of 25.1% and maleic acid was produced with 13.2% yield at 52.7% selectivity. The catalytic results obtained in the deionised water and acetic acid co-solvent are better than those achieved when employing deionised water and acetic acid as individual solvents (**Table 8-1**). Fumaric acid and formic acid were produced with respective yields of 2.0% and 4.8%, and the yield of the side products was 1.7%. The 2-furoic acid intermediate was produced with 3.3% yield and 13.3% selectivity. Increasing the reaction temperature from 100 °C to 120 °C resulted in an improved of furfural conversion from 25.1% to 30.7% with just a 0.6% increase in maleic acid yield to 13.8% and 2.6% increase in fumaric acid yield to 4.6%.

Table 8-3: Temperature effect on furfural oxidation rates with the Ti1Sn4 catalyst.

Temperature (°C)	Conversion (%)	Yield (%)				
		MA	FMA	FA	FOA	Other
100	25.1	13.2	2.0	3.3	4.8	1.7
120	30.7	13.8	4.6	3.5	7.2	1.6
140	42.4	17.5	8.7	4.9	9.9	1.0

Reaction conditions: 3 mmol furfural, 15 mmol 30% $_{(aq)}$ H_2O_2 (H_2O_2/furfural = 5), 15 mL AcOH and DI H_2O (1:1), 60 mg catalyst and t = 20 min.

Selectivity towards maleic acid decreased to 45.0% and selectivity towards fumaric acid also decreased from 19.1% to 15.0% when the temperature was increased from 100 °C to 120 °C. 2-Furoic acid was produced with 3.5% yield and 11.5% selectivity. An increase in the yield of formic acid was observed with in an increase in temperature to 7.2% with

selectivity also increasing from 19.1% to 23.4%. Increasing the temperature further to 140 °C led to increases in both the furfural conversion and maleic acid yield to 42.4% and 17.5%, respectively. The yield of fumaric acid also increased to 8.7%. The selectivity towards maleic acid decreased further to 41.3% despite the increase in yield while selectivity to fumaric acid increased to 20.6%. An increase in yield of 2-furoic acid to 4.9% was also observed with selectivity at 11.6%. The increase in temperature to 140 °C resulted in a further increase in yield of formic acid to 9.9% at 23.5% selectivity.
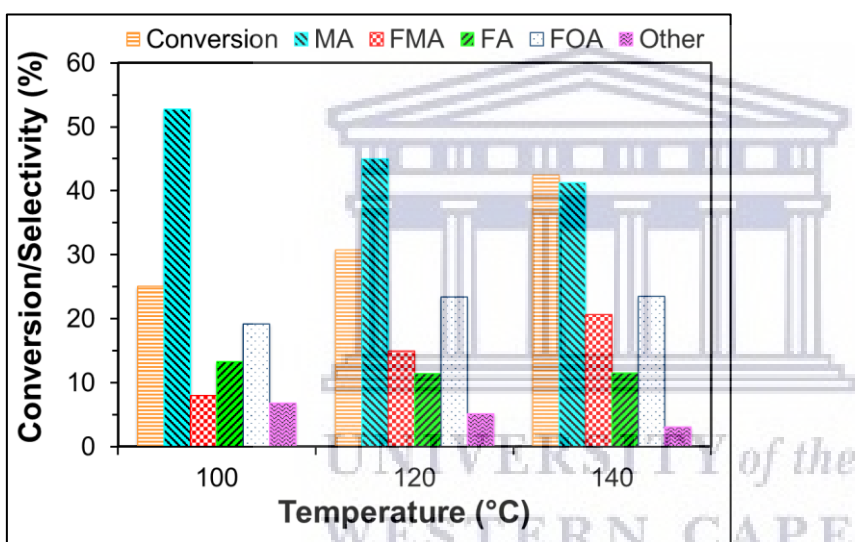
Fig. 8-2: Products selectivity for the microwave-assisted batch oxidation of furfural with Ti1Sn4 catalyst at different temperatures. Reaction conditions: 3 mmol furfural, 15 mmol 30% $_{(aq)}$ H_2O_2 (H_2O_2/furfural = 5), 15 mL AcOH and H_2O (1:1), 60 mg catalyst and t = 20 min.

The results above indicate that the reaction carried out at a higher temperature (140°C) favours the formation of maleic acid and fumaric acid with better yields as the thermal decomposition of H_2O_2 proceeds at a faster rate at high temperatures (as demonstrated in **Chapters 4** and **5**). Coupled with the rapid heating of microwave energy, the rapid H_2O_2 decomposition also leads to over-oxidation reactions to favour the formation of formic acid with increased yields and selectivity at the expense of maleic acid selectivity. Inversely,

the reaction carried out a lower temperature (100 °C) results in the thermal decomposition of H_2O_2 proceeding at a somewhat slower rate and thus favouring the formation of maleic acid with better selectivity. Consequently, the reaction temperature of 100 °C was determined to afford the maximum selectivity toward maleic acid and employed for further optimization reactions.

8.2.3 Effect of reaction time

Next, the effect of microwave irradiation time on the distribution of furfural oxidation products was investigated with the reaction being performed for 20, 30 and 40 min (**Table 8-4** and **Fig. 8-3**). Increasing the reaction time from 20 min to 30 min led to a 2% increase in furfural conversion from 25.1% to 27.1%. However, a slight decrease in maleic acid yield from 13.2% to 12.6% was observed with the selectivity also decreasing from 52.7% to 46.7%. An increase in fumaric acid yield from 2.0% to 3.2% was also observed. There was a slight increase in the yield of 2-furoic acid from 3.3% to 3.6%. Formic acid was once again the major by-product with its yield increasing from 4.8% to 6.2%.

Table 8-4: Effect of reaction time on furfural oxidation rates with the Ti1Sn4 catalyst.

Time (min)	Conversion (%)	Yield (%)				
		MA	FMA	FA	FOA	Other
20	25.1	13.2	2.0	3.3	4.8	1.7
30	27.1	12.6	3.2	3.6	6.2	1.5
40	29.2	14.7	3.0	3.5	7.1	1.0

Reaction conditions: 3 mmol furfural, 15 mmol 30% $_{(aq)}$ H_2O_2 (H_2O_2/furfural = 5), 15 mL AcOH and DI H_2O (1:1), 60 mg catalyst and T = 100 °C.

Further increasing the reaction time to 40 min resulted in an additional 2% increment in furfural conversion from 27.1% to 29.2%. The yield of maleic acid also increased to 14.7% at 50.2% selectivity. The yield of fumaric acid decreased further to 3.0% and formic acid

was produced with an increased yield of 7.1%. The yield of 2-furoic acid remained unchanged at 3.5% with 11.9% selectivity. Conducting the reaction for longer periods (30 and 40 minutes) had very minimal effects on furfural conversion and maleic acid yield with only a ~4% increase in conversion and a 1.5% increase in maleic acid yield obtained when the reaction time was doubled from 20 to 40 minutes. The increase in reaction time had a negative impact on maleic acid selectivity and fumaric acid yield as a result of over-oxidation to formic acid. The reaction time of 20 minutes afforded the best catalytic results and was employed for subsequent reactions.
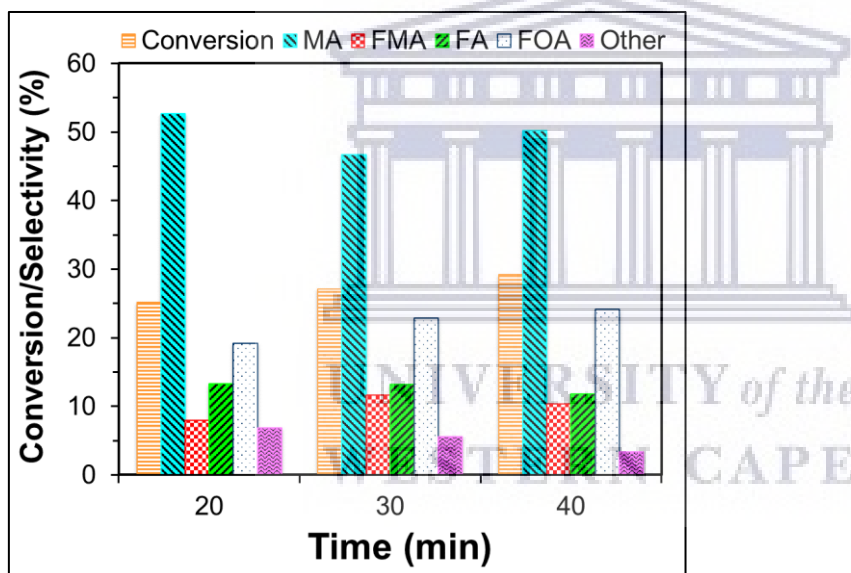
Fig. 8-3: Effect of reaction time on products selectivity for the microwave-assisted batch oxidation of furfural with Ti1Sn4 catalyst. Reaction conditions: 3 mmol furfural, 15 mmol 30% $_{(aq)}$ H_2O_2 (H_2O_2/furfural = 5), 15 mL AcOH and H_2O (1:1), 60 mg catalyst and T = 100 °C.

8.2.4 Effect of catalyst dosage

The amount of catalyst utilized in a catalytic reaction can influence the rate of reaction and distribution of products by altering the number of available catalyst active sites. Consequently, the effect of catalyst dosage on the furfural oxidation reaction was investigated next with the results displayed in **Fig. 8-4** and **Table 8-5**. Varying the amount

of catalyst from 60 mg to 180 mg resulted in an increase in both furfural conversion and maleic acid yield to 32.8% and 17.5% respectively. The selectivity towards maleic acid increased to 53.5%. A slight increase to 3.6% was observed for 2-furoic acid while the yield of fumaric acid increased to 4.9% with selectivity increasing from 8.0% to 15.1%. The yield of formic acid also increased to 5.5% when 180 mg of catalyst was utilized.

Table 8-5: Effect of catalyst dosage on furfural oxidation rates with the Ti1Sn4 catalyst.

Cat. Amount (mg)	Conversion (%)	Yield (%)				
		MA	FMA	FA	FOA	Other
60	25.1	13.2	2.0	3.3	4.8	1.7
180	32.8	17.5	4.9	3.6	5.5	1.2
240	18.3	8.5	2.2	3.0	3.9	0.6

Reaction conditions: 3 mmol furfural, 15 mmol 30% (aq) H_2O_2 (H_2O_2/furfural = 5), 15 mL AcOH and H_2O (1:1), T = 100 °C and t = 20 min.
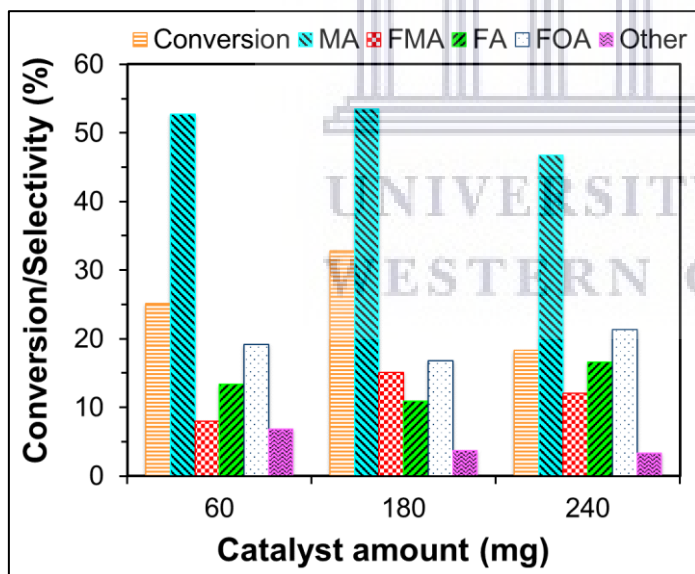

Fig. 8-4: Effect of catalyst dosage on products selectivity for the microwave-assisted batch oxidation of furfural with Ti1Sn4 catalyst. Reaction conditions: 3 mmol furfural, 15 mmol 30% (aq) H_2O_2 (H_2O_2/furfural = 5), 15 mL AcOH and H_2O (1:1), T = 100 °C and t = 20 min.

A further increase in catalyst amount to 240 mg led to a decrease in both furfural conversion and maleic acid yield to 18.3% and 8.5%, respectively, with selectivity towards

maleic acid also decreasing to 46.7%. The amount of fumaric acid and 2-furoic acid produced also continued to decrease to reach respective yields of 2.2% and 3.0%. A decrease in yield of the formic acid to 3.9% was also observed. The use of increased catalyst amounts can present an increase of catalyst active sites and thus lead to improved catalytic results while also providing a platform for over-oxidation of reaction products. This is evident by the observed increase in furfural conversion and the respective yields of maleic, furoic and formic acids. As a result, the catalyst dosage of 60 mg showed to afford the best catalytic activity for furfural oxidation with highest maleic acid selectivity and minimal over-oxidation of products, thus further reaction optimization was carried out with 60 mg catalyst.

8.2.5 Effect of H_2O_2 concentration

Next, the effect of aqueous H_2O_2 amount on furfural oxidation rates and product distribution was investigated by varying the H_2O_2/furfural (mmol/mmol) ratio and the results for these experiments are presented in **Fig. 8-5** and **Table 8-6**. The gradual increase of H_2O_2 concentration had a remarkably positive effect leading to faster furfural conversions and increased maleic acid yield. Incrementally increasing the H_2O_2/furfural molar ratio resulted in a linear increase in furfural conversion from 25.1% (mol ratio of 5) to 89.2% (mol ratio of 10) as a result of more H_2O_2 being available to oxidize the furfural substrate. Increasing the H_2O_2/furfural ratio from 5 to 6 increased the yield of maleic acid from 13.2% to 15.5% with selectivity decreasing slightly from 52.7% to 45.6%. Further increasing the ratio from 6 to 7 led to the maleic acid yield being more than doubled to reach 41.9% while the selectivity increased to a maximum of 70.5%. The selectivity remained unchanged when the ratio was increased from 7 to 8 with a just a 2% increase in maleic acid yield to 43.9%. The yield of maleic acid continued to increase reaching a

maximum of 56.7% at a H_2O_2/furfural ratio of 10. However, the excess H_2O_2 had a negative impact on maleic acid selectivity which decreased when the H_2O_2/furfural ratio was increased beyond 8 reaching 63.5% at a ratio of 10.

Table 8-6: Effect of H_2O_2 concentration on furfural oxidation rates with the Ti1Sn4 catalyst.

H_2O_2/furfural (mmol/mmol)	Conversion (%)	Yield (%)				
		MA	FMA	FA	FOA	Other
5	25.1	13.2	2.0	3.3	4.8	1.7
6	34.0	15.5	2.3	4.2	9.8	2.2
7	59.1	41.9	2.8	3.2	8.1	3.4
8	62.6	43.9	3.1	1.9	11.6	2.1
9	76.9	47.0	3.5	2.1	21.4	2.9
10	89.2	56.7	3.1	1.3	22.2	5.9

Reaction conditions: 3 mmol furfural, 60 mg catalyst, 15 mL AcOH and DI H_2O (1:1), T = 100 °C and t = 20 min.

The yield of fumaric acid also increased with increasing H_2O_2 concentration reaching a maximum of 3.5% with a H_2O_2/furfural ratio of 10. The yield of 2-furoic acid intermediate on the other hand decreased with increasing H_2O_2 concentration as a result of oxidation to the reaction products. The yield of the side products increased to reach 5.9% when a ratio of 10 was utilized thus indicating the over-oxidation of products due to the excess H_2O_2. The over-oxidation was confirmed by the increase of formic acid when the ratio was increased beyond 8. The yield of formic acid increased from 11.6% for a H_2O_2/furfural ratio of 8 to 22.2% for a ratio of 10. In terms of selectivity, the H_2O_2/furfural ratio of 7 provided the best catalytic results affording maleic acid with a yield of 41.9% at 70.5% selectivity. The lowest selectivity of 13.7% towards formic acid (8.1% yield) was also achieved at that H_2O_2 concentration.
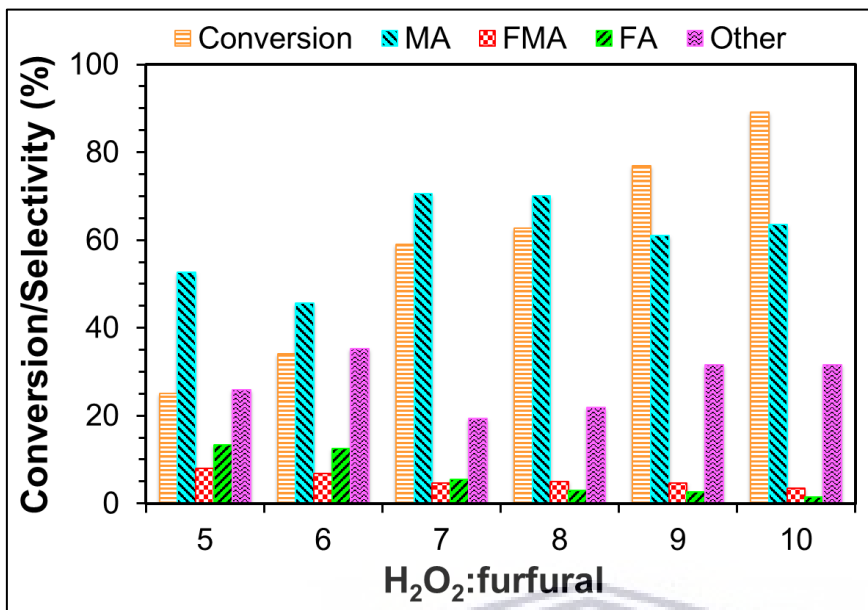
Fig. 8-5: Effect of H_2O_2 concentration on products selectivity for the microwave-assisted batch oxidation of furfural with Ti1Sn1 catalyst. Reaction conditions: 3 mmol furfural, 60 mg catalyst, 15 mL AcOH and DI H_2O (1:1), T = 100 °C and t = 20 min.

8.2.6 Comparison of microwave to conventional heating

To investigate the energy efficiency of microwave (MW) irradiation compared to the conventional heating (CH) method, the conversion and selectivity results obtained under optimal conditions are showed in **Fig. 8-6** along with those achieved under CH under the same reaction conditions. The differences between the two reaction systems are significant: a much higher reaction rate was achieved for the reaction conducted under MW heating with a 59.1% conversion achieved in just 20 min, in contrast to 59.8% achieved in 3 h for the CH method. In addition, a selectivity of 70.5% towards maleic acid was higher for the MW method compared 56.1% for the CH method. Maleic acid was also produced in a higher yield under MW heating (41.9%) in comparison to CH (33.4%). The striking differences between the results of the two heating methods can be explained in terms of microwave thermal effects. As a result of microwaves acting directly on molecules, rapid and volumetric heating of the reaction medium can be achieved leading

to higher reaction rates and selectivity as evidenced by the enhance catalytic results achieved under MW irradiation. Furthermore, microwave irradiation has been reported to induce hot spots in heterogenous catalysts as a result of the tan δ and dielectric constant of the catalyst material. These hot spots consequently lead to increased temperatures at the catalyst active surface compared to the bulk, thus resulting in increased reaction rates.[19-22] Thus, the high dielectric constant of TiO_2 makes it a good microwave absorber and can lead to the generation of such hot spots.[23] However, it should be mentioned that no additional experiments were conducted to test this hypothesis.
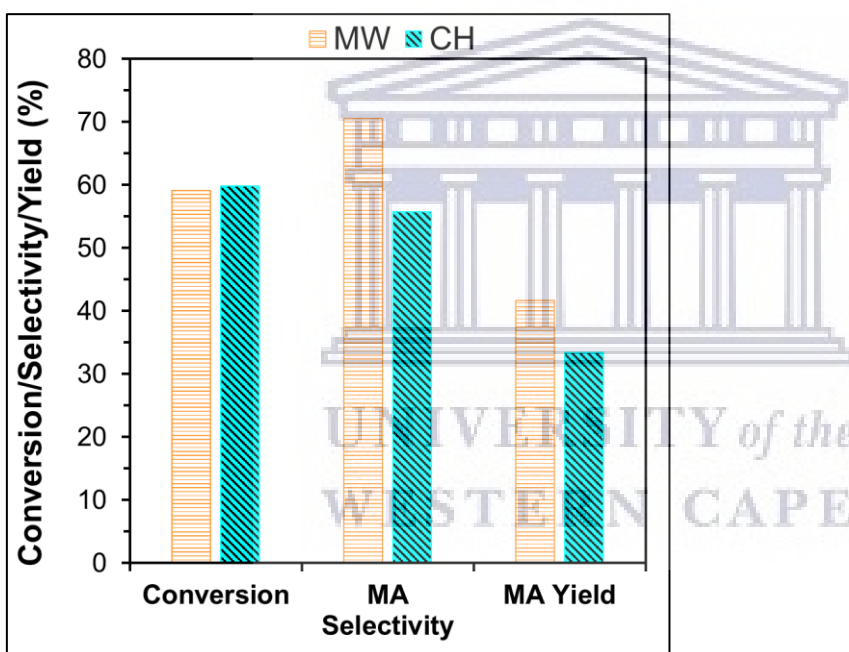
Fig. 8-6: Comparison of the MW irradiation and CH methods for batch oxidation of furfural with the Ti1Sn4 catalyst. Reaction conditions: 3 mmol furfural, 21 mmol 30% (aq) H_2O_2, co-solvent of H_2O (7.5 ml) and AcOH (7.5 ml), 60 mg catalyst and T = 100 °C.

8.2.7 Catalyst reutilization test

The recyclability of the catalyst was also investigated by conducting successive reutilization runs with the experiments conducted under optimized reaction conditions. To compensate for the loss of catalyst experienced during handling; the amount of catalyst

used and the amounts of furfural, aqueous H_2O_2, and solvent were all increased by a factor of 1.67 for the first reaction cycle and by a factor of 1.42 for the second cycle (i.e. 5 mmol furfural, 35 mmol 30% (aq) H_2O_2, 12.5 mL DI H_2O and 12.5 mL AcOH solvent, and 100 mg catalyst for the first cycle and 4 mmol furfural, 30 mmol 30% (aq) H_2O_2, 10.5 mL DI H_2O and 10.5 mL AcOH solvent, and 85 mg catalyst for the second cycle). After each reaction cycle, the catalyst was collected and washed by centrifuge three times with a mixture of ethanol, acetone and DI H_2O (1:1:1, vol/vol) and thereafter dried in an oven at 60 °C overnight.

Table 8-7: Recyclability performance test of the Ti1Sn4 catalyst in microwave-assisted furfural oxidation.

Cycle	Conversion (%)	Yield (%)				
		MA	FMA	FA	FOA	Others
1	75.9	34.4	8.0	21.2	0.6	11.7
2	44.0	22.7	4.2	16.3	0.0	0.8
3	30.1	12.7	3.0	11.2	0.1	3.1

Reaction conditions: T = 60 °C and t = 6 h, Cycle 1 = 5 mmol furfural, 35 mmol 30% (aq) H_2O_2, 12.5 mL H_2O and 12.5 mL AcOH solvent, and 100 mg catalyst. Cycle 2 = 4 mmol furfural, 30 mmol 30% (aq) H_2O_2, 10.5 mL H_2O and 10.5 mL AcOH solvent, and 85 mg catalyst. Cycle 3 = 3 mmol furfural, 21 mmol 30% (aq) H_2O_2, 7.5 mL H_2O and 7.5 mL AcOH solvent, and 60 mg catalyst.

After the first reaction cycle, a furfural conversion of 75.9% was achieved and a maleic acid yield of 34.4% at 45.4% selectivity. 2-Furoic acid and fumaric acid were produced with respective yields of 21.2% and 8.0%. A loss in catalytic activity was observed after the second reaction cycle with furfural conversion decreasing to 44.0% and the yield maleic acid achieved was 22.7% albeit at an increased selectivity of 51.5%. The yield of 2-furoic acid was also decreased to 16.3% while fumaric acid was produced with a decreased yield of 4.2%. The loss of catalyst activity became severe after the third reaction cycle. The conversion of furfural decreased further to 30.1% and the yield of

maleic acid decreased to 12.7% with 41.9% selectivity. Decreases in the yield of 2-furoic acid and fumaric acid were also observed, with respective yields of 11.2% and 3.0% obtained for the two acids. The loss of activity for the catalyst after each reaction cycle is indicative of leaching of the Ti1Sn4 catalyst active sites, which was also observed in **section 6.3.5**.
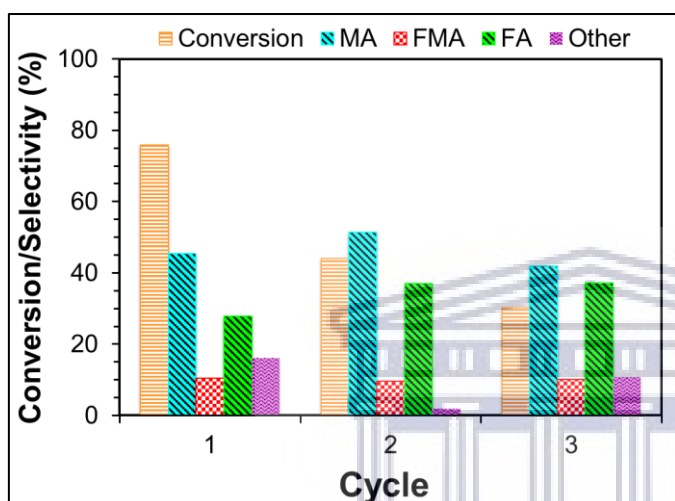

Fig. 8-7: The Ti1Sn4 catalyst recyclability results for the microwave-assisted batch oxidation of furfural. Reaction conditions: T = 100 °C and t = 20 min, Cycle 1 = 5 mmol furfural, 35 mmol 30% $_{(aq)}$ H_2O_2, 12.5 mL H_2O and 12.5 mL AcOH solvent, and 100 mg catalyst. Cycle 2 = 4 mmol furfural, 30 mmol 30% $_{(aq)}$ H_2O_2, 10.5 mL H_2O and 10.5 mL AcOH solvent, and 85 mg catalyst. Cycle 3 = 3 mmol furfural, 21 mmol 30% $_{(aq)}$ H_2O_2, 7.5 mL H_2O and 7.5 mL AcOH solvent, and 60 mg catalyst.

8.3 Concluding remarks

The process intensification of maleic acid synthesis by oxidation of furfural was successfully demonstrated by a simple and ultrafast microwave-assisted oxidation reaction using aqueous H_2O_2 oxidant employing a heterostructured TiO_2-SnO_2 catalyst. A maleic acid yield of 41.9% was obtained at 70.5% selectivity with a furfural conversion of 59.1% in 20 min reaction time. The space-time yields were significantly improved with the use of microwave irradiation as a heating method compared to conventional methods where longer reaction times (> 3 h) are required to achieve comparable yields.

Investigation of the reaction parameters revealed the polarity of the solvent to be critical with the most polar protic solvents affording increased maleic acid yields. Furthermore, conducting the reaction at longer reaction times and utilizing higher catalyst dosages proved detrimental to maleic acid selectivity resulting in over-oxidation to generate formic acid in increased yields. The same result was observed when employing increased concentrations of aqueous H_2O_2.

8.4 References

[1] G. Centi, S. Perathoner, Methods and tools of sustainable industrial chemistry: Process intensification. Sustainable Industrial Chemistry, **2009**, pp. 199-255.

[2] A. Stankiewicz, J.A. Moulijn, Process intensification. Industrial & Engineering Chemistry Research, **2002**, 41, pp. 1920-1924.

[3] T. Van Gerven, A. Stankiewicz, Structure, energy, synergy, time – The fundamentals of process intensification. Industrial & Engineering Chemistry Research, **2009**, 48, pp. 2465-2474.

[4] D. Reay, C. Ramshaw, A. Harvey, Chapter 2 - Process intensification – An overview, In: D. Reay, C. Ramshaw, A. Harvey (Ed.), Process Intensification: Engineering for efficiency, sustainability and flexibility (2nd Ed.). Butterworth-Heinemann, **2013**, pp. 27-55.

[5] F.J. Keil, R. Franke, Process intensification – An industrial point of view. Modeling of Process Intensification, **2007**, 2, pp. 2.

[6] V.L. Budarin, J.H. Clark, B.A. Lanigan, P. Shuttleworth, S.W. Breeden, A.J. Wilson, D.J. Macquarrie, K. Milkowski, J. Jones, T. Bridgeman, A. Ross, The preparation of high-grade bio-oils through the controlled, low temperature microwave activation of wheat straw. Bioresource Technology, **2009**, 100, pp. 6064-6068.

[7] A. Mittal, H.M. Pilath, D.K. Johnson, Direct conversion of biomass carbohydrates to platform chemicals: 5-Hydroxymethylfurfural (HMF) and furfural. Energy & Fuels, **2020**, 34, pp. 3284-3293.

[8] A. Rusanen, R. Kupila, K. Lappalainen, J. Kärkkäinen, T. Hu, U. Lassi, Conversion of xylose to furfural over lignin-based activated carbon-supported iron catalysts. Catalysts, **2020**, 10, pp. 821.

[9] N. Sweygers, R. Dewil, L. Appels, Production of levulinic acid and furfural by microwave-assisted hydrolysis from model compounds: Effect of temperature, acid concentration and reaction time. Waste and Biomass Valorization, **2018**, 9, pp. 343-355.

[10] T.S. Hansen, J.M. Woodley, A. Riisager, Efficient microwave-assisted synthesis of 5-hydroxymethylfurfural from concentrated aqueous fructose. Carbohydrate Research, **2009**, 344, pp. 2568-2572.

[11] S. Tabasso, D. Carnaroglio, E.C. Gaudino, G. Cravotto, Microwave, ultrasound and ball mill procedures for bio-waste valorisation. Green Chemistry, **2015**, 17, pp. 684-693.

[12] H. Pawar, A. Lali, Microwave assisted organocatalytic synthesis of 5-hydroxymethyl furfural in a monophasic green solvent system. RSC Advances, **2014**, 4, pp. 26714-26720.

[13] D. Zhao, D. Rodriguez-Padron, K.S. Triantafyllidis, Y. Wang, R. Luque, C. Len, Microwave-assisted oxidation of hydroxymethyl furfural to added-value compounds over a ruthenium-based catalyst. ACS Sustainable Chemistry & Engineering, **2020**, 8, pp. 3091-3102.

[14] T. Ji, C. Liu, X. Lu, J. Zhu, Coupled chemical and thermal drivers in microwaves toward ultrafast HMF oxidation to FDCA. ACS Sustainable Chemistry & Engineering, **2018**, 6, pp. 11493-11501.

[15] D. Zhao, D. Rodriguez-Padron, R. Luque, C. Len, Insights into the selective oxidation of 5-hydroxymethylfurfural to 5-hydroxymethyl-2-furancarboxylic acid using silver oxide. ACS Sustainable Chemistry & Engineering, **2020**, 8, pp. 8486-8495.

[16] Á Martín, A. Navarrete, Microwave-assisted process intensification techniques. Current Opinion in Green and Sustainable Chemistry, **2018**, 11, pp. 70-75.

[17] B.L. Hayes, Microwave synthesis: chemistry at the speed of light. Cem Corporation, **2002**.

[18] H. Li, C. Zhang, C. Pang, X. Li, X. Gao, The advances in the special microwave effects of the heterogeneous catalytic reactions. Frontiers in Chemistry, **2020**, *8*, pp. 355.

[19] H. Einaga, Y. Nasu, M. Oda, H. Saito, Catalytic performances of perovskite oxides for CO oxidation under microwave irradiation. Chemical Engineering Journal, **2016**, *283*, pp. 97-104.

[20] A. de la Hoz, A. Díaz-Ortiz, A. Moreno, Microwaves in organic synthesis. Thermal and non-thermal microwave effects. Chemical Society Reviews, **2005**, *34*, pp. 164-178.

[21] M.B. Gawande, S.N. Shelke, R. Zboril, R.S. Varma. Microwave-assisted chemistry: Synthetic applications for rapid assembly of nanomaterials and organics. Accounts of Chemical Research, **2014**, *47*, pp. 1338–1348.

[22] E.A. Anumol, P. Kundu, P.A. Deshpande, G. Madras, N. Ravishankar, New insights into selective heterogenous nucleation of metal nanoparticles on oxides by microwave-assisted reduction: Rapid synthesis of high-activity supported catalysts. ACS Nano, **2011**, *5*, pp. 8049–8061.

[23] P. N. Romano, J.M.A.R. de Almeida, Y. Carvalho, P. Priecel, E.F. Sousa-Aguiar, J.A. Lopez-Sanchez, Microwave-assisted selective hydrogenation of furfural to furfuryl alcohol employing a green and noble metal-free copper catalyst. ChemSusChem, **2016**, *9*, pp. 3387–3392.

CHAPTER 9

Summary, Conclusion and Recommendations

9.1 Summary and conclusions

In summary, the synthesis of heterostructured SnO_2 catalysts was successfully demonstrated via polyol and microwave assisted synthetic routes. These methods afforded the formation of high surface area and nanometre sized indistinguishable nanoparticles of Ti, V, Co, Cu, Mn, Ni and Sn metal oxides. The catalyst design strategy exploited the redox nature, low cost and abundance of Ti, V, Co, Cu, Mn and Ni metals as catalyst active sites for the development of efficient catalysts for use in the conversion of furfural and 5-hydroxymethylfurfural to bio-based maleic acid. Furthermore, the varying degree of intrinsic Lewis acidity and redox character of these metal oxides was key in bringing about enhanced intrinsic acid-base and redox properties required for efficient catalytic oxidations of furfural and 5-hydroxymethylfurfural via an accelerated electron transfer process and facilitation of the substrate C–C bond cleavage process.

Among the heterostructured VO_x-SnO_2 catalysts synthesised by the surfactant-free polyol method, the VO_x-SnO_2 catalyst loaded with 9.3 wt% V-metal (VSn-2) presented a highly active catalyst for the oxidation of both furfural and 5-hydroxymethylfurfural with H_2O_2 to maleic acid. Under optimized conditions, complete furfural and 5-hydroxymethylfurfural conversions were achieved with 60% maleic acid yield from furfural and 52% yield from 5-hydroxymethylfurfural being obtained in 20 h. The VSn-2 catalyst composed of VO_x mono- and polymeric active sites populated with balanced V^{5+}/V^{4+} redox pairs, which induced highly active sites amenable for oxidation of furfural and 5-hydroxymethylfurfural as evidenced by the XPS results. The easily exchangeable V^{4+}/V^{5+} redox pair was important

for accelerating the electron transfer processed and facilitating the C-C bond cleavage of the substrate for efficient maleic acid production. The V^{4+} species was determined to be the active phase and was found to be most exposed on the VSn-2 catalyst with the highest amount of surface vanadium. Moreover, the catalyst possessed a large concentration of lattice oxygen atoms which are necessary for facilitating the electron transfer process. Both the catalyst leaching and recyclability tests demonstrated the gradual decrease of catalytic activity for furfural oxidation, which exhibited to be due to the leaching of the V-metal.

The catalytic activity evaluation of a series of hetero-mixed SnO_2 interfaced metal oxides catalysts consisting of Co, Cu, Mn, and Ni metals synthesized by the polyol surfactant-assisted method in the liquid-phase oxidation of furfural to maleic acid using H_2O_2 oxidant revealed the CuO_x-SnO_2 to afford the best catalytic performance to afford a yield of 60.3% in 3 h for maleic acid under optimized conditions. The structure-activity correlation showed the retained morphology of SnO_2 for the CuO_x-SnO_2 catalyst along with the even distribution of the Cu^{2+}/Cu^+ redox pairs to be crucial for the effective oxidation of furfural to maleic acid. The Cu^{2+}/Cu^+ reactivity was crucial to facilitate the required free radical driven oxidation redox electron-transfer mechanism to create reactive oxygen species (ROS) effective for the efficient conversion of furfural substrate. In addition, the CuO_x-SnO_2 catalyst also showed the highest surface metal content thus exhibiting maximised exposure of surface Cu^{2+}/Cu^+ active sites. The catalyst also possessed a low concentration of surface defects (oxygen vacancies) which proved detrimental for the oxidation reaction and a large concentration of lattice oxygen atoms necessary for facilitating the electron transfer process. The high reducibility of the CuO_x-SnO_2 catalyst (TPR results) also proved beneficial for this purpose. Further, the small pore size, pore

volume and small crystallite size of the CuO$_x$-SnO$_2$ oxide catalyst showed to be influential on the yield of maleic acid. Moreover, the use of a co-solvent of water and acetic acid proved to enhance product selectivity and yield as well as minimize the over-oxidation of the products observed when employing H$_2$O as the solvent.

The heterostructure TiO$_2$-SnO$_2$ catalysts synthesised by a simple microwave-assisted method also proved to be highly active for the oxidation of both furfural and 5-hydroxymethylfurfural with H$_2$O$_2$ to maleic acid. The TiO$_2$-SnO$_2$ catalyst with a high surface area composing of Ti1Sn4 ratio showed to be most active for maleic acid synthesis. The Ti1Sn4 catalyst afforded total yield of 74.1% for maleic acid and 4.4% for its isomer fumaric acid from furfural under optimal reaction conditions. Moreover, the Ti1Sn4 catalyst afforded a 56.6% yield for maleic acid and 27.2% for its isomer fumaric acid from HMF oxidation. The catalyst structure-activity correlation showed the most active catalyst to possess a high amount of surface exposed Ti atoms and the highest surface area thusmaximized surface exposed Ti active sites. The highly exposed active sites were beneficial for accelerating the electron transfer processed and facilitating the C-C bond cleavage of the substrate for efficient maleic acid production. The Ti1Sn4 catalyst also possessed a low concentration of surface defects (oxygen vacancies) and a large concentration of lattice oxygen atoms necessary for facilitating the electron transfer process. Furthermore, the use of a co-solvent of water and acetic acid proved to enhance product selectivity, yield, and overall catalytic performance by forming a peracetic acid intermediate with stronger oxidizing strength. However, catalyst leaching and recyclability tests revealed the catalyst to suffer severe leaching of the Ti active site under these conditions.

A scalable maleic acid synthesis process by furfural oxidation with a bench top stirred glass batch reactor was successfully demonstrated with the heterostructured SnO_2 catalysts, achieving improved maleic acid yields with the VSn-2 and Ti1Sn4 catalysts compared to those obtained with the laboratory flask reaction. A maleic acid yield of 73.3% was obtained in 2 h with the VSn-2 catalyst compared to a 60 % maleic acid yield achieved in 20 h for the laboratory flask reaction. Similarly, for the Ti1Sn4 catalyst, a yield of 93.2% for maleic acid was obtained in 7 h compared to a 74.1 % maleic acid yield achieved in 6 h for the laboratory flask reaction. Furthermore, the method of aqueous H_2O_2 addition showed to affect the furfural oxidation rate and yield of maleic acid with the maximum yield of maleic acid produced (93.2%) when H_2O_2 was added periodically every 1 h. The issue of over-oxidation of the products was intensified when the CuO_x-SnO_2 catalyst was employed with a yield of 86.7% for side products obtained.

In addition, the maleic acid synthesis process by oxidation of furfural was successfully intensified by a simple and ultrafast microwave-assisted oxidation reaction using aqueous H_2O_2 oxidant employing a heterostructured Ti1Sn4 catalyst. The space-time yields were significantly improved with the use of microwave irradiation as a heating method compared to conventional methods where longer reaction times (> 3 h) are required to achieve comparable yields. A maleic acid yield of 41.9% was obtained at 70.5% selectivity with a furfural conversion of 59.1% in just 20 min reaction time. Investigation of the reaction parameters revealed the polarity of the solvent to be critical with the most polar protic solvents affording increased maleic acid yields while conducting the experiments at longer reaction times and utilizing higher catalyst dosages proved detrimental to maleic acid selectivity resulting in over-oxidation to generate formic acid in increased yields.

9.2 Recommendations

Although the heterostructured SnO_2 catalysts developed in this thesis for the synthesis of bio-based maleic acid from biomass-derived furfural and 5-hydroxymethylfurfural showed promising results, a considerable amount of work remains before industrial application can be considered. An understanding of the main issues such as the furfural and 5-hydroxymethylfurfural oxidation reaction mechanism with the different heterostructured SnO_2 catalysts and the role of the copper and vanadium redox pairs as well the TiO_2 Lewis character is still required. This will be important for the development of a stable and selective catalyst for maleic acid production. Thus, the following recommendations are made for future continuation of the maleic acid synthesis work employing heterostructured SnO_2 catalysts for furfural and 5-hydroxymethylfurfural oxidation reactions:

➤ The first recommendation pertains to improving the catalyst stability. Further studies are required to re-design the catalysts to improve on their recyclability and selectivity by preventing leaching of the active sites under optimal reaction conditions, which was experienced with all the catalyst, employed in this thesis. To perform this, thorough characterization of the spent catalyst (especially by XPS) is needed to understand how the catalyst structure is has changed after the reaction. The catalyst stability can be improved by strengthening the SnO_2-metal oxide interaction using an alternative catalyst synthesis method such as hydrothermal synthesis or chemical vapour deposition. Other possible remedies for leaching include replacing SnO_2 with another metal oxide resistant to leaching such as ZrO_2 or controlling the pH of the reaction medium as the acidic reaction medium obtained when the carboxylic acids are produced can induce leaching of the active sites.

➤ The second recommendation involves uncovering the furfural and 5-hydroxymethylfurfural oxidation reaction mechanism with the different

heterostructured SnO_2 catalysts. This can help in understanding the exact role of the metal redox pairs in accelerating the electron transfer process and how the Lewis character of the catalyst facilitates the C-C bond cleavage process and thus lead to improved and controlled catalyst re-design to improve selectivity towards maleic acid.

➢ Thirdly, the redox-acid properties of the different heterostructured SnO_2 catalysts need to be quantified by CO_2-TPD, H_2-TPR, pyridine-adsorption, etc. as this will further assist to uncover the role of these properties in the electron transfer and C-C bond cleavage processes for improved and controlled catalyst re-design.

➢ The fourth recommendation concerns optimization of the oxidation reaction. The periodic addition of aqueous H_2O_2 was shown to enhance the yield and selectivity towards maleic acid. As a result, transformation of the oxidation reaction from a batch to a continuous flow process should be studied as it can improve maleic acid yield and selectivity due to improved interfacial mass transfer dynamics of reactant contacts and tailored residue times. This can be especially beneficial for the up-scaled and microwave assisted reactions.

➢ Lastly, further refinement of the reaction parameters for the microwave assisted oxidation reaction should also be investigated to probe the effect of varying reaction parameters such as microwave irradiation energy and temperature ramp-up rates as this can further improve the space-time yields for the reaction.

APPENDIX A

**1.** **Nitrogen sorption analysis of heterostructured VO$_x$-SnO$_2$ catalysts**
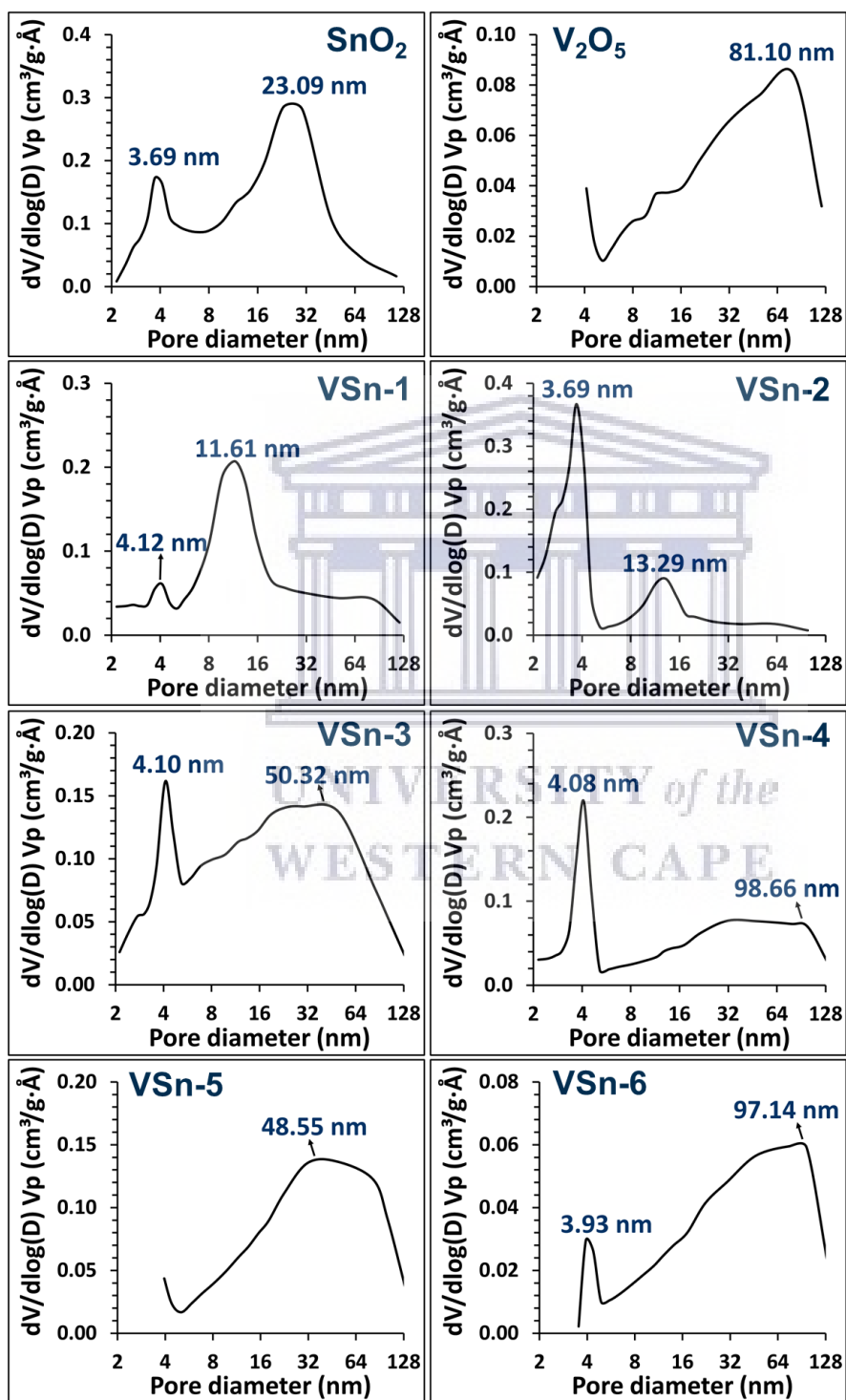
Fig. A-1: BJH pore size distribution plots of the heterostructure VO$_x$-SnO$_2$ catalysts.

## 2. SEM-EDX characterization of heterostructured VO$_x$-SnO$_2$ catalysts
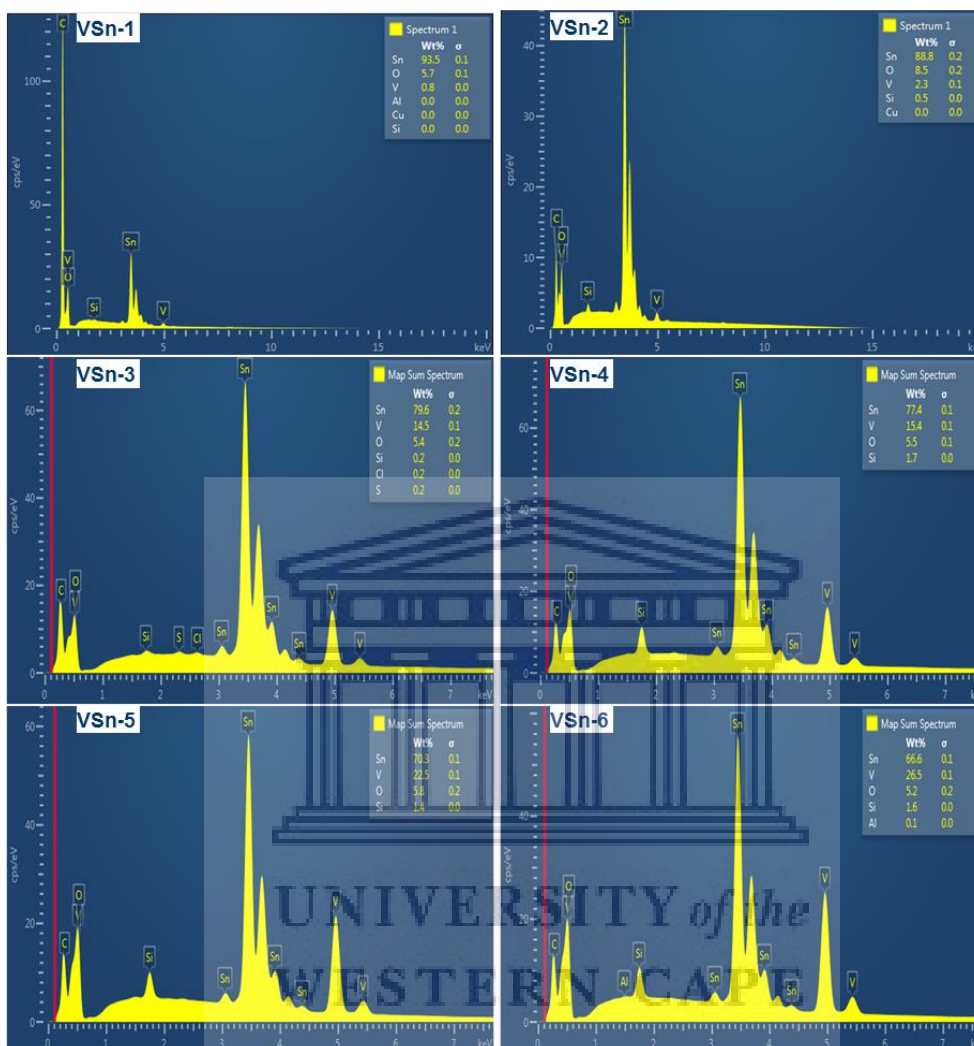
**Fig. A-2**: SEM-EDX spectra of the heterostructure VO$_x$-SnO$_2$ catalysts.
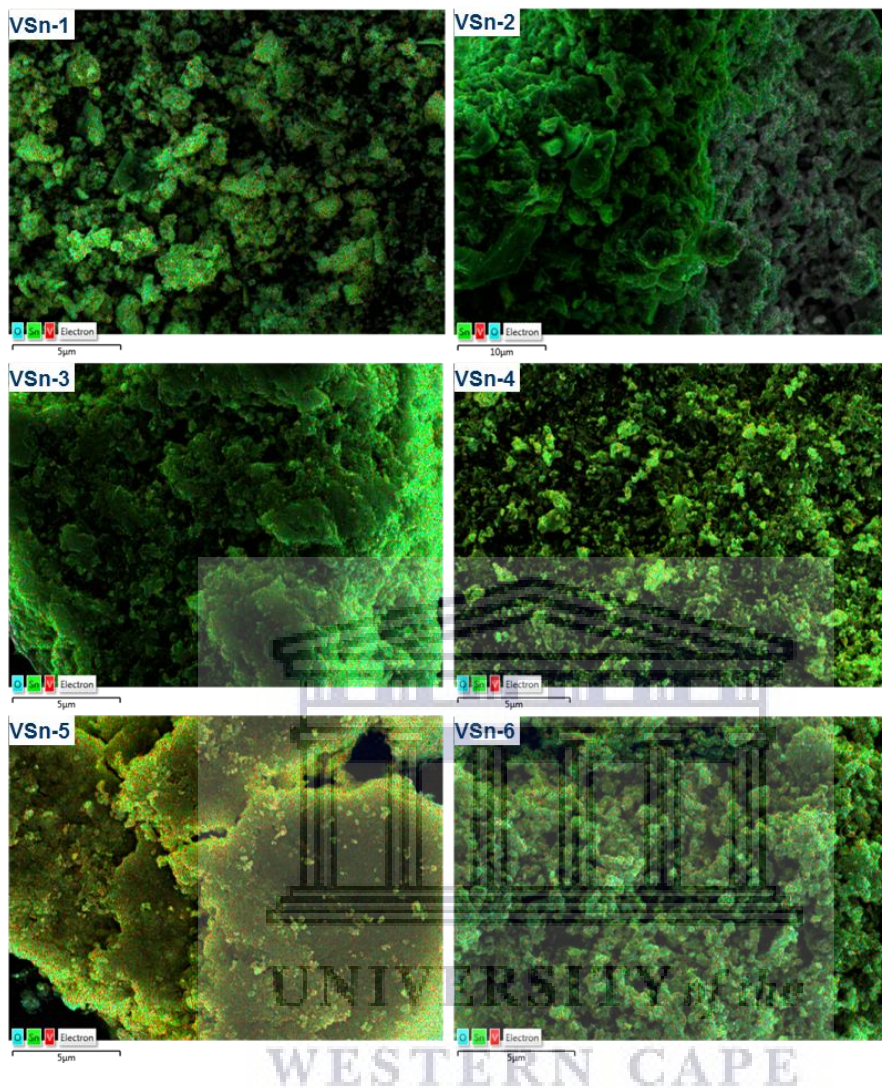
Fig. A-3: EDX elemental maps of the heterostructure VO_x-SnO_2 catalysts.

APPENDIX B

**1.** **Nitrogen sorption analysis of heterostructured BMO-SnO$_2$ catalysts**
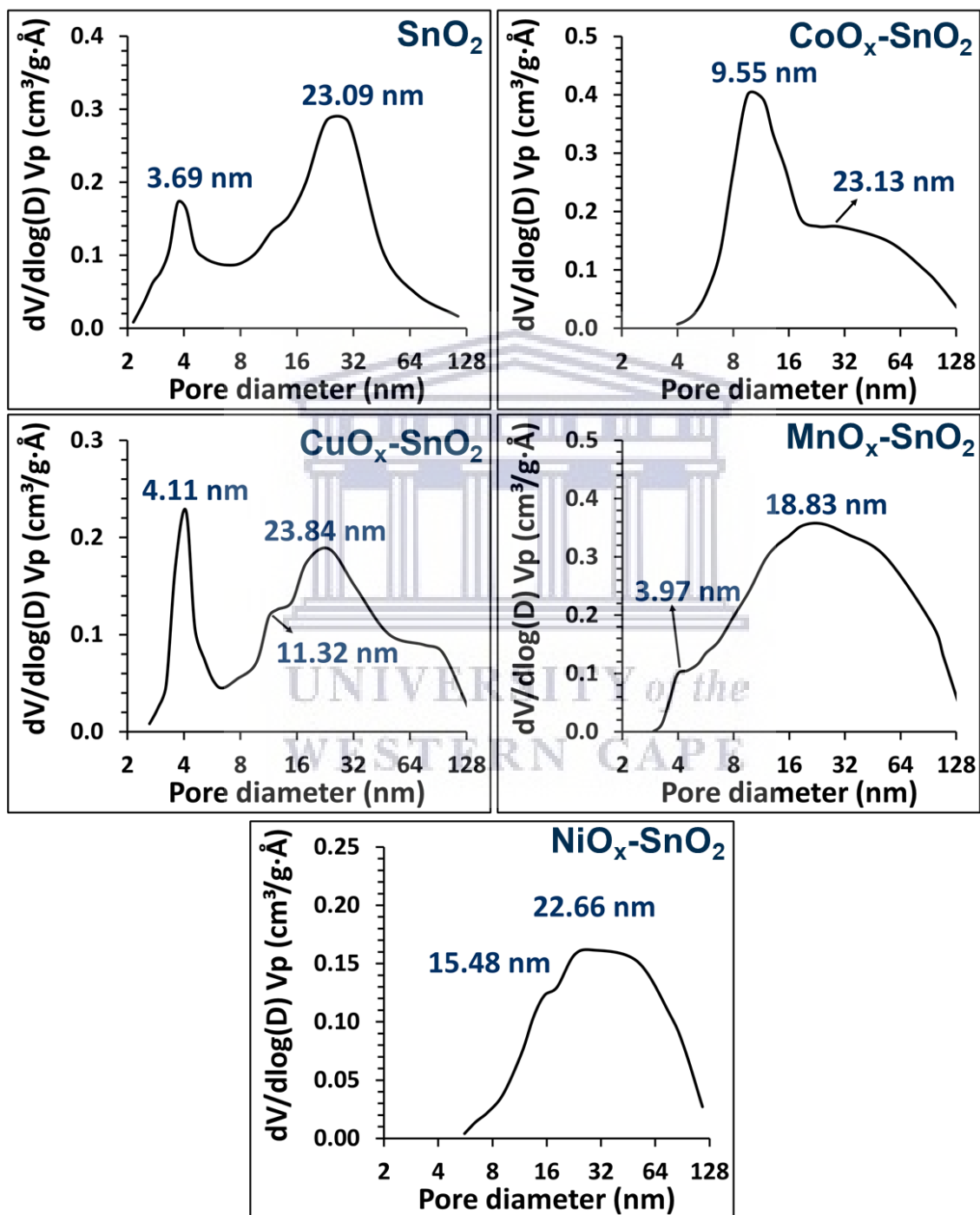
Fig. B-1: BJH pore size distribution plots of the heterostructure BMO-SnO$_2$ catalysts.

APPENDIX C

**1.** **Nitrogen sorption analysis of heterostructured TiO$_2$-SnO$_2$ catalysts**
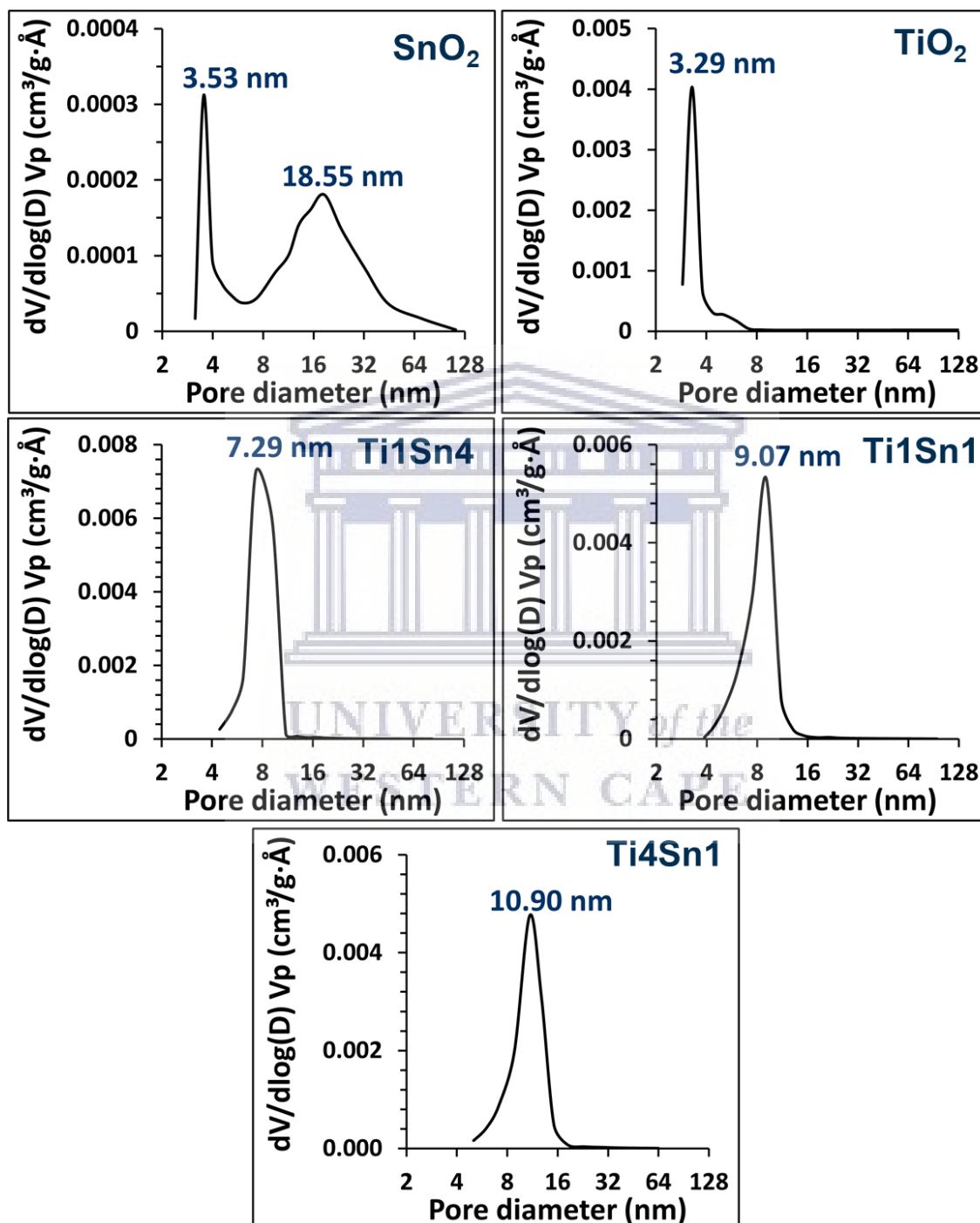
Fig. C-1: BJH pore size distribution plots of the heterostructure TiO$_2$-SnO$_2$ catalysts.

## 2. SEM-EDX characterization of heterostructured TiO₂-SnO₂ catalysts

Fig. B-2: SEM-EDX spectra of the heterostructure TiO₂-SnO₂ catalysts.

Fig. B-3: EDX elemental maps of the heterostructure TiO$_2$-SnO$_2$ catalysts.